

Underwater Acoustic Localisation in the context of Autonomous Submersibles

Navinda Kottege

A thesis submitted for the degree of Doctor of Philosophy of
The Australian National University



College of Engineering and Computer Science
The Australian National University

June 2009

Declaration

I certify that, except where otherwise stated, the contents of this thesis are my own original work based on research conducted at the Department of Information Engineering, College of Engineering and Computer Science at The Australian National University. No part of this has been submitted for a higher degree to any other university or institution. To the best of my knowledge, this does not contain any material previously published or written by any other person except where due reference is made in the text.

Navinda Kottege

Abstract

With the advancement of the field of underwater robotics, the amount of autonomy embodied in the vehicles themselves have considerably increased while making it possible to build and deploy swarms of small autonomous underwater vehicles (AUVs). Apart from the many environmental and mechanical challenges encountered in the underwater domain, the swarming paradigm demands the need for each vehicle to be aware of the positions of at least its near neighbours. The Serafina AUV project which was initiated with the goal of developing swarming technology for the small and highly agile Serafina class AUVs requires a localisation system which could cope with the dynamic and fast changing vehicle configurations while being small, reliable, robust, and energy efficient and not dependent on pre-deployed acoustic beacons.

The acoustical relative localisation system proposed here uses hyperbolic and spherical localisation concepts and provides each vehicle with the azimuth, range and heading of its near neighbours. The implementation utilises an acoustically transmitted maximum length sequence (MLS) signal which provides extremely high robustness against interference by stochastic and systematic disturbances which are typical for underwater environments. The azimuth is obtained via hyperbolic positioning with improved resolution and accuracy with respect to conventional methods. Range and heading estimation is performed utilising two independent methods for increased robustness. The first method uses the implicit synchronisation provided by the underlying inter-vehicle communication scheduling system to measure the difference in time of arrival of the acoustic and long-wave radio signals to estimate the time of flight (TOF) of the acoustic signal and hence measure range. The second method relies on multiple time differences of arrival (TDOA) and a *reverse hyperbolic* localisation scheme to measure range without any explicit knowledge of the sending times of the acoustic signals.

The localisation system performance with regard to accuracy, precision and robustness against interference is experimentally evaluated. Results of experiments conducted at a test tank as well as those obtained during open water lake experiments are presented along with detailed analyses of the behaviour of the errors associated with the measurements.

*To my parents Padmini & Neil with gratitude
& to my wife Himadhu with affection*

Acknowledgement

First and foremost I would like to convey my humble gratitude to Uwe Zimmer, who over the last four years became my guide not only in academia but in many other facets of my life. Thank you, for engaging me intellectually, may it be robotics research, programming real-time systems, photography, finer points of type-setting, world politics or cinema, your influence and insights have helped me mature as a person and to broaden my horizons of knowledge. Most of all, thank you for believing in me throughout this research, even at times when I was doubting my capabilities, and being a good friend.

Many years ago when I had no plans of pursuing postgraduate studies, it was while listening to the many interesting stories related by Dr. Keerthi Premadasa while conducting his first year algebra lectures at the University of Colombo, that the thought and ambition of doing further studies was imprinted in my mind. I only realised this a few years later by which time I was beginning to prepare myself to take the plunge in to the great unknown of PhD research. Henceforth I thank all those who inspired and encouraged me to continue with my studies, including Prof. Upul Sonnadara at the department of Physics and Dr. Ruvan Weerasinghe at the School of Computing.

I reminisce with appreciation and gratitude how Jayantha and Ranjula Kottege took us under their wing providing us with all the amenities, resources and knowledge to make a smooth transition to our new life in Australia when we moved to Canberra in 2004.

Thank you Chris Webers, for being my room-mate at RSISE for almost three years and for being a compassionate friend. I truly appreciate your approach in tackling life's many problems and in turn influencing me to re-evaluate my view of the world through the many engaging conversations we have had. I owe a debt of gratitude towards Felix Schill for being such a great colleague with endless enthusiasm, technical acumen and skill. Thank you for teaching me the dark art of 'hot glue engineering' and also for building the original gantry cart, upon which I based my design. Thank you Jan Zimmer for being a fan of my experiments and being an outstanding assistant during the lake experiments, volunteering to paddle the kayak (and maintaining a great

course) and above all, for convincing me to power my laptop in the way we did (which eventually saved the day) when I was in despair. I am sincerely grateful to Arvin Dehgani for being a great friend and colleague, for the intriguing conversations and for the encouragement and support given throughout my time at RSISE.

I would like to extend my appreciation to Rosemary Shepherd, Lesley Goldberg, Elspeth Davies and Julie Arnold who made my life at the RSISE so much more pleasant and easier by way of providing the highest standards of administrative support and a 'user-friendly' interface to the inner workings of bureaucracy, whether it was to book a hotel in Tokyo, to register for a conference in Paris or simply to place an order for the next critical component in the experimental setup.

I am sincerely thankful to Rod Kennedy, for the support provided for robotics research at our department, for believing in our 'real-world' experimental projects and offering to continue supporting me and my research activities in the immediate aftermath of submission. I gratefully credit Roy Featherstone for reviving the robotics group, for the encouraging conversations and most of all, for picking up my application from a pile many years ago. I also thankfully appreciate the support and encouragement given to me by Jochen Trumpp, especially when it came to tackling mathematical formulae and extending my scholarship. Thank you, Thushara Abhayapala for all the support given during my thesis preparations, your advice was extremely helpful during those stressful times.

My deep appreciation and gratitude extends to my parents Padmini and Neil Kottege, for guiding me from the very young days on to a path of knowledge and education and for providing for my wellbeing and setting the groundwork for me to embark on the journey to where I currently am. I acknowledge my sister, Isuruni Kottege for being all that a younger sister could be and in the process, giving me a new perspective in handling what life has to offer. I also wish to recognise the continued encouragement towards my studies by Amara and Ananda Peiris and Lakmini and Asoka Kottege. Lastly my wife, Himadhu, I thank you from the depths of my heart for being the ideal partner in life, for tolerating me, for caring for me and making sure that I have the best possible environment to help finish writing this thesis, for the many runs of proof reading and most of all, for being you.

Contents

<i>Chapter 1: Introduction</i>	1
1.1 Motivation	2
1.2 Contributions	8
1.3 Thesis outline	10
<i>Chapter 2: Background and related work</i>	15
2.1 Localisation	16
2.2 Underwater localisation	17
2.2.1 Sonar based localisation	17
2.2.2 Acoustic beacon based localisation	18
2.2.3 Vision based localisation	21
2.3 Relative localisation in multi-robot setups	21
2.3.1 Direct relative position sensing	22
2.3.2 Relative position information via communication	24
2.3.3 Position sensing by external centralised observer	30
2.3.4 Comparison of performance	33
2.4 Sensor utilisation strategies for localisation	34
2.5 Discussion	37
<i>Chapter 3: Source signals</i>	43
3.1 Full-range cross-correlation of time-domain signals	43
3.2 Choice of signal waveform	45

3.2.1 Chirps, pseudo-noise and shift-register sequences	45
3.2.2 Maximum Length Sequences	50
3.3 Cross-correlation of MLS signals	51
3.3.1 Effect of uncorrelated noise	52
3.3.2 Effect of mixing and shifting	52
3.3.3 Effect of non-linear transducers	53
3.4 Discussion	56
<i>Chapter 4: Acoustic source localisation</i>	59
4.1 Angle estimation	60
4.1.1 Mapping path length difference to an angle	60
4.1.2 TDOA measurement	62
4.2 Distance estimation	64
4.2.1 Modified matched filter for TOF extraction	65
4.2.2 Distance estimation using TOF	68
4.3 Source localisation and uncertainty of estimates	68
4.3.1 Propagation of errors	71
4.3.2 Sub-sample interpolation	75
4.4 Relative localisation of an AUV	78
4.4.1 Measuring conventions and ranges	79
4.4.2 Transducer placement	80
4.4.3 Geometric description	81
4.4.4 Reverse hyperbolic localisation	83
4.4.5 Estimation errors and resolution	87
4.5 Discussion	93
<i>Chapter 5: The relative localisation system</i>	95
5.1 System overview	96
5.2 Distributed relative localisation in a swarm	99
5.2.1 Pose vector	101
5.2.2 Update rates	102
5.2.3 Sensing range	104

5.3 Handling interference	107
5.3.1 Cluttered environments and multiple senders	108
5.3.2 Interference from extraneous noise sources	116
5.4 Handling outliers	116
5.4.1 Peak tracking	118
5.4.2 Threshold bounding	125
5.5 Computational complexity	126
5.5.1 Range tracking	127
5.6 Discussion	128
<i>Chapter 6: Experiments</i>	131
6.1 Experimental setup	131
6.1.1 Software modules	132
6.1.2 Electromechanical apparatus and firmware	135
6.2 Synchronisation	141
6.3 Experimental procedure	143
6.3.1 Variation of azimuth	144
6.3.2 Variation of heading	144
6.3.3 Variation of range	145
6.4 Calibration of experimental apparatus	145
6.5 Establishing ground truth	151
6.5.1 Definition of estimation errors	152
6.6 Measuring Signal-to-Noise Ratio	153
6.7 Discussion	154
<i>Chapter 7: Results and analysis</i>	157
7.1 Effects of filtering	159
7.2 Effects of peak tracking	160
7.3 Results and errors of short range experiments	166
7.3.1 Variation of azimuth	167
7.3.2 Variation of range	169
7.3.3 Variation of heading	172

7.4 Results and errors of medium range experiments	175
7.4.1 Variation of azimuth	177
7.4.2 Variation of range	179
7.4.3 Variation of heading	182
7.5 Results and errors of long range experiments	184
7.6 Analysis	186
7.6.1 Behaviour of errors	187
7.6.2 System performance	194
7.7 Discussion	202
<i>Chapter 8: Towards 3D source localisation</i>	205
8.1 Incorporating relative depth information	206
8.2 Using additional hydrophones	209
8.2.1 Vehicle motion to emulate additional hydrophones	211
8.3 Source localisation experiments in 3D	213
8.4 Discussion	215
<i>Chapter 9: Conclusions</i>	217
9.1 The relative localisation system	218
9.1.1 Accuracy and precision of position estimates	219
9.1.2 Can the localisation system support swarming?	220
9.2 Key contributions	222
9.2.1 Summary of contributions	224
9.3 Future considerations	225
<i>Appendix A</i>	227
A.1 Source signals before and after filtering	227
A.2 Azimuth variations for error comparison	228
A.3 Heading variations for error comparison	229
<i>Appendix B</i>	231
B.1 MLS generation routine	231

	231
<i>Appendix C</i>	235
C.1 Lower bound for peak tracking parameters	235
C.2 Values of peak tracking parameters used	237
<i>Bibliography</i>	239

“If you cause your ship to stop, and place the head of a long tube in the water, and place the other extremity to your ear, you will hear ships at a great distance from you”

-Leonardo da Vinci (1452-1519)

(MacCurdy, 1948)

Chapter 1

Introduction

Among the definitions for the term **navigation**, many still refer to its early roots in maritime transportation such as the following found in the Oxford English dictionary: “The art or science of directing the movements of a vessel on the sea or other open water; the process of determining and planning a vessel's position and course, by means of geometry, nautical astronomy, instruments”. A more concise interpretation is given by Kaplan and Hegarty (2006) where: “Navigation is defined as the science of getting a craft or person from one place to another”. A common feature among these is the reference to **localisation**, or position fixing which is the process of determining the location of a craft, person or platform¹ with respect to some point of reference. Hence localisation is an integral part of navigation, may it be land, underwater or aerial domains.

The process can be loosely classified as **self-localisation** with respect to one or many fixed beacons (landmarks), *e.g.* trying to find ones own location in an environment using a map based on correlating observed landmarks with those on the map; or **relative localisation (mapping)** when locating the position of one or many beacons with unknown positions with respect to your own position. These concepts are not exclusive and can have overlaps depending on the application

¹. The term ‘platform’ is used to refer to a robot or any vehicle performing the task of navigation.

concerned and sometimes can be simply referred to as **localisation** without the use of prefixes; these are used extensively in robotics especially in the context of navigation and target tracking. The field of simultaneous localisation and mapping (SLAM) research (also known as concurrent mapping and localisation (CML)) use both these concepts extensively. SLAM addresses the process of navigating in unknown environments where the features (landmarks) of the environment are localised based on sensory observations and incorporated in to a map while using the same map as a navigational aid for self-localisation (Thrun, 2002). In the case of known environments, the navigation task becomes somewhat simpler as *a priori* information about the surroundings would be available. This could either be in the form of active landmarks such as navigation beacons (used in aircraft and ship navigation) or passive features in the environment which corresponds to an already available map.

Another localisation scenario is when a communication channel is available between the navigating vehicle and an external observer. The observing platform/station would be actively or passively localising the navigating vehicle (control tower radar observing an aircraft, sonar station observing a submarine) and relaying that information to the navigation/path planning system of the vehicle. In these cases, the localisation task is external to the vehicle and receives the information via the communication channels.

The environments in which autonomous robots operate can be given three independent attributes of varying degree depending on a) the level of *a priori* knowledge about the environment, b) the 'structuredness' or the regularity of environmental features and c) the level of temporal persistence of the aforementioned features. As a guide, navigation in known, structured and static environments is considered relatively easy with currently available methodologies while unknown, unstructured and dynamic environments pose many unaddressed challenges.

1.1 Motivation

Drawing inspiration from nature, the use of multiple robots to solve a task in a collaborative manner, either as swarms or formations, has been growing as a vibrant sub-field in mobile robotics research for over two decades¹. Some of the attractive features of this concept are, the ability to perform spatially distributed tasks quicker, reliably and more robustly, easier reconfigurability of a system and complex emergent behaviour of a swarm comprising of relatively simple individuals. A large body of accumulating literature had been addressing different aspects of swarming from the higher level swarm behaviours to the lower level sensing strategies. One common thread that emerges throughout the literature is the importance of each vehicle being aware of relative

¹. See Liu (2008), pp. 9- 50 for a survey of swarm robotics research.

locations of others¹ (at least of the immediate neighbourhood) for the success of the swarming paradigm.

Relative localisation in multi-robot systems

In his work Reynolds (1987) published a set of simple ‘swarming rules’ aimed at achieving ‘life-like’ animation of boids². The underlying distributed behavioural model states that individuals’ knowledge of the relative positions of neighbouring members is sufficient for sustaining and controlling swarm behaviour. In her seminal work Mataric (1994) postulates that “the ability to distinguish the agents with whom one is interacting from everything else in the environment is a necessary condition for intelligent interaction and group behaviour”³.

In swarm robotics research, the problem of acquiring information regarding the relative position of other members have been addressed in three broad approaches:

- 1) Use of explicit on-board exteroceptive sensing to directly detect relative positions of other members (*e.g.* using cameras, acoustic transponders *etc.*).
- 2) Use of communication channels to exchange/broadcast own localised positions (in reference to a common global frame) with/to the neighbourhood (*e.g.* using radio communication to distribute GPS fixes or self-localised map coordinates obtained via laser range finders, using acoustic communication to distribute self-localised position with respect to an acoustic beacon network *etc.*).
- 3) Use of external “God’s eye view” observations to explicitly sense the position of each individual and relaying that information back to the swarm via communication channels (*e.g.* using over head cameras, acoustic transponders to observe motion and detect positions of individual members *etc.*).

This is not a strict exclusive categorisation but rather a classification based on prominent attributes observed among different implementations for the ease of analysis. Except for the first approach, the other two heavily relies on the existence and reliability of communication channels. In addition, the third approach precludes the notion of decentralised control of the swarm. However in practise, these three approaches are often inter-mixed to varying degrees depending on the application, the availability of communication channels and the level of autonomy assigned to each member of the swarm.

¹. In addition to the knowledge about the operating environment (Fenwick et al., 2002; Howard et al., 2003; Pugh and Martinioli, 2006)

². Simulated bird-like “bird-oid” objects generically called “boids” even when representing other creatures such as schooling fish.

³. In her experiments, members of the ‘Nerd Herd’ recognised other robots using short range radio broadcasts and their positions were detected using infra red sensors - in the related simulations, precise position information such as distance and direction of nearest neighbours were available to each member.

With the maturity of the field of mobile robotics and the ubiquity of position sensing and communication methodology (*e.g.* miniature portable GPS receivers, laser range finders, advanced vision processing systems, small low-cost RF transceivers) relative localisation in land based applications has been successfully addressed utilising multitudes of these techniques. Consequently, a substantial portion of the literature assumes an underlying ‘localisation sensor’ and ‘communication channel’ when addressing the higher level swarm behaviour/control and navigation problems. For example, Martinelli et al. (2005) assumes the existence of exteroceptive sensors capable of measuring relative bearing, distance and orientation of other robots in their multi-robot localisation work. In addition, the cooperative navigation and localisation work presented by Roumeliotis and Bekey (2000b) as well as Moore et al. (2004) assumes the existence of a fast and reliable communication channel between all participants. While the assumption of accessible localisation sensors and communication channels holds true for most in-air applications, it is not necessarily the case in the underwater environment.

Underwater swarms

As the field of underwater robotics progressed with the advancement of mechanical and electronic technology, the amount of autonomy embodied in the vehicles themselves have considerably increased while making it possible to build and deploy even smaller autonomous underwater vehicles (AUVs). However, the cost of most ocean going scientific AUVs has remained relatively high. The oceanographic research community as well as scientists of many other fields (geological, chemical, biological *etc.*) who need to map and survey large bodies of water rely on AUVs for data collection. Apart from the financial aspects, a loss of an autonomous robot during a mission¹ usually means loss of mission data as well. Under these circumstances, the concept of multiple cooperative underwater robots started to emerge combining expertise from the areas of underwater robotics and distributed sensor networks (Curtin et al., 1993). This was not meant necessarily as a replacement for larger AUVs, but rather to offer a viable alternative for missions which would naturally yield themselves to this approach (Bellingham and Rajan, 2007, p. 1100). Multiple smaller autonomous robots collaborating and sharing information improve reliability and enhance robustness against loss of mission data in the event of an individual vehicle being damaged or lost. Apart from making many surveying tasks much more efficient in terms of area coverage and power requirements, the paradigm of a small school of AUVs instead of a single main robot makes possible certain tasks which were not possible earlier, such as dynamically and simultaneously obtaining spatio-temporal measurements of a body of water at multiple locations, cooperative searching, plume tracking and gradient following (Stojanovic et al., 2002; Kalantar and Zimmer, 2007; Leonard et al., 2007; Ramp et al., 2008).

¹ *Kaiko (JAMSTEC) lost in 2003 (Maki et al., 2005), Autosub-1 (NERC) lost in 2005 (Manley, 2007).*



Figure 1.1: Serafina Mk I AUVs [top left], prototype Serafina Mk II AUVs [bottom left] and the author and Jan Zimmer setting up localisation experiments using mock-up hulls [right].

[PHOTOGRAPHY BY UWE R. ZIMMER]

While many researchers are actively engaged in developing cooperative multiple AUV technology, the development of the **Serafina AUV** project (figure 1.1) at The Australian National University (ANU) was initiated with the goal of developing swarming/schooling technology for small submersible robots (Kalantar, 2006; Schill, 2007; Serafina website, 2009).

Relative localisation for underwater swarms

Apart from the many challenges encountered by roboticists when it comes to designing and developing underwater vehicles, the swarming paradigm introduces yet another. As discussed earlier, for multiple vehicles to collaborate, *i.e.* “behave as a swarm”, it is essential that each member is aware of the positions of at least its near neighbours. In the existing literature, the problem of underwater localisation in the context of multi-robot systems has been addressed in a number of ways combining the three approaches mentioned earlier in various degrees.

One method is to have a centralised controller which has a “God’s eye view” over the swarm using some form of sensing modality to track the positions of each individual vehicle. This task is usually designated to a surface vehicle acting as a base station. Depending on the level of autonomy allocated to the members of the swarm, the controller issues either control commands, way-points or position information via communication channels maintained with each vehicle¹.

¹. *E.g. a fleet of gliders surface every 2hrs to obtain a GPS fix and transmits information via satellite phone links to a base station which performs necessary processing and relays back way-points via the same communication channel (Leonard et al., 2007).*

Reliable and fast communication channels underwater are by themselves a challenging problem (Proakis et al., 2001; Lucani et al., 2008). As the number of members in a swarm increase, so does the required bandwidth of the communication. Furthermore, it is preferred to have a decentralised swarm which otherwise impedes some of the attractiveness of this paradigm.

Another approach is for a designated leader vehicle to regularly fix its position with respect to a landmark (acoustic beacon network) and then broadcast this information to the rest of the swarm in the first phase. In the second phase, the members of the swarm individually interrogates the leader vehicle to measure the range between them and the leader. This two phase process leads to each member of the swarm being aware of its position. Once the members are aware of their locations, it is communicated to the rest of the vehicles. This method relies on a designated leader and improves performance over a method where each member of the swarm individually localise with respect to an acoustic beacon network and communicates its position fix to its neighbours. Usually the beacons used can only serve one vehicle at a time where they first need to be interrogated by the vehicle attempting to fix its position. This aspect makes the process of vehicle positions propagating throughout the swarm considerably slow as the number of vehicles increase.

In a variant of the above approach, which does not depend on deployed acoustic beacon networks, the leader vehicle is meant to surface occasionally to get a GPS position fix. The follower vehicles individually interrogate the leader to find its position and uses dead-reckoning in the mean time to update their positions. An underlying feature of these methods apart from the reliance of explicit communication between vehicles for navigation, is that most of the approaches described in the literature are built on a leader-follower paradigm rather than a fully-fledged homogeneous swarm. As a result, the emphasis has been to update the vehicles with their own position and not on each member of the swarm getting regular position updates of vehicles in its local neighbourhood.

It must be emphasised that the existence of communication channels between members is considered essential for the swarming paradigm in light of sharing mission data. However, the speed and bandwidth requirements for such communication tends to be lower compared to those required for multi-robot navigation, especially considering the above mentioned approaches. With the limitations faced by underwater communication techniques at present, it is preferable to make navigation less dependant on inter-vehicle communication, especially in the context of AUV swarms, whose manoeuvrability would otherwise be limited by the speed of the communications network.

Under these circumstances, with the growing research interest in the field of underwater swarm robotics, shortcomings in transferring concepts and methodologies from land based multi-robot systems are emerging. This is especially the case in relative localisation for underwater swarms

given the limitations and unavailability of appropriate 'localisation sensors' and communication channels in the underwater medium. With the advent of swarms comprising of small agile vehicles, the conventional schemes such as beacon network based localisation and reliance on slow acoustic communication channels for localisation are becoming inadequate.

The Serafina AUV project was initiated with the goal of developing swarming technology for the small, agile and highly manoeuvrable Serafina class AUVs¹. Smith et al. (1998) elaborates the attractiveness of using multiple AUVs for synoptic and pseudosynoptic oceanographic data collection while highlighting operational logistics as a key challenge. Using smaller AUVs contribute to greatly reducing the time and cost involved in transport, deployment and recovery while allowing more AUVs to be used in missions with a similar or lower cost and effort compared to the use of larger conventional vehicles.

The use of multiple homogenous vehicles with similar sensing and navigation capabilities further assists in managing operational logistics and yields itself to distributed and decentralised control of the swarm. Additionally, use of such homogenous vehicles can contribute to an overall reduction of navigation errors as pointed out by Roumeliotis and Bekey (2002) in their distributed multi-robot localisation work. The distributed and decentralised control paradigm provides safeguards against mission failures due to loss of or damage to a few individual members of a swarm. By considering these aspects, a decentralised concept of localisation was preferred over strategies requiring a designated leader or centralised controllers.

As pointed out by Leonard et al. (2007), the number of vehicles and their speeds needs to be matched with the spatial and temporal scales of interest when monitoring and sampling time varying spatially distributed fields using swarms of AUVs. This emphasises the need for fast and agile vehicles for applications in environments whose dynamic features vary in short time scales.

With the relatively small size, and scenarios which require a large number of the AUVs to swarm, the localisation system would need to efficiently scale with the number of vehicles involved. In order to make maximum use of the agility of these vehicles and provide the swarm with fast and dynamic manoeuvres, the position update rates needed to be much faster, accurate and precise than those provided by state of the art strategies. In addition, a system which does not depend on pre-deployed acoustic beacons was preferred as well. This eliminates the need for preparing the area of operation and calibrating the beacons and also lifts any constraints placed upon the swarm by a beacon network covering only a limited underwater area. Moreover, the small size of the individual vehicles make it impossible to incorporate existing technology such as underwater

¹. The Serafina class vehicles are just over 50cm in length, 10cm in diameter, actuated by five thrusters giving it five direct degrees of freedom (roll, pitch, yaw, heave and thrust) with sway motion achieved by a combination of roll and heave. The maximum forward speed is 1.5ms^{-1} .

acoustic modems, ultra-short baseline transponders and sonar modules due to physical size limitations and power consumption requirements.

Problem statement

The research presented in this thesis addresses the challenging problem of designing, developing and evaluating a decentralised relative localisation system capable of facilitating swarming of autonomous submersibles - a system that scales up with increasing swarm size and does not depend on pre-deployed beacon networks or the speed and bandwidth of the communication channels. The design specifications and constraints are drawn from the requirements of providing relative localisation capability for the small and agile Serafina class AUVs.

1.2 Contributions

In order to design a relative localisation system while considering the aspects discussed earlier, the emphasis was shifted more towards direct position sensing as opposed to explicit and active communication being used to exchange self-localised position information between neighbouring vehicles. This line of thought was further reinforced by observing swarms, flocks and schools of animals in nature. For example, a school of fish would change its swimming direction either by all members reacting after sensing the same stimuli or by individuals reacting after sensing a position change of their local neighbourhood - without explicit communication. Furthermore, the swarming behaviour of the AUVs only required positions of vehicles in the local neighbourhood *relative to the observing vehicle* and not relative to a global frame since there is no global controller. Despite a number of challenges being posed by the requirements and specification of a decentralised swarm consisting of small and fast AUVs, the benefits provided are the relatively shorter distances between vehicles and being able to exploit the existing underlying communication and scheduling scheme developed by Schill (2007).

The relative localisation system

In order to address the requirements of the **Serafina AUV** project, a relative localisation system was designed, developed and evaluated experimentally. This system draws insights from hyperbolic and spherical positioning schemes (Deffenbaugh et al., 1996a) and provides each vehicle with a regularly updated pose vector (consisting of the azimuth, range and heading) of its near neighbours with respect to its own frame of reference. As opposed to most relative localisation schemes described in the literature which treats swarm members as point objects and hence provide no heading direction (apart from integrating multiple position updates), this implementation explicitly estimates the heading direction and is included in the pose vector with each update. The implementation utilises an acoustically transmitted **Maximum Length Sequence**

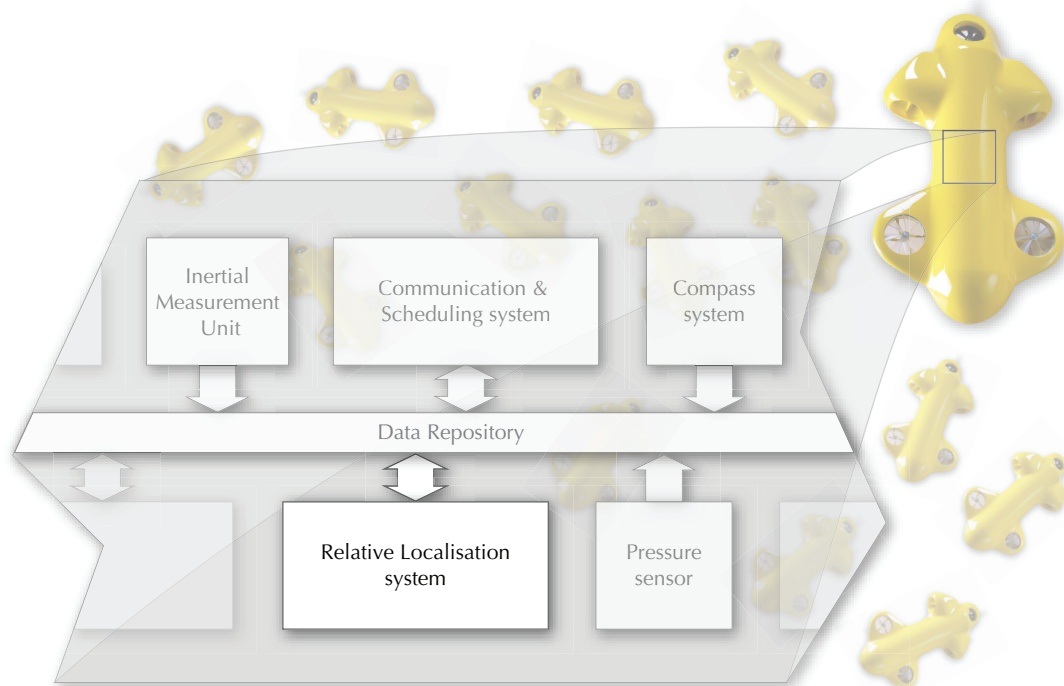


Figure 1.2: Simplified block diagram showing some of the main components that facilitates decentralised swarming capability on a Serafina AUV along with their data flows. This thesis focuses on the relative localisation system.

(MLS) signal from **projectors** on the bow and stern ends of each ‘sender’ vehicle which in turn is received by a pair of **hydrophones** on the ‘observer’ vehicles at each update cycle. The statistical properties of the MLS signals provide extremely high robustness against interference by multipath arrivals, cross-talk and noise sources and other inherent detrimental effects in the underwater environment as well as the non-linear characteristics of the transducers used.

While the azimuth is obtained via **hyperbolic positioning** techniques measuring multiple **time-difference-of-arrivals** (TDOA) between the hydrophones, the resolution and accuracy is greatly improved over those achieved by conventional methods using effective outlier handling schemes. The range and heading estimation is performed utilising two independent methods which provide higher reliability and robustness in a fast changing and dynamic environment. One method uses the implicit synchronisation provided by the underlying scheduling system to measure the difference of **time-of-arrivals** (TOA) of the acoustic and electromagnetic (long-wave radio) signals. This gives an equivalent measure to the **time-of-flight** (TOF) of the acoustic signal which is converted to a distance as done in spherical positioning schemes. The second method which only relies on multiple TDOAs, estimates the range without any explicit knowledge of the sending times of the acoustic signals. The **reverse hyperbolic** estimation scheme used here provides a

safeguard against erroneous range and heading estimation due to loss or drift of synchronisation between the neighbouring vehicles.

Figure 1.2 shows a simplified block diagram of some of the main components that facilitates decentralised swarming capability on a Serafina AUV. In his thesis Schill (2007) addresses the problem of establishing effective distributed communication in underwater robotic swarms while the work presented in this thesis addresses the problem of achieving localised relative position sensing amongst swarm members. While the implementation characteristics focus on the Serafina AUVs, the relative localisation strategy and innovative methodologies developed in this research can in general be utilised to implement ‘localisation sensors’ for many other underwater applications (underwater sensor network localisation, tracking of underwater life forms *etc.*) which are not limited to small AUV swarms. The experimental results and analyses presented therein contributes to the growing field of localisation in the context of understanding limitations and opportunities presented by underwater environments. Aspects such as the choice of signal waveform and techniques of handling interference and outliers have potential applications beyond underwater robotics and can be transferred to other application domains with minimal modifications to serve localisation requirements.

Solution synopsis

The work presented in this thesis proposes a novel distributed relative localisation strategy to be used in underwater multi-robot setups with an emphasis on providing swarming capability to small agile AUVs. This strategy is implemented with a relative localisation system comprising of a ‘localisation sensor’ capable of producing estimates for azimuth, range and heading of neighbouring submersibles. The system is experimentally evaluated and its performance is analysed with regard to aspects such as update rate, sensing range, accuracy and precision of the produced estimates. According to the obtained experimental results, within the required sensing range, the system outperforms state of the art techniques with regard to the speed of updates and the localised position accuracy.

1.3 Thesis outline

The structure of the thesis is outlined in the following sections. A brief introduction is given to each of the chapters which contain the background, methodology developed during the research, experimental results and analyses, extensions and conclusions.

Chapter 2 - Background and related work

This chapter gives a brief insight in to the background of localisation technology, the drivers behind the choice of sensing strategies and methodologies and focuses on work related to the

research presented in this thesis. Underwater localisation methods and modalities are discussed first and different strategies used to perform relative localisation in multi-robot setups are reviewed next with an emphasis on ‘real-world’ implementations addressing the problem of simultaneous navigation of multiple AUVs. Finally, drawbacks and benefits of existing underwater localisation systems with respect to the constraints and requirements of the motivating application is discussed.

Chapter 3 - Source signals

Description of the time-domain cross-correlation used by the relative localisation system as well as the motivation behind the choice of maximum length sequences (MLS) as the source signal is given in this chapter. This includes performance evaluation of several classes of signals with regard to cross-correlation peak detection and signal to noise ratios (SNR). Also presented in this chapter is an empirical method for overcoming the frequency filtering introduced by the transducers to improve the cross-correlation peak detection performance.

Chapter 4 - Acoustic source localisation

The specific distance and angle measurements and estimations carried out during the process of localisation is explained in this chapter. The methodology and basic measurement schemes are described in detail along with identification of different classes of errors affecting the estimated quantities. An analysis is presented on how the uncertainties associated with the basic measurements propagate towards uncertainties in the estimated quantities which is followed by an explanation of how sub-sample interpolation contributes towards increased precision of the estimation system. Descriptions of how the sub-azimuths and sub-ranges are combined to derive the compound estimates for azimuth, range and heading are given along with theoretical error models associated with each of these quantities.

Chapter 5 - The relative localisation system

An overview of the functional components of the relative localisation system is presented in this chapter and goes on to explain how the relative localisation system can provide a distributed localisation solution for swarming of AUVs. The relationship between the relative localisation system and the underlying communication and scheduling system is elaborated while expanding on how multiple senders and observers are accommodated in the context of a local neighbourhood belonging to a larger swarm of AUVs. This chapter also discusses the interference caused by delayed multipath arrivals, cross-talk due to multiple senders and effects of environmental noise on the system along with strategies to address them. Furthermore, outlier handling schemes are introduced and the performance of the proposed **peak tracking** scheme is experimentally evaluated. In addition, the computational complexity of the system is discussed along with a

proposed **range tracking** scheme to overcome the problem of increasing computational cost as the effective sensing range increases.

Chapter 6 - Experiments

The configuration, apparatus and procedure used for the experimental evaluation of the relative localisation system is elaborated in this chapter. The experiments were aimed at gauging the accuracy and precision of the estimates under operational conditions, the angular and radial sensing limits of the system and the overall suitability of the approach to solve the task of relative localisation for small AUVs. Most of the experiments were carried out at the ANU test tank¹ while other experiments were carried out at Lake Burley Griffin². This chapter also explains how ground truth references were established to compare the localisation estimates produced by the system.

Chapter 7 - Results and analysis

The effects of the inverse frequency filtering scheme and the peak tracking scheme have on the estimated quantities are explained and analysed in this chapter, while the results of selected short, medium and long range experiments are presented in detail. The performance of the localisation system is analysed in terms of accuracy, precision while the angular and radial sensing ranges of the system are evaluated with respect to SNR of the received hydrophone channels and position errors resulting from pose vector estimates. Experimental data is also used to demonstrate how the system recovers from degradation of position estimation accuracy.

Chapter 8 - Towards 3D source localisation

The localisation system discussed throughout this thesis focuses on 2-dimensional or planar localisation, where the localised position is expressed in polar coordinates with an azimuth and a range. The source to be localised is assumed to be on the same plane containing the two receivers and their main axes of directivity. When the source leaves this plane, the range estimation remains valid while the estimated angle is no longer contained within the plane for which the azimuth was defined. This chapter proposes several strategies to incorporate additional information about the source position with the estimated range and azimuth quantities to produce the true azimuth and elevation angles. The experimental results are also presented to validate the feasibility of the presented relative localisation system in handling 3-dimensional localisation, either with relative depth information or with additional sensors without further modification of the sensing and processing methodologies.

¹ *Cylindrical tank with corrugated metal walls filled with tap water. Diameter 4.2m, depth 1.5m.*

² *Lake Burley Griffin has an approximate surface area of 6.64km² situated in the centre of Canberra, ACT, Australia.*

Chapter 9 - Conclusions

The performance of the relative localisation system is critically compared against the state of the art in terms of accuracy and precision of the obtained localisation estimates. This chapter concludes the thesis summarising key contributions and drawing insights upon the research conducted. Additional work needed to implement a deployable system are enumerated and future research directions are indicated which could benefit from the outcomes of this thesis.

Chapter 2

Background and related work

Over the last few decades, sensor modalities and methodologies for navigation of robots over land have developed and propagated rapidly when compared to its underwater counterparts. Apart from the challenges presented by the harsher environment for the mechanical aspects of robots, the underwater media itself presents a number of considerable challenges in localisation, navigation and communication for autonomous underwater vehicles (AUVs). This chapter gives a brief insight in to the background of localisation technology, the drivers behind the choice of sensing strategies and methodologies while focusing on work related to the research presented in this thesis.

The following section gives a general introduction to the sensor modalities available for underwater applications with regard to robot localisation. Next, different strategies used to perform relative localisation in multi-robot setups are reviewed with an emphasis on ‘real-world’ implementations addressing the problem of simultaneous navigation of multiple AUVs. The subsequent section discusses some sensor utilisation strategies for localisation available in the literature and their applicability in the localisation system being developed in this thesis. Finally, drawbacks and benefits of existing underwater localisation systems with respect to the constraints and requirements of the motivating application are discussed.

2.1 Localisation

Localisation, or position fixing, is a topic of interest covered by many diverse research fields. Animal hearing/binaural localisation (Wallach, 1938; Konishi, 1993; Roman and DeLiang, 2003; Stern et al., 2006), Acoustic source localisation/Speaker tracking (Svaizer et al., 1997; Benesty, 2000; Lehmann, 2004), Sensor network localisation (Ajdlar et al., 2004; Priyantha, 2005; Mao et al., 2007), target motion analysis (Altes, 1979; Farina, 1999; Arulampalam et al., 2004) and mobile robot navigation (Thrun et al., 2001; Howard et al., 2003; Valin et al., 2003; Kenn and Pfeil, 2004) are some of them. The research presented in this thesis draws insights from many of these areas in designing and developing the relative localisation system. The choice of sensing strategy and methodology mainly depend on the constraints (size, weight, power budget *etc.*), requirements (range, accuracy/precision, update rate *etc.*) of the application and the operating environment (structuredness, degree of clutter, medium *i.e.* in-air, underwater *etc.*). For example, underwater electrolocation schemes such as those presented by Solberg et al. (2008) are only viable for very short ranges (less than 0.5 m). While visual localisation methods (Dellaert et al., 1999b; Huster, 2003) require well lit (or artificially lit) environments, the use of sensors such as laser range finders are more suited to structured environments with laser reflective surfaces.

While localisation schemes involving the electromagnetic spectrum have become ubiquitous for all forms of in-air applications¹, in the underwater domain these are unavailable due to the high rate of attenuation of electromagnetic waves in water. For example, global positioning system (GPS) signals experience an attenuation of well over 50 dB at 1.0 m depth in sea water². Ergo, vehicles operating underwater are deprived of access to navigational aids and wireless communication methods using high frequency electromagnetic waves.

Early localisation systems

During the mid 20th century, maritime and later aircraft navigation used localisation schemes utilising low frequency (LF) and very low frequency (VLF) electromagnetic waves. Among these were the Decca Navigator System, Omega Navigation System and the LORAN system to name a few (Palmer, 1970; Kasper and Hutchinson, 1978; Klepczynski, 1983; Last, 1989). By now these systems (except for the LORAN-c variant which is also in decline) have been superseded by GPS based navigation systems (Kaplan and Hegarty, 2006; Hofmann-Wellenhof et al., 2001). Most of the aforementioned obsolete systems used hyperbolic localisation (also known as multilateration) which operated either by locating the position of a single transmitter using

¹ See Kayton (1988) for a comprehensive survey article on the historical development of navigation technology.

² GPS signals use a frequency of approximately 1.5 GHz and electromagnetic loss in sea water is given by $1400 \sqrt{f}$ dB km⁻¹ where f is in kHz (Waite, 2002).

multiple receivers (at least three) or by locating the position of a single receiver using at least three synchronised transmitters. Despite the fact that these systems are non-operational, the developed localisation concepts have been adopted by acoustic beacon localisation schemes that are currently used for subsea navigation.

2.2 Underwater localisation

The following sections give a brief evolution of underwater localisation methodologies. While this section concentrates mostly on single vehicle localisation schemes, later sections will elaborate on how some of these methods have been extended to facilitate multi-robot localisation and navigation in the underwater domain.

2.2.1 Sonar based localisation

While the concept of target detection in the underwater environment using acoustics can be traced back to a late 15th century postulate by Leonardo da Vinci¹ (MacCurdy, 1948), practical systems came into use only in the early 20th century. The earliest adoption of this method was sonar (sound navigation and ranging) in its passive and active forms which performed very similar to radar (radio detection and ranging) in target detection, ranging and mapping applications (Altes, 1979). Though sonar was primarily developed for underwater applications, its principles have also been successfully used in air to complement radar systems as well. Sonar sensors have also been successfully used in mobile robotic applications to aid navigation (Elfes, 1987). As the role of electromagnetic waves in air is taken over by acoustics in water, Burdic (1984) gives a comprehensive chapter on the historical developments and technologies that led to modern day sonar systems. In addition see Nielsen (1991), Waite (2002) and Ricker (2003) for more detailed descriptions about these concepts and Etter (2003) regarding further mathematical treatment for both active and passive sonar operation.

In his survey of different localisation and map building methods, Thrun (2002) presents a number of approaches used by land based robots deployed mostly in static and structured environments. As he points out, for the dynamic and unstructured environments in the underwater domain, most of these techniques are inadequate. However, terrain sensing sonar based mapping and localisation has been successfully implemented and demonstrated for AUV navigation. In this regard, Feder, et al. (1998), presents a concurrent mapping and localisation algorithm and tests its long term performance using simulated forward looking sonar data covering an area of 1.2km × 1.2km. Leonard et al. (2001) applies a modified version of this algorithm to sonar data

¹. *"If you cause your ship to stop, and place the head of a long tube in the water, and place the other extremity to your ear, you will hear ships at a great distance from you"*

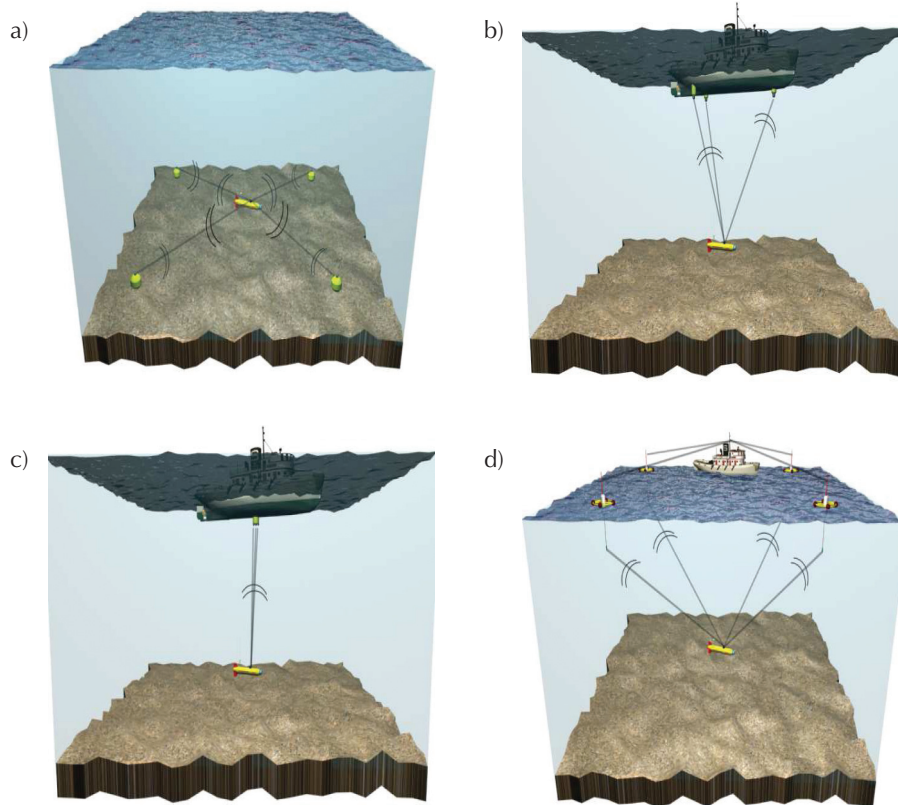


Figure 2.1: Illustrations of acoustic beacon based underwater localisation techniques reproduced from work presented by Alcocer et al. (2006) showing a) Long baseline (LBL), b) Short baseline (SBL), c) Ultra short baseline (USBL) and d) LBL with GPS Intelligent Buoys (GIB).

collected from a test tank experiment and later to forward looking sonar data sets obtained in the ocean by a US Navy vessel equipped with an 87kHz high resolution array (HRA) sonar. Williams et al. (2001a) presents results of ocean experiments where a simultaneous mapping and localisation algorithm operating on sonar data was deployed on the Oberon AUV with artificial landmarks distributed along a 50m stretch of Sydney shoreline. Supplementing this scheme, Majumder et al. (2001) presents a framework to fuse vision and sonar data obtained in shallow water environments to perform localisation of an AUV. Williams and Mahon (2004a) further apply and develop this concept in their work to perform simultaneous localisation and mapping in 3D. In addition Newman et al. (2003) presents results of applying simultaneous mapping and localisation schemes for AUVs using a synthetic aperture sonar for terrain sensing and compares its performance to acoustic beacon network based position fixes along with data from an on-board Doppler velocity log (DVL).

2.2.2 Acoustic beacon based localisation

While there is no equivalent to GPS underwater, considering its availability at almost any location on the surface of the planet, underwater acoustic beacons provide a somewhat similar service

for position fixing in a much smaller area where the beacons are deployed. Therefore, the use of acoustic beacon networks has been the localisation method of choice for most underwater robotic applications for many years (Bellingham et al., 1994; Deffenbaugh et al., 1996a). In the context of AUVs, on-board omnidirectional transducers are used to interrogate a transponder beacon using an acoustic signal with a predefined frequency signature. Upon receiving the signal, the transponder responds by transmitting an acoustic signal with a different frequency signature after a predetermined delay. The navigation system on-board the AUV measures the round-trip time for the acoustic signal upon receiving the reply from the transponder; thus estimating the distance between the transponder and the vehicle. However, to accurately obtain a position fix, the AUV needs to interrogate multiple transponder beacons. Depending on the distance between transponders (which could be deployed on the sea floor, attached to floating buoys or mounted on surface vessels), they are categorised as long baseline (LBL) short baseline (SBL) or ultra-short baseline (USBL) techniques. Alcocer et al. (2006) and the references therein gives an introduction to the traditional methods of underwater localisation including LBL, SBL and USBL techniques. Some diagrams illustrating these different acoustic localisation schemes are reproduced in figure 2.1.

A large body of literature exists covering many aspects of acoustic beacon based navigation and localisation, among those; Vaganay et al. (1999) and Matos et al. (1999) discusses the use of dead-reckoning in between position fixes using on-board inertial measurements, while Olson et al. (2004) presents an outlier rejection scheme for localisation using LBL methods. Bingham and Seering (2006) discuss the use of hypothesis grids for improving LBL navigation for AUVs and Larsen (2000) proposes a method called 'synthetic LBL' where a single transponder and dead-reckoned vehicle motion simulates multiple transponders.

A significant challenge faced when using a pre-deployed beacon network (LBL) had been the lack of precise position information of the transponders themselves. Once they are dropped to the bottom of the ocean, careful surveying involving multiple surface vessels is required to accurately calibrate the positions of the transponders. However, these positions can change over time due to shifting sediments and other geological and environmental activity, necessitating periodic recalibration which makes maintaining such a beacon network extremely costly. Additionally, in the case of sea-floor based, or floating buoy based beacons, the theatre of operation for AUVs is limited by the area serviced by the transponder network. In the case of ship/boat mounted technologies such as SBL and USBL, the area coverage is once again limited to the sensing range of these transponders. However, these techniques have been successfully used for underwater localisation, especially in the context of single AUV missions. The work presented by Rigby et al. (2006) demonstrates accurate geo-referenced underwater navigation in 3-dimensions by fusing

measurements from an on-board DVL with localisation information obtained via a boat mounted USBL system.

A slightly different approach is used in the work presented by Liu and Milios (2005) which is later used to track the AQUA robot (Dudek et al., 2007). Instead of a conventional USBL system, a surface floating buoy with an array of four hydrophones are used to localise a sound source located on the robot (using hyperbolic localisation techniques). The localised relative positions are mapped to a global reference frame using the position of the floating buoy acquired via GPS, compass, inclinometers, and inertial sensors. The passive localisation sensor ‘raft’ used initially had later been developed in to a self-propelled buoy which is capable of positioning itself on the surface to track the AQUA robot using acoustic source localisation.

With the emergence of the field of underwater acoustic sensor networks (UWASN), much effort had been focused on localising static or mobile sensor nodes with respect to a number of ‘anchor nodes’ whose positions are known (Pompili et al., 2008). These techniques draw insights from traditional acoustic beacon based localisation schemes (Chandrasekhar et al., 2006). Cheng et al. (2007) describes such a strategy and presents simulation results for self-localisation of a mobile (AUV) or stationary underwater sensor node with respect to four anchor nodes with known positions using trilateration. Dive and rise (DNR) beacon networks involve mobile beacons which acquire a GPS position fix by periodical surfacing (Erol et al., 2007). Once the position fix is obtained, they dive becoming anchor nodes which transmit their positions. In ‘multi-stage localisation’ studies presented by Erol et al. (2008), other nodes (static or mobile) can localise with respect to these anchor nodes by additionally using a communication channel. With results of their simulations, it is concluded that the communication overhead is higher for mobile node localisation compared to static nodes.

In the recent years, traditional long baseline navigation concepts have been extended to accommodate multiple AUV missions with autonomous surface crafts equipped with GPS antennae and underwater acoustic modems implementing ‘moving long baseline’ (MLBL) concepts (Vaganay et al., 2004; Curcio et al., 2005a). These mitigate some of the drawbacks such as limited area coverage and need for survey and re-calibration of pre-deployed beacon networks. In these MLBL applications, the conventional acoustic transponders are replaced with underwater acoustic modems such as the WHOI micro-modem (Freitag et al., 2005).

Although with the advantage of a much faster speed of propagation of acoustic signals in water (approximately 1500ms^{-1}) compared to air, sonar ranging systems and transponder beacon localisation schemes operate much slower than their in-air counterparts which utilise electromagnetic waves. This characteristic is shared by communication systems as well. Though underwater acoustic modems are now available with usable bandwidth, range and speed as off-the-shelf products, they are far limited in bandwidth and speed in comparison to other common

in-air wireless communication solutions. Apart from the speed of operation, most of the communication and navigation applications involving underwater acoustics are prone to adverse effects such as those introduced by sound speed profiles caused by changing water temperature, multipath propagation, frequency dependent fading, scattering and noise as elaborated by Baggeroer et al. (1993), Collins and Kuperman (1994) and Kilfoyle and Baggeroer (2000).

2.2.3 Vision based localisation

Depending on the application domain, the requirements for localisation varies widely. While the most popular modality is to use variants of acoustic positioning and sonar sensing, a few vision based methods have been successfully used as well. Huster (2003) proposes a localisation system based on monocular vision and an inertial measurement unit for underwater object manipulation while Plotnik and Rock (2005) describes a stereo vision based system used by an AUV for tracking marine organisms in the ocean. Sáez et al. (2006) use a ‘trinocular’ stereo rig with three grey scale cameras to perform underwater simultaneous localisation and mapping in 3D. Corke et al. (2007) presents experimental results of underwater localisation using visual odometry and scaled optical flow obtained from stereo cameras. The localisation performance is also compared with that of an acoustic localisation system using static acoustical sensor nodes. However, the existing literature suggests that the use of vision underwater is limited to short range sensing in non-turbid, shallow and illuminated (or deep and artificially illuminated) environments.

2.3 Relative localisation in multi-robot setups

Coordination and manoeuvring of multiple vehicles presents additional localisation and navigation requirements. Self-localisation by each vehicle with respect to a common global reference frame is no longer sufficient for most such applications. In the previous chapter, it was established that a minimum requirement for a swarm to operate is for each vehicle to at least be aware of the relative locations of vehicles in its immediate neighbourhood. Different approaches used to achieve this were loosely categorised in section 1.1 as a) direct relative position sensing of other members, b) use of communication channels to exchange own self-localised positions (with respect to a common global reference frame) with the neighbourhood and c) use of external centralised observations to explicitly sense the position of each individual and relaying that information back to the navigation systems of each swarm member via communication channels.

The following sections give few of the examples available in the literature which address the problem of relative localisation in multi-robot setups, not limited to underwater environments nor acoustical methods. However, approaches addressing underwater multi-robot localisation are

given more emphasis and experimental results showing position estimation performance are also presented where available.

2.3.1 Direct relative position sensing

A few examples of implementations which do not rely on any communication channel to broadcast/exchange self-localised position information while facilitating multi-robot localisation are described in the following sub-sections.

As acoustical navigation system for multi-vehicle operations

A customised LBL method proposed by Atwood et al. (1995) is among the earliest work addressing the problem of multiple AUV navigation. They highlight the need for either the LBL beacons to synchronously emit navigation pings (to implement hyperbolic techniques for localisation) or for the AUVs themselves to schedule their interrogation cycles (to implement spherical techniques for localisation) to avoid confusion caused by overlapping acoustic pings. The latter method is favoured and implemented via a master-slave (leader-follower) approach. The designated master vehicle initiates a cycle by emitting an interrogation ping which is heard by the slave vehicles. Each of them initiate their own interrogation ping after waiting for different preset delays. The master, being aware of the schedule would be able to localise the positions of all slave vehicles, which is identified as an advantage of this approach along with the ability to acoustically monitor the positions of all vehicles if the master interrogation cycle is triggered by a ping from a surface vessel. The main drawback however is the reduction of the 'navigation duty cycle' as the number of slave vehicles are increased. As described by the authors, doubling the number of vehicles more than doubles the time between interrogation cycles.

This technique is demonstrated with two AUVs, one acting as a master and the other as a slave. The ping period of the master was 10s and the slave emitted an interrogation ping 5s after hearing the 9kHz interrogation ping of the master. Apart from the drawbacks associated with conventional LBL beacon networks with regard to deployment and maintenance, the viability of such a system decreases as the number of vehicles increase, due to the long delays between position fixing.

Multi-frequency LBL beacon network for multiple AUV navigation

Cruz et al. (2001) proposes a multiple AUV navigation system with a network of multi-frequency (20-30kHz) transponders attached to surface buoys with known locations. While each AUV separately interrogates the transponders as in traditional LBL systems, the other AUVs are supposed to listen to these interrogation pings and derive the relative positions of the vehicles attempting localisation. This is facilitated by the different frequency pairs used by each vehicle

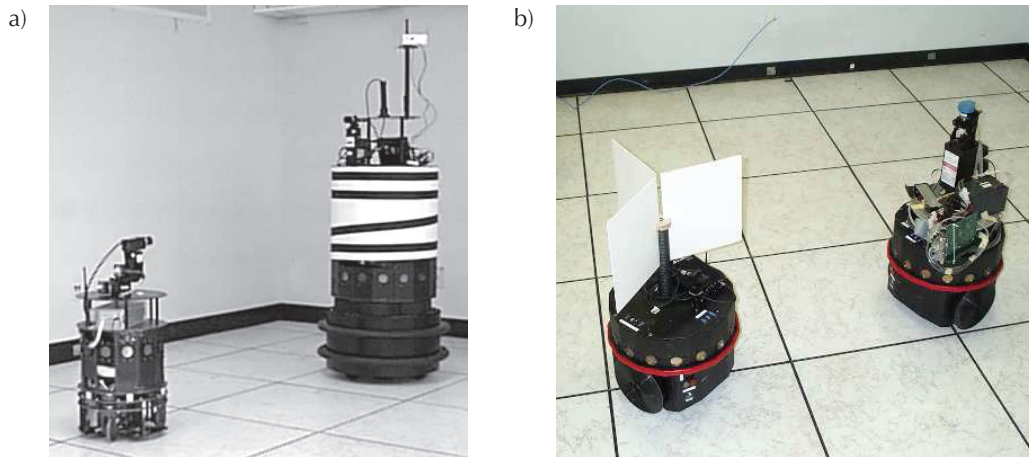


Figure 2.2: Images of the two implementations of the robot tracker sensor, reproduced from work presented by Rekleitis (2003). a) Robot tracker with helical pattern and camera, b) robot tracker with three vertical planes and laser range finder.

to interrogate each transponder. By attaching radio transmitters to these buoys, a land based station can track the position of each of the AUVs while in operation. While the system is purported to facilitate multiple AUV navigation, the presented experiments (in a $8\text{km} \times 3\text{km}$ effective area) only show remote tracking involving one REMUS class AUV (1.5m in length, 0.2m in diameter). The authors report the externally tracked position was in agreement with the internally logged vehicle position within 5-10m.

Robot tracker for indoor multi-robot exploration

The ‘robot tracker’ sensor described by Rekleitis (2003) is used to localise and track the position of another robot during cooperative localisation in multi-robot exploration. The experiments involving two robots demonstrate how one stationary robot provides a salient landmark for the other robot to navigate, a strategy to compensate for non-salient environmental features interfering with longer term navigation. In the first of the two implementations of the ‘robot sensor’, a camera on one robot is used to identify a unique helical pattern on the other robot and derive the relative position and orientation from the observed visual pattern. In the second implementation, a laser range finder is used to identify a unique target mounted on the other robot comprising of three vertical planes made of laser reflecting material. The relative position of the target robot is derived using the laser range finder measurements based on reflected intensities. The two robot tracker implementations are depicted in figure 2.2.

Infra-Red relative position sensing for small scale robot formations

Pugh and Martinoli (2006) presents a relative position sensing methodology for small scale indoor robots using an infra-red based system. Here, relative range and bearing of a neighbouring

robot is measured using the received signal strength indication (RSSI). This approach has the added advantage of being able to use the infra-red localisation system for low bandwidth communication between the robots. However, relative localisation does not depend on the availability of the communication channel in this approach. Navigation of multiple robots using this scheme is simulated while experiments (with and without communication) involving 4 real robots are also presented. The results suggest that the localisation error is reduced when the communication channels are used to exchange relative position information between localising robots.

2.3.2 Relative position information via communication

Examples of implementations which require some form of position information exchange via communication channels to realise relative position updates to facilitate multi-robot navigation are appraised in the following sub-sections.

Positioning for multiple AUVs using GPS and acoustic communication

This methodology is presented and tested in simulation by Baccou et al. (2001) as a low cost solution for multiple AUV navigation where a flotilla of AUVs consists of a designated leader vehicle and followers. The leader vehicle using dead-reckoning based on inertial data (velocity calculated using the propellor rotation speed), periodically reaches the surface to obtain a GPS position fix. Its displacement with regard to the initial position based on dead-reckoning corrected using the GPS fix is then broadcast to the rest of the followers using acoustic communication modems. Once the information is received, each of the follower vehicles interrogate the leader vehicle which now acts as an acoustic transponder in order to find their distances to the leader. Based on their own dead-reckoned displacements, the leader's displacement and their distances to the leader, the followers update their own positions. This simulation only describes a scenario with one follower, therefore scheduling issues arising from multiple followers trying to interrogate the leader is not addressed. Another aspect of this method is that the leader vehicle is not aware of the positions of the followers. While it is applicable in a single follower scenario, this scheme does not provide a method for followers to be aware of each others positions either, as each localise with respect to the leader only and does not maintain communication between followers.

Localisation and navigation for multiple AUVs using acoustic communication

Freitag et al. (2001) proposes an improved system for multiple vehicles to use LBL transponders efficiently with passive listening and inter-vehicle acoustic communication. This work includes results of tests carried out in a shallow ocean environment using static sensor nodes and a surface

vessel mounted mobile node later replaced by a bottom crawling (surf zone crawler) unmanned vehicle. In this scenario, a designated leader vehicle interrogates an LBL transponder network and each of the other vehicles passively listens to the responses by the transponders. This is possible as the other vehicles are equipped with acoustic modems (WHOI utility acoustic modem) which utilises the same frequency band as used by the LBL transponders. The frequency shift keyed (FSK) signals emitted from the transponders are used to calculate the distances to each of the vehicles. The acoustic modems are then used to communicate the position of each of the vehicles to a surface vehicle for monitoring and coordination. The bidirectional modem communication makes it possible for an external controller to provide mission commands to the individual vehicles. Two LBL transponders with a baseline distance of 1500m, at a depth of 18m was used during the experiments. The mobile node operated at a depth of 12-18m and the bottom crawling vehicle reached depths as shallow as 1.5m. The results report an accuracy within 6m of the corresponding ground truth obtained via GPS fixes (which had an error of the same magnitude). The ranges used during the experiments were up to 2000m.

Stojanovic et al. (2002) draws upon the work presented above and presents a concurrent mapping and localisation scheme for multiple AUV operation which is based on inter-vehicle distances. This is achieved by measuring inter-vehicle delays using matched filtering which are later refined using Doppler frequency shifts when communicating with each other using acoustic modems (WHOI micro-modems). These modems utilise high rate phase shift keyed (PSK) or quadrature amplitude modulated (QAM) acoustic signals. The authors also presents a slot based communication protocol including an initialization phase such that the network can be built up dynamically. The communication process exchanges local position maps containing the positions of other vehicles in its neighbourhood as measured by the individual vehicle. This enables each vehicle to be aware of the positions of other vehicles. Since the localisation scheme suggested here is tightly coupled with the communication system whose speed and bandwidth is limited, the position update rate can be adversely affected as the number of vehicles increase. Furthermore, the refinement of distance estimation using Doppler frequency shifts is only viable when the vehicles are in motion.

A two hydrophone heading sensor for multiple AUV navigation

A two hydrophone heading sensor presented by Reeder et al. (2004) and a leader-follower navigation algorithm presented by Edwards et al. (2004) is implemented in work presented by Baker et al. (2005b) which facilitates simultaneous navigation of multiple AUVs. The presented scheme requires one designated vehicle (leader) to perform conventional LBL localisation while the others (followers) are equipped with the 'two hydrophone heading sensor' which intercepts acoustic pings emitted by the leader and each of the transponders to derive their relative heading. These are then fused with other information (known geometry of the transponders, inertial

heading of vehicle) to ascertain the position of the follower. The presented simulations with five followers assume the leader vehicle position is broadcast to the followers via a parallel acoustic communication channel. While it is purported to be a leader-follower scheme, since the presented experiments only involve one follower, the problems arising due to multiple followers not knowing each others positions are not addressed. In this scheme, as in the previously described approach, the leader vehicle is not aware of the positions of the followers.

The presented experiments involved two fixed transponders at a depth of 12m with a base distance of 146m. In the first instance the two hydrophone heading sensor, representing the follower vehicle was mounted below a surface vessel while the acoustic source (projector driven using a WHOI micro-modem) representing the leader vehicle was suspended from a tethered stationary moorage. In the second instance the acoustic source representing the leader vehicle was also mounted below a surface craft which was driven on a straight course at a velocity of 1.05ms^{-1} by a human driver. In the earlier instance the follower surface craft was driven past the stationary leader at velocities of $1.0\text{-}1.8\text{ms}^{-1}$. In each case the hydrophones and projectors were at a depth of 2m and the distances varied between 20-40m.

The authors report an acoustic source level of 183 dB (re $1\mu\text{Pa}$ @ 1 yd) using an ITC-1032 omnidirectional transducer (resonance at 32kHz) and the signal comprised of a binary phase shift keyed (BPSK) navigation ping with a carrier frequency of 26kHz and bandwidth of 4kHz with a signal duration of 7 ms. Receiving hydrophones were two omnidirectional ITC-8140 transducers (flat frequency response for 1- 40kHz) separated by a base distance of 0.457m. The received signals were sampled at 65 536Hz with a resolution of 16 bits.

During these experiments the angles were measured using cross-correlation as well as matched filtering and the results were compared. Sub-sample interpolation had been used to enhance the resolution of the bearing estimates. The maximum heading errors are reported as 4° and 9° with cross-correlation providing the greater error. The authors state that the reason for this discrepancy is unknown at the time of publication. Furthermore, it is reported that the first 100s of the experiment produced only 2 valid bearings out of 7 attempted and the next 100s produced 11 valid bearings out of 15 attempted. Overall, a precision of 10m within an area of $500\text{m} \times 500\text{m}$ is reported.

Cooperative localisation for AUVs using moving baseline navigation

Bahr and Leonard (2008) presents a method for multiple AUVs to perform cooperative localisation using WHOI micro-modems for underwater communication. The individual vehicles are meant to localise with respect to a few CNAs (Communication and Navigation Aid AUVs) equipped with sensors to obtain accurate self-localisation information. All clocks on the multiple AUVs and CNAs are assumed to be synchronised via the acoustic modems and externally

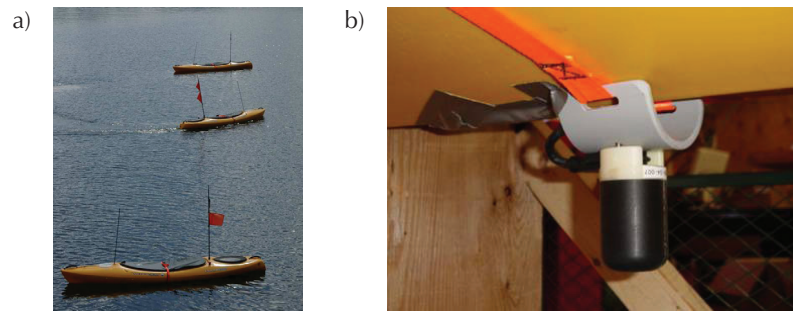


Figure 2.3: Cooperative localisation experiments using autonomous surface crafts (ASCs) with a) an image of three ASCs reproduced from work presented by Bahr and Leonard (2008) and b) an image of a WHOI micro-modem mounted to an ASC reproduced from work presented by Curcio et al. (2005b).

supplied (from GPS receivers) pulse per second (PPS) signals. The presented navigation principle is similar to the moving baseline concept described and demonstrated by Curcio et al. (2005b) where some drawbacks of conventional LBL schemes are mitigated by the use of a mobile transponder network. With each signal transmission by a CNA which includes its absolute position (longitude, latitude and depth), the listening nodes can estimate the distance between themselves and the CNA using one-way range calculations due to synchrony of clocks.

Experiments presented in this work use three autonomous kayaks - ASCs (Autonomous surface crafts) described by Curcio et al., (2005a) in place of AUVs, each equipped with a WHOI micro-modem (mounted to the bottom of the kayaks). Two are designated as CNAs with access to GPS positioning while the third operates as an AUV. The 'AUV kayak' navigates according to a pre-programmed mission using GPS way points while tracking its own position and those of the two CNAs which moved in formation to stay within range of the acoustic modems (figure 2.3). The tracked position is compared to ground truth obtained via the GPS position fixes. Since these experiments only involved one 'AUV kayak', the problem of multiple AUVs trying to localise each other had not been addressed. It can be assumed that some form of communication schedule is to be adopted in such a case where each AUV would make acoustic broadcasts of its depth and position in addition to the CNAs to allow all members of a swarm to localise each other. The authors report a maximum position update rate of 0.1Hz with regard to the localisation algorithm used during the experiments.

Experiments presented by Curcio et al. (2005b) involving three ASCs use round-trip range measurements as well as one-way range measurements using the WHOI micro-modems for localisation and navigation. Among the many experiments conducted with surface crafts emulating AUVs, a maximum range of 400m is reported while a nominal separation of 25m to 100m was maintained between vehicles. Cooperative localisation was performed with inter-vehicle communication using leader-follower and formation keeping configurations during these experiments. The authors report a nominal position error of approximately 1% compared to

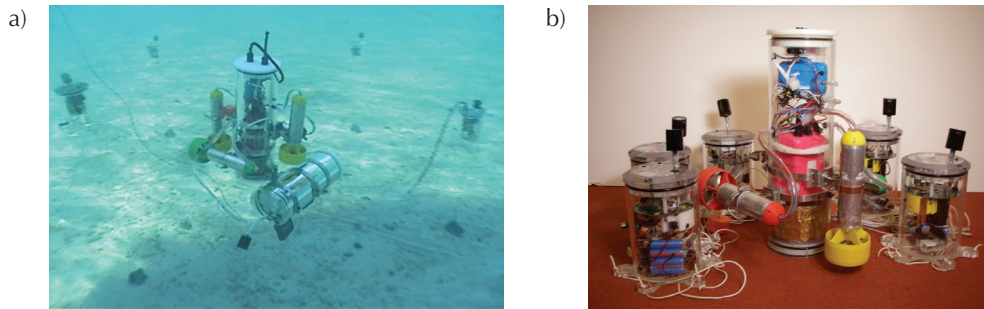


Figure 2.4: Images of the AMOUR AUV and acoustic sensor nodes a) during an underwater localisation experiment reproduced from work presented by Corke et al. (2007) and b) reproduced from work presented by Detweiler et al. (2007).

GPS ground truth while nominal range errors are around 2m according to the presented plots. While an experiment where one ASC was replaced with an Odyssey III AUV is mentioned, the localisation performance was not presented.

Navigation of multiple AUVs using synchronous clock one way travel time

The work presented by Eustice et al. (2007) uses the same synchronised clock concept described in the previous approach to estimate ranges between nodes using WHOI micro-modems. On board navigational data is broadcast by each vehicle and all receiving vehicles estimate distances between themselves and the broadcasting vehicle based on one-way travel times facilitated by synchronised clocks.

During the experiments presented in this work the node on the surface uses highly accurate GPS based clocks to maintain synchrony while the submerged nodes are equipped with temperature compensated crystal oscillator based clock sources with a drift rate of approximately 1ms per 14h. This translates to a maximum drift induced range error of 1.5m per dive which the authors claim to be similar to errors due to a conventional LBL navigation system. As with the previous cases, while the system is purported to support multiple AUV navigation, the experiments only demonstrate the localisation of one SeaBED AUV with respect to a ship (both equipped with acoustic modems) and does not address the issue of multiple AUVs localising each other. The experiments cover an area of $200\text{m} \times 200\text{m}$ and nominal position errors range from 2m to 5m according to the presented plots when compared to ground truth obtained via an LBL system.

Static sensor node networks for AUV localisation

The work presented by Corke et al. (2007) describes the use of a static underwater acoustic sensor node network which can be utilised for localisation and navigation of multiple AUVs. Unlike traditional LBL beacon networks, these nodes are equipped with acoustic modems capable of bidirectional communication. These nodes can localise each other using three methods:

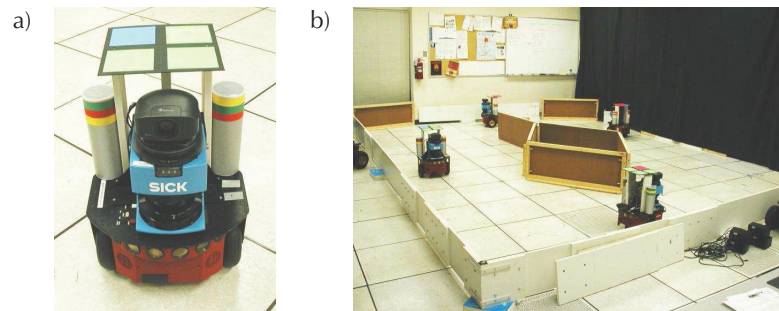


Figure 2.5: Images reproduced from work presented by Howard et al. (2003) showing a) One of the robots used in the localisation experiments equipped with a scanning laser range finder, a pan-tilt-zoom camera, a pair of retro-reflective and colour-coded fiducials, and a second colour-coded fiducial for use with the overhead tracking/ground-truth system and b) the experimental environment.

a) inter-node distance measurement with round-trip time delay when two nodes exchange messages, b) a node broadcasting a range request to which other nodes respond after specific delays allowing inter-node distance measurement with round-trip time delay and c) use of on-board synchronized clocks for nodes to ping at specified intervals allowing listening nodes to compute the distances based on differences in time of arrival of the acoustic signals. The sensor node network performs self calibration (Vasilescu et al., 2007) using a distributed localisation algorithm based on work by Moore et al. (2004) which allows the sensor nodes to be thrown overboard eliminating the need for the precise deployment and survey as in the case of conventional LBL transponders.

The authors claim these sensor networks can be used to localise multiple mobile nodes (AUVs), each equipped with similar acoustic modems, to concurrently perform localisation. However, the presented experiments involve only one mobile node (AMOUR AUV) and four static sensor nodes in one instance and one mobile node (Starbug AUV) and six static sensor nodes in the other (figure 2.4). The mobile node obtained range measurements to some of the static nodes every two seconds which results in a position update rate is 0.5 Hz. The acoustic localisation performance is compared to GPS position fixes (the AUV navigated near the surface of the water allowing it to log GPS positions) and a nominal location error of approximately 2.5 m is reported.

In-air multi-robot localisation with inter-node communication

There are many examples in the literature where relative position sensing coupled with communication channels between robots have been used to perform in-air cooperative multi-robot localisation and navigation. A few of these relative localisation methods are briefly reviewed here. Fox et al. (2000) introduces a Markov localisation technique for probabilistic multi-robot localisation in known environments (a map is available *a priori*) where position estimates are

exchanged between robots. In the physical experiments presented, two Pioneer mobile robots were used in an indoor environment. The ‘robot sensor’ used to perform relative localisation consisted of a laser range finder and a colour camera mounted on each robot. Each robot was marked with a unique colour marker which can be recognized by the vision system of the robots. Once a robot is recognized, its relative position (angle and distance) was measured using the laser range finder.

In work presented by Howard et al. (2003) Bayesian formalisms are used to perform cooperative relative localisation in multi-robot teams. The Pioneer robots used in the experiments are each equipped with a laser range finder and a camera which constitutes a ‘robot sensor’ to detect the position of a nearby robot (figure 2.5). Each robot has a unique colour coded fiducial for recognition by the vision system. As in the previous case, once another robot is detected (and recognized - using the unique fiducials, unlike the previous case) using the vision system, the laser range finder measurements are used to obtain the relative position of that robot. At each instance of localising another robot, that information is wirelessly broadcast using the user datagram protocol (UDP) such that the localisation information is shared amongst other robots.

In their work, Mourikis and Roumeliotis (2006) presents a study of various cooperative localisation algorithms used in multi-robot setups. They analyse the dependence of localisation performance of robot teams on factors such as the size of the team and accuracy of the robots’ sensors. For this analysis, they perform experiments in a rectangular arena with four Pioneer mobile robots each equipped with a laser range finder for self-localisation. Each robot is mounted with a visual marker which is used to track the position of the robots using an overhead camera based vision system. Since the robots do not have exteroceptive sensors capable of sensing the relative locations of other robots directly, these relative position measurements are synthesized using the individual robot positions tracked via the vision system. The self-localisation information is assumed to be exchanged between robots using a communication channel (the processing was performed offline). The results show that the localisation accuracy of the robot team improves when position information is exchanged between robots while performing relative localisation.

2.3.3 Position sensing by external centralised observer

A few examples of implementations where an external “God’s eye view” perspective was used to achieve relative localisation to facilitate multi-robot navigation are presented in the following sub-sections.

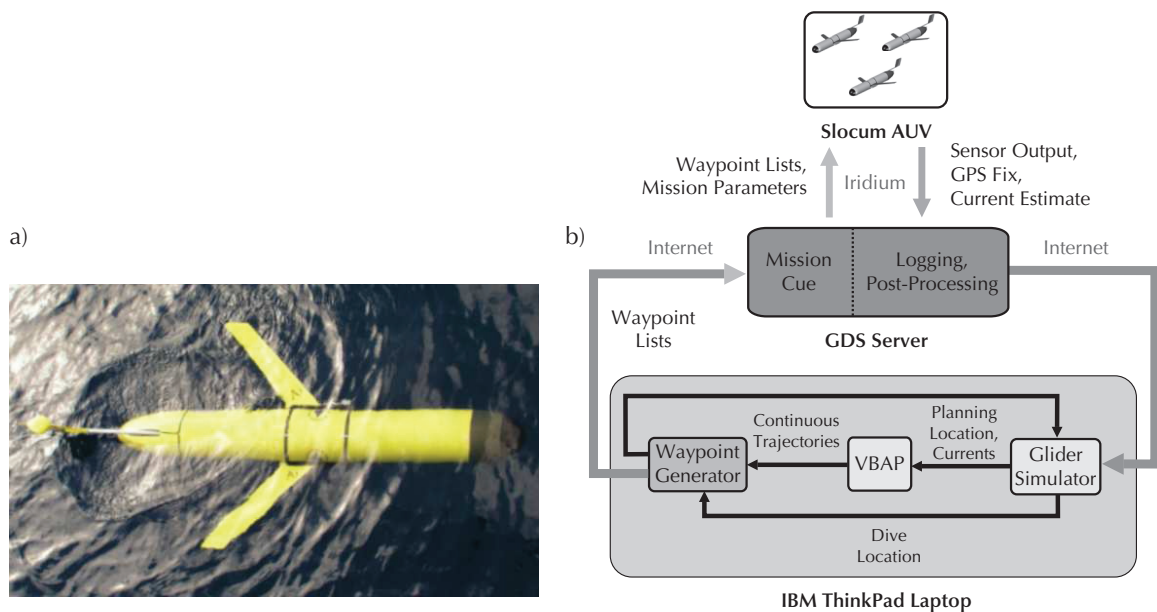


Figure 2.6: The image and diagram reproduced from work presented by Fiorelli et al. (2006) shows a) a Slocum underwater glider and b) the operational configuration and data flow of the system used to coordinate the fleet of gliders.

Coordination and control of an underwater glider fleet

Underwater gliders (Bachmayer et al., 2004) have drawn much attention in recent years for long duration wide area coverage missions due to their superior endurance compared to other AUVs. Many sea trials have been performed with these including participation in the autonomous oceanographic sampling network (AOSN) experiments (Bellingham and Zhang, 2005; Ramp et al., 2008).

Over a number of years Naomi Leonard and colleagues have developed strategies and methods for coordination and navigation of a fleet of underwater gliders for adaptive oceanographic sampling (Paley et al., 2008; Davis et al., 2008). The central concept of ‘virtual bodies and artificial potentials’ (VBAP) used for navigation of these gliders is explained by Ögren et al. (2004). In order to maintain a stable formation of the reference points (gliders) constituting the virtual body and to perform adaptive sampling based on artificial potential gradients, each vehicle needs to know the position of at least its near neighbours (Leonard et al., 2007, p.52). However, the Slocum underwater gliders do not have a facility for inter-vehicle communication, especially in the context of the large inter-vehicle distances maintained during typical glider fleet missions. The sea trial experiments presented by Fiorelli et al. (2006) involve inter-vehicle distances of 6km and 3km for three Slocum gliders attempting to maintain a formation at the vertices of an equilateral triangle. Given these large inter-vehicle distances and the slow effective speed of the gliders (0.35ms^{-1}), a relatively slow position update can be tolerated by the navigation system. During operation, each vehicle reach the ocean surface periodically (every two hours) to obtain a GPS

position fix and asynchronously transmit its position to an on-land base station via satellite phone links. The navigation coordination system located on the base station transmit waypoints back to the gliders via the same satellite phone links (figure 2.6). It must be noted that while the vehicles were operating in the underwater medium, the self-localisation (using GPS) and communication (Iridium satellite phone links) were all conducted in air. Relative positions between vehicles are measured using an external centralised system and relayed back to the vehicles. In addition, unlike other examples, this implementation does not use acoustical methods for localisation or communication.

Experiments with cooperative aerobots to simulate underwater swarms

In a novel approach, Honary et al. (2009) uses aerobots (automated blimps) to simulate a swarm of underwater robots in their experiments to test cooperative navigation algorithms. For the formation flying and cooperative area coverage missions, each member of the swarm needed position information of other members in the neighbourhood. Since the aerobots lacked an appropriate exteroceptive sensor capable of performing relative localisation, this capability was simulated using external sensors. During the experiments conducted inside a large auditorium, each of the blimps (three were used) were affixed with custom reflective markers which were tracked using a network of 12 infrared cameras. The positions of individual vehicles were then broadcast via wireless local area network. Each vehicle then derived relative positions of other swarm members using this information.

Air traffic control, take off and landing approaches of aircraft

While it is arguable if modern aircraft can be classified as ‘robots’, the role played by human air traffic controllers at airports is an example of localisation and navigation using a “God’s eye view” perspective. Even though most aircraft are equipped with sensors to detect other aircraft in the vicinity, these are meant to be used for collision avoidance rather than relative localisation. During the ‘cruising’ phase of navigation, aircraft perform self-localisation with respect to a suite of sensors ranging from precise inertial navigation systems, GPS and radio navigation beacons. However, when approaching or leaving airports where a large number of aircraft converge, localisation is usually taken over by ground based air traffic controllers. Powerful radar, radio beacons and radio communication channels are used to localise and track individual members among the ‘swarm’ of aircraft in the vicinity of most major airports. Navigation waypoints, landing approach and take off patterns are relayed back to the aircraft from the ground based control centres based on this localisation information.

2.3.4 Comparison of performance

The earlier sections gave examples of relative localisation strategies implemented in multi-robot setups with an emphasis on those operating in the underwater environment. All presented underwater implementations except one, utilise underwater acoustics for either localisation, communication or both. Despite the fact that the discussed multi-robot implementations all performed either explicit or implicit forms of position sensing of other members in the ‘swarm’, the objectives were varied. In some cases it was motivated by maintaining rigid formations, to perform cooperative localisation aiming to minimise navigation errors or to facilitate adaptive spatio-temporal sampling.

Description	Number of nodes (Type)	Used comms?	Internode distance or survey area	Position errors (Reference)
Navigation of multiple AUVs using synchronous clock one way travel time (Eustice et al., 2007)	2 (1 AUV, 1 ship)	yes	200m × 200m	~2m - 5m (LBL)
Static sensor node networks for AUV localisation (Corke et al., 2007)	5 (4 static, 1 AUV)	yes	80m × 80m	~2.5m (GPS)
Coordination and control of an underwater glider fleet (Fiorelli et al., 2006)	3 (Gliders)	yes *	3000m - 6000m	255m - 623m (GPS)
Cooperative localisation for AUVs using moving baseline navigation (Curcio et al., 2005b; Bahr and Leonard, 2008)	3 (Autonomous Kayaks)	yes	25m-100m	~1% of range (GPS)
A two hydrophone heading sensor for multiple AUV navigation (Baker et al., 2005b)	2 (1 static, 1 boat)	no**	500m × 500m	~10m (LBL)
Localisation and navigation for multiple AUVs using acoustic communication (Freitag et al., 2001; Stojanovic et al., 2002)	3 (2 static, 1 boat / surf zone crawler)	yes	up to 2000m	~6m (GPS)
Multi-frequency LBL beacon network for multiple AUV navigation (Cruz et al., 2001)	3 (2 static, 1 AUV)	no	4000m × 8000m	~5m - 10m (LBL/ Inertial)

Table 2.1: Summary of experimental setups and results extracted from the literature where the problem of simultaneous navigation of multiple AUVs was addressed. The position errors are either nominal or average errors explicitly reported by the authors or derived from the provided plots.

* Communication with external base station via satellite phone links once at the water surface.

** The proposed strategy requires inter-vehicle communication but not used during experiment.

Given the various experimental platforms, spatial scales of operation and performance metrics used by the different research groups it is extremely difficult to qualitatively compare the performance of different localisation methods and strategies against each other. Summarised experimental results extracted from the literature (where available) associated with seven of the ‘real-world’ underwater multi-robot implementations discussed earlier are tabulated in table 2.1 in reverse chronological order. While each method attempt to address the problem of simultaneous navigation of multiple AUVs, it must be noted that most of these strategies are highly specialised and specifically adapted to the experimental platforms and the application. Therefore, attempting to derive an overall performance ranking is not realistic.

2.4 Sensor utilisation strategies for localisation

Configuration of localisation sensors as well as processing techniques have been extensively studied in fields of target motion analysis (active and passive detection/tracking), acoustic source localisation (ASL) and wireless sensor network research. Additionally, it also has overlap in the field of wireless communication with regard to receiver/transmitter configuration and processing. The following sections give brief overviews of techniques which have relevance to the problem of relative localisation in multi-robot setups.

Multiple Input Multiple Output (MIMO) methods

In most cases, any system which involves multiple receivers and multiple transmitters can be classified as a MIMO system while in some cases the specific signal processing strategy involving multiple inputs and outputs is a pre-requisite for a system to be identified as a MIMO system. In wireless communication systems, use of multiple receiver and transmitter antennae had led to remarkable improvements in overcoming problems caused by multipath propagation, interference and behaviour of time-varying channel characteristics such as fading. Instead of treating it as a problem, multipath propagation is in fact exploited by MIMO techniques to improve reliability and throughput of the communication channels without any further increase of channel bandwidth or transmission power (Gesbert et al., 2000; Goldsmith et al., 2003). These aspects such as channel reliability and capacity which attract a lot of attention in wireless communication research is of limited relevance for localisation. However, researchers in the field of acoustic source localisation have adopted some MIMO strategies to implement target tracking in noisy reverberant environments (Huang et al., 2006; Fallon and Godsill, 2008).

Time delay estimation is essential in a number of signal processing techniques used for source localisation where two or more input channels are involved. The methods used by many researchers can be classified as adaptations of the generalised cross-correlation (GCC) approach introduced by Knapp and Carter (1976). However, these methods have limitations when applied

in the presence of multipath arrivals in highly reverberant environments. Influenced by MIMO techniques, the adaptive eigenvalue decomposition (AED) approach proposed by Benesty (2000) makes use of the additional information presented by multipath arrivals to perform passive acoustic source localisation. These techniques have been used in applications such as acoustic echo cancellation, time delay estimation, cross-talk cancellation and speech de-reverberation as described by the extensive survey presented by Huang et al. (2006).

Another area which benefits from MIMO techniques is when multiple source signals need to be separated from a mixture without explicit knowledge about the source signals, which is referred to as blind source separation (BSS). This is used in areas such as multiple speaker tracking and speech recovery using at least as many microphones as the number of sources to be separated. Buchner et al. (2005) presents an approach for simultaneous estimation of multiple time difference of arrivals (TDOAs) based on blind adaptive MIMO filtering using a microphone array to track multiple speakers in a reverberant environment. Lombard et al. (2008) presents experimental evaluation of a BSS-based real-time demonstrator for the localisation of two sound sources using MIMO processing. The authors report that the system is capable of accurately localising two speech sources in two dimensional space within a few seconds and with a precision better than one degree. The experimental implementation which used four microphones (two pairs) did not rely on any prior knowledge of the source positions.

Beamforming methods using sensor arrays

Beamforming with receiver arrays (usually three or more sensors) is used in sonar detection, source localisation and target tracking to improve performance. Time domain beamforming is achieved by setting delays and gain factors for each of the array elements appropriately such that a larger more sensitive sensor can be simulated using multiple smaller less sensitive sensors. In frequency domain beamforming, the received signals are separated in to different frequencies using a fast Fourier transform (FFT) either across time or across different array elements and gain factors are set to each separated frequency¹. Additionally, by dynamically changing the delays and gain factors, the 'beam' can be steered in an arbitrary direction. Adaptive beamforming strategies are used in localisation where the beam is dynamically steered to point to the signal source to maximise the signal to noise ratio. These techniques are also used to locate and track multiple simultaneous signal sources. Chen et al. (2003) demonstrates such methods in acoustic source localisation. Valin et al. (2004) presents an experimental evaluation of a mobile robot mounted frequency-domain steered beamformer approach capable of localising up to two simultaneous moving sound sources using an array of eight microphones.

¹. See Van Veen and Buckley (1988) for an in-depth description of beamforming techniques.

Applicability of MIMO and beamforming techniques

As mentioned before, advantages presented by MIMO processing techniques such as improvement in channel reliability and capacity are of interest for communication applications but not necessarily for localisation. However performance gains are demonstrated in acoustic source localisation applications with regard to multiple source tracking and speech separation in reverberant environments when MIMO techniques are applied. The approach used in this thesis to address the localisation problem stated in chapter 1 differs from these applications as explained below.

The use of broadband source signal pings with known statistical properties and relatively short durations can mitigate detrimental effects caused by delayed multipath arrivals when operating in reverberant environments. For localisation purposes, the direct path arrival of the source signal ping is sufficient and this can be recovered using time-domain channel windowing coupled with cross-correlation and matched filtering techniques. However, since the duration of the signal can be considered continuous in speaker tracking and speech separation applications, multipath arrivals can cause echoes and interference. Channel windowing techniques can still be used for source tracking but not in the context of speech recovery as the source signal needs to be recovered in its entirety.

Both in MIMO processing and beamforming techniques, for accurate simultaneous localisation of multiple signal sources a relatively large number of receivers need to be used. The approach used in this thesis minimises the chance of multiple sources from emitting pings simultaneously¹ within the range of a receiver. This is achieved by a) temporally separating the multiple pings emitted by a single vehicle, b) exploiting time division multiple access (TDMA) scheduling within a local neighbourhood and c) implicitly synchronised signal transmission across the swarm². Under these circumstances, the utility of a technique for simultaneous localisation of multiple sources becomes redundant. Additionally, the approach presented in this thesis aims to perform localisation with minimum possible hardware, space, power and processing requirements. In this context, while MIMO and beamforming techniques might well achieve the same localisation performance, the additional processing and sensors required for the effective implementation of these methods place a strain on limited resources available on the small Serafina class AUVs.

In summary, the strong points of MIMO and beamforming techniques are a) being able to accurately localise and extract continuous signal sources in reverberant environments and b) being able to effectively separate multiple simultaneous signal sources. In order to realise the full

¹ Handling of such occurrences is addressed in section 5.3 of chapter 5.

² The relationship between the localisation system and the scheduling system is discussed in section 5.2 of chapter 5. See work by Schill (2007) for an in depth explanation of the communication scheduling system developed for Serafina class AUV swarms.

potential of these techniques, it is desirable to have spatially distributed arrays with many sensor elements. Since a) and b) stated above are not high priority requirements of the approach used in this thesis to address the localisation problem, the additional hardware, space, power and processing requirements imposed by MIMO and beamforming techniques are difficult to justify.

2.5 Discussion

Localisation is an integral part of mobile robot navigation regardless of the operating environment. Due to the non-availability and limitations of sensor modalities, robots operating in the underwater environment face a number of obstacles as discussed by Leonard et al. (1998) and Loebis et al. (2002). Unlike in operation of a single AUV, the multi-robot paradigm presents many additional challenges for localisation and navigation along with the bounty of new applications it makes possible. Smith et al. (1998) identifies navigation, synchronisation techniques and logistics as key problems in realising the full potential of multiple AUV missions for synoptic and pseudosynoptic data collection.

LBL navigation

It was established in the previous chapter that each member of a multi-robot setup having access to position information of at least their near neighbours is a minimal requirement for the successful operation of a swarm or a formation. In principle, it is possible for multiple AUVs to be deployed with pre-programmed navigation waypoints to conduct 'formation flying' with only self-localisation information obtained via LBL beacon networks without relative position awareness or inter-vehicle communication. However, this approach precludes many of the synergistic benefits championed by the swarm robotics research community and cannot be used for applications such as adaptive oceanographic sampling (Martins et al., 2003; Bhatta et al., 2005). The strategy used in many in-air applications had been to establish communication links between the vehicles to exchange absolute position information which is then used to derive relative position of other members of the swarm. In the face of limitations in speed and bandwidth of underwater communication channels, this strategy has had limited success when applied to multiple AUV navigation. The other problem of LBL navigation is that the operational area is limited to a pre-instrumented segment of the ocean. While USBL navigation provides independence of pre-deployed beacon networks, this method imposes harsher limits on maximum transponder-vehicle distances (Smith and Kronen, 1997). In both cases (LBL and USBL navigation) beacons need to be individually interrogated by each vehicle to update its own position causing the position update rate to decrease as the number of vehicles increase. As Eustice et al. (2007) points out, this limits LBL and USBL navigation to multi-robot groups of only few members.

Underwater acoustic modems with ranging capability

In the backdrop of the circumstances mentioned above, the WHOI micro-modem for underwater acoustic communication and navigation and its availability as an ‘off the shelf’ package was considered a significant innovation and the oceanographic community had been quick to adopt this technology. Despite its relatively low data rate of 80bps, the use of frequency hopping FSK (Frequency Shift Keying) modulation technology provide reliable communication links up to about 4km even in shallow water environments with multipath propagation. In addition to providing a communication link, the micro-modem has the capability of supporting LBL type navigation by acting as a transponder and up to four vehicles can share the acoustic navigation beacons, by using different broadband interrogation codes. The modem network protocol also supports up to 15 nodes to facilitate underwater acoustic networks (Freitag et al., 2005). Another feature which had been exploited for localisation is the ability to do ranging between modem nodes using round-trip travel time or one-way travel time when externally provided pulse per second (PPS) reference clock signals are available. Apart from the examples described in earlier sections (Curcio et al., 2005b; Eustice et al., 2007; Bahr and Leonard, 2008) a number of additional underwater acoustic navigation applications demonstrating the versatility of the WHOI micro-modem are given by Singh et al. (2006). With the availability of inter-vehicle communication channels and flexible and versatile transponder beacons which can easily be mounted on AUVs or ASCs (autonomous surface crafts) such as the MIT SCOUT, the concept of ‘moving long baseline’ (MLBL) navigation for multiple AUVs have been proposed (Vaganay et al., 2004; Curcio et al., 2005a).

Building on the success of the WHOI micro-modem, novel underwater acoustic sensor nodes with modem and ranging capability have been developed and presented by Vasilescu et al. (2007). This implementation also uses FSK modulation and reports a data rate of 300bps verified up to 300 m in freshwater and ocean environments. These nodes also support a time division multiple access (TDMA) scheduling protocol which can be used to perform self-synchronisation and self-calibration of the network. Given their small size and versatility, as proposed in work presented by Corke et al. (2007), these sensor node networks can be used to facilitate localisation for multi-vehicle AUV missions.

Moving away from the ‘self-localise and communicate’ strategy for relative localisation, the ranging capability of acoustic modems and the possibility to mount these modems on AUVs makes other cooperative localisation approaches possible. These methods based on sensor node localisation research presented by Moore et al. (2004) attempts to directly measure distances to others vehicles without relying on beacons or anchor nodes. Proposed multi-AUV localisation strategies reviewed previously (Bahr and Leonard, 2008; Corke et al., 2007) are hybrid approaches which use relative range measurements, self-localisation with respect to beacons (static sensor nodes or

mobile CNAs) and communication channels to propagate position information among other members in the group. A fully decentralised ‘real-world’ implementation of an AUV swarm (more than two AUVs instead of leader-follower schemes) is yet to be deployed at the time of writing as the references in the current literature all point to either software simulations or hardware simulations using maximally two AUVs and additional surface crafts.

Localisation for small agile AUVs in dynamic unstructured environments

To facilitate the swarming paradigm, the rate at which relative position information needs to be updated depends on the application and the robotic platforms being used. For larger inter-vehicle distances and slower vehicle speeds the position update rate can afford to be relatively low¹ while on the other hand, a swarm consisting of agile vehicles operating in highly dynamic and unstructured environments with relatively short inter-vehicle distances would require a much higher position update rate for successful operation. The Serafina class AUVs (Serafina website, 2009) are highly agile² with their small size and five thruster actuation compared to both traditional AUVs of ‘torpedo style’ and ‘crate style’³ designs. They are less than half the length of the Starbug AUVs which are similarly actuated (Dunbabin et al., 2004). This unique design, the level of agility and small size will allow the Serafina AUVs to be deployed in large dense swarms with relatively short inter-vehicle distances (up to 20m) operating in dynamic and unstructured environments. This is an unprecedented prospect in underwater robotics and opens up many application possibilities in scales which were previously infeasible. Since fast and reliable communication links are essential for the operation of a swarm of Serafina AUVs as described above, a specialised short range inter-vehicle communication system using a 122880Hz long-wave radio carrier signal with a maximum data rate of 8192bps have been developed and tested (Schill, 2007, pp. 66-69). The projected range of this system is up to 30m (at full drive voltage) while the current state of experimentation verifies ranges of over 15m. Due to the small size of the AUVs, available space inside the hull is extremely limited. This precludes possibilities of using existing acoustic modem technology. Moreover, the data rate achievable by the long-wave radio communication system is far superior than those provided by state of the art underwater acoustic modems. As further elaborated by Schill (2007), the communication system is reinforced with fully decentralised spatially distributed TDMA routing schedules which allow dynamic re-configuration, addition and deletion of communication nodes. The two ‘flavours’ of scheduling regimes enforced by the **distributed dynamical omnicast routing** (DDOR)

¹. E.g. for underwater glider fleets with large inter-vehicle distances of 3km to 6km and low effective speeds 0.35ms^{-1} , a relatively slow position update rate of once every 2 hours can be tolerated (Fiorelli et al., 2006).

². Serafina class AUVs are 50cm in length, 10cm in diameter with a maximum forward speed of 1.5ms^{-1} and roll, pitch and yaw rates of 360°s^{-1} , 180°s^{-1} and 90°s^{-1} respectively.

³. REMUS class AUVs (Allen et al., 2000) are examples of ‘torpedo style’ design while Kambara and Oberon AUVs are examples of ‘crate style’ designs (Wettergreen et al., 1999; Williams et al., 2001a).

algorithm (Schill and Zimmer, 2006b) and the **pruned distributed omnicast routing** (PDOR) algorithm (Schill and Zimmer, 2007) are both fully scalable and places no upper bounds to the number of participating swarm members. By facilitating simultaneous broadcasts within spatially distributed local neighbourhoods, these routing schedules implement ‘every node to every node’ (omnicast) communication within the swarm in a fast and efficient manner within one scheduling run.

Despite the availability of a fast and reliable communication system, the problem of relative localisation was not yet addressed for the realisation of a swarm of Serafina AUVs. With shorter inter-vehicle distances and small fast moving members, the accuracy and update rate requirements placed on the localisation system is high. Self-localisation methods such as individually interrogating transponder beacons was not possible due to limitations imposed on update rates by swarm size when using such methodologies as elucidated earlier. Inter-vehicle ranging methods such as those used by applications using state of the art underwater acoustic modems offer certain possibilities in this regard. Nevertheless, in the absence of externally supplied precise reference clock signals and synchronised clocks on all swarm members, these methods have to rely on round-trip travel time for range measurement. This feature coupled with the space constraints within the Serafina AUVs mentioned earlier makes this solution undesirable for the problem at hand¹.

The relative localisation system

‘Robot sensors’ or ‘localisation sensors’ such as those mentioned in the literature (Fox et al., 2000; Rekleitis, 2003; Howard et al., 2003) with regard to land based multi-robot setups which provides relative estimates for range (distance), azimuth (bearing) and heading (rotation) of another robot based on observation and sensing does not have equivalents in underwater robotics. The nearest related work in this regard is the two hydrophone heading sensor proposed and tested by Baker et al. (2005b) but fails to deliver a fully decentralised and accurate position estimation methodology.

The research presented in this thesis addresses the problem of designing, developing and evaluating a fully decentralised relative localisation system comprising of a ‘localisation sensor’ capable of producing relative estimates for range, azimuth and heading of other nodes aimed at facilitating swarming of small and agile Serafina class AUVs. Drawing insights from strengths and weaknesses of underwater localisation methods referred earlier, the proposed strategy exploits the available communication scheduling system developed by Schill (2007). While they communicate, the vehicles synchronously sends out short acoustic pings with long-wave radio broadcasts

¹ *In the future, maturity of technology and miniaturization coupled with availability of precise clocks, this method might be a feasible alternative.*

within a local neighbourhood. In addition to measuring the azimuth of the acoustic source using hyperbolic techniques, the rest of the members of the neighbourhood can each measure ranges to the sender using the arrival time difference between the electromagnetic and acoustic signals using matched filtering techniques. By sequentially sending two acoustic pings from the two ends of each vehicle, it also enables the observers to measure the relative heading of the sender. Additionally, the sensor geometry used in the implementation allows for additional ‘reverse hyperbolic’ techniques to be used to derive alternate heading and range estimates which do not rely on the synchrony provided by the communication and scheduling system. This adds redundancy to the position estimation thus improving reliability.

The availability of such a low level ‘localisation sensor’ makes it possible to explore the abundant swarm robotics literature to find many candidate high level cooperative navigation and localisation strategies that have been developed and studied over the years which assumes the availability of such sensors. In addition, using the communication system to exchange the relative localisation system leads to each swarm member being aware of positions of all other swarm members (at least within the local neighbourhood). Not only does this facilitate a platform for robust swarming applications, it also improves overall localisation accuracy as evident from studies presented in available literature (Mourikis and Roumeliotis, 2006; Pugh and Martinoli, 2006). Moreover, by using the communication channel to broadcast depth measurements derived from on-board pressure sensors with each acoustic sending event, the observing submersibles can all calculate relative depth information based on their own pressure sensor reading and incorporate this information with the 2-dimensional position given by the acoustic localisation system to estimate the 3-dimensional position of the sending submersible. This approach has been extensively used to derive 3-dimensional position information by reducing the underwater localisation problem to 2-dimensions (Bellingham et al., 1992; Vaganay et al, 2000; Baccou et al., 2001; Cheng et al., 2008; Bahr and Leonard, 2008).

The next few chapters give in-depth descriptions of the enabling technologies and methodology used to develop the relative localisation system. This is followed by experimental evaluations and performance analyses of the setup to discern its suitability to address the stated problem of facilitating swarming of small agile autonomous submersibles with an accurate, precise and robust localisation system that scales up with increasing swarm size and independent of pre-deployed beacon networks.

Chapter 3

Source signals

This chapter describes the time-domain cross-correlation used by the relative localisation system as well as the motivation behind the choice of maximum length sequences (MLS) as the source signal. Several classes of signals are considered and their performance is experimentally evaluated against the required characteristics of the source signal to be used in an underwater acoustic localisation system. The main criteria are the cross-correlation peak detection performance and interference robustness when used in noisy, reverberant environments. In addition, the effects of uncorrelated additive white noise, mixing of multiple MLS signals as well as detrimental effects of non-linear transducers on the transmitted MLS signal's spectral properties are also discussed in the subsequent sections. An empirical method for overcoming the frequency filtering introduced by the transducer to improve the cross-correlation performance is presented as well.

3.1 Full-range cross-correlation of time-domain signals

In the relative localisation system presented in this thesis, cross-correlation is used as the main tool for extracting delays between signal channels. The usual approach suggested in the literature involves the generalised cross-correlation (GCC) or its variations first suggested by Knapp and

Carter (1976). Applications of this method including the work done by Carter (1981) and Piersol (1981) is based on performing the cross-correlation in the frequency domain, i.e, using the Fourier transforms of the original time-domain signals to produce a cross-power spectrum. Arguments supporting this approach include lower processing complexity and being able to achieve a narrow peak in the resulting cross-correlogram by applying appropriate pre-filters for the signals. The latter requires *a priori* knowledge about the signal characteristics to properly apply the pre-filters, which otherwise would make the delay estimation system susceptible to external noise.

In this research, cross-correlation of signals is performed in the time-domain. With relatively short duration signals (as explained in the next section), the issue of computational complexity does not arise and the narrowness of the cross-correlogram peak is maintained by the characteristics of the source signal being used and compensating for the transducer effects.

For two finite, discrete sequences $s_1(n)$ and $s_2(n)$ of length N (with $s_1(n) = s_2(n) = 0$ for $n < 0$ and $n \geq N$) the cross-correlation can be expressed as:

$$R_{s_1s_2}(\tau) = \sum_{n=i}^{N-|k|-1} s_1(n)s_2(n-\tau) \quad (3.1)$$

where $i = \tau$, $k = 0$ for $\tau \geq 0$, and $i = 0$, $k = \tau$ for $\tau < 0$. The auto-correlation of the sequence $s_1(n)$ can be derived by setting $s_2(n) = s_1(n)$ in the above formula (Burdic, 1984; Proakis and Manolakis, 1996).

By using the relationship:

$$R_{s_1s_2}(\tau) = R_{s_2s_1}(-\tau) \quad (3.2)$$

negative lags can be measured as well. Considering signed lags instead of an absolute value helps to avoid the *left-right ambiguity* otherwise encountered in TDOA based source localisation. Combining cross-correlations for both positive and negative lags, a full-range cross-correlation function can be constructed, which represents all possible delays between the two sequences. For the localisation system, the sequences consist of discrete samples of the acoustic signals output by the analogue to digital converter. These **sample-domain** signal lags can be easily converted to the **time-domain** by considering the sampling frequency of the converter (f_s) and the **spatial-domain**¹ by considering both the sampling frequency and propagation speed of the signal (v). The quantity τ_0 which maximises $R_{s_1s_2}(\tau)$ corresponds to the delay between the two signals. The resolution of τ_0 depends on the characteristics of the signal waveform being used, as explained in the following sections.

¹. The distance travelled by a wavefront of the signal during the delay period.

3.2 Choice of signal waveform

In acoustic source localisation, it is preferable to avoid pure tone periodic signals since the TDOA can only be unambiguously estimated for frequencies whose wavelengths are at least twice the base distance of the receivers. Therefore, for a base distance of 0.3 m used by the proposed system explained in chapter 4.4.3, the frequency needs to be 2500 Hz or lower. Cross-correlation of such signals results in a wide peak in the cross-correlogram causing the delay estimates to have a lower resolution. In addition, due to frequency dependent fading effects caused by multipath propagation (Sozer et al., 2000; Kilfoyle and Baggeroer, 2000) encountered in underwater acoustics, the signals of choice for localisation applications have been mostly non-periodic and broadband.

For the localisation application presented in this thesis, the primary requirement of the source signal is to provide a unique narrow peak in the cross-correlogram. The secondary requirements are to provide a high signal-to-noise ratio (SNR) when used in noisy environments¹ (*i.e.* robustness against interference) and to maintain a broad frequency spectrum to counter the fading effects of the underwater channel. While a ‘flat’ frequency spectrum is highly desirable, it is extremely difficult to find transducers that faithfully reproduce such a response.

Based on prior research in the fields of acoustical localisation in air (Girod et al., 2006), sonar signal processing (Nielsen, 1991; Waite, 2002) and room acoustics (Bradley, 1996), three broad classes of signal waveforms were identified as chirps, pseudo-noise and linear feedback shift register sequences. Samples from each of those classes were evaluated against the performance criteria mentioned above and compared.

3.2.1 Chirps, pseudo-noise and shift-register sequences

Sine sweeps or ‘chirps’ are signals where the base frequency is changed with time. The rate of change in frequency is referred to as the ‘chirp rate’ where linear (linear frequency modulated - LFM) and logarithmic chirp rates are commonly used to synthesise source signals. These signals are popular in sonar and radar applications where the reflected signal is utilised for localisation of a target rather than localising the sound source itself (Ma and Goh, 2006). Studies have revealed that bats use ‘down sweeps’, among other waveform structures, for precise echolocation of prey (Neuweiler, 2003). Sine sweeps with logarithmically increasing chirp rates are considered to be better suited for moving target detection as they behave more gracefully with the introduced doppler shifts in frequency. In addition, sine sweeps with arbitrary bandwidths can be synthesised to match the operational bandwidth of the transducers used.

¹. Noise in this context includes ambient background noise, stray impulsive signals emitted from nearby sources as well as reflections of the main signal when used in reverberant, cluttered environments.

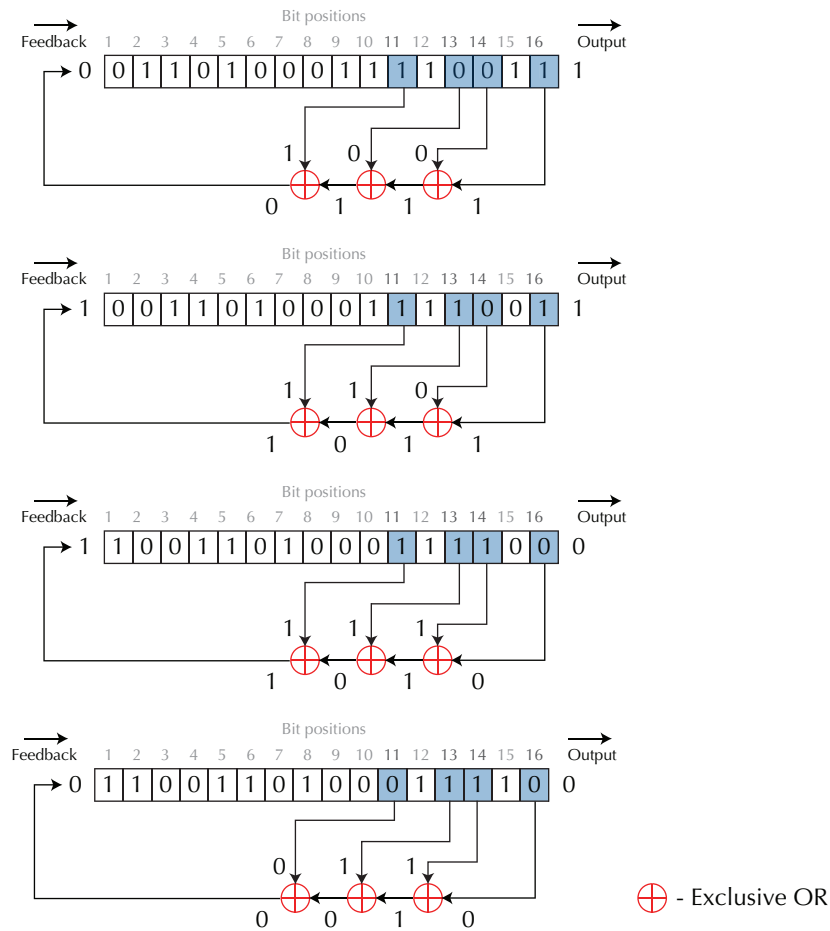


Figure 3.1: Generation of a linear feedback shift register sequence adapted from Aguirre and Kerr (2009) is depicted above (some errors in the third iteration had been corrected). The bit positions of ‘taps’ in the shift register corresponds to the exponents of the primitive polynomial $x^{16} + x^{14} + x^{13} + x^{11} + 1$.

Pseudo-noise consists of a wide variety of broadband signals which have a quasi-flat frequency spectrum however without a deterministic progression of frequency as in chirps. ‘White noise’ referred to in many theoretical analyses, falls under this category as well. These signals are generated based on a random number sequence. The broadband qualities of the signal depends on the quality of the pseudo-random generator used. Pseudo-noise signals can either be uniform, or binary. Normalised uniform signals are generated with a pseudo-random sequence of uniformly distributed real numbers in the range 0 (or -1) to 1 while a normalised binary signal can be generated with the same pseudo-random sequence with an additional function which outputs 0 (or -1) and 1 depending on the random number being less than or greater than 0.5 (or being negative or positive). Unlike chirp signals, pseudo-noise signals do not display gradual phase transitions.

The third class of signals, linear feedback shift register sequences based signals have identical spectral properties to pseudo-noise signals but also have a number of desirable statistical

properties including being deterministic sequences and the possibility to generate multiple unique sequences of the same length having identical spectral properties but with minimal correlation between the sequences (Golomb, 1982; Golomb and Gong, 2004). These sequences and signals are widely used in applications such as cryptography and digital communication systems. A polynomial over the Galois Field $GF(2)$ can be used with a linear feedback shift register as shown in figure 3.1 to generate a binary sequence. When the generating polynomial (such as $x^{16} + x^{14} + x^{13} + x^{11} + 1$ used in the example is figure 3.1) is primitive, the class of generated sequences are known as *maximum length sequences* (MLS) or *m-sequences* and they contain every possible sequence which can be produced by the shift register (Peterson and Weldon, 1972; Cohn and Lempel, 1977). Further description of properties and characteristics of MLS signals is given in section 3.2.2.

Experimental evaluation of different signal waveforms

In order to compare the cross-correlation performance under ‘real’ conditions, sample signals of five different types were transmitted and received using actual transducers (same **projectors** and **hydrophones** used in the experimental evaluation of the relative localisation system) in an enclosed reverberant underwater environment¹. Each of the signals (1.3ms in duration - 127 samples, sampled at 96 000Hz) were repeated 25 times at 5.0Hz. The signal amplitudes of all source signals were normalised such that the transmission power was equivalent for each type. The compared source signals were:

- An MLS signal of length 127.
- A chirp with an up sweep of 750 - 48 000Hz with a logarithmic chirp rate².
- A chirp with an up sweep of 750 - 48 000Hz with a linear chirp rate.
- A pseudo-noise signal based on the MT19937 pseudo-random generator³.
- A uniform pseudo-noise signal based on the MT19937 pseudo-random generator.

MLS	Chirp (Logarithmic)	Chirp (Linear)	Pseudo-noise	Pseudo-noise (uniform)
34.03dB	29.71dB	32.27dB	34.02dB	30.64dB

Table 3.1: Average signal to noise ratios of the different source signals used for cross-correlation as illustrated in figure 3.3.

¹ Cylindrical tank with corrugated metal walls filled with tap water. Diameter 4.2m, depth 1.5m.

² Due to the length of the signal and the sampling rate used, the lowest and highest producible frequencies are 750Hz and 48 000Hz.

³ Implementation of the Mersenne Twister pseudo-random generator are given by Hoe (2002) and Matsumoto (2007) while the theory behind the implementation is given by Matsumoto and Nishimura (1998).

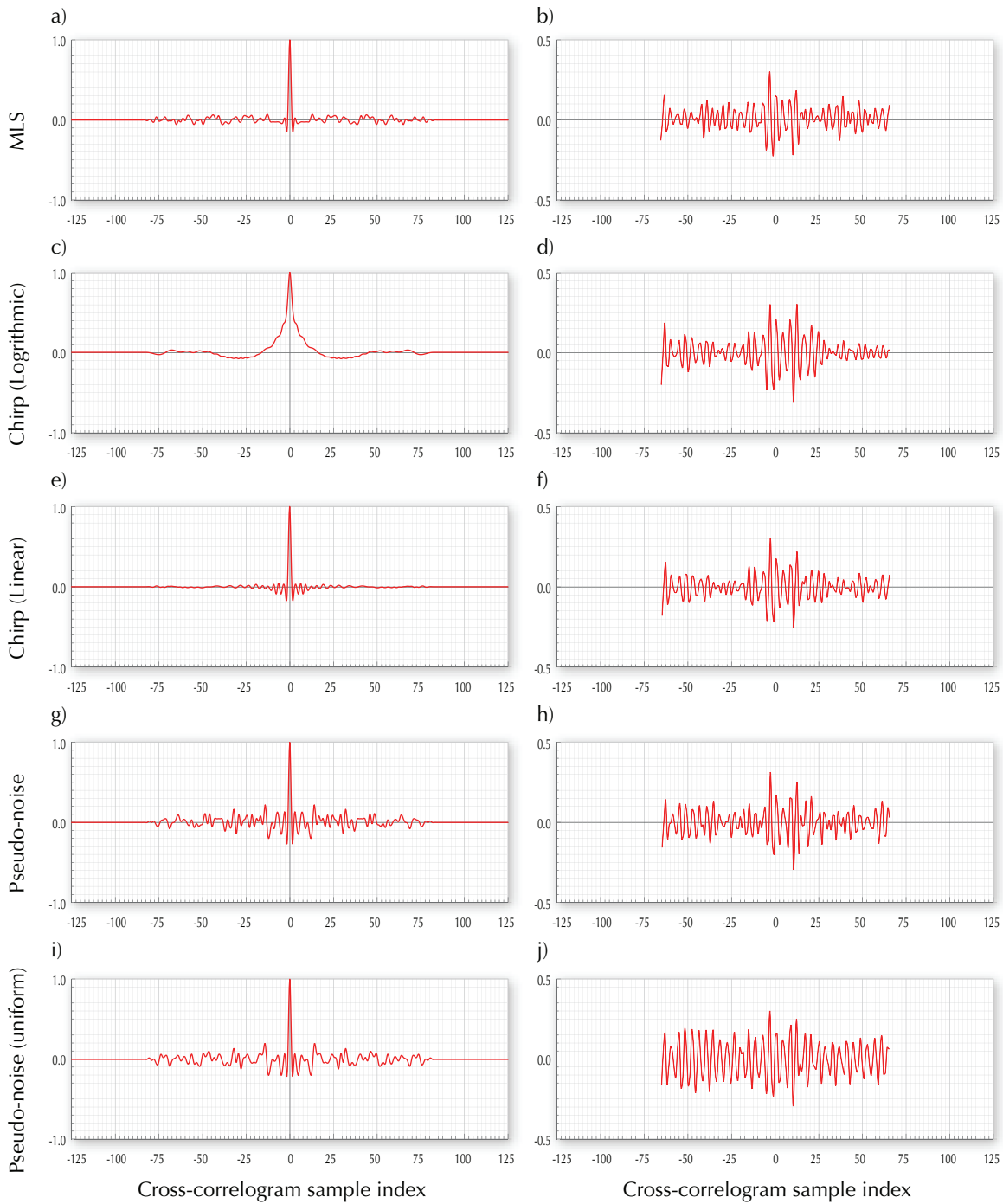


Figure 3.2: The left column shows the auto-correlograms of the five evaluated source signals while the right column shows the cross-correlograms of the experimentally recorded versions of the same signals. The y -axes of these plots represent normalised amplitude.

The signal source was placed 2.0 m away from a pair of receivers and the received signal channels were cross-correlated in the time-domain as described in section 3.1. To compare the ‘real’ and ideal performances, representative cross-correlograms of each of the different experimentally recorded signals are given alongside the auto-correlograms of the source signals in figure 3.2. Due

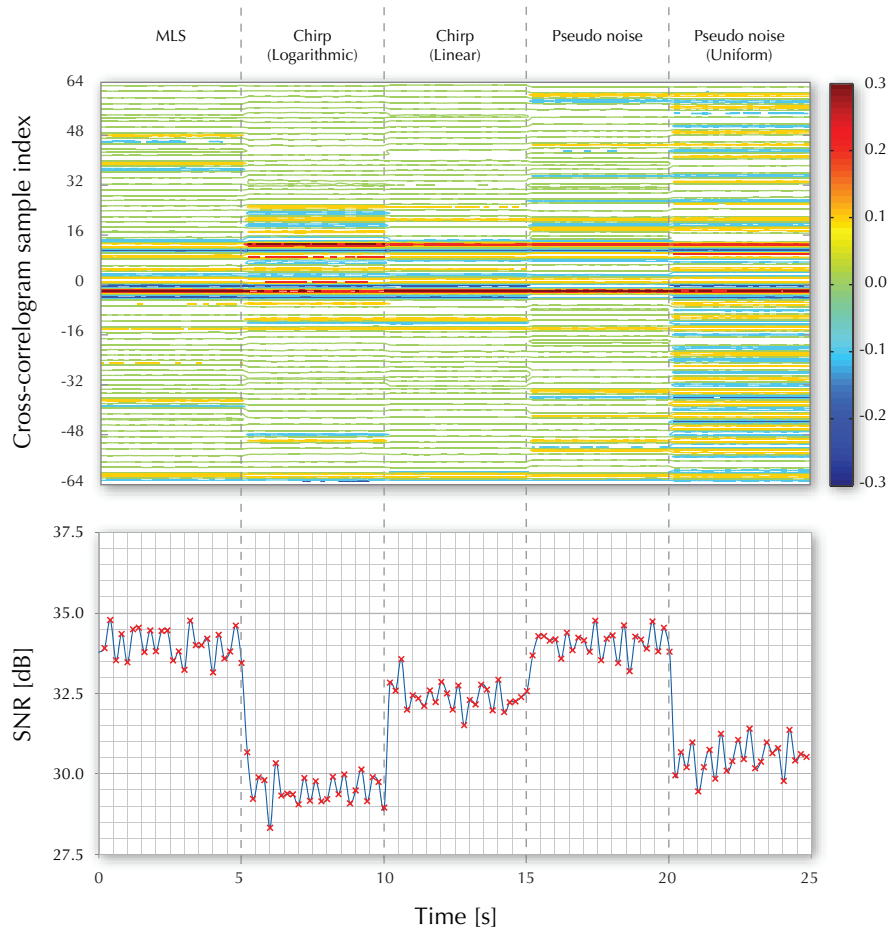


Figure 3.3: Contour plot of the 125 cross-correlograms with colours representing peak heights shown on top with the measured SNR for each of the corresponding signals.

to the placement of the source signal relative to the receivers, cross-correlations of the experimentally recorded signals have a peak in the vicinity of -3 samples. Figure 3.3 shows the contour plots of all 125 cross-correlograms (25 each for the five source signal types) along with the measured signal-to-noise ratio (SNR)¹. The average SNR for each signal type is given in table 3.1. By inspecting the auto-correlation of the different signals shown in figure 3.2, the linear chirp appears to have the most unique peak with side-lobe peak amplitudes at a minimum while the logarithmic chirp has the widest peak. The side-lobe peak amplitudes of the two pseudo-noise signals are comparatively higher than those of the MLS signal. Observing the performance of the experimentally recorded signals, it is apparent that each of them were severely affected by reflected signals which are represented by the many significant side-lobe peaks present in the cross-correlogram. The most prominent secondary peak near the vicinity of $+12$ samples correspond to the bottom reflected signal received on one channel, according to the experimental

¹. The methods used for SNR measurement is explained in section 6.6.

configuration of the transducers within the test tank. When considering the cross-correlation peak detection performance as well as the delivered SNR, MLS signals appeared to perform better than the other compared signals.

3.2.2 Maximum Length Sequences

As mentioned earlier, an MLS is a pseudo-random binary sequence. The statistical properties of these sequences which were first introduced by Golomb (1982) in his first edition published in 1967 have been widely studied since then (Peterson and Weldon, 1972; Cohn and Lempel, 1977; Dunn and Hawksford, 1993; Vanderkooy, 1994). The most attractive of its properties is its auto-correlation function which is essentially a *Dirac delta function* (single sharp peak at zero-shift). Some additional properties of these sequences as given by Aguirre and Kerr (2009) are:

- The number of '0's in the sequence is one less than the number of '1's (balance property)
- For any q which is relatively prime to N , if you choose every q^{th} element in an MLS until the length of the new sequence is N , the resulting sequence is also an MLS.
- Another MLS can also be created by adding a shifted version of the original sequence to the original sequence.

Acoustically transmitted MLS signals (instead of '0's and '1's, these signals consist of -1 and $+1$) are widely used in fields such as room acoustics to measure the impulse response of linear systems without actually using impulsive signal sources (Borish and Angell, 1983; Bradley, 1996). Farina (1998) presents an experimental study of using MLS signals instead of impulsive sources for underwater bottom profiling and concludes that the MLS approach yields a higher SNR and better spatial resolution compared to conventional methods.

While behaving similarly to band-limited white noise in the frequency domain with a *quasi-flat* spectrum up to the Nyquist frequency, MLS signals have the additional advantage of being fully deterministic which makes them accurately reproducible and the ability to have multiple unique signals with the same spectral properties with guaranteed minimal cross-correlation amongst them. These properties combined with the experimental performance mentioned in the previous section makes MLS signals an ideal candidate for the source signal to be used in the relative localisation system presented in this thesis.

There exists many standard algorithms for the generation of MLSs by using generating polynomials with different degrees which result in MLS signal sets of different lengths. The degree n of the generating polynomial, which is also the length of the shift register (also known as the degree of the MLS signal) governs the length l_{MLS} of the sequence as:

$$l_{MLS} = 2^n - 1 \quad (3.3)$$

The length of the sequence and the employed sampling rate of the analogue to digital converter determines the duration of the signal. Even though longer MLS signals give a better resolution of the cross-correlation peak resulting in higher precision of the consequent estimation, a longer duration has its drawbacks. Due to undesirable echoes in cluttered or enclosed environments, higher processing overheads and lower update rate for the overall estimation system (presented in chapter 5) associated with a longer duration signal, a relatively short MLS signal of degree 7 (length 127) is employed as a compromise. The MLS generation algorithm (see appendix B) produces 18 unique sequences of this length which exhibits extremely low correlation between each other.

3.3 Cross-correlation of MLS signals

Plots a) and b) in figure 3.4 depict two unique MLS signals picked out of the different length-127 sequences produced by the generating algorithm. The original pure square-wave signals have been conditioned with sub-sample interpolation and the amplitude have been normalised. The auto-correlation of the first signal is shown in plot c) with a maximum lag equal to the length of the signal. The highly desirable narrowness and height of the correlation peak can be observed from this plot. Plot d) is the result of a cross-correlation between the two different MLS signals shown in plots a) and b). As is evident, different MLS signals show almost no correlation amongst each other.

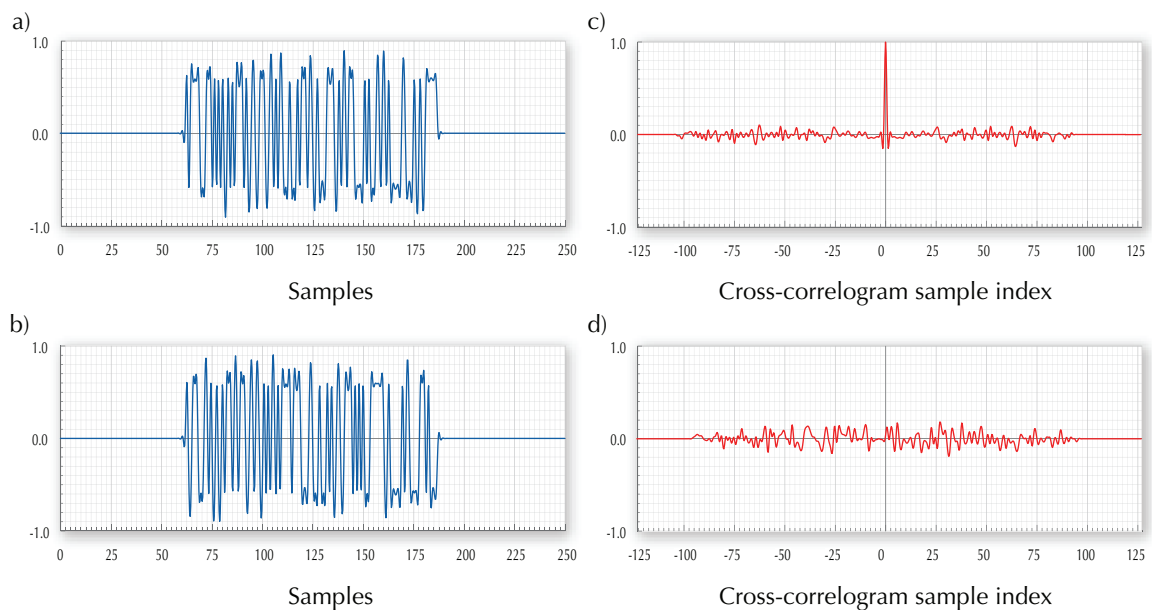


Figure 3.4: Plot c) shows the narrow sharp peak resulting from the auto-correlation of the MLS signal shown in a) while plot d) shows the cross-correlation between the two different MLS signals given in plots a) and b). In each plot, the *y-axis* represents normalised amplitude.

3.3.1 Effect of uncorrelated noise

The robustness of MLS signals against uncorrelated noise, even at relatively short lengths, is demonstrated as follows. Two copies of the MLS signal shown in figure 3.4a are used where one is shifted by 8 samples, such that the first channel (figure 3.5.b) leads. Then the two signals are contaminated with additive white Gaussian noise and cross-correlated. The average signal powers were equal (-3 dBFS) when mixing white noise with the MLS signal representing a SNR of 0dB. The two signals (plots a) and b)) and the resulting cross-correlogram (plot c)) is shown in figure 3.5. The position and width of the peak of the cross-correlation as well as the area surrounding the peak remains unaltered in this case. However, the height of the peak has been reduced to about 70% of its original value compared to the auto-correlation plot in figure 3.4c.

3.3.2 Effect of mixing and shifting

The plots in figure 3.6 show the behaviour of the cross-correlation for shifted signals. Instead of cross-correlating a simple sample-shifted signal, which might suggest a role played by the relative difference in the leading edges of the two signals, a mixed signal was used on one channel. The two different MLS signals shown in plots b) and e) were shifted by 16 samples and added such that the signal in b) leads. This mixed signal was cross-correlated separately with its component signals, each shifted by 8 samples such that the mixed signal leads. If it was merely leading edge detection, in both cases the relative delay between the two channels would have been measured as -8 samples. However, as seen in plots c) and f), the lags are correctly represented in the cross-

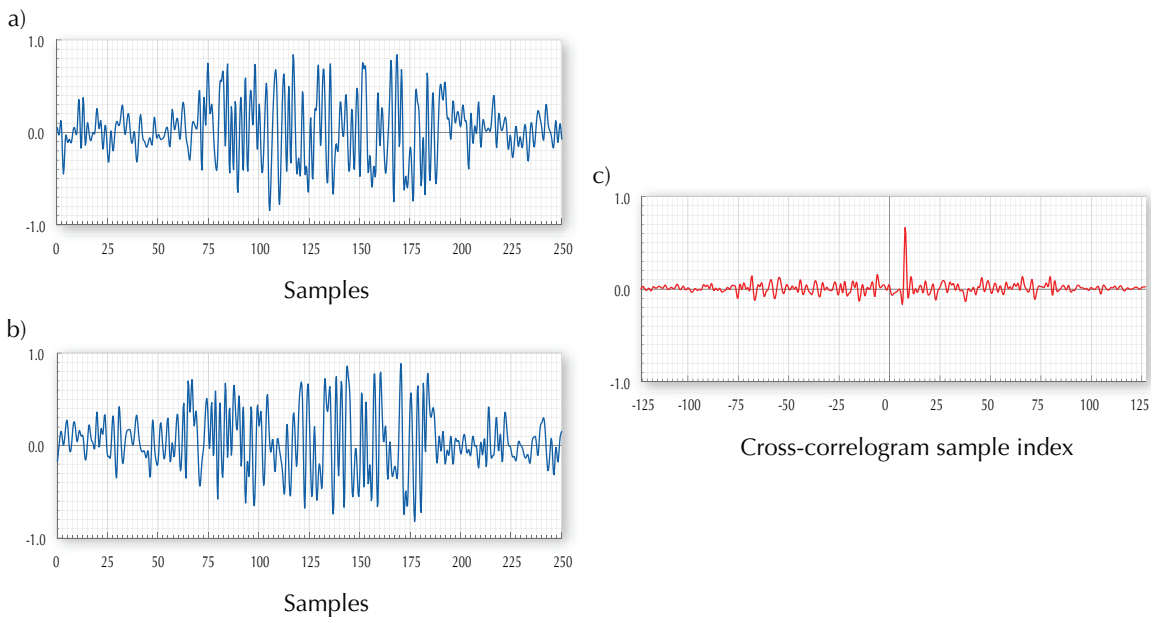


Figure 3.5: Plot shown in c) results from the cross-correlation of the shifted noisy MLS signals shown in a) and b). In each plot, the *y-axis* represents normalised amplitude.

correlogram with peaks at -8 samples and $+8$ samples respectively. In addition, the height reduction of the two cross-correlogram peaks are similar to that observed in the noise contamination earlier. This suggests that the sporadic peaks introduced to the frequency spectrum during the mixing process behaves as uncorrelated noise, hence lowering the effective SNR of the signals.

3.3.3 Effect of non-linear transducers

As it was shown by figure 3.5.c, contamination by additive white noise does not contribute to a noticeable deterioration of the cross-correlation performance of MLS signals, apart from a slightly lower height for the peak. In theory, addition of two 'flat' frequency spectra should again result in a 'flat' frequency spectrum, hence the spectral properties of the MLS signal which provides the narrowness of the peak are preserved. However, this is not necessarily the case when these signals are transmitted and received via transducers with a non-linear frequency response

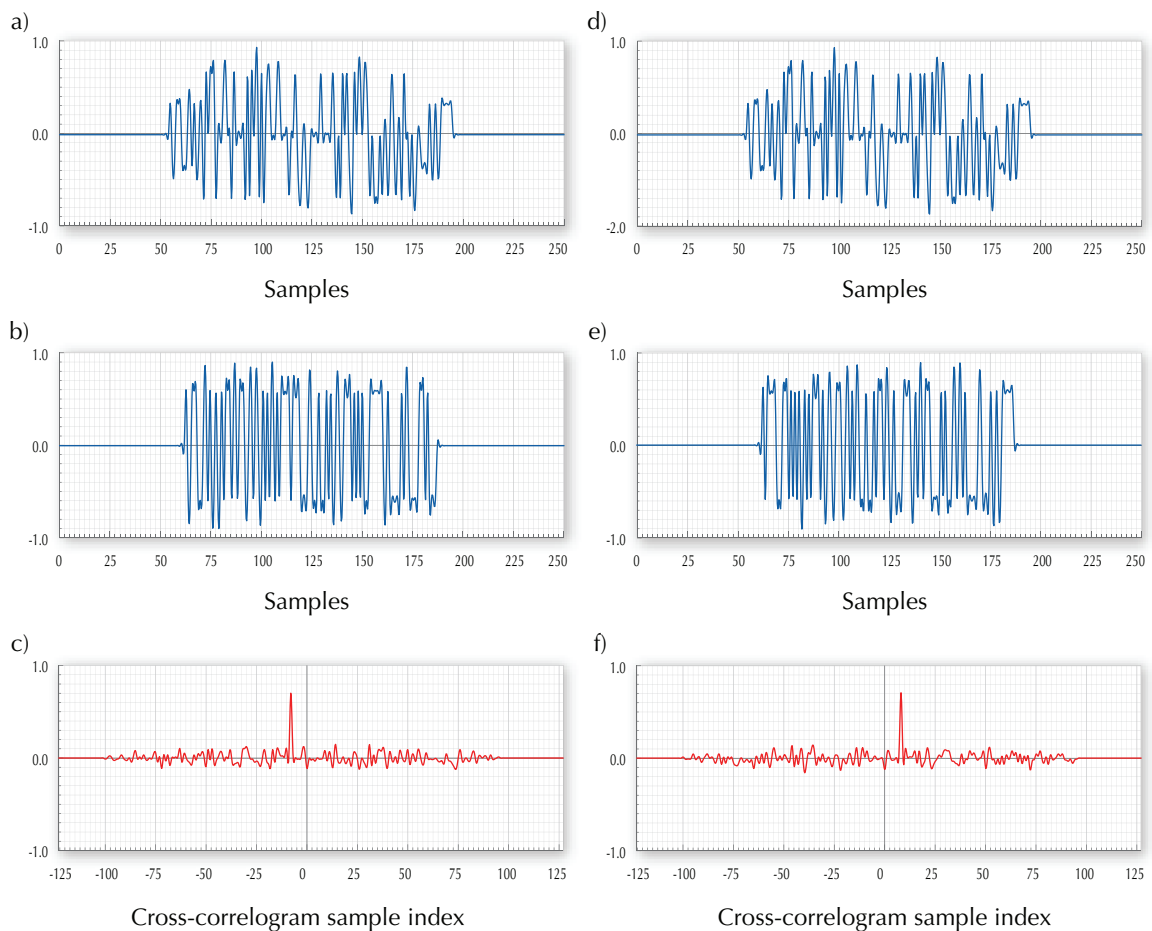


Figure 3.6: Plots in a) and d) represents a signal which is a mixture of the signals in b) and e). This mixed signal is cross-correlated with each of the two component signals and the resulting cross-correlograms are depicted in c) and f). In each plot, the *y-axis* represents normalised amplitude.

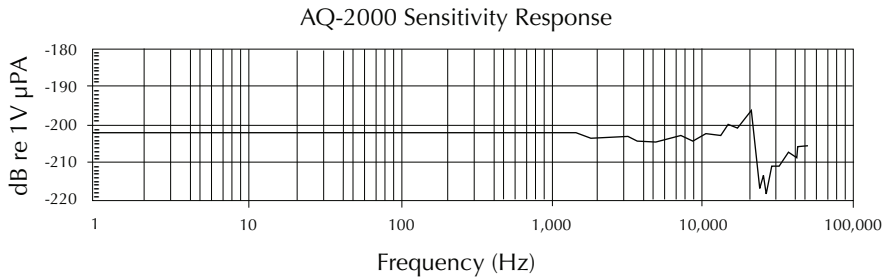


Figure 3.7: The frequency response curve of the hydrophone reproduced from the AQ-2000 data sheet (Benthos, 2001)

within the bandwidth of the signal. Due to the sampling rate used ($f_s=96\,000\text{Hz}$), the signals are band limited by $48\,000\text{Hz}$. The frequency response of the Benthos AQ-2000 transducers which are used as transmitting projectors as well as receiving hydrophones in the relative localisation system is shown in figure 3.7. As seen from this logarithmic plot, the transducers have a resonance near $20\,000\text{Hz}$ and an anti-resonance near $25\,000\text{Hz}$ which results in a highly non-linear response within the signal bandwidth.

To test the effect of this potential frequency filtering effect introduced by the transducers, the frequency response shown in figure 3.7 was empirically modelled¹ and implemented as an FFT filter. The filter was then applied to white noise contaminated MLS signals shown earlier in plots a) and b) of figure 3.5 and the two filtered signals were cross-correlated. This setup is illustrated in figure 3.8.a. The effect it has on the cross-correlogram shown in plot a) of figure 3.9 can be compared to the cross-correlogram shown in plot c) of figure 3.5, which was produced by the same source signals but without frequency filtering. Resonance of the transducer near $20\,000\text{Hz}$ appears as the dominant frequency in the resulting cross-correlogram. For comparison, plot c) of figure 3.9 shows the cross-correlogram of two signal channels received via two AQ-2000 transducers (separated by 0.3m) when an MLS (length-127, duration 1.3ms) signal was transmitted via another AQ-2000 transducer. The signal travelled a distance of 2.0m underwater and the cross-correlation reveals a delay of $+8$ samples ($83.33\mu\text{s}$) between the channels. This setup is schematically illustrated in figure 3.8.c. Both the cross-correlograms, one from cross-correlating the ‘real’ and the other from cross-correlating the ‘simulated’ signals, shows the dominance of the $20\,000\text{Hz}$ resonance of the transducer throughout the plots. Even though the position and height of the peak is not affected, the uniqueness of the peak had been lost by being surrounded by an envelope of decaying side-lobes. As revealed in chapter 7, this decreases the accuracy of the localisation system when used in enclosed and cluttered environments due to peaks caused by reflected signals.

¹. The shape of the frequency response curve was replicated as the shape of a frequency response curve of an FFT filter.

In order to address this issue, another filter was empirically modelled which had the inverse frequency response of the one modelled earlier to represent the response of the transducer. The results of applying the new FFT filter¹ to the simulated and the real signals used earlier and cross-correlating the channels are shown in plots b) and d) of figure 3.9 respectively. The source signals, before and after being filtered is shown in appendix A (figure A.1). The setups used in these instances are schematically depicted in figures 3.8.b and 3.8.d. As depicted by the plots the uniqueness, narrowness and the height of the peak is restored making it possible to unambiguously locate it.

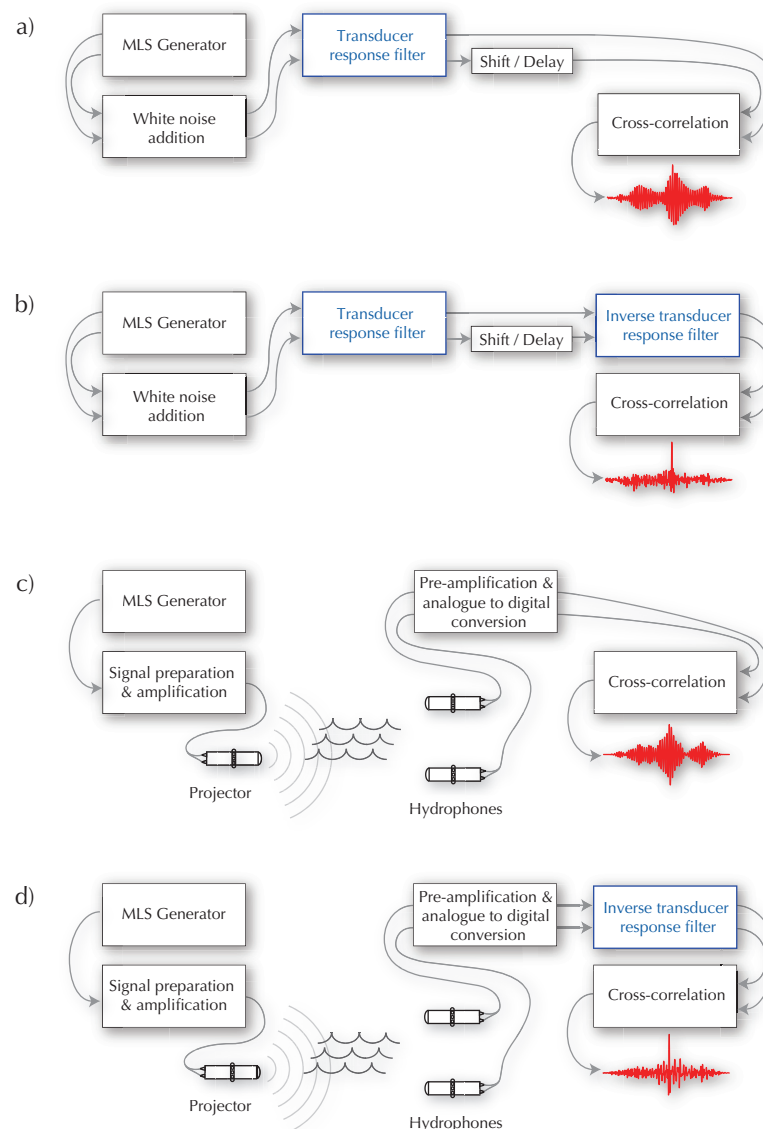


Figure 3.8: The four different setups producing the four different cross-correlograms shown in figure 3.9. The source signals that provide inputs to the cross-correlation are given in section A.1.

¹ The filter was applied to the two signal channels prior to being cross-correlated.

3.4 Discussion

An experimental evaluation of the performance of MLS signals alongside other types of broadband signals with regard to cross-correlation peak detection and measured SNR was presented earlier in this chapter. In a harsh reverberant acoustical environment, the MLS signals performed better with regard to peak detection and delivered SNR, in comparison with chirps and pseudo-noise signals. Further statistical properties of MLS signals, their behaviour characteristics with regard to exposure to noise and the effect mixing and shifting signals are given in the subsequent sections.

Finally, the effects of the non-linear frequency response of transducers on the transmitted MLS signals are discussed and a strategy to address this effect is proposed. It must be emphasised that the filter process described in the earlier section only accounts for the transducer characteristics and not those of the propagation medium. Since channel characteristics of the underwater medium greatly varies with depth, temperature and salinity as well as environmental features such as the composition and texture of the bottom (sediment/sand/vegetation), modelling the transducer characteristics are more practical. In the context of an autonomous underwater vehicle, it is far more convenient to account for the characteristics of on-board sensors than to have access to a model of the channel characteristics of the operating medium. However, the underwater channel does indeed have an effect on the transmitted MLS signal as seen in figure 3.9.d

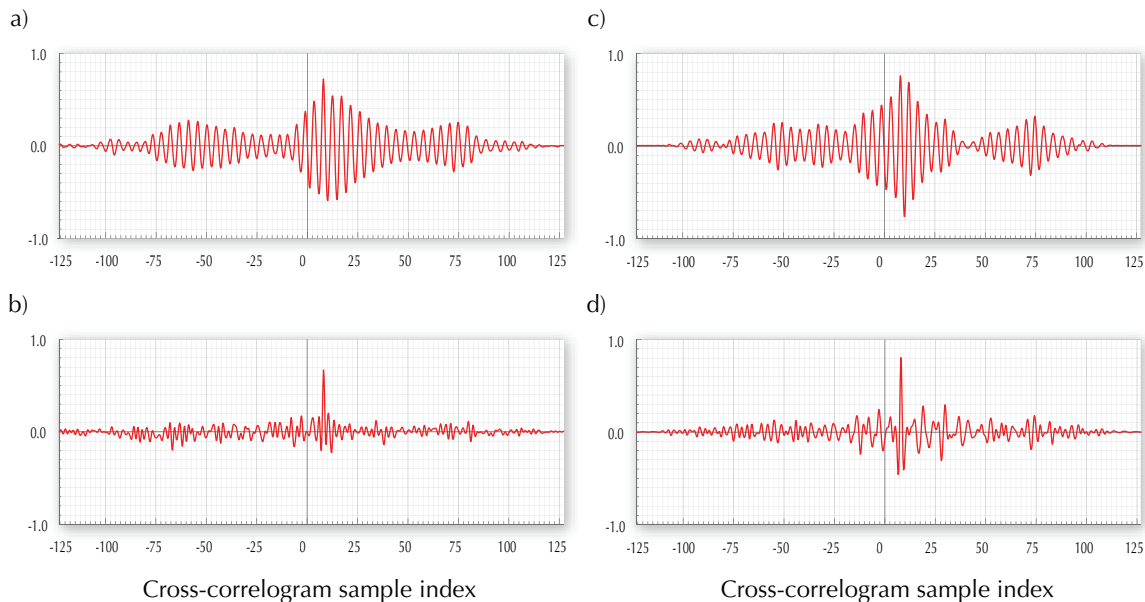


Figure 3.9: Plots in a) and b) represents the cross-correlograms of the shifted MLS signals contaminated with additive white noise, first filtered with the transducer frequency response model, then filtered with the inverse of that filter. Plot c) shows the cross-correlogram resulting from two actual signal channels (with a shift of +8 samples) which were transmitted and received using the transducers. Plot d) shows the resulting cross-correlogram when the inverse transducer filter was applied to the signal channels prior to cross-correlation. In each plot, the y -axis represents the normalised amplitude of the signals.

where the filtering process does not completely reconstruct the original cross-correlogram (figure 3.4.c). Furthermore, the power of the received signals are greatly reduced by the inverse filtration process since most of the transmitted signal power is around the resonance frequency of the transducer. This attenuation affects the distance which the MLS signals can be effectively transmitted at a given transmission power. For the application concerned, the achievable operating distances at a low transmission power and the cross-correlation peak detection performance given by the use of MLS signals are amply sufficient and far surpasses other alternative signal waveforms which were evaluated.

The next chapter describes the distance and angle estimations carried out during the process of localising source signal pings. The methodology and basic measurement schemes are also described along with identification and analysis of different classes of errors affecting the estimated quantities.

Chapter 4

Acoustic source localisation

The basic sequence of operation of the relative localisation system can be explained as follows: an AUV (**sender**) emits two acoustic ‘pings’ in sequence, first from the bow (front) end and next from the stern (rear) end. These two pings constitute one **sending event**. AUVs (**observers**) which have the sender within their sensing range would attempt to estimate the angle and the distance to each of the source upon receiving the acoustic pings. These angles (**sub-azimuths**) and distances (**sub-ranges**) are then used to estimate the compound azimuth, range and heading of the sending AUV, relative to each of the observers. These azimuth, range and heading estimates are later used as components to assemble a pose vector which contains the position information of the localised AUV.

The specific measurements and estimations carried out by an observing vehicle in this process are explained in the next sections, starting with the angle and distance estimation for a single acoustic source. The methodology and basic measurement schemes are described in detail along with identification of different classes of errors affecting the estimated quantities. An analysis of how the uncertainties associated with the basic measurements propagate towards uncertainties in the estimated quantities is given and a strategy for minimising the random errors of the estimates is also presented which contributes towards improving the precision of the relative

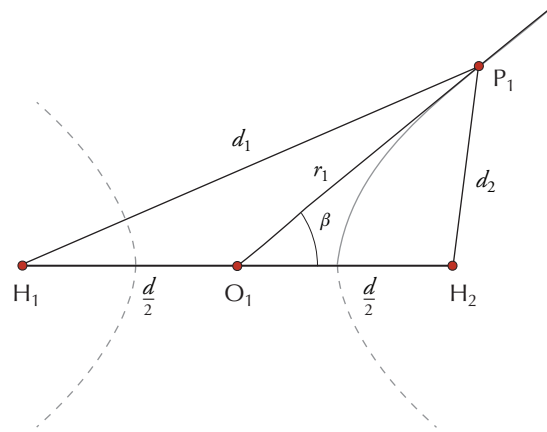


Figure 4.1: As a signal is emitted from P_1 , it reaches the receivers H_1 and H_2 after travelling distances d_1 and d_2 respectively. The path length difference $d_1 - d_2$ can be used to derive the angle of arrival β .

localisation system. Later sections describe how the sub-azimuths and sub-ranges are used to derive the compound estimates for azimuth, range and heading in addition to an alternative scheme of estimating heading and range independent of implicit sender-observer synchronisation. Formulae showing the relationship of the component quantities and their uncertainties with the uncertainty of the compound quantities are also derived and plotted. These are used to analyse the behaviour of the relative localisation estimates with regard to resolution and upper bounds for errors.

4.1 Angle estimation

As mentioned in chapter 2, TDOA measurement is the basis of hyperbolic localisation and navigation schemes as well as many bearing only tracking systems. Bellingham et al. (1992) presents such a self-localisation system for multiple AUVs using TDOA measurements with respect to multiple acoustic beacons. TDOA, as the term suggests, is the difference of arrival times at two receiver locations, of a signal transmitted from a third location. This quantity is then converted to an angle, from which the source signal arrive towards the two receivers. In the context of this research, the source signal consist of an acoustically transmitted MLS signal and transmitters and receivers are projectors and hydrophones as described in the previous chapter.

4.1.1 Mapping path length difference to an angle

Figure 4.1 depicts a source at P_1 and two receivers at H_1 and H_2 . The signal from P_1 takes two different paths to reach H_1 and H_2 , traversing path lengths of d_1 and d_2 respectively. This difference in path lengths as a distance is denoted by δ and given as:

$$\delta = d_1 - d_2 \quad (4.1)$$

With the spacing between the receivers denoted by d and following the standard definition of a hyperbola, the locus of P_1 can be defined as lying on a branch of a hyperbola with its foci at H_1 , H_2 and eccentricity $d/|\delta|$.

If the distance to P_1 from the midpoint of the two receivers (O_1) is denoted by r_1 and considering the polar coordinates of P_1 as (r_1, β) where the polar axis lies along H_1H_2 with the pole at O_1 , the polar coordinate equation of the hyperbola yields the angle of arrival of a signal originating from P_1 as:

$$\beta = \pm \tan^{-1} \left(\frac{\sqrt{(4r_1^2 - \delta^2)(d^2 - \delta^2)}}{\delta \sqrt{4r_1^2 + d^2 - \delta^2}} \right) \quad (4.2)$$

Usually, the quantity r_1 is not available at the time of measuring the angle. When the source is located sufficiently far away from the receivers compared to the spacing between the receivers¹, the same angle can be expressed using the polar coordinate equation of the asymptotes of the hyperbola as follows:

$$\beta = \pm \tan^{-1} \left(\frac{\sqrt{d^2 - \delta^2}}{\delta} \right) \quad (4.3)$$

where $\tan\beta$ is the gradient of the asymptotes.

As can be seen from the diagram in figure 4.1 as well as by inspecting the formulae, the path length difference δ varies between $-d$ and $+d$. The sign of δ determines which branch of the hyperbola contains P_1 . However, as seen from figure 4.2, a given value of δ yielding a value for β still holds an ambiguity, referred to as the *front-back ambiguity*. Any location of P_1 and its reflection about H_1H_2 would give the same path length difference. The \pm sign in the formulae (4.2) and (4.3) can be considered to represent this ambiguity. In the absence of extra information from additional sensors, omnidirectional receivers cannot usually resolve this ambiguity. The relative localisation system presented in this thesis uses non-omnidirectional hydrophones as receivers and consequently avoids this problem². Therefore, the \pm sign will be dropped from the formulae in the subsequent discussions. Furthermore, the signal source is assumed to be on the same plane containing the two receivers and their main axes of directivity, hence the localisation system is restricted to two dimensions. However, the principle of path length difference extends to the third dimension where the source lie outside the aforementioned plane. In this case, the branches of the hyperbola are replaced by sheets of a three dimensional hyperboloid and the asymptote lines are replaced by cones. Strategies for extending the localisation system into the

¹ In practise, this condition is satisfied when $r_1 > 2d$

² The experimental results presented in chapter 7 demonstrates the use of non-omnidirectional hydrophones.

third dimension by fusing additional sensor information (relative depth) and utilising additional hydrophones, are proposed and experimentally validated in chapter 8.

4.1.2 TDOA measurement

While the path length difference described earlier is given as a distance, the speed of propagation of the signal relates it to a time delay t_D as:

$$t_D = \frac{\delta}{v} \quad (4.4)$$

where v is the speed of propagation of the source signal. Since it is not possible to explicitly measure the path length difference, the actual measurement is of this delay t_D which is referred to as the time difference of arrival (TDOA) of the signal.

When $s(t)$ denotes the source signal at P_1 , the two signal channels at receivers H_1, H_2 represented by $s_1(t), s_2(t)$ respectively, can be modelled as:

$$\begin{aligned} s_1(t) &= s(t) + n_1(t) \\ s_2(t) &= a \times s(t + t_D) + n_2(t) \end{aligned} \quad (4.5)$$

where a is an attenuation coefficient, $n_1(t)$ and $n_2(t)$ being the uncorrelated noise present in each channel and t_D being the time difference of arrival between the two channels corresponding to the difference in path length δ . Transformation of the signal due to receiving and transmitting transducer characteristics and the propagation medium is not explicitly modelled. These transformations do not affect the measurement of t_D when they are assumed to be common to

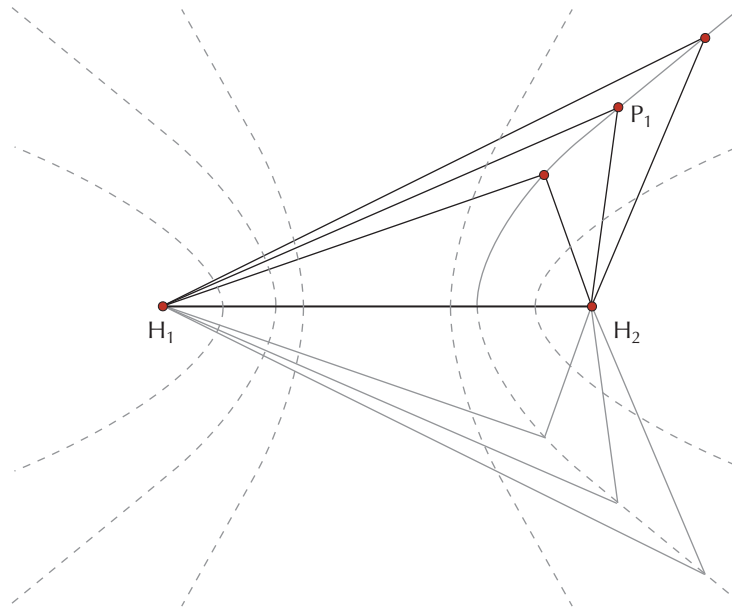


Figure 4.2: A given path length difference, while restricting the locus of P_1 to one branch of the hyperbola, introduces a *front-back ambiguity* when using omnidirectional receivers at H_1 and H_2 .

both channels. Knapp and Carter (1976) gives the estimate for t_D as the argument τ that maximise the following cross-correlation function:

$$R_{s_1 s_2}(\tau) = E[s_1(t)s_2(t-\tau)] \quad (4.6)$$

where E denotes the expectation.

A continuous-time representation of the cross-correlation function of the time-domain signals $s_1(t)$ and $s_2(t)$ can be expressed as:

$$R_{s_1 s_2}(\tau) = \int_{-\infty}^{+\infty} s_1(t)s_2(t-\tau)dt \quad (4.7)$$

However, in the relative localisation system being discussed, the signals received by the hydrophone channels are two discretely-sampled time-series signals of finite length N which can be denoted by $s_1(n)$ and $s_2(n)$ which gives the cross-correlation function using (3.1) given in chapter 3 as follows:

$$R_{s_1 s_2}(\tau) = \sum_{n=i}^{N-|k|-1} s_1(n)s_2(n-\tau) \quad (4.8)$$

where $i = \tau$, $k = 0$ for $\tau \geq 0$, and $i = 0$, $k = \tau$ for $\tau < 0$. When considering the full-range cross-correlation described in section 3.1, which includes both positive and negative lags, the resulting cross-correlation function is of length $2N+1$ with the sample index spanning $-N$ to $+N$. The sample index which corresponds to the maximum value of $R_{s_1 s_2}$ denoted by τ_0 can be expressed as:

$$\tau_0 = \min\{n_0 \in \{-N \dots N\} \text{ s.t. } \forall n \in \{-N \dots N\}, x(n_0) \geq x(n)\} \quad (4.9)$$

where

$$x(n) \in \{x_{-N} \dots x_N\} = R_{s_1 s_2} \quad (4.10)$$

Here $R_{s_1 s_2}$ denotes the full-range cross-correlation containing values corresponding to both negative and positive lags. τ_0 relates to the TDOA as follows:

$$t_D = \frac{\tau_0}{f_s} \quad (4.11)$$

where f_s is the sampling frequency of the analogue to digital converters used. In order to measure the angle of arrival of the signal using (4.3), τ_0 is related to δ by (4.4) and (4.11) as:

$$\delta = \frac{\tau_0 v}{f_s} \quad (4.12)$$

The sequence of angular measurements carried out by the relative localisation system using the methodology explained above to obtain the azimuth angle of the sender AUV is explained later in this chapter.

4.2 Distance estimation

Time of flight (TOF) of a signal is usually used to estimate distance between the signal source and the receiver. While sonar and radar systems (Nielsen, 1991; Waite, 2002; Ricker, 2003) estimate distance to targets by measuring the round-trip time of a signal reflected off the target, the method used in this system does not involve a reflected signal. The direct-path range estimation using TOF of acoustic signals employed in this work is related to the spherical positioning schemes used in acoustic beacon based underwater localisation (Liang, 1999; Larsen, 2000; Olson et al., 2004).

To measure the travel time of a signal, knowledge of the exact time at which the signal was emitted is required. When localising relative to acoustic beacons, this is achieved by maintaining explicitly synchronised clocks at both the receiver and transmitter locations. The **logical time-step**¹ concept used in the relative localisation system achieves synchronisation in an implicit manner compared to maintaining clocks synchronised with absolute time. The long-wave radio communication system on-board each Serafina Mk II AUV which transmits according to a **distributed omnicast routing** schedule (Schill and Zimmer, 2006b; Schill and Zimmer, 2007) is coupled with the relative localisation system such that each acoustic sending event is initiated simultaneously² with the start of a long-wave radio transmission from a sender AUV which also marks the start of a logical time-step. Upon receiving the long-wave radio signal, each of the observer AUVs within communication range increments their respective logical clocks marking the start of their logical time-steps.

Due to the sufficient difference in speed of propagation for electromagnetic and acoustic signals underwater, it can be safely assumed that the long-wave radio signal reaches an observer AUV earlier than the acoustic signal. The consequent start of the logical time-step on the observer triggers the acoustic receivers which begins to await the acoustic signal. If it takes time t for the acoustic signal to arrive since the start of the logical time-step, the distance r between the sender and observer can be given by:

$$r = \frac{tv_e v}{(v_e - v)} \quad (4.13)$$

¹. Logical time increments with each update and not necessarily on a fixed absolute time related to a real-time clock as explained by Lamport (1978)

². The time jitter involved in this process is taken into consideration in the uncertainty analysis of the range estimates and later discussed in chapter 5.

where v_e and v are the speeds of propagation for electromagnetic and acoustic signals underwater. However, with the relatively short distances between AUVs in a local neighbourhood and comparing the magnitudes of the quantities¹ v_e and v , it can be assumed that the long-wave radio signals are transmitted between the neighbouring vehicles instantaneously, which reduces (4.13) to:

$$r = tv \quad (4.14)$$

where t can be expressed as the TOF of the acoustic signal.

A similar in-air distance estimation approach which does not rely on explicitly synchronised clocks on the sender and the receiver is used on the Cricket indoor location system developed by Priyantha (2005) and discussed by Balakrishnan et al. (2003) and Smith et al. (2004). The beacon nodes deployed in the Cricket system simultaneously transmit a radio frequency message packet with a narrow ultrasound pulse. The receiving nodes then use the difference of arrival time of the electromagnetic and acoustic signals to estimate the distance between the beacon and the receiver.

4.2.1 Modified matched filter for TOF extraction

A common approach used in echo signal detection is the use of a matched filter. In one of the earliest and most comprehensive contributions, Turin (1960) introduces the concept of matched filter processing as a means for recovering a known waveform from a noisy signal. In its conventional form, a noise-free replica of the original signal is cross-correlated with the received signal channel to locate the return signal and thus extract the TOF. Hermand and Roderick (1993) introduces an improved ‘model based’ matched filter which uses a copy of the original signal which is convolved with the impulse response of the transmission medium as the reference signal instead of a noise-free replica. This approach requires some *a priori* knowledge about the characteristics of the underwater environment in which the AUVs operate in order to construct the impulse response.

The proposed relative localisation system uses an actual received signal channel as the reference for cross-correlation. The system initialises with a pre-recorded reference channel consisting of the MLS signal (which is used by the localisation system as the source signal waveform) which has been transmitted and received underwater via the transducers used in the system. This technique compensates for the frequency distortions introduced by the transducers as explained in chapter 3 as well as the transmission characteristics of the underwater medium. As the operation progresses (when the swarm moves to areas with different underwater channel characteristics),

¹. $v_e \approx 3.0 \times 10^8 \text{ ms}^{-1}$ and $v \approx 1.5 \times 10^3 \text{ ms}^{-1}$

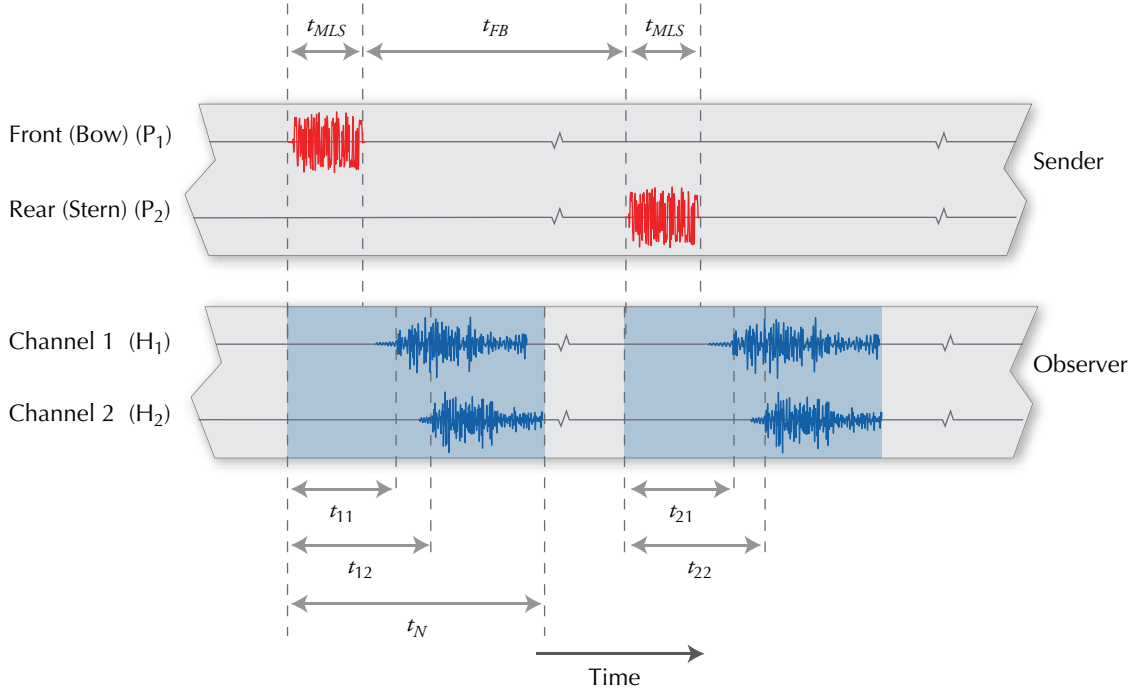


Figure 4.3: Time durations involving the sender and observer within one sending event.

this initial reference signal can be replaced by a newly received signal which encompasses more up to date characteristics of the transmission medium if and when the performance of the range estimation system drops below a pre-set threshold value. This methodology presents a technique which can cope with changing underwater channel characteristics without explicit measurements or *a priori* information about the transmission medium.

The cross-correlation scheme described in the previous section is used for this ‘modified’ match filter as well, where one signal channel is replaced by the reference signal in (4.8). Two cross-correlations are performed to extract the TOF to each of the two receivers for each signal received from the sender AUV. The diagram given in figure 4.3 shows the four TOFs associated with the two pings. The TOFs t_{11} and t_{12} are related to the front (bow) ping and the TOFs t_{21} and t_{22} are related to the rear (stern) ping. As mentioned in the previous section, the long-wave radio signal emitted from the sender simultaneously with the first acoustic ping is assumed to be received instantaneously by the observer, triggering the start of the sending event. The subsequent TOFs are measured from this starting trigger. When implemented in hardware, there is finite latency and timing jitter associated with detection of the long-wave signal and the synchronised sending of the acoustic pings. If this synchronisation latency of the receiving hardware is denoted by t_L , then the sample-domain latency τ_L is given by:

$$\tau_L = f_s t_L \quad (4.15)$$

where f_s is the sampling rate. The variation in latency, which is the timing jitter is denoted by Δt_L . From (4.15), its sample domain counterpart $\Delta \tau_L$ is given by:

$$\Delta \tau_L = f_s \Delta t_L \quad (4.16)$$

The quantity $\Delta \tau_L$ will be included in the uncertainty analysis of the range estimates in the following sections.

Without loss of generality, the range estimation will be explained in the next section using only the two TOFs where the front (bow) ping is the source signal. For this purpose, the two sample-domain delays obtained from (4.9) corresponding to the receivers H_1, H_2 are denoted by τ_0^{11} and τ_0^{12} with regard to a signal transmitted from P_1 , (figure 4.4) the two TOFs t_{11} and t_{12} can be calculated as:

$$t_{11} = \frac{\tau_0^{11} - \tau_L}{f_s} \quad (4.17)$$

$$t_{12} = \frac{\tau_0^{12} - \tau_L}{f_s}$$

where τ_L is the sample-domain latency given in (4.15) and f_s is the sampling frequency of the analogue to digital converters used.

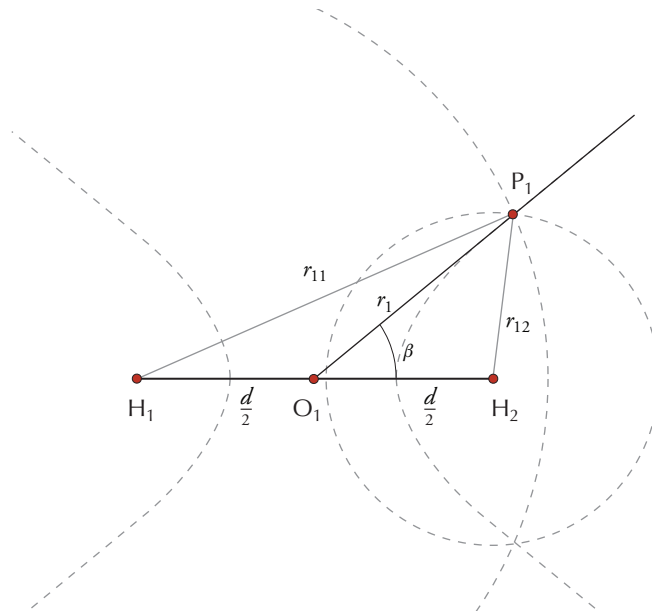


Figure 4.4: Intersecting two circles centred at H_1 and H_2 with the line defining angle of arrival of the signal uniquely localises the source position P_1 .

4.2.2 Distance estimation using TOF

As explained by Deffenbaugh et al. (1996a), in spherical localisation, measuring the travel time of an acoustic signal emitted by a single synchronised beacon with a known location defines a sphere centred at the beacon on which the receiver must lie. Conversely, if the position of the beacon is unknown, the signal source must lie on a sphere centred at the receiver. In the planar case considered in the relative localisation system, the said sphere reduces to a circle. However, instead of the multiple spheres (or circles in the planar case) needed to uniquely identify a position as done in traditional spherical localisation, using a single circle and its intersection with the line defining the angle of arrival of the signal which was described in the previous sections, uniquely defines the position of the signal source.

In order to achieve better accuracy, two circles centred at the two receivers at H_1 and H_2 and the line defining the angle of arrival is used as shown in figure 4.4. The radii of the circles centred at H_1 and H_2 are denoted by r_{11} ($=P_1H_1$) and r_{12} ($=P_1H_2$) are obtained by substituting (4.17) in (4.14). The distance r_1 ($=P_1O_1$) needed to complete the polar coordinates (r_1, β) of signal source P_1 can be derived by:

$$r_1 = \sqrt{\frac{r_{11}^2 + r_{12}^2}{2} - \left(\frac{d}{2}\right)^2} \quad (4.18)$$

where d ($=H_1H_2$) is the spacing between the receivers.

4.3 Source localisation and uncertainty of estimates

The TDOA of the source signal between the receivers at the point of observation O_1 (mid point between receivers) defines an angle of arrival β , while the TOFs of the source signal to the two receivers combined as explained in the previous section defines a radius r_1 , centred at the point of observation. The intersection of the line along the angle of arrival β through O_1 and the semi-circle (considering the directivity of the receivers) with this radius r_1 would uniquely define the position of the source in two dimensions. The equation in (4.3) gives the angle of arrival and (4.18) gives the radius mentioned above.

The previous sections described and explained the methodology used in localising an acoustic source by measuring TDOAs and TOFs in the context of the relative localisation system being presented. During the estimation process, these measurements are done twice per sending event, once for the front ping, then again for the rear ping yielding two TDOAs and four TOFs. These are then used for deriving two angles and two distances - the **sub-azimuths** and **sub-ranges**, corresponding to the front and rear of the sender relative to the observing submersible.

Subsequently in section 4.4.3, these quantities are used as the basis for deriving compound estimates based on the geometrical relationship of the transducer positions.

The angle and distance estimates derived earlier have uncertainties associated with them. Since these quantities will later be used to derive compound estimates which constitute the pose vector¹ describing the azimuth, range and heading of the sender vehicle, it is important to identify and analyse the possible sources of errors and the effect of uncertainty associated with the component quantities on the derived estimates. The following subsections classify errors based on the sources and their effect on the estimated quantity. In section 4.3.1, error formulae are derived to show the relationship between the estimated quantities and the uncertainties of the component measurements. While this does not constitute a comprehensive error model for the system, it provides a statistical basis to analyse the behaviour of the system in the presence of random errors and to provide theoretical bounds to the precision of the estimates. As compound localisation estimates are derived from these component estimates later in this chapter, similar error propagation formulae will be presented with respect to the uncertainties associated with these compound estimates.

Random errors

The primary measurements in each of the estimates are sample-domain delays, measured by detecting the peak position after cross-correlation of pairs of discretized time-domain signal waveforms. By virtue of this discretization, the position of the peak has an uncertainty of 0.5 samples which manifests itself as a form of quantization error with an assumed uniform distribution. Apart from this, which affects the TDOA measurement, the TOF measurement is also affected by the uncertainty introduced by synchronisation time-jitter mentioned earlier. The time-jitter is assumed to have a Gaussian distribution. Both these sources of uncertainty lead to random errors, effects of which are non-deterministic, and contributes to the lowering of precision of the estimated quantities. A strategy for reducing the impact of these random errors is presented and discussed in section 4.3.2. There also are random measurement errors associated with the constant quantities such as the speed of sound in water v , sampling rate f_s and the base distance between hydrophones d on the observer (and the separation between projectors l on the sender, introduced later in section 4.4.3) as well. Considering typical values for the upper bounds of these errors, section 4.3.1 discusses the contributions of these quantities to the final estimates.

Systematic errors

In addition to these random errors, biases and variations associated with the constant quantities such as the speed of sound in water v , sampling rate f_s , the base distance between hydrophones

¹. The structure of the pose vector is described in section 5.2.1 of chapter 5.

d on the observer (and the separation between projectors l on the sender) as well as the synchronisation latency t_L manifest themselves as systematic errors in the estimation process. These errors affect the accuracy of the estimated quantities. While it is extremely difficult to individually identify the contributions of these different errors to the final estimates, most of these systematic errors can be compensated by careful calibration of the system and applying compound corrections.

Errors due to low SNR

Apart from the two forms of errors, another class of errors arise due to the deterioration of the signal-to-noise ratio (SNR). Loss of signal could occur due to the source being out of the sensing range (radial or angular) of the utilised transducers. In such situations, in the absence of a distinct waveform, the cross-correlation is between channels containing ambient noise, which in the ideal cases would act as uncorrelated noise. As a result, both forms of the cross-correlation peak detection (For TDOA and TOF measurement) would return uniformly distributed random positions, affecting the accuracy of the consequent estimates. In most real cases, the ambient noise appears weakly correlated on the two received channels yielding a discernible peak near '0' for the TDOA measurement, resulting in an angular estimate in the vicinity of 90° (or 0° after the measuring conventions are applied as described later in section 4.4.1). The TOF measurement however is uninfluenced, by correlated noise in the absence of the signal of interest, due to the matched filter processing and would continue to return random estimates.

Operating in highly cluttered, reverberant environments result in interference of the direct path signals by reflected (multipath) signals. A similar form of interference occurs in the presence of multiple sending events within the (1-hop) neighbourhood of an observer due to colliding sending schedules. In such situations, without explicit identification and handling of the situation, both the TDOA and TOF measurements would respond to the louder signal source which gives a higher peak in the cross-correlogram (not necessarily the first arriving signal) which could lead to inaccurate estimates for the source angle and range. With respect to the intended/ direct-path signal of interest, the other signals (with the same wave form) due to colliding sending events and multipath can be considered noise, which contributes to the lowering of the effective SNR. Though not always¹, in most operating conditions, due to short-range propagation loss caused by acoustic spreading (Urick, 1983), the first arriving signal would indeed be louder, yielding a higher peak.

Yet another form of interference could occur due to extraneous acoustic sources present in the environment. Detrimental effects due to this last form of interference is largely avoided by the

¹: Due to the directivity pattern of receivers, for some source positions, a reflected signal can appear louder than the direct path signal in the presence of multipath arrivals.

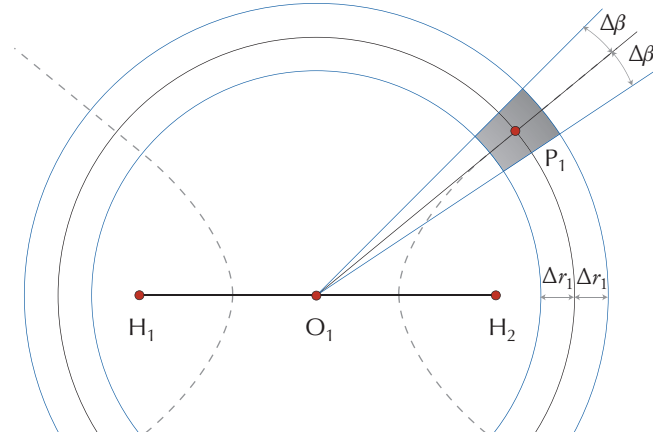


Figure 4.5: Localising the source P_1 by intersecting a branch of an asymptote of the hyperbola and a circle. The blue lines depict the theoretical error bounds for r_1 and β .

choice of MLS signals as the source waveform due to their robustness against most such noise sources as discussed in the previous chapter. However in the presence of intense broadband noise, due to the deterioration of the SNR, the TDOA measurement could yield estimates which corresponds to the angular position of the noise source rather than the signal source. The TOF measurements are usually unaffected by such extraneous noise but could result in random errors caused by loss of cross-correlation peak height due to severe deterioration of SNR.

These errors due to deterioration of the SNR usually appear as transient effects when considering mobile platforms operating in a dynamic environment. The time history of previous estimates, the transient nature of these errors and additional information derived from the underlying long-wave radio communication system can be utilised to handle these errors. Such strategies are presented in chapter 5 and further experimentally evaluated in chapter 7.

4.3.1 Propagation of errors

Inspecting (4.3), (4.12) by which angle β is derived from and (4.14), (4.17), (4.18) which are used to derive range r_1 , the sources of random errors can be identified as the uncertainties associated with the sample-domain delay estimations τ_0 , τ_0^{11} , τ_0^{12} and the sample-domain sender-observer synchronisation latency τ_L . If these uncertainties for the quantities τ_0 , τ_0^{11} and τ_0^{12} are denoted by $\Delta\tau_0$, $\Delta\tau_0^{11}$ and $\Delta\tau_0^{12}$ respectively, using the general error propagation formula¹ gives the uncertainty for β as:

$$\Delta\beta = \pm\Delta\tau_0 \frac{\partial\beta}{\partial\tau_0} \quad (4.19)$$

¹. See Bock and Krischer (1998) for a basic introduction to the error propagation formula or Figliola and Beasley (2005) for a comprehensive treatment of uncertainty analysis and error propagation.

and the uncertainty for r_1 as:

$$\Delta r_1 = \pm \sqrt{(\Delta \tau_0^{11})^2 \left(\frac{\partial r_1}{\partial \tau_0^{11}} \right)^2 + (\Delta \tau_0^{12})^2 \left(\frac{\partial r_1}{\partial \tau_0^{12}} \right)^2 + (\Delta \tau_L)^2 \left(\frac{\partial r_1}{\partial \tau_L} \right)^2} \quad (4.20)$$

where $\Delta \tau_L$ is the synchronisation timing jitter mentioned in section 4.2.1. As depicted in figure 4.5 these uncertainties associated with the angle and distance estimates places the source in an error bounded area rather than a point.

Since the sample-domain delay estimates are obtained from the same cross-correlation peak detection process, the associated uncertainties for the TDOA and TOF measurements are assumed to be similar ($\Delta \tau_0 = \Delta \tau_0^{11} = \Delta \tau_0^{12}$) and represented by $\Delta \tau$. The random measurement errors associated with the quantities d , v and f_s are denoted by Δd , Δv and Δf_s respectively. Evaluating (4.19) and (4.20) gives:

$$\Delta \beta = \pm \sqrt{\left(\frac{v \Delta \tau}{f_s d \sin \beta} \right)^2 + \frac{1}{\tan^2 \beta} \left(\left(\frac{\Delta d}{d} \right)^2 + \left(\frac{\Delta v}{v} \right)^2 + \left(\frac{\Delta f_s}{f_s} \right)^2 \right)} \quad (4.21)$$

$$\Delta r_1 = \pm \frac{v}{2 r_1 f_s} \sqrt{2(\Delta \tau^2 + \Delta \tau_L^2) \left(r_1^2 + \left(\frac{d}{2} \right)^2 \right) + X} \quad (4.22)$$

$$X = \left(\frac{d \Delta d}{2} \right)^2 + 4 \left(r_1^2 + \left(\frac{d}{2} \right)^2 \right)^2 \left(\left(\frac{\Delta v}{v} \right)^2 + \left(\frac{\Delta f_s}{f_s} \right)^2 \right) \quad (4.23)$$

The uncertainty for d arises directly from the instrument error of the measuring device (standard measuring tape), which in this case has a minimum measurement of 0.001 m. Hence the maximum random uncertainty associated with the base distance is $\Delta d = 0.0005$ m. It is assumed d remains constant¹ at 0.3 m throughout the estimation process due to the mechanical mounting of the hydrophones. By inspecting the structure of the above equations, the contribution of terms containing Δd^2 are negligible compared to the other contributing components.

The sampling rate of 96000 Hz which is used by the experimental system is provided by an Edirol FA-101 sampling device (Roland, 2004). Once again, considering typical values for Δf_s caused by clock drifts, the contribution of terms with this quantity to the uncertainty equations are negligible.

The speed of sound in water v , is not a direct measurement. While initial explicit measurements were done during experimental calibration described later in chapter 6, the empirical formula

¹. However, any minor variations of this base distance will manifest itself as a systematic error in the final estimates as discussed earlier and is not accounted for by Δd mentioned here.

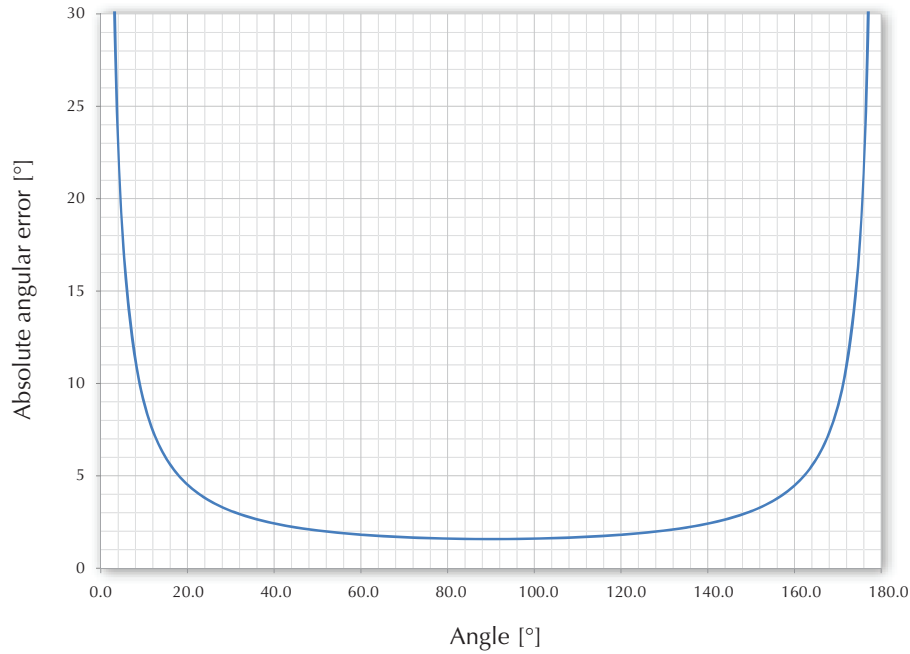


Figure 4.6: Plot showing the uncertainty of angular estimates $\Delta\beta$, varying with the angle β .

given by Coppens (1981) was used for uncertainty calculations. The formula for speed of sound in water which uses the depth D , temperature T and salinity S as input parameters is as follows:

$$\begin{aligned}
 v = & 1449.05 + 4.57T - 0.0521T^2 + 2.3 \times 10^{-4}T^3 + \\
 & (1.333 + 0.0126T + 9.0 \times 10^{-5}T^2)(S - 35) + (0.1623 + 2.53 \times 10^{-4}T)D + \\
 & (2.13 + 0.1T) - 5D^2 + (0.016 + 2.0 \times 10^{-4}(S - 35))(S - 35) \times 10^{-4}TD
 \end{aligned} \tag{4.24}$$

The speed of sound is obtained in meters per second when units for temperature, depth and salinity are degrees Celsius ($^{\circ}\text{C}$), meters (m) and parts per thousand (ppt) respectively. The standard error for speed of sound calculated using this formula is 0.1 ms^{-1} . While the nine term equation given by Mackenzie (1981) has a lower standard error of 0.07 ms^{-1} , it is only valid for salinities between 25ppt to 40ppt. The formula given above is valid from 0ppt to 42ppt and this range includes the nominal salinity of 0.5ppt for freshwater in which the ensuing experiments were carried out. By considering the value of Δv to be 0.1 ms^{-1} and the calculated¹ speed of sound in water to be 1497 ms^{-1} , the contribution of terms associated with Δv in the uncertainty formulae can therefore be considered negligible as well. Ignoring the terms with Δd , Δf_s and Δv the uncertainty for β can be expressed as follows:

$$\Delta\beta = \pm \frac{v\Delta\tau}{f_s d \sin\beta} \tag{4.25}$$

¹. The input parameters used were $D = 1.0\text{m}$, $T = 25^{\circ}\text{C}$ and $S = 0.5\text{ppt}$.

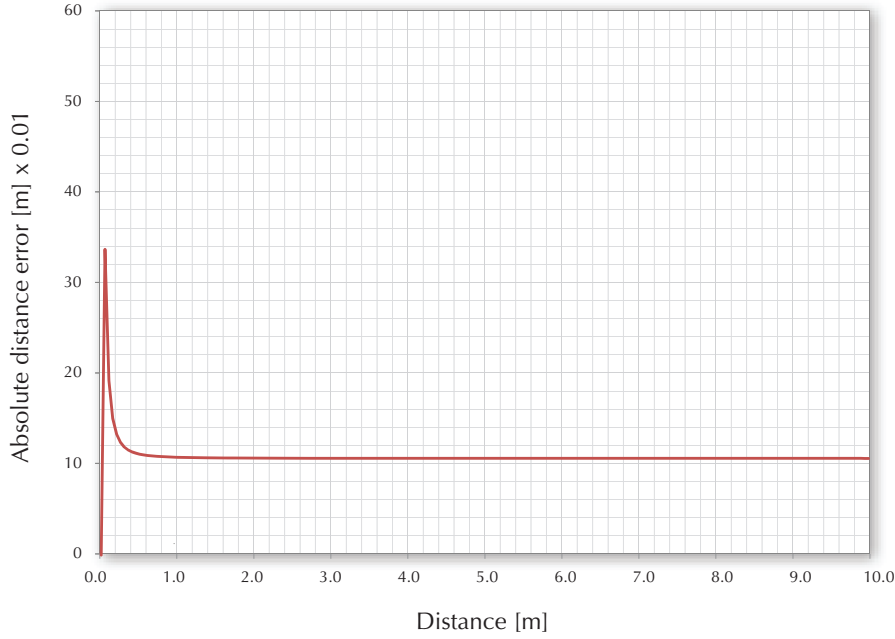


Figure 4.7: Plot showing how uncertainty in distance estimates Δr_1 is related to the distance r_1 . The uncertainty remains constant for distances where $r_1 > d$ is satisfied.

while the uncertainty for r_1 can be expressed as follows:

$$\Delta r_1 = \pm \frac{v}{2f_s r_1} \sqrt{2(\Delta \tau^2 + \Delta \tau_L^2) \left(r_1^2 + \left(\frac{d}{2} \right)^2 \right)} \quad (4.26)$$

These formulae shows how the uncertainties associated with the basic sample-domain delay measurements and timing jitter propagates to the estimated quantity. They also show the relationship between uncertainties associated with estimates and the estimates themselves and other constant quantities¹. The terms Δd , Δf_s and Δv that were ignored due to their negligible contributions to (4.21) and (4.22), represented the random measurement errors and do not account for any bias in these quantities assumed to be constant. Furthermore, it shows both estimate uncertainties reduce in magnitude with a higher sampling rate f_s , the only constant that can be arbitrarily chosen within constraints².

The uncertainties given by (4.26) and (4.25) were plotted against distance and angle respectively by substituting typical values for the constant parameters d , f_s , v , setting $\Delta \tau = 0.5$ and $\Delta \tau_L = 9.6$. This value for sample domain synchronisation timing jitter (equivalent to a

¹ The constant assumptions hold for the speed of sound in water and the sampling rate considering the relatively short distances travelled by the acoustic signals and the short sampling duration of the pings.

² Lower limit is governed by the required frequency bandwidth of the source signals and the upper limit governed by the available processing capacity.

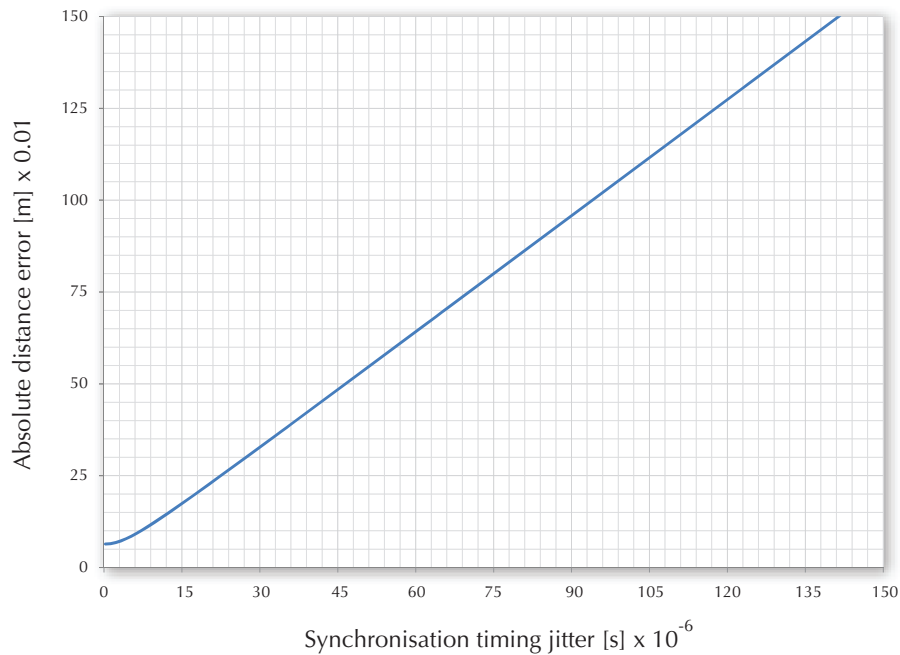


Figure 4.8: Plot showing how uncertainty in distance estimates Δr_1 is related to synchronisation timing jitter Δt_L for $r_1 = 5.0\text{m}$.

synchronisation timing jitter of $\Delta t_L = 0.0001\text{s}$) is considered nominal based upon experimentally measured values given later in section 6.2 of chapter 6.

The angular uncertainty is independent of the source distance but as seen from figure 4.6, it changes with angle giving the smallest uncertainty close to 90° . The errors rapidly increase as the angle approach either 0° or 180° . This corresponds to P_1 being aligned with the two receivers at H_1, H_2 .

By observing the plot in figure 4.7, it can be seen that the distance uncertainty does not depend on the distance when $r_1 > d$. This condition is satisfied in the physical implementation of the localisation system and therefore it can be considered that the uncertainty in distance is invariant with the distance measured within the sensing range of the system.

Figure 4.8 plots the variation of the distance uncertainty against synchronisation timing jitter for $r_1 = 5.0\text{m}$. Beyond extremely small jitter values ($\Delta t_L \geq 5.0 \times 10^{-6}\text{s}$) the relation between these quantities tends to be linear.

4.3.2 Sub-sample interpolation

Both the uncertainties for distance and angle estimates derived in the previous sections depend on the quantity $\Delta\tau$. This measurement error in the sample-domain remains at 0.5 regardless of the sampling frequency used. A reduction of this value is desirable to minimise its contribution

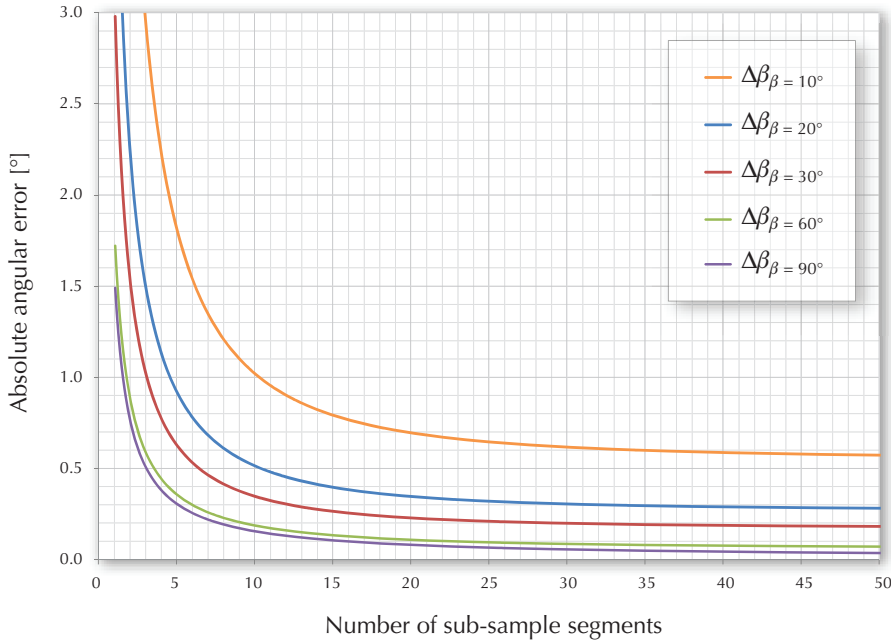


Figure 4.9: Variation of angular uncertainty $\Delta\beta$ with the number of sub-sample interpolation points n_{int} for different values of β .

to the random errors in the estimates which ultimately leads to improving the precision of the estimation system.

A sub-sample interpolation scheme¹ is used in the relative localisation system where the process of finding τ_0 , the value which maximise the cross-correlation function according to (4.9) is done in two steps. First, a simple search finds the maximum value of the sample sequence $R_{s_1 s_2}$ and its corresponding sample index. This index is then used to do a more refined search in the neighbourhood on either side of this point using a cubic spline interpolation routine, which subdivides each sample interval in to n_{int} segments. This has the same effect as increasing the sampling frequency by a factor of n_{int} , where $n_{int} = 1$ means no sub-sample interpolation. This term relates to $\Delta\tau$ as:

$$\Delta\tau = 1/2n_{int} \quad (4.27)$$

Just as for the sampling frequency f_s , increasing the number of sub-sample interpolation segments n_{int} , improves the performance of the estimation. Plots in figure 4.9 show how the angular uncertainty $\Delta\beta$ varies with an increasing number of sub-sample interpolation points at multiple values for β . Figure 4.10 shows plots of Δr_1 varying with n_{int} for multiple values of r_1 . Nevertheless, this parameter cannot be arbitrarily increased due to the higher processing overheads it adds to the relative localisation system. As a compromise, $n_{int} = 10$ is used by the

¹. Sub-sample interpolation to avoid sample-interval round-off when detecting the cross-correlation peak using various interpolation routines is mentioned in work presented by Reeder et al. (2004) and Baker et al. (2005a).

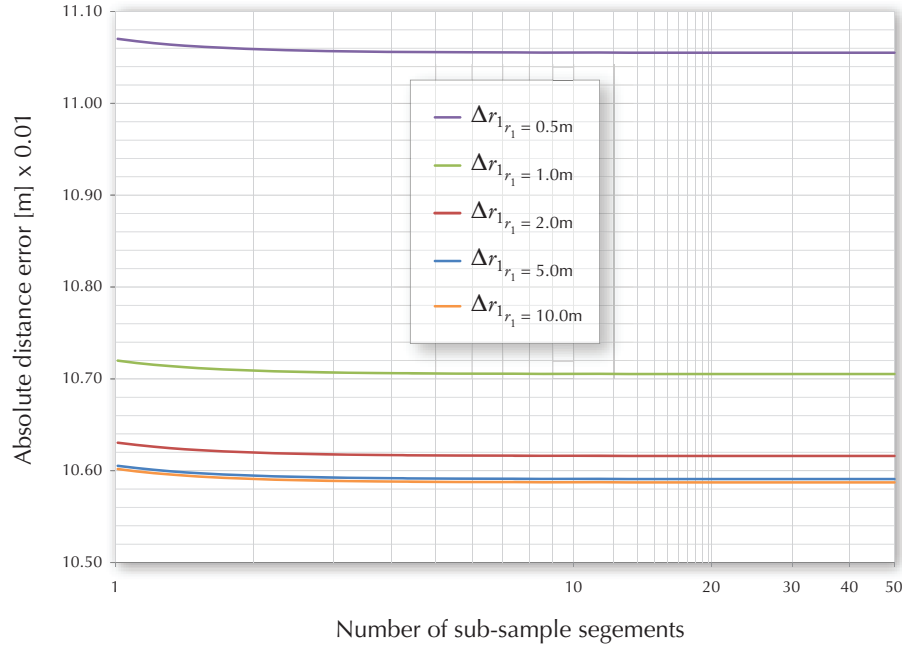


Figure 4.10: Variation of uncertainty in distance Δr_1 with n_{int} for different values of r_1 .

relative localisation system to improve the performance of the system. According to the plots shown in figures 4.9 and 4.10, increasing n_{int} beyond 10 does not yield a substantial improvement in the uncertainty to justify the additional processing cost. By changing the value of n_{int} from 1 to 10, with a sampling frequency $f_s = 96000$ kHz, the best and worst average¹ absolute uncertainty for angle estimation is improved from 1.49° to 0.14° and 4.85° to 1.07° . The best values correspond to angles close to 90° and worst is in the vicinity of 0° and 180° .

The resolution of an estimate is the smallest measurable change, *i.e.* the minimum ‘reading’ of the estimation system which can also be defined as twice the measurement error. The absolute angular resolution $\rho\beta$ can also be calculated as follows:

$$\rho\beta = \left| \beta - \tan^{-1*} \left(\sqrt{\frac{1 + \tan^2\beta}{(1 - 2v\Delta\tau\sqrt{1 + \tan^2\beta}/f_s d)^2} - 1} \right) \right| \quad (4.28)$$

where

$$\tan^{-1*}(\cdot) = \begin{cases} \tan^{-1}(\cdot), & \beta < 90^\circ \\ 180^\circ - \tan^{-1}(\cdot), & \beta \geq 90^\circ \end{cases} \quad (4.29)$$

¹. The average for minimum (best) errors was calculated using four points around 90° with $\tau_0 = 0, 1, 2, 3$ for $n_{int} = 1$ and with $\tau_0 = 0, 0.1, 0.2, 0.3$ for $n_{int} = 10$ using (4.3), (4.12) and (4.25). Due to symmetry around 90° , only positive lags were considered. The average for maximum (worst) errors was calculated using four points around 180° with $\tau_0 = 16, 17, 18, 19$ for $n_{int} = 1$ and with $\tau_0 = 18.8, 18.9, 19.0, 19.1$ for $n_{int} = 10$.

This $\tan^{-1}(\cdot)$ function expands the range of the inverse tangent function from $0^\circ \rightarrow 90^\circ$ to $-90^\circ \rightarrow 90^\circ$.

The angular resolution as calculated by (4.28) can be explained as the difference between two adjacent angular estimates. By selecting $n_{Int} = 10$, the average¹ resolving power of the relative localisation improves from 2.98° to 0.29° and from 9.71° to 2.14° for angular measurements (for best and worst conditions mentioned earlier) and from $11.0 \times 10^{-3} \text{ m}$ to $3.2 \times 10^{-3} \text{ m}$ for distance measurements². The increase in resolution reduces quantization effects which otherwise affects the output of the relative localisation system. This directly contributes to the higher precision of estimates shown by the experimental results presented later in chapter 7.

4.4 Relative localisation of an AUV

Previous sections focused on how acoustic source localisation concepts can be utilised to produce an angle and a distance to an acoustic source. The sources of uncertainty of estimates were identified and analysed and a scheme for improving the resolution and precision of the estimates was also presented. In the relative localisation system being presented in this thesis, an acoustic

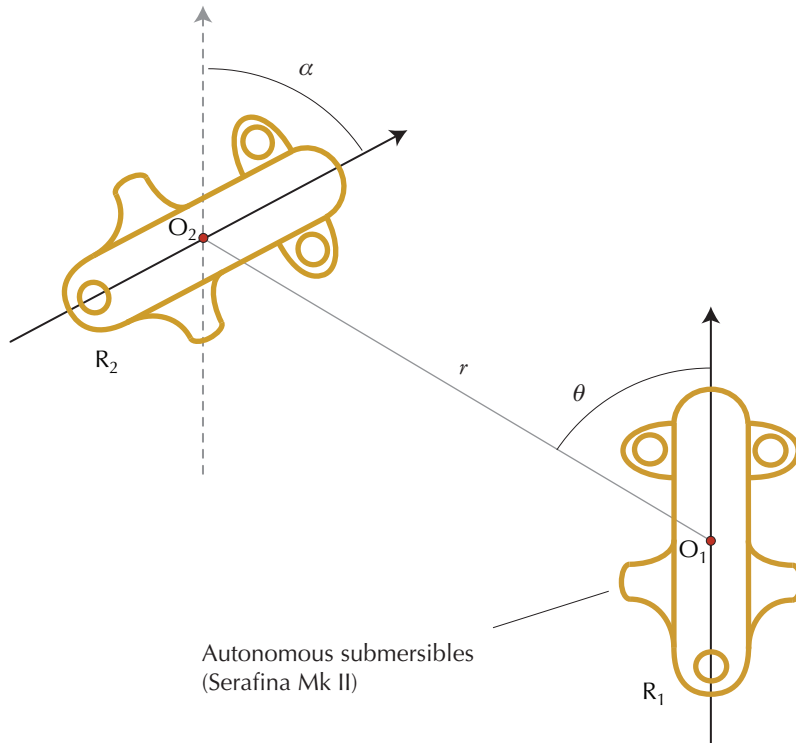


Figure 4.11: Azimuth θ , range r and heading α of sending AUV R_2 with respect to the observing AUV R_1 .

¹ Using the three differences between each of the four points selected to calculate the average best and worst errors.

² Under ideal synchronisation conditions with zero time-jitter.

sending event consists of two pings emitted by the sender AUV, first from the bow end and the next from the stern end. Observer AUVs which have the sender within their sensing range would estimate the angle and the distance to each of the two sources upon receiving the acoustic pings, resulting in two sub-azimuth and four sub-range estimates. These are then used to derive the compound localisation estimates of azimuth θ , range r and heading α of the sender relative to each of their *body-fixed* coordinate frames of the observers. Figure 4.11 illustrates these compound estimates when considering one observer AUV (R_1) and a sender AUV (R_2). The measuring conventions, the derivation and uncertainty analyses of these quantities are presented in the subsequent sections.

4.4.1 Measuring conventions and ranges

Figure 4.11 illustrates AUV labelled R_1 (observer) measuring the azimuth, range and heading of AUV R_2 (sender). These relative measurements are based upon a polar coordinate system fixed on R_1 . The pole O_1 is at the center of the AUV coinciding with the center of buoyancy and the polar axis runs across the pole along the center line of the vehicle, pointing towards the bow end.

Azimuth

The azimuth θ is the angle between the line O_1O_2 and the polar axis on R_1 . This quantity, with a range of $-180^\circ < \theta \leq 180^\circ$ is measured as positive clockwise and as negative counter-clockwise from the polar axis. For example, if R_2 was directly ahead of R_1 , the azimuth would be 0° and if R_2 was in parallel alongside R_1 either on port side or starboard side would result in an azimuth of 90° or -90° respectively.

Range

The range r is a positive scalar quantity which gives the Euclidean distance between the poles O_1 and O_2 , of the coordinate systems fixed on the observer (R_1) and sender (R_2). Even though the subsequent formula used to derive the range allows this quantity to be zero, in practise it is strictly greater than zero due to the physical size of the AUVs as can be seen from the diagram in figure 4.11.

Heading

The heading α is the relative rotation angle between the polar axes of R_1 and R_2 , measured with respect to the observer, R_1 . As depicted in figure 4.11, it can be seen as translating the coordinate system of R_1 on to R_2 , such that the two poles coincide and then measure the angle between the two polar axes. Similar to the azimuth, the heading has a range of $-180^\circ < \alpha \leq 180^\circ$ and is measured positive and negative for clock-wise and counter-clock-wise rotations respectively. That is,

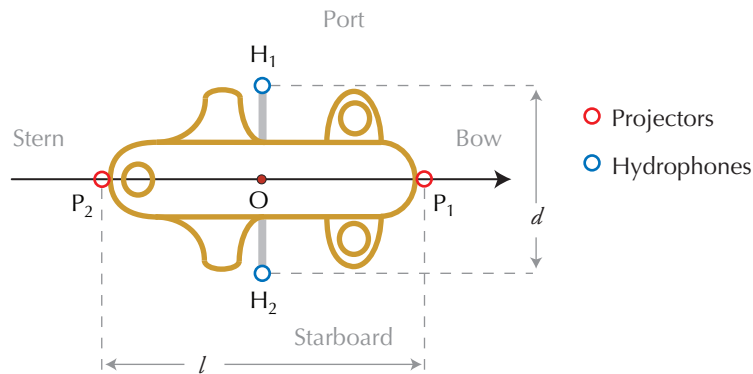


Figure 4.12: Hydrophones H_1 and H_2 are positioned on the port and starboard sides while projectors P_1 and P_2 are positioned on the bow and stern ends of Serafina AUV hulls. The diagram illustrates a top view.

for whatever azimuth if the two AUVs are travelling (or pointing) in the same direction (same heading), then the relative heading of R_2 measured by R_1 would be 0° .

The relative behaviour of the two AUVs R_1 and R_2 can be interpreted using the azimuth and heading as follows; if the azimuth and heading of R_2 measured by R_1 is the same ($\alpha = \theta$), then R_2 is pointed away from R_1 (heading directly away, if in motion *i.e.* the range r is increasing) and if the two quantities are separated by 180° ($\alpha = -\theta$), then R_2 is pointed at R_1 (heading directly towards, if in motion *i.e.* range r is decreasing).

4.4.2 Transducer placement

Chapter 4 described and explained how TDOAs and TOFs of acoustically transmitted MLS signals are used to measure angles and distances to a sound source. The following sections will describe how these measurements are incorporated into the relative localisation system to produce azimuth, range and heading estimates. Figure 4.12 shows the mounting configuration of hydrophones and projectors on a hull of a Serafina Mk II class AUV (Serafina website, 2009) and how it corresponds with the sender and receiver positions P_1 , P_2 and H_1 , H_2 mentioned in chapter 4. The hydrophone spacing d is set to 0.3m and projector spacing l is set to 0.5m, based on the physical size of the AUV hull. The pole of the coordinate frame O lies at the intersection of two lines H_1H_2 and P_1P_2 and the polar axis is along the center line of the AUV which goes through the projectors P_1 and P_2 and points towards the bow end of the vehicle. This configuration of hydrophone and projector placement is further illustrated in chapter 6 which explains the experimental setup.

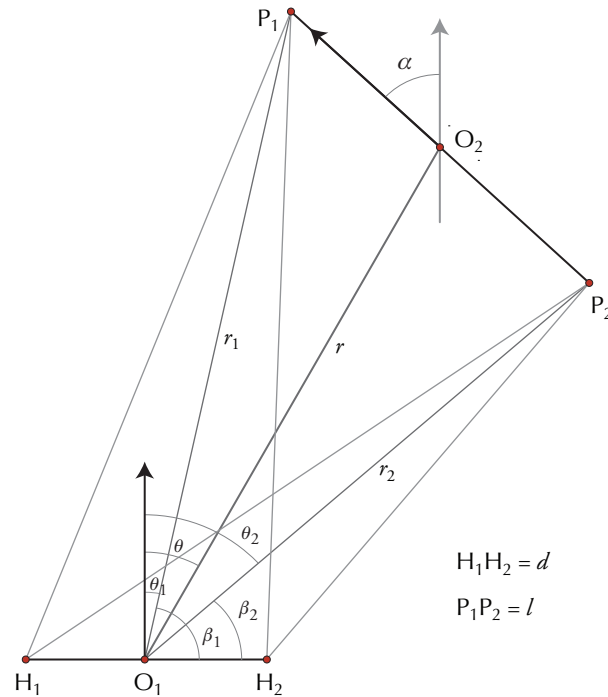


Figure 4.13: The geometric description of the angles and distances used to calculate the components of the pose vector, azimuth θ , range r and heading α . Here θ_1 and θ_2 are sub-azimuths while r_1 and r_2 are sub-ranges.

4.4.3 Geometric description

Figure 4.13 shows a geometrical abstraction of two vehicles, the sender with its two projectors P_1 and P_2 and the observer with its two hydrophones H_1 and H_2 . O_1 and O_2 represent the poles of the body fixed polar coordinate frames of the observer and the sender respectively. The azimuth, range and heading of the sender, relative to the observer is given by θ , r and α . As explained in the previous chapter, emission of two MLS signal pings constitutes a sending event. These pings are emitted from the projectors P_1 and P_2 , first from the bow end (P_1) then the stern end (P_2) of the sender AUV. Each of these signals are received by two hydrophones H_1 and H_2 mounted on port and starboard sides of the observer AUV.

Azimuth

According to the diagram in figure 4.13 and the definition given in section 4.4, the azimuth θ is the angle between the polar axis going through O_1 and the line O_1O_2 . However, according to the source localisation scheme given in chapter 4, the angles are measured to the actual sound sources, and with regard to the diagram the sources are at P_1 and P_2 . The angle measurement

using TDOA gives β_1 and β_2 corresponding to the angles which the lines P_1O_1 and P_2O_2 makes with H_1H_2 using (4.3) as follows:

$$\beta_i = \tan^{-1}\left(\frac{\sqrt{d^2 - \delta_i^2}}{\delta_i}\right), i = 1, 2 \quad (4.30)$$

where d is the base distance between the hydrophones H_1 and H_2 . δ_1 and δ_2 are the acoustic path length differences calculated according to (4.12), based on the two TDOAs corresponding to the two MLS signals emitted from P_1 and P_2 . According to the measurement convention given in section 4.4, the two angles returned by (4.30) need to be transformed to θ_1 and θ_2 which are measured against the polar axis instead of the line H_1H_2 . This transformation is given by:

$$\theta_i = [90^\circ - \beta_i]_{adj}, i = 1, 2 \quad (4.31)$$

where the adjustment function $[]_{adj}$ is defined as:

$$[x]_{adj} = \begin{cases} x, & -180^\circ < x \leq 180^\circ \\ \text{sgn}(x)(|x| - 360^\circ), & x \leq -180^\circ, x > 180^\circ \end{cases} \quad (4.32)$$

which return the angles conforming to the measuring convention.

This adjustment is required since (4.3) produces β_i with the range $-180^\circ < \beta_i \leq 180^\circ$ when implemented with the $\tan^{-1}(x, y)$ function which considers the quadrant of the complex value $x + iy$ where $y/x = \tan\beta$. However, in the experimental implementation of the relative localisation system, the range of (4.3) was limited to $0^\circ \leq \beta_i \leq 180^\circ$ due to the directivity of the hydrophones used as explained in section 4.1.1.

The two angular measurements θ_1 and θ_2 obtained from (4.31) are combined to produce the azimuth estimate θ according to the geometry of the diagram in figure 4.13 as follows:

$$\theta = \frac{\theta_1 + \theta_2}{2} \quad (4.33)$$

Range

According to figure 4.13 the range r , which is the Euclidean distance between the poles of the coordinate frames fixed to the sender and observer vehicles, is given as the length of line O_1O_2 . However, as with the azimuth measurement, the actual measurements are the distances to the sound sources P_1 and P_2 from each of the receivers H_1 and H_2 . If P_1H_1 , P_1H_2 are denoted as r_{11} , r_{12} , and P_2H_1 , P_2H_2 as r_{21} , r_{22} the distances r_1 (P_1O_1) and r_2 (P_2O_1) can be calculated using (4.18) based on the TOF measurements given in chapter 4 as follows:

$$r_i = \sqrt{\frac{r_{i1}^2 + r_{i2}^2}{2} - \left(\frac{d}{2}\right)^2}, i = 1, 2 \quad (4.34)$$

where d is the distance between hydrophones on the observer vehicle. Once r_1 and r_2 are calculated, the range r can be calculated using the formula:

$$r = \sqrt{\frac{r_1^2 + r_2^2}{2} - \left(\frac{l}{2}\right)^2} \quad (4.35)$$

where l is the separation between the projectors on the sender vehicle.

Heading

The relative heading α of the sender vehicle as seen by the observer vehicle can be estimated with the aid of the component measurements θ_1 , θ_2 , r_1 and r_2 used earlier to derive the azimuth and the range. The range adjusted heading can be expressed as:

$$\alpha = \left[\tan^{-1} \left(\frac{r_1 \sin \theta_1 - r_2 \sin \theta_2}{r_1 \cos \theta_1 - r_2 \cos \theta_2} \right) \right]_{adj} \quad (4.36)$$

where the θ_i values are given by (4.31) with the range $-180^\circ < \theta_i \leq 180^\circ$ and r_i values are given by (4.34). The adjustment function is the same as given in (4.32). While $r_1, r_2 \geq 0$, by inspecting figure 4.13 it is also clear that they cannot both be zero at the same time given the constraint $l > d$ which holds true in practise.

As with the azimuth calculation given previously in the current section, the returned α value has a range of $-180^\circ < \alpha \leq 180^\circ$ when implemented with the $\tan^{-1}(x, y)$ function which considers the quadrant of the complex value $x + iy$ where $y/x = \tan \alpha$.

4.4.4 Reverse hyperbolic localisation

The azimuth estimation presented in the previous sections is based on hyperbolic localisation (TDOA measurement) schemes while the range estimation is based on spherical localisation (TOF measurement) schemes. Overall, the source localisation presented can be viewed as a hybrid approach. The heading estimation relies on the azimuth and range as shown by (4.36). However, the range estimation and the subsequent heading estimation requires implicit synchronisation between the sender and observer as with traditional TOF based spherical localisation schemes. This synchronisation provided by the underlying communication scheduling system enables the relative localisation system to measure TOF as described in section 4.2.

With the two sound sources at P_1, P_2 and the two receivers at H_1, H_2 , a novel reverse hyperbolic scheme was devised to calculate the range and heading which does not require a TOF measurement, consequently eliminating the dependence on sender-observer synchronisation.

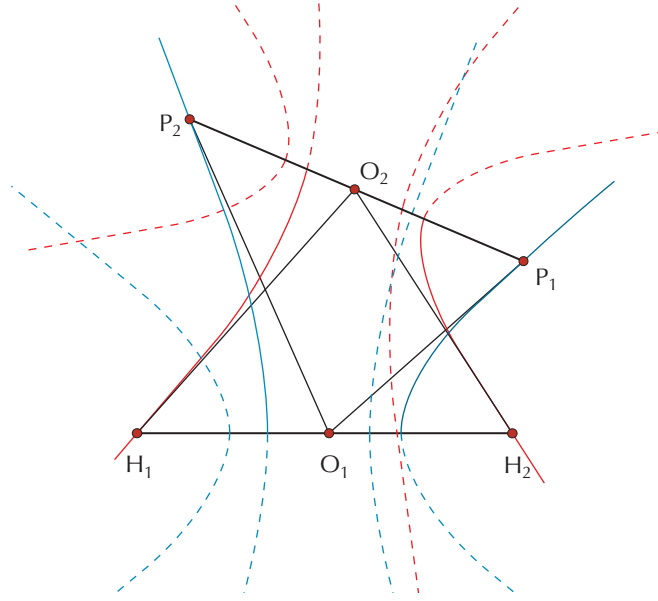


Figure 4.14: The two hyperbolae centred on P_1, P_2 depicted in red and the hyperbolae centred on H_1, H_2 shown in blue.

Reverse azimuth estimation

The acoustic path length differences δ_1 ($P_1H_1 - P_1H_2$) and δ_2 ($P_2H_1 - P_2H_2$) mentioned in section were based on the two hyperbolae centred on H_1 and H_2 corresponding to the two acoustic sources at P_1 and P_2 . By considering two more path length differences denoted by η_1 and η_2 which are equivalent to the quantities $P_1H_1 - P_2H_1$ and $P_1H_2 - P_2H_2$, two additional hyperbolae centred on P_1 and P_2 can be realised. The diagram in figure 4.14 depicts the two hyperbolae centred on H_1, H_2 in blue and the two hyperbolae centred on P_1, P_2 in red.

The observer vehicle receives four acoustic signal channels for each sending event. They comprise of two channels received by the hydrophones H_1, H_2 with P_1 as the source, denoted by $x_{11}(t)$, $x_{12}(t)$ and the two channels received with P_2 as the source denoted by $x_{21}(t)$, $x_{22}(t)$. The values for δ_1 and δ_2 were obtained from (4.12) after performing cross-correlation as described in section 4.1.2 on the channel pairs $x_{11}(t)$, $x_{12}(t)$ and $x_{21}(t)$, $x_{22}(t)$ respectively. Similarly, cross-correlating channel pairs $x_{11}(t)$, $x_{21}(t)$ and $x_{12}(t)$, $x_{22}(t)$ would give the corresponding sample-domain delays which can be converted to the required path length differences η_1 and η_2 using the following modified version of (4.12):

$$\eta_i = \frac{\tau'_{0i} v}{f_s}, \quad i = 1, 2 \quad (4.37)$$

where v is the speed of sound underwater, f_s the sampling frequency of the analogue to digital converter and τ'_{01}, τ'_{02} the sample-domain delays that maximise the respective cross-correlation

functions. Just as β_1 and β_2 defined the angles P_1O_1 and P_2O_1 made with H_1H_2 , two new angles φ_1 and φ_2 can be defined as the angles H_1O_2 and H_2O_2 makes with P_1P_2 . These two angles can be obtained from a slightly modified version of (4.30) using the path length differences η_1 and η_2 as follows:

$$\varphi_i = \text{sgn}^*(\theta_2 - \theta_1) \tan^{-1} \left(\frac{\sqrt{l^2 - \eta_i^2}}{\eta_i} \right), \quad i = 1, 2 \quad (4.38)$$

where l is the separation between the two projectors P_1, P_2 and the modified sign function is defined as:

$$\text{sgn}^*(y) = \begin{cases} \frac{y}{|y|}, & |y| > 0 \\ 1, & y = 0 \end{cases} \quad (4.39)$$

The angles returned from (4.38) has the range $-180^\circ < \varphi_1, \varphi_2 \leq 180^\circ$ and can be combined to produce the angle φ as:

$$\varphi = \frac{\varphi_1 + \varphi_2}{2} \quad (4.40)$$

This angle φ can be identified as the reverse azimuth of the sender vehicle or the azimuth of the observer relative to the sender vehicle. The geometry of these quantities along with the measuring convention is shown in figure 4.15.

Heading and range estimates based on reverse azimuth

According to the geometry shown in figure 4.15, an alternate relative heading (α') of the sender with respect to the observer vehicle can be given as:

$$\alpha' = [\varphi - \theta]_{adj} \quad (4.41)$$

The adjustment function is the same as given in (4.32). The azimuth θ is as given by (4.33).

A new calculation for range based on the reverse azimuth φ and α' derived above yields r' as follows:

$$r' = \left| \frac{d \cos(\varphi_1 + \alpha')}{2 \sin(\theta - (\varphi_1 + \alpha'))} \right| \quad (4.42)$$

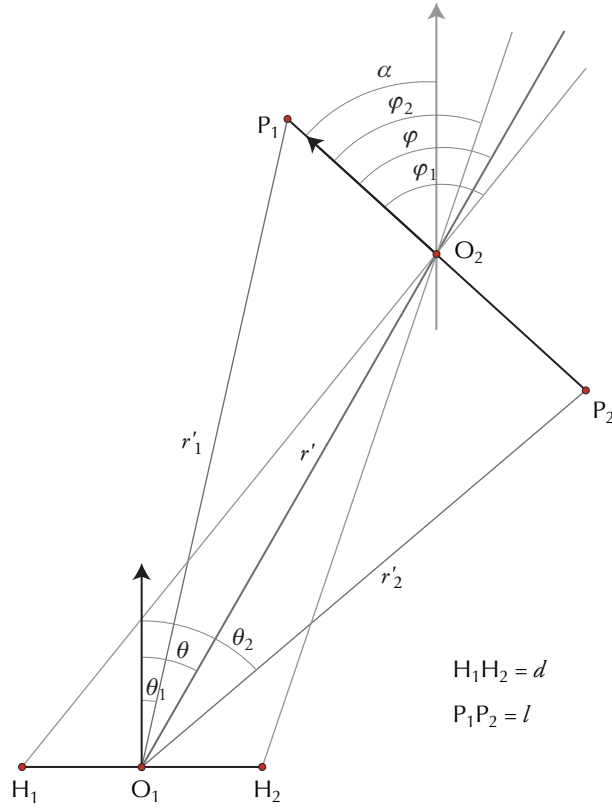


Figure 4.15: The geometric description of the new angles φ_1 , φ_2 , φ and their relationship to azimuth θ and alternate values for range r and heading α' .

where d is the base distance between the hydrophones H_1 , H_2 . The other variables have the ranges $-180^\circ < \varphi_1, \alpha', \theta \leq 180^\circ$. As explained earlier in section 4.4.1, even though (4.42) allows for r' to be zero, in practise it is always strictly greater than zero.

As these alternate calculations are based on two hyperbolas, each with foci at P_1 and P_2 , considering their asymptotes which pass through H_1 and H_2 , substituting these points in the polar coordinate equations for O_2H_1 and O_2H_2 and adjusting for the measuring conventions, the separate range components can be calculated using the following formula:

$$r'_i = \left| r' \cos(\theta_1 - \theta) \pm \operatorname{sgn}^*(\alpha') \operatorname{sgn}^*(\theta) \sqrt{r'^2 \cos^2(\theta_1 - \theta) - \left(r'^2 - \left(\frac{l}{2}\right)^2\right)} \right|, i = 1, 2 \quad (4.43)$$

where the '+' sign yield r'_1 and the '-' sign yield r'_2 . The variables have the following ranges; $r', l > 0$, $-180^\circ < \theta_1, \alpha', \theta \leq 180^\circ$ and the modified sign function is as defined in (4.39). The sign functions are used in this formula to resolve the ambiguity introduced by the existence of two asymptotes per hyperbola mentioned earlier.

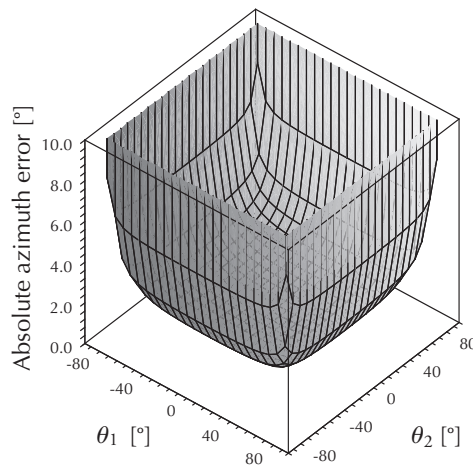


Figure 4.16: Variation of $|\Delta\theta|$ as the sub-azimuths θ_1 and θ_2 varies between -90° and 90° .

Properties of alternate heading and range estimates

The alternate heading and range estimates obtained above do not require sender-observer synchronisation or any knowledge of the sending time of the acoustic signal. This is due to the calculations being purely based on TDOA measurements. This form of independence from the underlying scheduling system provides an additional level of redundancy and increases the robustness of the relative localisation system against synchronisation failures and timing drifts. This also facilitates a more fault tolerant outlier rejection scheme with two independent estimates for the range and heading.

However, in its current form, the independence from sender-observer synchronisation comes at a cost. The errors associated with the alternate range are greater than those of the direct estimation. On the other hand, the errors associated with the alternate heading are lower than its direct counterpart and these errors are not dependant on the range as with the case of the direct heading estimation. The errors and associated resolution of the direct and alternate estimates are discussed in the following sections.

4.4.5 Estimation errors and resolution

The previous chapter presented the uncertainties associated with the angle and distance estimates in (4.26) and (4.25). These angle and distance estimates were further developed earlier in this chapter to form the components of the pose vector; azimuth, range, heading and the alternate versions of range and heading.

Azimuth

By applying the transformation given in (4.31), the angular uncertainties given by (4.25) in the previous chapter can be expressed as:

$$\Delta\theta_i = \pm \frac{v\Delta\tau}{f_s d \cos\theta_i}, \quad i = 1, 2 \quad (4.44)$$

By applying the general error propagation formula to (4.33) and substituting for the sub-azimuths errors given above, the error for the main azimuth estimate is given as:

$$\Delta\theta = \pm \frac{v\Delta\tau}{2f_s d} \sqrt{\frac{1}{\cos^2\theta_1} + \frac{1}{\cos^2\theta_2}} \quad (4.45)$$

Typical values for v , f_s and d are substituted while using $\Delta\tau = 0.05$, which corresponds to a sub-sample segmentation of $n_{\text{int}} = 10$ as explained in section 4.3.2, to plot the absolute variation of $\Delta\theta$ as θ_1 and θ_2 spans the range $-90^\circ \rightarrow 90^\circ$. This plot is shown in figure 4.16. The error associated with azimuth is independent of the distance between the sender and the observer. The minimum errors are achieved around 0° for both the sub-azimuths and the cross-sections of this plot retains the shape described by the initial plot given in figure 4.6 with an offset of -90° along the x -axis due to (4.31). The resolution of the azimuth estimation follows a similar shape as the surface of the plot in figure 4.16 multiplied by a scaling factor of 2.0. This suggests that the estimation can resolve changes in azimuth of less than 1.0° for most of

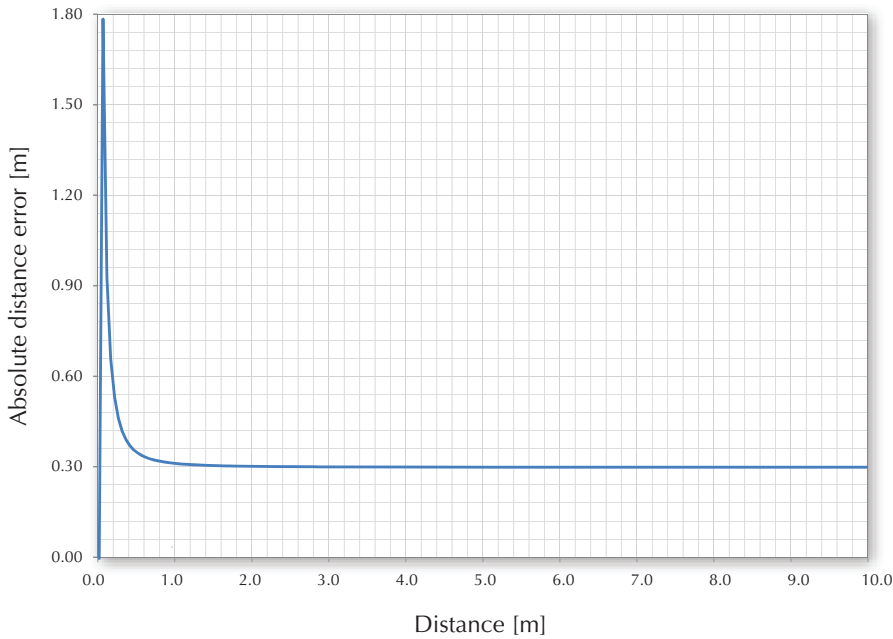


Figure 4.17: Variation of the absolute range error $|\Delta r|$ as the range r increases.

the θ_1 and θ_2 combinations, but performance trails off as either of the sub-azimuths approach $\pm 90^\circ$.

Range

The uncertainty for distance given by (4.26) in the previous chapter can be extended to both sub-ranges r_1 and r_2 as:

$$\Delta r_i = \pm \frac{v}{2f_s r_i} \sqrt{2(\Delta \tau^2 + \Delta \tau_L^2) \left(r_i^2 + \left(\frac{d}{2} \right)^2 \right)}, \quad i = 1, 2 \quad (4.46)$$

By applying the general error propagation formula to (4.35) and substituting Δr_1 and Δr_2 from (4.46) the estimation error for range can be derived by:

$$\Delta r = \pm \frac{v}{4f_s r} \sqrt{(\Delta \tau^2 + \Delta \tau_L^2)(4r^2 + l^2 + d^2)} \quad (4.47)$$

Despite the fact that r is used in the above equation, as the plot in figure 4.17 suggests, the absolute error in range Δr tends to be constant and independent of r for ranges satisfying $r > l$. As with the error in azimuth, this plot is obtained by substituting typical values to the parameters v , f_s , d and l in (4.47), using $\Delta \tau_L = 9.6$ and $\Delta \tau = 0.05$ corresponding to $n_{Int} = 10$. The initial spike shown in the plot is for ranges where $r < d$ which does not occur due to physical constraints of the system.

Accordingly the range estimates produced by the relative localisation system would have an upper error bound of $\pm 0.3\text{m}$ as suggested by the constant estimation error depicted in the plot. However, the experimental results presented in chapter 7 shows that the nominal errors are much

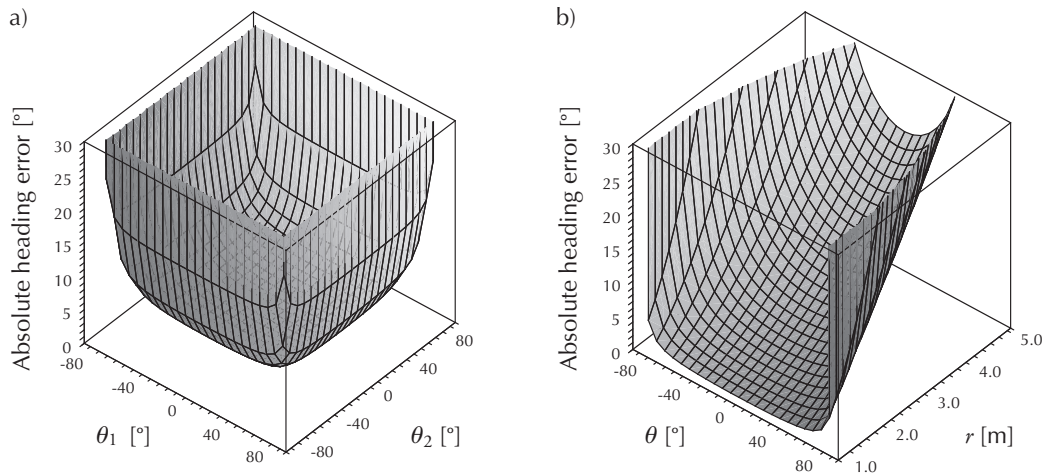


Figure 4.18: Variation of absolute error in heading $|\Delta \alpha|$; a) as sub-azimuths are varied while $r = 2.0\text{m}$, b) as azimuth and range are varied.

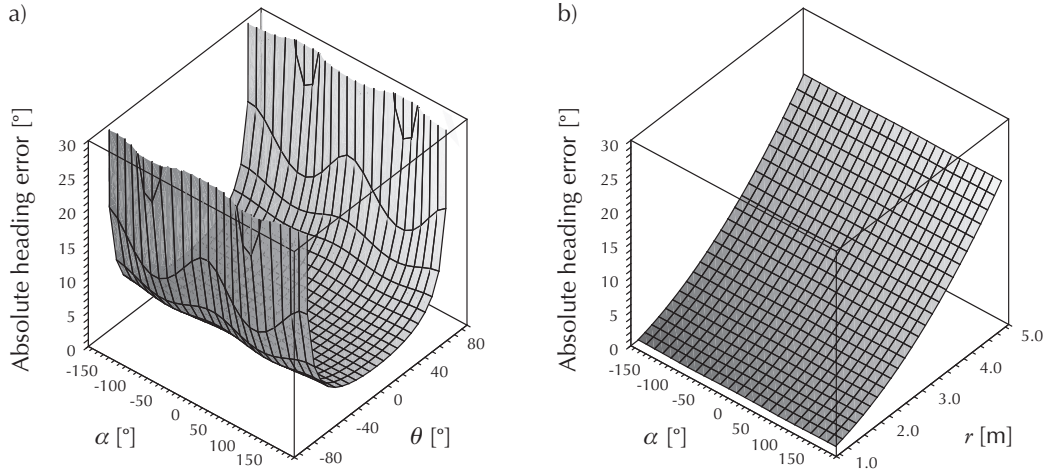


Figure 4.19: Variation of $|\Delta\alpha|$ a) as α and θ are varied at $r = 2.0\text{m}$, b) as α and r are varied with $\theta = 0^\circ$.

lower than this bound and the resolving power approaches $3.2 \times 10^{-3}\text{m}$, which is the value predicted in section 4.3.2 for zero-jitter conditions.

Heading

Unlike the azimuth and range which are independently estimated, the heading is a compound estimation based on both the sub-azimuths and sub-ranges as shown in (4.36). As a consequence, applying the general error propagation formula results in an error for the heading estimate which is related to all four quantities; θ_1 , θ_2 , r_1 and r_2 as:

$$\Delta\alpha = \pm \frac{v\Delta\tau}{f_s l^2} \sqrt{\frac{\sin^2(\theta_1 - \theta_2)}{8} \left[4(r_1^2 + r_2^2) + \frac{d^2}{r_1^2 r_2^2} (r_1^4 + r_2^4) \right] + \frac{1}{d^2} \left[\frac{(l^2 - r_2^2)^2}{\cos^2 \theta_1} + \frac{(l^2 - r_1^2)^2}{\cos^2 \theta_2} \right]} \quad (4.48)$$

The plots in figures 4.18 and 4.19 show the variation of $|\Delta\alpha|$ as two quantities are changed while the others are kept constant. By observing plots shown in figure 4.18.b and figure 4.19.b, it is apparent that the error in heading and subsequently the resolution of the heading estimate is very sensitive to the range, i.e. the distance between the sender and the observer. This predicts that the performance of the heading estimation would deteriorate with increasing range and would be unable to resolve heading changes of $\pm 45^\circ$ for ranges beyond 5.0m.

Alternate heading

The estimation error associated with the alternate calculation for heading given by (4.41) is

$$\Delta\alpha' = \pm \frac{v\Delta\tau}{2f_s} \sqrt{\frac{1}{d^2} \left(\frac{1}{\cos^2 \theta_1} + \frac{1}{\cos^2 \theta_2} \right) + \frac{1}{l^2} \left(\frac{1}{\sin^2 \varphi_1} + \frac{1}{\sin^2 \varphi_2} \right)} \quad (4.49)$$

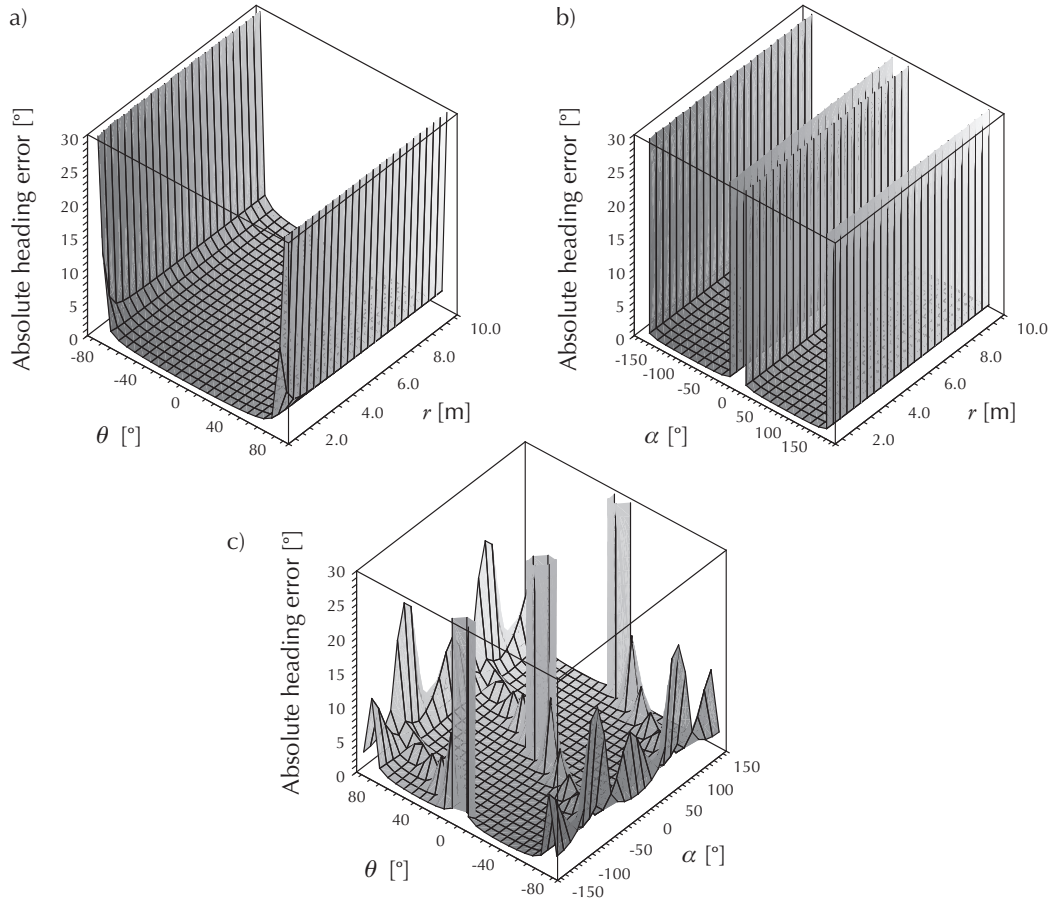


Figure 4.20: Variation of $|\Delta\alpha'|$ a) as r and θ are varied with $\alpha = 90^\circ$, b) as α and r are varied with $\theta = 0^\circ$ and c) as α and θ varied with $r = 2.0\text{m}$.

where φ_1 and φ_2 are the reverse sub-azimuths introduced in section . Figure 4.20 shows how $|\Delta\alpha'|$ varies with the pose vector components, θ , r and α , considering two at a time. It can be seen from plots b) and c) in figure 4.20 that the errors increase whenever $|\theta + \alpha| \approx 0^\circ, 180^\circ$. By inspecting the formula in (4.41), this condition corresponds to the reverse azimuth φ approaching 0° or 180° . Since the reverse azimuth errors behave similar to the azimuth errors explained earlier section 4.3 (before applying the adjustments given in (4.31)), the magnitude of the errors rapidly increases as $\varphi \rightarrow 0^\circ, 180^\circ$. However, these errors do not display the deterioration with increasing range as displayed by the direct heading estimation errors explained in the previous section. In fact, apart from the areas affected by the aforementioned condition related to the reverse azimuth, the alternate heading estimation errors remain invariant with increasing range. Furthermore, precisely knowing the behaviour of the error when $|\theta + \alpha| \approx 0^\circ, 180^\circ$ and being able to separately estimate θ and α (although with lower precision) allows the relative localisation system to gracefully handle this situation.

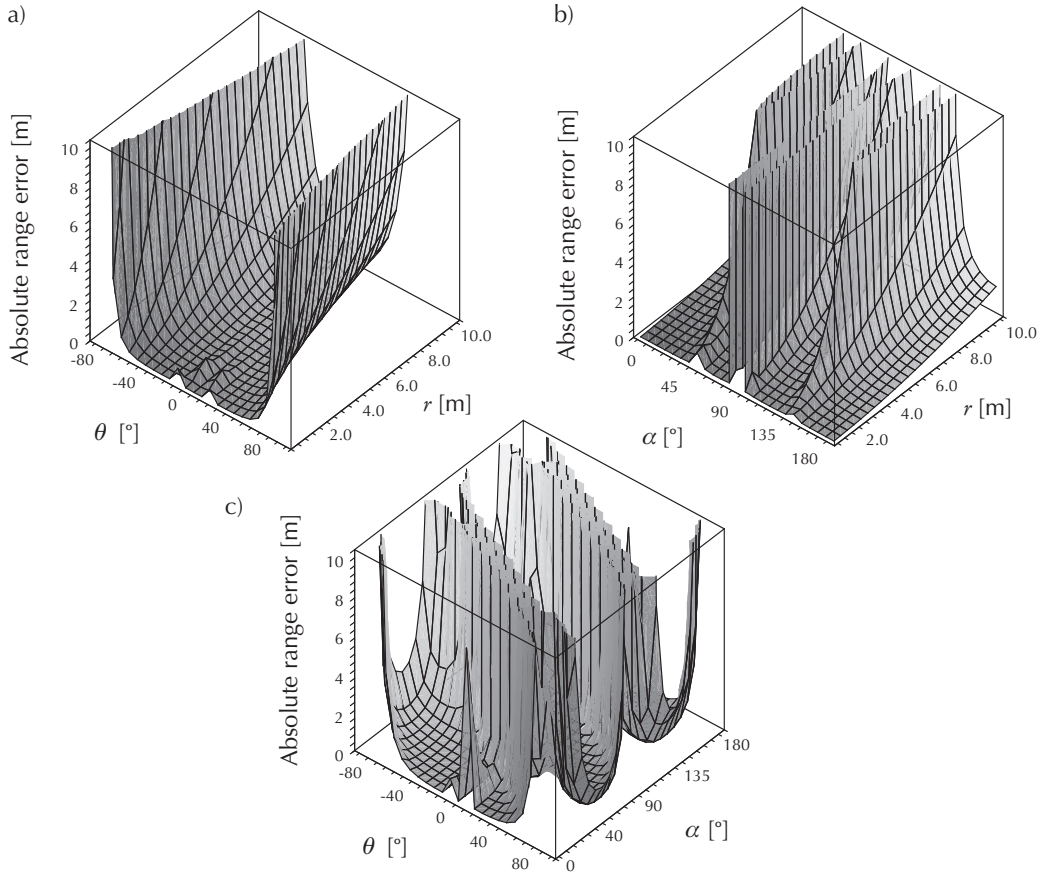


Figure 4.21: Variation of $|\Delta r'|$ a) as r and θ are varied with $\alpha = 0^\circ$, b) as α and r are varied with $\theta = 0^\circ$ and c) as α and θ varied with $r = 2.0\text{m}$.

Alternate range

Estimation error associated with the alternate range given by (4.42) can be stated as follows:

$$\Delta r' = \pm \frac{vr'\Delta\tau}{2f_s d} \sqrt{4\left(\frac{X}{l^2} + \frac{Y}{d^2}\right) \left(\frac{d + 2r' \sin((\theta_1 + \theta_2)/2)}{\sin(2(\varphi_1 + \alpha'))}\right)^2 + \frac{Y(4r'^2 - d^2 \cos^2(\varphi_1 + \alpha'))}{4d^2 \cos^2(\varphi_1 + \alpha')}} \quad (4.50)$$

where X and Y are:

$$X = \frac{5}{\sin^2 \varphi_1} + \frac{1}{\sin^2 \varphi_2}, \quad Y = \frac{1}{\cos^2 \theta_1} + \frac{1}{\cos^2 \theta_2} \quad (4.51)$$

As with the alternate heading, the absolute errors associated with the estimation of the alternate range are plotted in figure 4.21 as they vary with θ , r and α , considering two at a time while keeping the third quantity constant. Since the alternate range is coupled with the alternate heading, errors associated with these two quantities show similarity in behaviour. Therefore the condition $|\theta + \alpha| \approx 90^\circ$ causes the errors to increase. However, due to the structure of (4.50), the

plots in figure 4.21 show additional instabilities. Especially in plot b), the ridges increasing in height on either side of the $\alpha = 0^\circ$ uncertainty, can be traced to the individual uncertainties associated with the reverse sub-azimuths φ_1 and φ_2 which could reach 0° or 180° independent of φ . Once again, the knowledge of this behaviour and the ability to detect this condition by way of having access to φ_1 , φ_2 , θ and direct α estimates, the system can handle this situation with minimum degradation of overall system performance.

4.5 Discussion

This chapter described the methodology and techniques used in the measurement and estimation process which leads to the derivation of the compound estimates for azimuth, range and heading. In addition, an alternative scheme to estimate heading and short ranges without the need for sender-observer synchronisation was also presented. These quantities are used in assembling the pose vector which is described in chapter 5. Formulae of relationships between the component quantities and the uncertainty of the compound quantities were also derived. They give a statistical basis to analyse the behaviour of the system in the presence of random errors and provides theoretical bounds to the precision of the estimates. By inspecting these and the associated plots, it was shown that the uncertainties of azimuth, range and alternative heading estimates are independent of distance between the sender and the observers. However, as the sender position approaches the angular and radial sensing limits of the hydrophones on the observers, the resulting loss of SNR leads to deterioration of the estimation accuracy. This effect will be discussed along with strategies to handle such situations in chapter 5 with experimental evaluation presented in chapter 7. The uncertainty analysis reveals that the precision of compound estimates for direct heading and alternative range are severely affected as the sender-observer distance increases. The behaviour of these estimates are experimentally evaluated in chapter 7.

The following chapter explains the way in which the techniques and methodologies presented throughout this as well as the previous chapter are combined in developing the distributed relative localisation system. Furthermore, issues such as interference handling, outlier handling and computational complexity will also be addressed.

Chapter 5

The relative localisation system

This chapter will explain how the techniques and methodologies presented and described in previous chapters fuse together in building up the relative localisation system. Furthermore, the chapter will discuss how the relative localisation system can provide a distributed localisation solution for swarming of AUVs, while addressing issues such as interference handling, outlier handling and computational complexity.

The first section will present an overview of the functional components of the relative localisation system with regard to a single localisation event involving one sender-observer pair. The relationship between the relative localisation system and the underlying communication and scheduling system in terms of synchronisation and information flow will be explained in the context of distributed relative localisation in a swarm in the next section. It also expands on how multiple senders and observers are accommodated in the context of a local neighbourhood belonging to a larger swarm of AUVs. Effective sensing ranges and different update rates will also be introduced in this context.

In the following sections issues related to interference caused by delayed multipath arrivals, crosstalk due to multiple senders and effects of environmental noise on the acoustic localisation are discussed along with strategies to address them. In addition, the peak detection performance of

the cross-correlation scheme is experimentally evaluated in the presence of cross-talk due to multiple senders within a reverberant acoustic environment.

Subsequently, strategies of outlier handling utilised by the relative localisation system is presented along with a brief motivational background. The performance of the proposed **peak tracking** scheme is experimentally evaluated in comparison to a Kalman filter approach. Finally, the computational complexity of the system is discussed along with a **range tracking** scheme which is proposed to overcome the problem of increasing computational cost as the effective sensing range increases.

5.1 System overview

The previous chapter gave detailed explanations as to how each of the localisation estimates are calculated and also a description of the associated errors and their behaviour. Furthermore, an alternate method for estimating the heading and range was introduced by way of the reverse hyperbolic localisation concept. The localisation estimates are assembled into a pose vector (section 5.2.1) which is the output of the localisation system. The block diagram in figure 5.1 gives the functional components of the relative localisation system while depicting the flow of

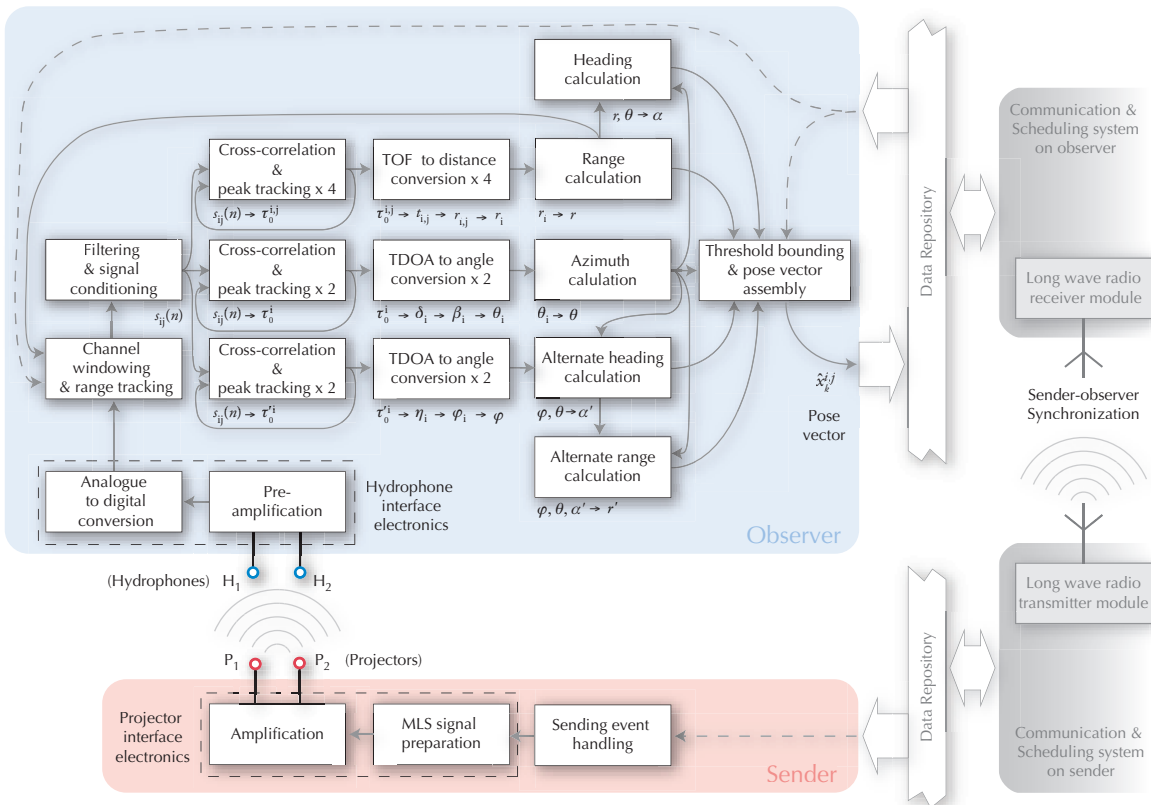


Figure 5.1: Block diagram showing main modules and components of the relative localisation system.

information from the acoustic pings received by the hydrophones to the final pose vector assembly. Specific hardware and software modules used in the experimental implementation of the system are described in chapter 6 while overviews of the main components of the information flow are explained in the following sections.

Acoustic signal reception and preparation

The main external inputs to the system are provided via the hydrophones which receive the MLS pings transmitted by the sender. The received signals are first pre-amplified and converted to two digital audio channels by analogue to digital converters. Once in digital form, the channels are ‘windowed’ in to finite length segments. The length N of the channel window in sample space is related to the sampling frequency of the analogue to digital converters f_s , the speed of sound underwater v , length of the MLS ping l_{MLS} and the maximum effective range of the localisation system r_{max} , introduced later in section 5.2.3. This length can be given as:

$$N = r_{max} \left(\frac{f_s}{v} \right) + l_{MLS} \quad (5.1)$$

The two separate pings emitted by projectors P_1 and P_2 of the sender which constitute a sending event, are separated in time by t_{FB} to avoid interference. Therefore, the channel windowing module assembles two length N signal segments, each with two channels corresponding to the two hydrophones H_1 and H_2 . The start of a sending event is signalled to the channel windowing module via the long-wave radio receiver module, which is part of the communication and scheduling system residing on the observer, as soon as it receives a message from a sender. Therefore, the beginning of the first windowed segment is aligned with the start of the sending event which resets a sample counter. The beginning of the second segment is aligned with sample $t_{FB}f_s + l_{MLS}$. In order to overcome the computational cost of range estimation for longer ranges, a range tracking scheme is introduced in section 5.5.1. Here, the windowed channel segments are further cropped based on the previous range estimates related to a particular sender.

The two channels of the first segment (ping emitted by P_1) are denoted by $s_{11}(n)$ and $s_{12}(n)$ while the two channels of the second segment (ping emitted by P_2) are denoted by $s_{21}(n)$ and $s_{22}(n)$. Once assembled, these are filtered with the frequency filter introduced in section 3.3.3. This is done by transforming the signals into the frequency domain using an FFT, multiplying with the response of the filter and then transforming back into the sample domain using an inverse FFT. These channels serve as inputs to the subsequent cross-correlations which derive the TDOAs and TOFs used for the pose vector estimation.

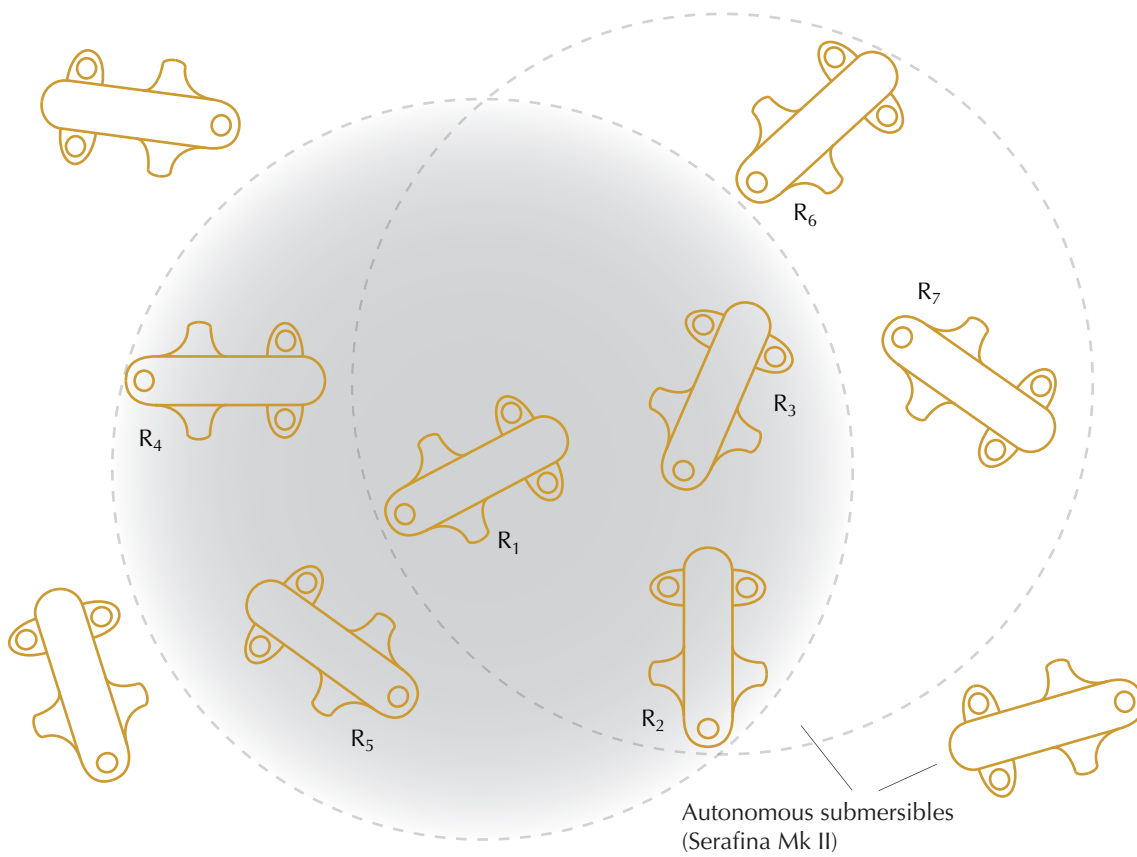


Figure 5.2: AUVs labelled R_2 , R_3 , R_4 and R_5 receive the acoustic signals when the ‘sending’ vehicle R_1 is within their sensing range. The four vehicles which receive the signals sent out by R_1 constitutes its local neighbourhood. When R_3 is ‘sending’, R_1 , R_2 , R_6 and R_7 makes up the local neighbourhood of R_3 . The number of vehicles in a local neighbourhood depends on the swarm density and the range of the localisation system.

TDOA and TOF measurements

As depicted in figure 5.1, the cross-correlations for deriving the TOFs for range estimations and TDOAs for azimuth and alternate heading estimations are processed in parallel. The **peak tracking** scheme which is presented later in section 5.4.1 operates at a very low level in the processing chain utilising the information about the peak positions of cross-correlograms derived in the previous estimation step. This peak tracking technique, in conjunction with the sub-sample interpolation scheme described previously in section 4.3.2 contributes to improved accuracy and precision of the relative localisation estimates produced by the system.

Localisation estimates and pose vector assembly

Once appropriate intermediate quantities are calculated, the pose vector components azimuth, range and heading along with alternate heading and range are calculated using the formulae given previously in chapter 4. Out of these, azimuth, range and alternate heading can be

categorised as primary estimates while those calculated using these quantities, namely the heading and alternate range can be categorised as secondary estimates. Outliers resulting from the numerical instability of formulae used to derive these secondary estimates are handled with the threshold bounding scheme described later in section 5.4.2.

Each of the assembled pose vectors are attributed with the node IDs of the sender vehicles which are localised by the system. The information about which member of the local neighbourhood triggered the sending event is provided to the localisation system via the communication and scheduling system residing on the observer.

Synchronisation

The synchronisation for relative localisation system is provided by the scheduling scheme used by the underlying communication system present on both sender and observer AUVs. As depicted by the block diagram in figure 5.1, an acoustic sending event on a sender AUV is triggered by the communication system which simultaneously transmits its message via the long-wave radio transmitter module. On the observer, the communication system, upon receiving a message via the long-wave radio receiver module, signals the start of a sending event to the relative localisation system, providing implicit synchronisation between the sender and the observer AUVs.

5.2 Distributed relative localisation in a swarm

The methodologies discussed in the previous chapters focused on one sender and one observer, as it was sufficient to describe the process of relative localisation to be used by individual AUVs. However, it was elucidated that for each sending event initiated by a sender, multiple observers within its local neighbourhood can localise it. Furthermore, multiple simultaneous sending events can occur within a swarm depending upon the structure of the distributed omnicast routing schedule used by the underlying long-wave radio communication system (Schill, 2007).

The simplified¹ diagram given in figure 5.2 can be used to explain the concept of a **local neighbourhood** with regard to an acoustic sending event. As the AUV labelled R_1 is ‘sending’, vehicles R_2 , R_3 , R_4 and R_5 which has it within their sensing range would be able to receive the acoustic signals. In this case, the four vehicles which receive the signals sent out by R_1 constitute its local neighbourhood. Similarly when R_3 is ‘sending’, R_1 , R_2 , R_6 and R_7 makes up its neighbourhood. Assuming a large swarm consists of many such local neighbourhoods, the time division multiple access (TDMA) scheduling scheme allows multiple sending events to occur simultaneously (Schill et al., 2005; Somaraju and Schill, 2007). Within one schedule run, (consisting maximally

¹. While the diagram depicts the sending range of an AUV as a circle, in practise it is a more complex shape depending on transducer directivity and occlusion effects.

of $2N_0 - 2$ time-steps for a swarm of N_0 AUVs) each member of the swarm would have information about the relative positions of each of its neighbourhood members via the relative localisation system.

While a given sending event allows multiple observers to fix the static position of a sender, the time history of pose vectors (corresponding to that particular sender) would describe the relative motion of the vehicle with respect to the frame fixed on each of the observers. Furthermore, at each sending event, the sender is meant to broadcast (via the long-wave radio communication system, within the local neighbourhood of the sender) the pose vectors estimated thus far within the scheduling run. Therefore, at the end of each local schedule run, each member of a local neighbourhood would have position fixes for all its neighbours obtained directly from the localisation system as well as the pose vectors assembled by all other neighbours via the communication system. This position data received via multiple methods is meant to be fused with proprioceptive measurements from other systems such as the inertial measurement unit (IMU), magnetic compass and pressure sensor on board the Serafina class AUVs to perform cooperative localisation within the swarm.

There is a considerable body of literature which addresses cooperative localisation in multi-robot setups. Martinelli et al. (2005) who expands on work presented by Roumeliotis and Bekey (2002) describe an extended Kalman filter approach for fusing of proprioceptive measurements with exteroceptive estimates such as relative bearing (azimuth), distance (range) and orientation (heading). Information is exchanged between robots when they localise each other in realising this cooperative localisation scheme. Particle filter based methods for multi-robot localisation which involves exchange of position estimates through communication is presented by Fox et al. (2000) and Howard et al. (2003) and shows that the overall position accuracy is greatly improved by this collaborative approach. These schemes address issues such as irregular update rates and noisy position estimates which are also relevant to the relative localisation system being discussed in this thesis. Work presented by Roumeliotis and Rekleitis (2004) analyses the propagation of uncertainty in such cooperative multi-robot localisation schemes where information is exchanged between robots when they detect each other.

As most of the work addressing distributed relative localisation in multi-robot setups have focussed on land based mobile robots, there has not been much emphasis on the actual means of obtaining the position fix of a nearby robot. While some simulation based literature use an emulated 'conceptual' localisation sensor, the others use readily available sensors such as laser range finders and cameras or combinations of such modules (*e.g.* the robot tracker sensor given by Rekleitis (2003)). As discussed in chapters 1 and 2, the constraints introduced by the underwater environment, available power budget and size requirements motivated the development of the relative localisation system being presented in this text. While it is beyond the scope of this

thesis to present a detailed description of how cooperative localisation is realised in a swarm of Serafina class AUVs with dynamically changing spatial configurations and irregular update rates, the localisation estimates (*i.e.* pose vectors) produced by the system presented in this text can be used as inputs for such a ‘higher level’ swarm localisation and navigation scheme.

From a graph theoretic perspective, the spatially distributed swarm can be converted to a network model by defining edges between nodes (AUVs) within sensing range of each other. Therefore, a ‘collision’ will occur if two or more nodes within a 2-hop neighbourhood of each other initiate sending events simultaneously. While the **distributed dynamical omnicast routing** (DDOR) algorithm (Schill and Zimmer, 2006b) guarantees locally collision free schedules, the **pruned distributed omnicast routing** (PDOR) algorithm (Schill and Zimmer, 2007) which produces schedules that allow collisions displays better performance under certain conditions (dense networks) in comparison. Section 5.3 will describe how the relative localisation system behaves with regard to interference caused by colliding sending events.

5.2.1 Pose vector

During a sending event, all members of the local neighbourhood would assemble a pose vector corresponding to the sender vehicle, relative to each of their *body-fixed* coordinate frames. The **sender node ID** provided by the communications schedule, identifying the sender, is used to label each of the pose vectors.

The azimuth θ , the range r and the heading α of the sender vehicles relative to the observer vehicle constitutes the pose vector (figure 4.11). For an observer AUV with node ID j which receives acoustic pings after an AUV with node ID i initiates a sending event, corresponding to a **logical time-step**¹ k , the estimated pose vector $\hat{x}_k^{i,j}$ is expressed as follows:

$$\hat{x}_k^{i,j} = [\theta, r, \alpha]^T, k \in \mathbb{N}, i, j = 1, 2, 3 \dots N_0, i \neq j \quad (5.2)$$

where N_0 is the total number of vehicles in the swarm. Though components of this pose vector are considered individual estimates for simplicity, this construct allows them to be multidimensional quantities depending on the requirements of the overall swarming system. Each component can be an array of estimates obtained by different methodologies (*e.g.* the inclusion of both the direct and alternate estimates for range and heading) or multiple hypotheses in the presence of interfering signals. In addition, the components can also consist of a finite time history² of each of the individual estimates preceding the current estimate.

¹. Logical time is not necessarily related to a real-time clock as explained by Lamport (1978).

². Length of which is governed by the specific application and amount of available memory.

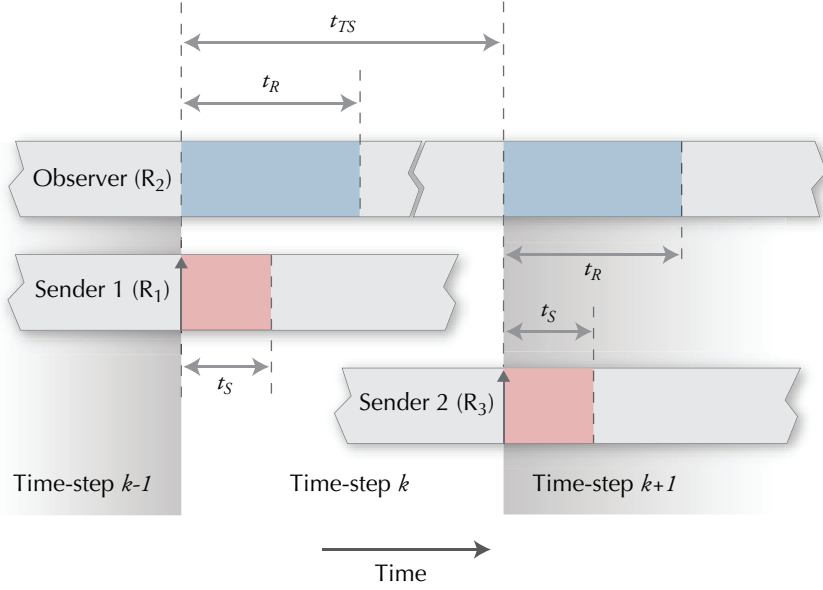


Figure 5.3: The time-line of an observer receiving signals from two sending events initiated by two senders in consecutive schedule slots. The labels R_1 , R_2 and R_3 relate to the diagram in figure 5.2.

5.2.2 Update rates

Multiple update rates operating at different levels can be identified with regard to distributed localisation in a swarm. The lowest level is the rate at which the pose vector is updated by a particular observer vehicle. That is, how often a vehicle would be able to get a position fix of some other vehicle in the local neighbourhood. This depends on the duration of a **schedule slot** (logical time-step). The possible duration of the time-step has a lower bound introduced by the effective sensing range of the localisation system, which is equivalent to the maximum radius of a local neighbourhood. If the time-step duration is t_{TS} and the maximum effective sensing range of the localisation system is r_{max} , this constraint based on the composition of a sending event which includes two send-receive cycles can be expressed as:

$$t_{TS} \geq t_R = 2 \frac{r_{max}}{v} \quad (5.3)$$

where v is the speed of sound in water and t_R is denoted as the receiving time associated with one sending event. Accordingly, the low level update rate is inversely proportional to the effective sensing range of the relative localisation system. Figure 5.3 illustrates the time-line of an observer (R_2) with regard to two sending events initiated in time-steps k and $k + 1$ by two senders (R_1 and R_3). The sending time, denoted by t_S can be expressed as:

$$t_S = 2t_{MLS} + t_{FB} \quad (5.4)$$

where t_{MLS} is the duration of one acoustic ping and t_{FB} is the temporal separation between the two pings.

Another update rate is how often an observer would be able to localise a given sender in its local neighbourhood (*e.g.* according to figures 5.2 and 5.3, how often R_2 can get a position fix for R_1). This would occur at least once in each schedule run. The exact update rate is governed by the structure and the length of the local routing schedule as well as the duration of a schedule slot (same as the logical time-step described earlier). The schedule length is a function of the number of vehicles in the local neighbourhood while the structure is dependent on the spatial configuration of swarm members (*e.g.* swarm density, shape). As expected, the update rate is inversely proportional to the number of members in a local neighbourhood as well as the effective sensing range of the localisation system.

Related to the above update rate are the rates at which a whole local neighbourhood updates pose vectors of each of the members and the whole swarm updates position fixes for each of the members in their respective local neighbourhoods. These too are governed by the characteristics of the communication schedule and would not remain constant for a dynamically changing swarm configuration. The schedule lengths produced by the omnicast routing algorithms have an upper bound of $2N_0 - 2$ where N_0 is the number of AUVs in the swarm. Hence, the upper bound on the duration for each member of the swarm to update the relative positions of each of its neighbourhood members via the relative localisation system is $2N_0 - 2$ logical time-steps. A detailed analysis of omnicast routing schedules and their characteristics are beyond the scope of this thesis¹.

Effects of motion and update rate on estimation error

The components of the pose vector, namely the azimuth, range and heading are all relative measurements where the frame of reference is fixed on the observer AUV. During the two estimations within a sending event, the sender and observers are assumed to be static with the estimates providing an instantaneous snapshot of the relative positions of the vehicles. For the Serafina AUVs, nominal linear and angular velocities can be given as 1.0ms^{-1} and 90°s^{-1} . These in turn could produce maximum relative linear and angular velocities of 2.0ms^{-1} and 180°s^{-1} . Given that t_{FB} is non-zero, there can indeed be an amount of relative motion between the two pings despite the static assumption (*e.g.* for $t_{FB} = 5.0 \times 10^{-2}\text{s}$ used during the experiments, a maximum range variation of 0.1 m could occur between the pings). However, the assumption would still be valid considering the slow relative motion between local members in a swarm for most typical swarm applications despite their absolute motion. For applications requiring higher relative motion between swarm members, the errors caused by motion between pings can be kept within bounds

¹. See Schill (2007) for a detailed description about omnicast routing schedules and their timing characteristics.

by appropriately selecting a value for t_{FB} or by simultaneously emitting pings ($t_{FB} = 0s$) employing different MLS signals for the two projectors¹.

Furthermore, the relative motion between the observer and sender introduces dynamic errors for each of the estimated quantities. For an update rate of u and relative velocity ω , the dynamic error for an estimate denoted by $\Delta\phi_{dynamic}$ can be expressed as:

$$\Delta\phi_{dynamic} = \omega/2u, \quad \phi \in \{\theta, r, \alpha\} \quad (5.5)$$

Here ϕ is used as a placeholder for azimuth θ , range r , heading α . With the update rate u given in Hertz, a relative linear velocity measured in meters per second this will return a dynamic range error of $\Delta r_{dynamic}$ in meters while relative angular velocities corresponding to azimuth and heading variations measured in degrees per second will return $\Delta\theta_{dynamic}$ and $\Delta\alpha_{dynamic}$ in degrees.

If the theoretically derived uncertainty values in section 4.4.5 are denoted by $\Delta\phi$ then the effective error when the system is in motion is given by:

$$\Delta\phi_{effective} = \begin{cases} \Delta\phi, & \Delta\phi > \Delta\phi_{dynamic} \\ \Delta\phi_{dynamic}, & \Delta\phi \leq \Delta\phi_{dynamic} \end{cases} \quad (5.6)$$

For the nominal linear and angular velocities stated earlier, the corresponding maximum relative linear and angular velocity were $2.0ms^{-1}$ and $180^\circ s^{-1}$. For the actual low level update rate of 5.0Hz corresponding to a t_{FB} value of $5.0 \times 10^{-2}s$ used during the experiments presented in chapter 7 these values would be $\pm 20.0 \times 10^{-2}m$ and $\pm 18.0^\circ$ respectively.

It must be noted that the maximum relative velocities used above to derive these quantities are not realistic in a swarming context as stated before, the relative velocities between neighbouring vehicles would be quite low compared to the absolute velocities of the vehicle, hence the corresponding dynamic errors would be lower than the values stated above.

5.2.3 Sensing range

For the localisation scheme to be effective, it is not essential to have symmetric acoustic links where sending and receiving ranges are the same, since the localisation itself does not require two-way communication between the sender and observer vehicles. The requirement is for the acoustic sending to have a similar range as the long-wave radio communication.

The maximum effective range of the localisation system is less than or equal to the maximum range at which the SNR of the acoustic signals still provide acceptable localisation estimates within error bounds. The maximum range is dependent upon a number of external parameters such as the sensitivity of the hydrophones used, the transmission power of the acoustic pings, the

¹. A similar situation is discussed in section 5.3.1 where peak detection performance is experimentally evaluated for two different MLS signal pings are emitted simultaneously.

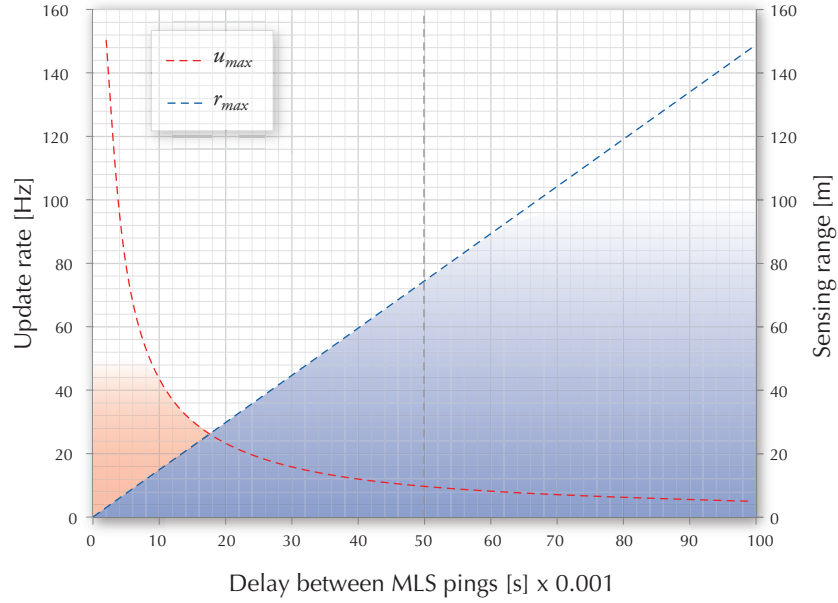


Figure 5.4: Maximum theoretically achievable update rate u_{max} and detectable range r_{max} are plotted against the delay between the two MLS pings within a sending event. Considering the deterioration of the SNR with increasing range and limits imposed by the speed of the processor being used, the shaded area represents the practically feasible values for these quantities.

pre-amplifiers and the dynamic range of the analogue-to-digital converters used while the effective range of the localisation system is related to the length N of the truncating window applied to the received signal channels.

For the relatively short inter-vehicular distances proposed for the Serafina Mk II class AUV swarms, matching ranges of the localisation system and the communication system can be achieved by either of two methods. One is to adjust the projector (transmission) power, changing the maximum range of the acoustic pings. The other is to manipulate the length N of the truncating window mentioned earlier, changing the effective range of the localisation system. Furthermore, the utility of effective range limitation in handling interference is explained later in section 5.3.1.

Relationship between effective sensing range and the update rate

As explained earlier, incoming acoustic channels are windowed in to two length N segments each containing a ping emitted within the sending event. The window length determines the maximum distance travelled by the acoustic signal before reaching the hydrophones. This in turn is the maximum effective sensing range r_{max} of the system which is related to N according to (5.1). However the time delay t_{FB} separating the two pings emitted during a sending event imposes an upper limit on the maximum detectable range given as:

$$r_{max} \leq vt_{FB} \tag{5.7}$$

where the speed of sound in water v is in meters per second, t_{FB} in seconds and r_{max} in meters.

Furthermore, the duration t_{FB} also dictates the maximum achievable low level update rate for the system mentioned at the beginning of section 5.2.2. Considering (5.1) and (5.3), the maximum low level update rate for the system u_{max} has an upper bound based on t_{FB} and t_{MLS} which can be expressed as:

$$u_{max} \leq \frac{1}{2(t_{FB} + t_{MLS})} \quad (5.8)$$

with $t_{MLS} = l_{MLS}/f_s$, where l_{MLS} is the length of an MLS ping and f_s the sampling frequency of the analogue to digital converters. The update rate is in Hertz when t_{FB} is in seconds and f_s is also in Hertz while l_{MLS} is unitless, given in sample points.

The upper bounds for r_{max} and u_{max} are plotted against t_{FB} in figure 5.4. The vertical dashed line on the plot represents the t_{FB} value used in the experiments presented in the following chapters which is 5.0×10^{-2} s. For this value, (5.7) and (5.8) suggests a maximum low level update rate of 9.74Hz and a maximum detectable range of 75m. The update rate actually used during the experiments was 5.0Hz. Considering the upper bounds plotted in figure 5.4, the optimal value for the time delay t_{FB} suggested by the plot is 1.74×10^{-2} s and the corresponding maximum update rate is 26.4Hz and the maximum detectable range is 26.4m.

However, though theoretically possible, the upper bounds suggested by the plot are not quite realistic. In order to reach the linearly increasing maximum ranges suggested, the transmission power needs to be increased accordingly, as the deterioration of the SNR is not considered by (5.7). The blue shading on the plot attempts to depict a more realistic representation of the maximum distance travelled by the acoustic signals where attenuation, multipath propagation and fading effects of the underwater sound channel would further shorten the maximum detectable range. Furthermore, the maximum update rate will be limited at an upper bound depending on the processor used by the system. This limiting level is represented by the red shading of the plot as opposed to the exponential increase suggested by (5.8).

Depending on how reverberant the operating environment is, t_{FB} cannot be reduced beyond a threshold value. This threshold would ensure that all the echoes/reflections of the first ping has sufficiently attenuated before the start of the second. These constraints would govern the selection of the threshold value for t_{FB} and dictate the maximum low level update rate and maximum detectable range of the system. However, the range tracking strategy described in section 5.5.1 eliminates the constraint on the maximum effective range imposed by (5.7) based on t_{FB} .

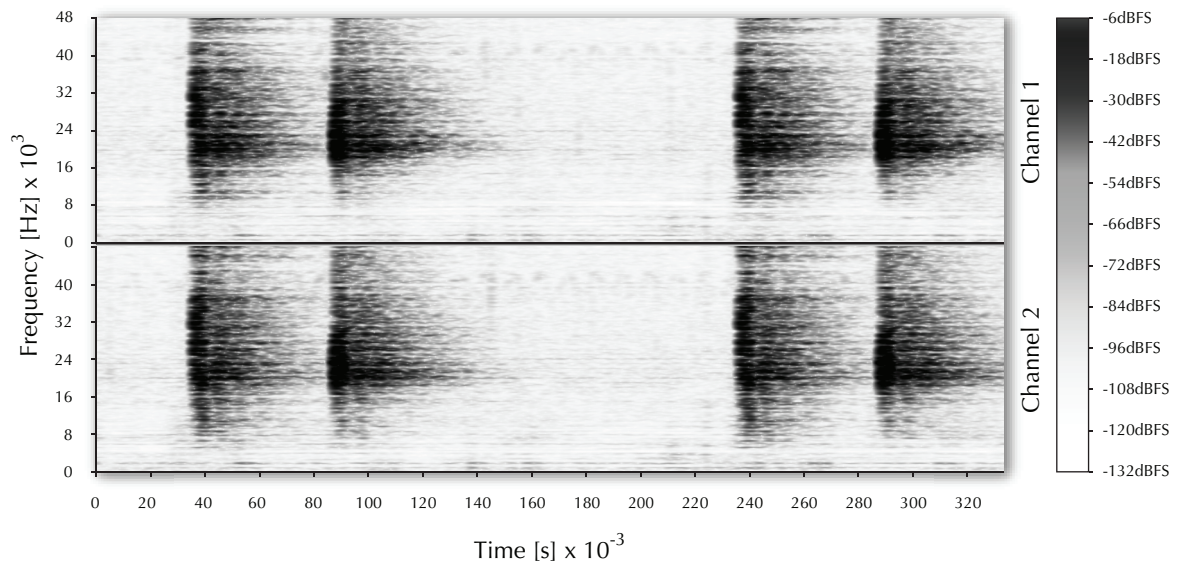


Figure 5.5: Spectrogram showing received hydrophone channels corresponding to two consecutive sending events during an experiment in the test tank ($r \approx 2\text{m}$).

5.3 Handling interference

Interference experienced by the acoustic signals used in the relative localisation system can be broadly classified in to three categories¹ (briefly introduced in the previous chapter under *Errors due to low SNR* in section 4.3). The first category is interference of the direct path signals by reflected (multipath) signals when operating in highly cluttered, reverberant environments. The second category, which has a similar effect on the localisation system is the interference in the presence of multiple sending events within a 2-hop neighbourhood due to colliding sending schedules. As mentioned in the previous section, the underlying scheduling scheme, depending on the routing algorithm used, can produce colliding sending events within a local neighbourhood.

The third category of interference occurs due to extraneous acoustic sources present in the environment. While detrimental effects due to this form of interference is largely avoided by the use of MLS signals, in the presence of intense broadband noise, the SNR can deteriorate to a level where the TDOA measurement could yield estimates which corresponds to the angular position of the noise source rather than the signal source. Furthermore, deterioration of the SNR can occur in two ways, either with higher noise levels or lower signal levels (as the signal source reaches the sensing limits of the receivers). The following subsections discuss how the relative localisation system behaves in the presence of these different sources of interference and what methodologies are adopted to maintain the accuracy and precision of the position estimates.

¹. Some texts refer to these effects as reverberation, cross-talk and noise but here they are treated as different forms of interference.

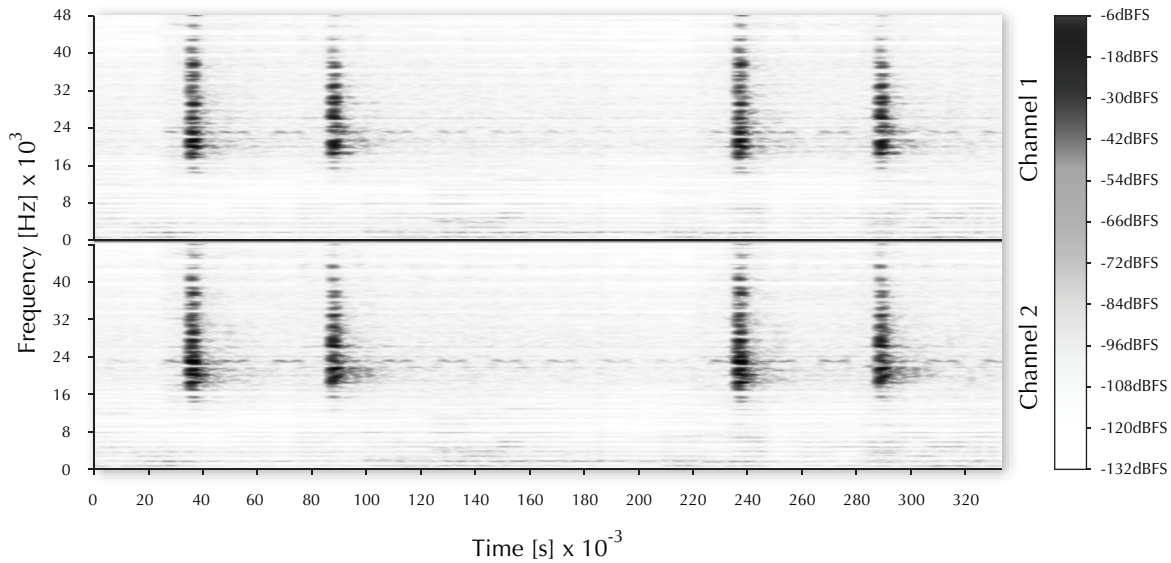


Figure 5.6: Spectrogram showing received hydrophone channels corresponding to two consecutive sending events during an experiment in the lake ($r \approx 8\text{m}$).

5.3.1 Cluttered environments and multiple senders

Operating in cluttered, reverberant environments, the acoustic source localisation is susceptible to inaccurate position fixes due to multipath arrivals of the signal. The test tank¹ in which the relative localisation system was experimentally evaluated constitutes such a harsh acoustic environment with strong reverberations. Figure 5.5 shows a spectrogram² of the two received hydrophone channels corresponding to two consecutive sending events (each consisting of two MLS pings) recorded during an experiment in the test tank. The broadband intensity of the reflected signals decays slowly with frequencies near the resonance of the transducers ($\sim 20\text{kHz}$) being the most persistent. Figures 5.6 and 5.7 shows spectrograms of received channels recorded during two experiments conducted at lake Burley Griffin³. The difference in the intensity and persistence of reverberations within the two acoustic environments can be observed by comparing these spectrograms with the one shown in figure 5.5. As a result of the delayed multipath signal arrivals, the cross-correlations used by the relative localisation system to measure TDOAs and TOFs would yield multiple peaks in close proximity to the peak representing the direct path signal.

With regard to the underwater swarm communication system presented by Schill (2007), the efficiency of the communication systems, in terms of information propagation throughout the swarm improves with multiple sending events taking place within the swarm in multiple disjoint

¹ Cylindrical tank with corrugated metal walls filled with tap water. Diameter 4.2m, depth 1.5m

² Generated with short-time Fourier transforms with a window size of 512samples.

³ Lake Burley Griffin has an approximate surface area of 6.64km^2 situated in the centre of Canberra, ACT, Australia.

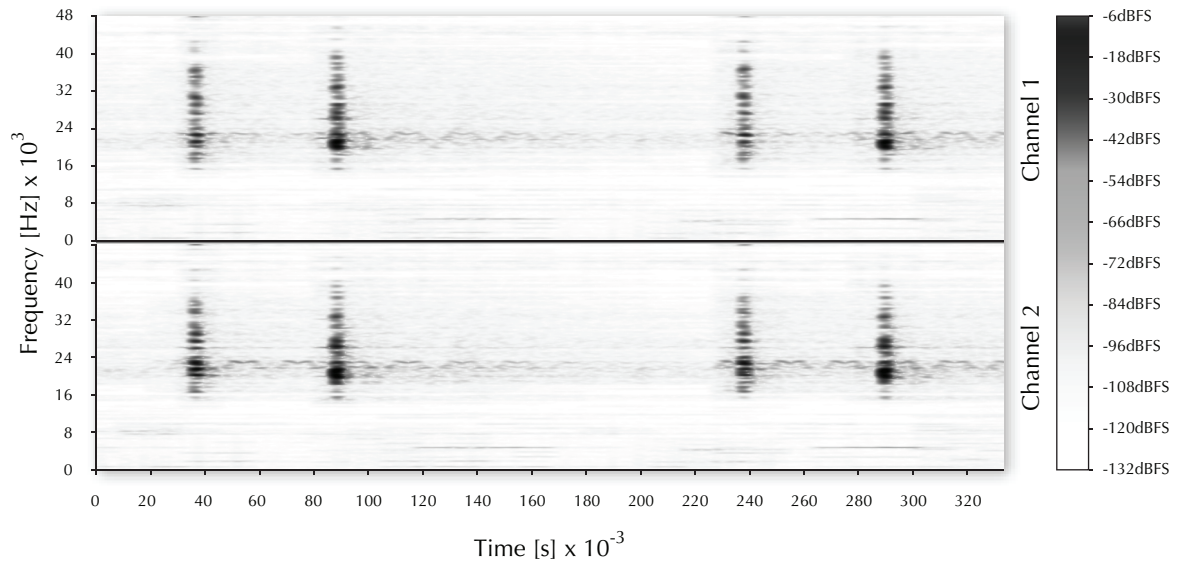


Figure 5.7: Spectrogram showing received hydrophone channels corresponding to two consecutive sending events during an experiment in the lake ($r \approx 20\text{m}$).

neighbourhoods. However depending on the routing algorithm used, sending schedules may contain “collisions” within a local (2-hop) neighbourhood. Since the communication system and the localisation system are synchronised to the same sending schedule, these colliding schedules trigger multiple AUVs in a neighbourhood to simultaneously emit acoustic pings.

Propagation loss, causality and channel windowing

In the case of long-wave radio signals used by the communication system, when multiple nearby sources simultaneously transmit, due to the high speed of propagation, the signals would arrive simultaneously at a receiver within range, regardless of the relative distances between each transmitter and the receiver. However, due to propagation loss through the media, the signal from the transmitter closest to the receiver appears stronger. This phenomenon is experimentally validated by Schill and Zimmer (2006a) and shows that the communication system can indeed receive and decode messages sent from the nearer transmitter despite the theoretical network model suggesting otherwise. According to the results of experiments conducted with two long-wave radio transmitters and one receiver, it was found that collisions where the signals could not be received occurred only in a relatively narrow band (less than 0.5 m on average) where the transmitters were approximately equidistant to the receiver. Due to this, the communication system adopts a geometrical collision model where a signal from the nearer source would be decoded and interpreted, under the assumption that the signal strength monotonically decreases with distance.

While the above assumption does not hold true for long range underwater acoustic channels (Urick, 1983), it is valid for the shorter ranges applicable to the inter-vehicle distances in a local neighbourhood being discussed here. In addition to the higher received signal strength, unlike

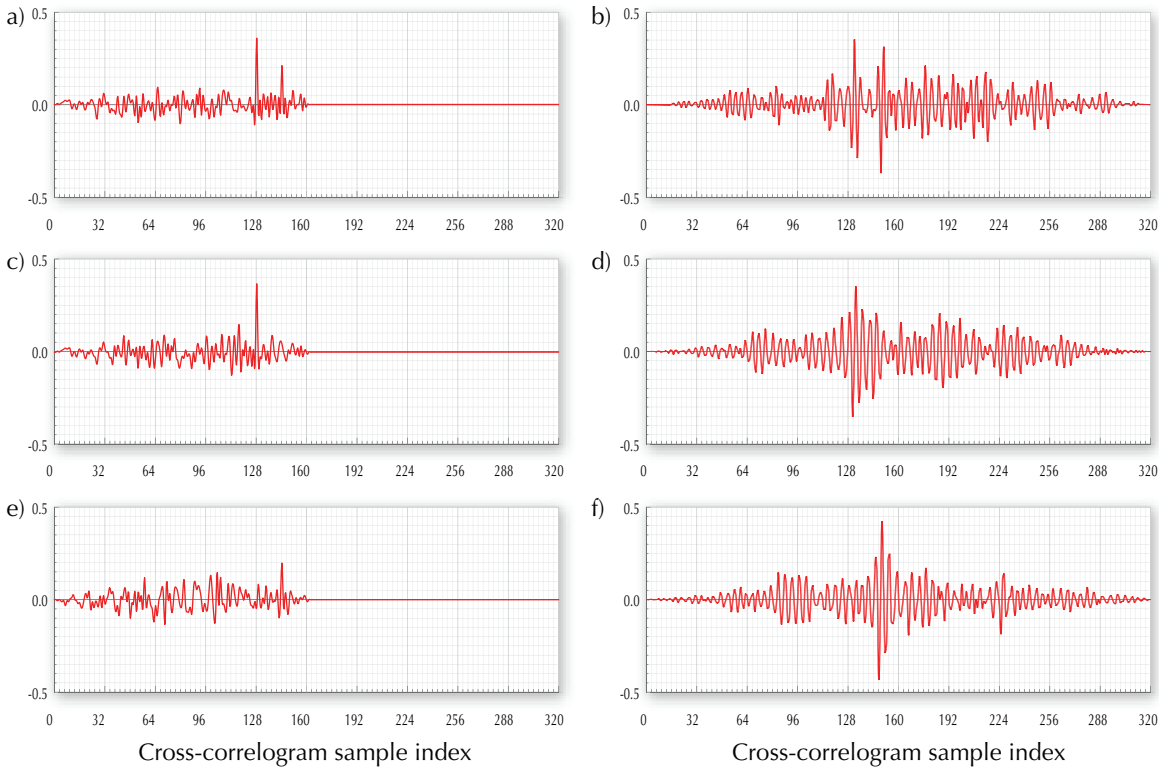


Figure 5.8: Cross-correlograms resulting from matched filter processing with two simultaneously emitted MLS pings, left column from ‘simulated’ uncorrupted MLS signals, the right column from experimentally recorded signals. First row corresponds to similar MLS signals being used while second and third rows correspond to two different MLS signals being used as sources. The two projectors are offset by 0.25 m.

the electromagnetic signals, when multiple sources send simultaneously, the direct-path acoustic signals from a nearer source would also arrive *earlier* at the observer. This is due to the relatively slower speed of propagation of acoustic signals compared to its electromagnetic counterpart. This is very similar to the earlier scenario where the direct-path signal is accompanied by delayed multipath signals when operating in reverberant environments. In both cases, the direct-path signal / signal from the nearer sender arrives first at the observer and yield a higher peak in the subsequent cross-correlations due to the higher signal strength. However, if the simultaneous senders are approximately equidistant from the observer or if the multipath arrivals are caused by reflectors in very close proximity to the source, the resulting cross-correlation peaks would have very small temporal separation and will have similar peak heights which in turn would cause errors in the final localisation estimates. Considering the dynamic nature of mobile platforms operating in real environments, the effect of such situations on the localisation estimates are assumed to be transient. The **peak tracking** scheme introduced in section 5.4.1 attempts to address such effects.

As mentioned in section 5.2.2, the maximum effective range of the relative localisation system is enforced by applying a truncating window upon the received signals. This scheme is similar to

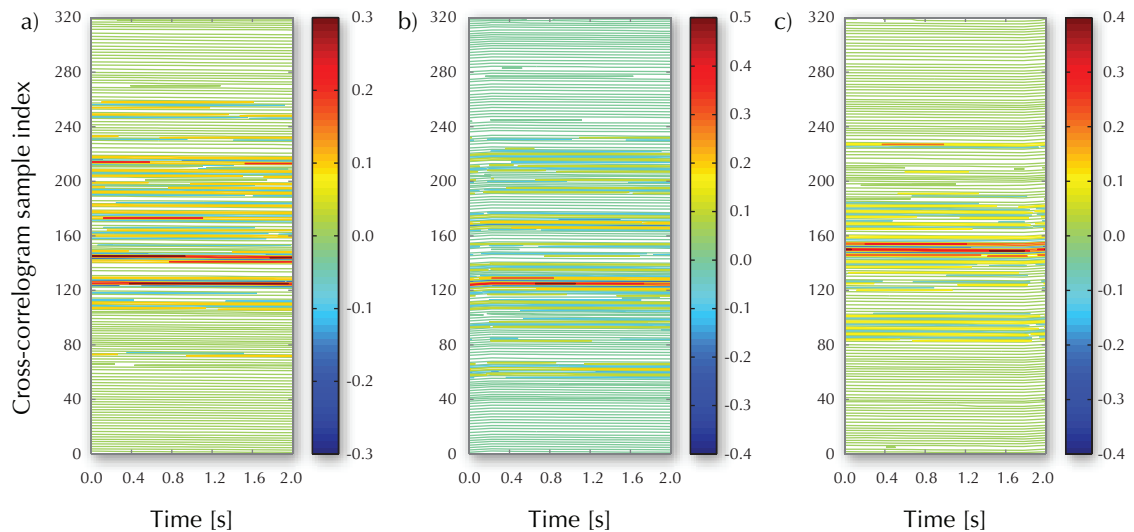


Figure 5.9: Contour plots of multiple cross-correlograms resulting from matched filter processing of one received hydrophone channel with two simultaneously emitted MLS pings where a) similar MLS signals, b) and c) two different MLS signals are being used as acoustic sources.

the *precedence effect* phenomenon studied in human hearing and binaural localisation research (Wallach et al., 1949; Blauert and Cobben, 1978) and truncates the two hydrophone channels in the time-domain. Due to the synchrony introduced by the omnicast routing scheme, sending events throughout the swarm are triggered simultaneously¹. Therefore, acoustic pings from distant senders (beyond the 1-hop neighbourhood of an observer) during a particular sending event will arrive much later than the ping from a local sender (within the 1-hop neighbourhood of an observer). The aforementioned windowing scheme prevents acoustic signals from far (non local) senders from affecting the subsequent cross-correlations.

In the test tank experiments presented in chapter 7, the delayed multipath signals act as interfering pings emitted simultaneously from distant sources. The windowing technique mentioned earlier and implemented in these experiments was effective in discarding most of these interfering signals. The interfering events not handled in this manner (reflected signals which are within the sensing range) are handled via the **peak tracking** scheme.

Experimental evaluation of cross-talk and reverberation handling

In chapter 3, it was shown how MLS signals perform with regard to peak resolution under harsh conditions including signal mixing. The performance of peak detection by the relative localisation system was experimentally tested in a situation where the detrimental effects of a reverberant environment and multiple colliding sending events were combined.

¹. Based on the assumption that the logical clocks are in-sync up to sufficient accuracy (Schill, 2007, pp.111-112).

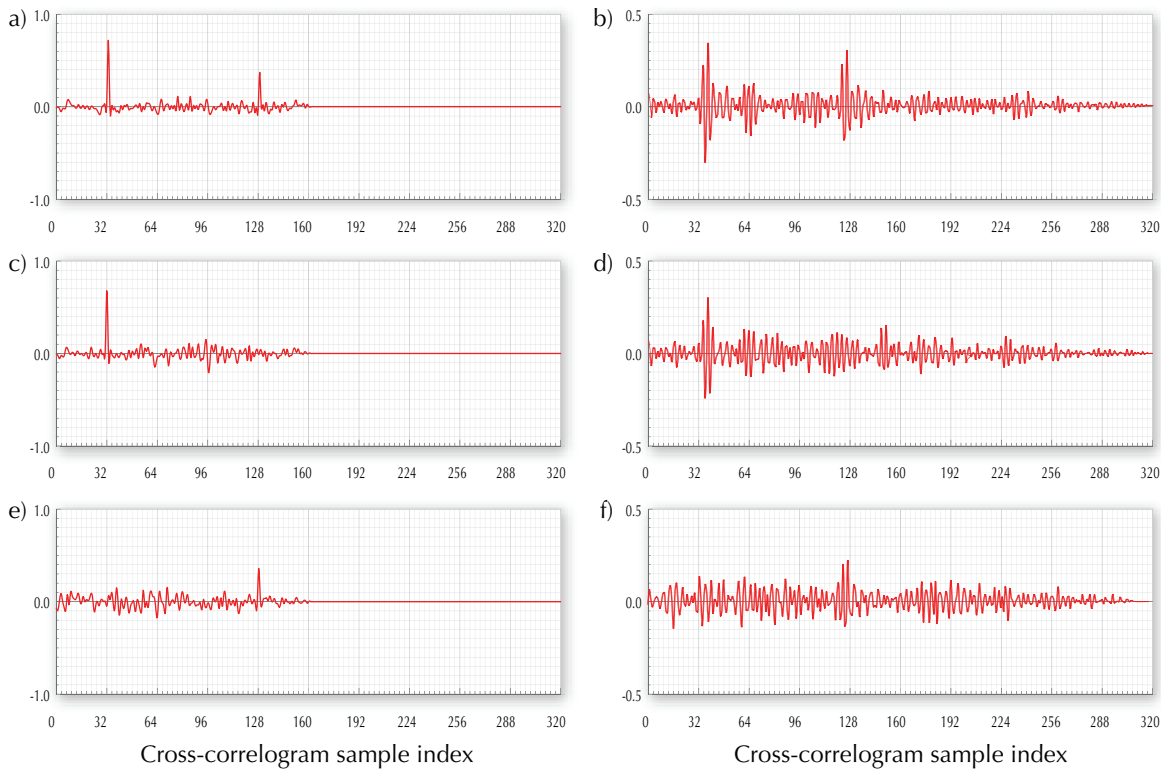


Figure 5.10: Cross-correlograms resulting from matched filter processing with two simultaneously emitted MLS pings, left column from ‘simulated’ uncorrupted MLS signals, the right column from experimentally recorded signals. First row corresponds to similar MLS signals being used while second and third rows correspond to two different MLS signals being used as sources. The two projectors are offset by 1.40 m.

First, two similar 128 sample MLS pings were emitted simultaneously from two projectors placed approximately equidistant¹ from the observer (hydrophone pair) to emulate two senders within its 1-hop neighbourhood. The duration of the pings were approximately 1.3 ms due to the sampling rate of 96000 Hz. The received channels contained the two direct path arrivals of the pings overlapping each other by over 85% due to the placement and simultaneous emission in addition to the multiple delayed arrivals due to reflections. Figure 5.8.b shows a cross-correlogram used to extract the TOF for subsequent range estimation by the relative localisation system using the modified matched filter introduced in section 4.2.1. For comparison, figure 5.8.a shows a cross-correlogram obtained by applying the matched filter to two similar uncorrupted MLS signal channels (as opposed to the experimentally recorded signal channels) of 1.3 ms duration which were mixed such that they overlap each other by 87.5%.

Later, two different MLS signals were emitted from the same projectors without changing their positions. The modified matched filter was applied to the received hydrophone channels twice,

¹: 2.05 m and 2.30 m from the observer which induces an offset of 0.25 m. This is well within the ‘collision’ band of approximately 0.50 m experienced by the long-wave radio communication system during experiments presented by Schill and Zimmer (2006a).

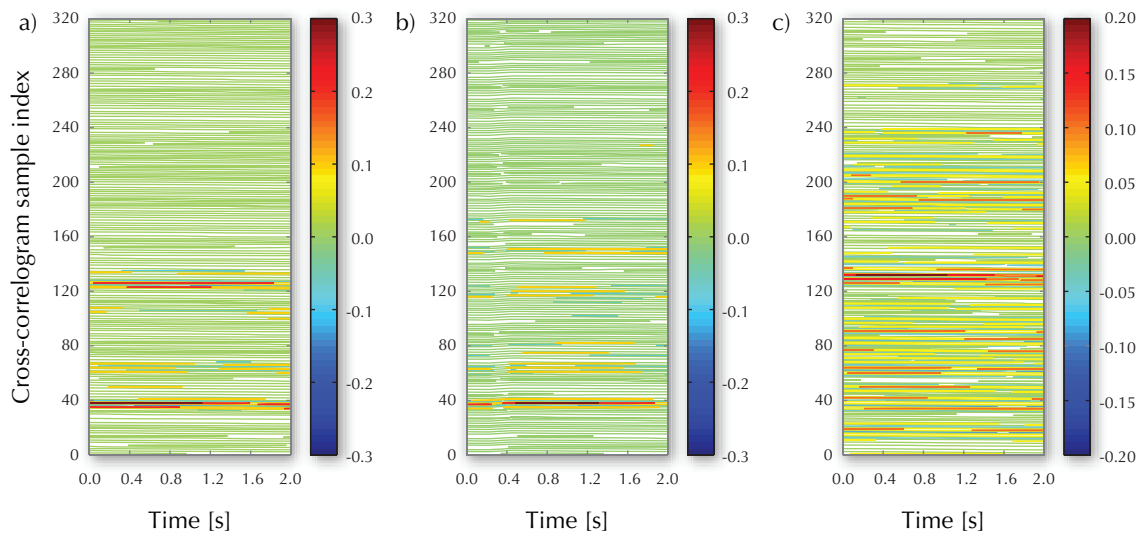


Figure 5.11: Contour plots of multiple cross-correlograms resulting from matched filter processing of one received hydrophone channel with two simultaneously emitted MLS pings where a) similar MLS signals, b) and c) two different MLS signals are being used as acoustic sources.

corresponding to the two different MLS source signals. Figures 5.8.d and 5.8.f shows two cross-correlograms resulting from this process, each showing a peak region corresponding to one of the source signals. The corresponding cross-correlograms obtained by the matched filter with uncorrupted MLS signals is shown in figures 5.8.c and 5.8.e for comparison. Contour plots of multiple cross-correlograms (segments of 2.0s duration) corresponding to the matched filtering of the experimentally recorded hydrophone channels described earlier are shown in figure 5.9. The colour index represents the heights of the cross-correlogram peaks.

The same experimental procedure was repeated with the two projectors placed 0.55m and 1.95m away from the hydrophone pair. First, two similar MLS pings were emitted simultaneously as before. Due to this spatial configuration, the received channels contained the two direct path arrivals of the pings overlapping each other by 30%. One of the cross-correlograms resulting from the modified matched filter is shown in figure 5.10.b. Later, two different MLS pings were emitted simultaneously from the two projectors and two cross-correlograms resulting from the corresponding matched filter processing is shown in figures 5.10.d and 5.10.f. As before, corresponding cross-correlograms resulting from applying the matched filter to uncorrupted versions of the MLS signals are shown in figures 5.10.a, 5.10.c and 5.10.e for comparison. Figure 5.11 shows the contour plots of multiple cross-correlograms corresponding to the matched filtering described earlier. Once again, the colour index represents the heights of the cross-correlogram peaks.

Cross-correlogram peak regions of the experimentally recorded signals presented earlier shows the impact of spatial separation of the sending events in the absence of temporal separation. All

cross-correlograms resulting from matched filter processing of experimentally recorded hydrophone channels also shows the effect of multipath arrivals due to reflections. Secondary peak regions in these cross-correlograms have relatively lower heights compared to the primary peak regions caused by the two direct path signals. This can be attributed to the lower signal strengths of the reflected signals. In the second instance where the relative spatial separation between the projectors was increased to 1.4 m from the earlier 0.25 m, the primary peak region from the far source has a lower height than the primary peak region from the near source. Here, one of the prominent secondary peak regions due to a strong reflection of the near source (off the bottom of the tank, 0.5 m below the near source) still has a lower peak height compared to the primary peak region of the far source. Therefore, as long as there is minimal relative spatial separation (down to 0.25 m as presented in the earlier experiments), the relative localisation system can resolve acoustic signals emitted from simultaneous sending events initiated within the 1-hop neighbourhood of an observer. In the case of reverberant environments, assuming direct path signals have a higher signal strength¹ than the delayed multipath arrivals, the relative localisation system can still accurately resolve the acoustic source position. The precision of the localisation estimates produced in reverberant environments is further improved by the peak tracking scheme introduced in section 5.4.1, which deals with transient outliers. More experimental evidence to support these claims are presented in chapter 7.

Incorporating geometric information to resolve cross-talk

In the previous section, it was demonstrated that the localisation system can handle simultaneous sending events provided that there is sufficient relative spatial separation between the senders. However, a sending event consists of two pings emitted from the bow and stern ends of a sender AUV separated in time by t_{FB} . This potentially could lead to a situation where pings emitted simultaneously from two separate sender AUVs could no longer be separated. An example of this situation could be when the bow end of sender A is nearer to the observer than the bow end of sender B while the stern end of sender B is nearer to the observer than the stern end of sender A. In such a situation, the two pings emitted from the two bow ends and the two pings emitted from the two stern ends can be identified separately as belonging to two senders, however there is no apparent way of matching up the pairs correctly without any additional information, giving rise to an ambiguity. Nevertheless, the two pings emitted from each sender during a sending event are separated in space by l as well.

Here, each of the four identified pings would yield a sub-azimuth and a sub-range. Considering the diagram given in figure 5.12, if O_1 , O_2 and O_3 are the origins of coordinate frames attached

¹. This assumption holds true except in situations where reflected signals can appear louder than the direct path signal due to the non-omnidirectional directivity pattern of the receivers used.

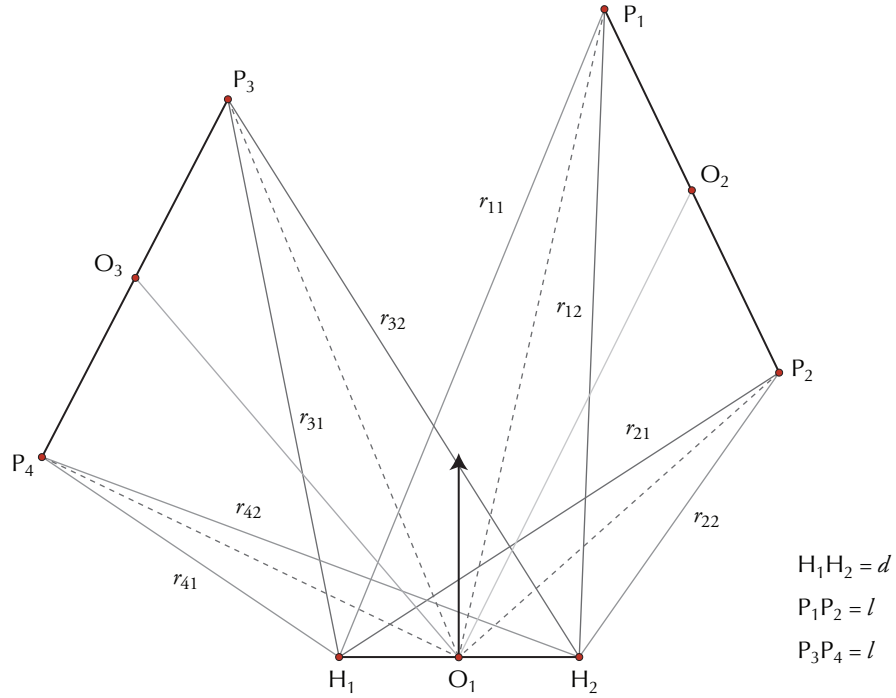


Figure 5.12: Positions of projectors on two senders within the 1-hop neighbourhood of an observer which could lead to a potential ambiguity in the localisation estimates when both senders initiate sending events simultaneously.

to the observer, sender A and sender B described earlier then $P_1O_1 > P_3O_1$ and $P_4O_1 > P_2O_1$. The four sub-azimuths are denoted by $\beta_1 (P_1\hat{O}_1H_2)$, $\beta_2 (P_2\hat{O}_1H_2)$, $\beta_3 (P_3\hat{O}_1H_2)$ and $\beta_4 (P_4\hat{O}_1H_2)$ while the four sub-ranges denoted by $r_1 (P_1O_1)$, $r_2 (P_2O_1)$, $r_3 (P_3O_1)$ and $r_4 (P_4O_1)$ are derived from r_{11} , r_{12} , r_{21} , r_{22} , r_{31} , r_{32} , r_{41} and r_{42} using (4.18) given in chapter 4. Considering the formula for the distance between two points given in polar coordinates, sub-azimuths and sub-ranges can be tested in pairs to check if they satisfy the following inequality:

$$\left| r_i^2 + r_j^2 - 2r_i r_j \cos(\beta_i - \beta_j) - l^2 \right| < \Delta_l \quad (5.9)$$

where $i, j = 1, 2, 3, 4$ and $i \neq j$. Δ_l is some small tolerance value (typically less than 10% of l) to accommodate the minor variations due to estimation errors. Pairs of sub-azimuths and sub-ranges satisfying (5.9) can be considered as belonging to one particular sender, thus resolving the ambiguity. This method explained for two simultaneous senders within the 1-hop neighbourhood of an observer can be extended to any number of simultaneous senders at the cost of the additional computations involved. Each observer would have knowledge of any potentially colliding schedules and which senders (node IDs) are involved in simultaneously initiating sending events via the underlying communication and scheduling system, which has access to the local sending schedules of the neighbourhood. This information can be used to initiate the additional computations to resolve ambiguities as explained earlier only when required.

5.3.2 Interference from extraneous noise sources

For a given constant source signal strength, the SNR on the received channels could deteriorate in either of two ways; with a higher noise level or with lower signal levels induced by the source position reaching the sensing limits of the receivers. Effects of spurious noise is largely avoided by the use of MLS signals as the acoustic source. In the face of broadband noise, cross-correlation of MLS signals were shown to withstand a SNR as low as 0 dB in section 3.3. The effect of lower SNR manifests itself in lowering the peak height in the ensuing cross-correlations but does not directly contribute to alter the peak position. In the experimental results given in section 7.5, it is shown that the relative localisation system can produce accurate localisation estimates under conditions where the SNR is near 0 dB.

As the source position reaches the sensing limits (angular or radial) of the receiver, the ambient noise in the underwater environment itself contributes towards lowering the SNR. Urick (1986) and Dahl et al. (2007) presents and discuss general characteristics of underwater ambient noise while Cato et al. (1992) and Pieng et al. (2004) are among many who have studied ambient noise in specific shallow water bodies. Shipping noise and snapping shrimp noise are two prominent noise sources identified in ocean environments. Inland water bodies such as lakes and reservoirs are comparatively silent. These background ambient noise levels are sufficiently low as to not have a detrimental effect on the SNR for the source signal levels at sender-observer distances considered for the relative localisation system presented in this text. Relatively short duration drops in SNR are handled as transient effects by the peak tracking scheme introduced later in section 5.4.1 while prolonged drops would lead to inaccurate localisation estimates. In the long range experiments presented in section 7.5, the effect of prolonged drops in SNR (below 0 dB) on the relative localisation system is discussed.

5.4 Handling outliers

Exteroceptive and proprioceptive sensors used in localisation tasks especially in position tracking in mobile robotics are assumed to produce noisy measurements leading to outliers, low accuracy and low precision in position estimates. The use of Kalman filters (Welch and Bishop, 1995) and particle filters (Gordon et al., 1993) are among the most popular approaches to address the aforementioned issues. In order to overcome the limitations¹ of the simple Kalman filter, a large class of Extended Kalman filters (EKF) have been used in the literature. Leonard and Durrant-Whyte (1991) present an EKF based approach for localisation and tracking of a mobile robot equipped with Sonar sensors. More recently Olson et al. (2004) presents an EKF technique for outlier rejection in long baseline navigation for AUVs. Thrun et al. (2001) presents an improved

¹ Regarding non-linear or non-Gaussian motion and measurement models (Julier and Uhlmann, 1997; Dellaert et al., 1999a).

particle filtering approach called mixed Monte Carlo localisation while discussing the attributes and drawbacks of conventional methods. Their work presents the results of applying particle filter techniques to sensor data obtained via a laser range finder and an upward looking camera for mobile robot localisation in an indoor environment. Compared to Kalman filter based methods, particle filter based methods perform better in dealing with non-Gaussian error distributions and multiple hypotheses.

The general approach of most of the filtering applications used in localisation can be summarised as follows; the position of the robot changes in time according to a dynamic model in response to some control input and noise. The sensor that observes the position of the vehicle produces readings according to some measurement model which are also corrupted by noise. Under these circumstances, initial/previous position estimates and initial/previous error (noise) distributions are used to predict the time evolution of these quantities and to update them with the information gathered from the actual measurement in the current time step to produce a current position estimate. The effectiveness of the approaches are improved with additional knowledge about the motion characteristics of the localisation target and more precise information about the measurement/noise models.

While these techniques are quite effective in position tracking applications, the handling of outliers by the localisation system presented in this thesis involve paradigm shifts in several important aspects. Instead of a particular sensor providing a noisy measurement (*e.g.* odometry, laser range finder, sonar sensor, vision processing system) which is then used as the input to a localisation system, the relative localisation system itself is treated as a ‘sensor’ which produces a position estimate with the possibility to handle outliers at very low level in the localisation processing chain. Instead of rejecting outliers and estimating a position based on a posterior error distribution given a noisy measurement per time step, the raw data (cross-correlograms used for TDOA and TOF measurements) of the relative localisation system at each time step are seen as containing true position information along with many outliers caused due to environmental interference. Therefore the emphasis is on recovering the true position rather than on rejecting the outliers.

The view that the raw data contains the true position along with outliers is shared by Ward et al. (2003) and Lehmann (2004) in their work regarding acoustical source localisation in reverberant indoor environments. They assume that the true position will follow a dynamic model in time evolution and the outliers will show no temporal consistency between time steps. Empirical data collected while experimentally evaluating the relative localisation system presented in this text suggests that while this first part of the assumption holds, the second part does not. The outliers caused by side lobe peaks in the cross-correlograms, especially when operating in reverberant

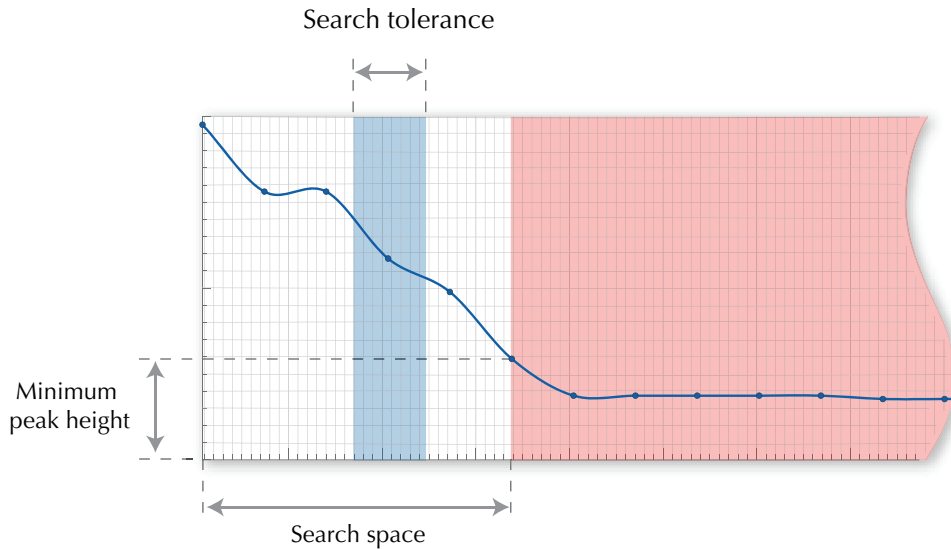


Figure 5.13: Local maxima search space and tolerance on a cross-correlogram sorted by peak magnitude.

environments follow a very similar dynamic model to the true position (See cross-correlogram peak evolutions shown in figures 7.1 and 7.3 in chapter 7).

While avoiding drawbacks of conventional approaches (assuming linear motion, requiring information about the sensor models / motion dynamics) and drawing insights from Markov localisation methods (Fox et al., 2000; Roman and DeLiang, 2003; Arulampalam et al., 2004) a novel yet simple strategy for peak recovery from the measurement cross-correlograms are presented in the next section. This peak tracking scheme uses a local maxima search to ‘predict’ the true peak position and exploits the underlying sub-sample interpolation scheme to ‘update’ and refine the peak position.

5.4.1 Peak tracking

While (4.9) in chapter 4 suggests a simple routine for finding the peak of a cross-correlogram and the corresponding position of the peak, the following **peak tracking** scheme contributes to effective handling of outliers arising due to interference. The main feature of this scheme is that it enforces continuity assumptions of the estimated quantities. Apart from the assumption that the variation of peak position in sample space follows a Markov process (*i.e.* current peak position only depends on the previous peak position) and *a priori* information about maximum variation of each raw estimate¹, this method does not rely on specific motion models, sensor models or error distributions. Furthermore, since the update and refinement of the peak position is done

¹ Maximum physically possible sample space variation within one estimation step based on maximum angular and linear relative velocities between observers and senders.

with the underlying sub-sample interpolation scheme, the additional computational cost is minimal.

As with the simple search in (4.9) $R_{s_1 s_2}$ refers to the full range cross-correlation of two length N signal channels $s_1(n)$ and $s_2(n)$ which includes both positive and negative discrete lags in sample space. For clarity, the following sections will always refer to a cross-correlogram spanning a sample space of $\{-N \dots N\}$ but in the actual implementation, the cross-correlations related to azimuth estimation and reverse azimuth estimation is limited to lags between $-f_s d / v$, $f_s d / v$ and between $-f_s l / v$, $f_s l / v$ respectively. The cross-correlation corresponding to the matched filtering required for the direct range estimation spans the full $-N$ to N range¹.

$x(n)$ denotes an ‘element’ of the resulting cross-correlation with a lag of n samples and can be expressed as:

$$x(n) \in \{x_{-N} \dots x_N\} = R_{s_1 s_2} \quad (5.10)$$

$X(n)$ is defined as a set containing all ordered pairs of lags and corresponding values of the cross-correlogram as follows:

$$X(n) = \{(n, x(n)), \forall n \in \{-N \dots N\}\} \quad (5.11)$$

Another set $X_{Sorted}(m)$ is formed by sorting $X(n)$ in descending order by the value of $x(n)$ as:

$$X_{Sorted}(m) = \{(m, y(m)), \forall m \in \{-N \dots N\}\} \quad (5.12)$$

Therefore, the following conditions are satisfied by the elements of $X_{Sorted}(m)$ and $X(n)$:

$$\forall m \in \{-N \dots N\}, \exists n \in \{-N \dots N\} \text{ s.t. } x(n) = y(m) \quad (5.13)$$

$$\forall n \in \{-N \dots N\}, \exists m \in \{-N \dots N\} \text{ s.t. } y(m) = x(n) \quad (5.14)$$

$$\forall m \in \{-N \dots (N-1)\}, y(m) \geq y(m+1) \quad (5.15)$$

where $n, m \in \{-N \dots N\} \subseteq \mathbb{Z}$, $x(n), y(m) \in [-1, 1] \subseteq \mathbb{R}$ and (5.13), (5.14) maintains bijectivity between $X(n)$ and $X_{Sorted}(m)$. A set $M(k)$ corresponding to estimation step² k is defined as follows:

$$M(k) = \{m \in \{-N \dots N\} \text{ s.t. } |m - \tau_0^l(k-1)| < \Delta_{Tolerance}\} \quad (5.16)$$

where m is drawn from the ordered pairs in the set $X_{Sorted}(m)$, $\Delta_{Tolerance}$ being a tolerance value based on the continuity assumptions of the quantity being estimated and $\tau_0^l(k-1)$ being the sub-sample interpolated lag at estimation step $k-1$. The ‘refined’ lag for estimation step k is

¹. or $-N_{RT}$ to N_{RT} if range tracking is implemented as explained later in section 5.5.1.

². This also corresponds to the k^{th} sending event initiated by the particular sender which is being localised.

returned by the cubic spline interpolation function I_{Spline} which takes in n_{Int} as a parameter as introduced in section 4.3.2, can be defined as:

$$\tau_0^l(k) = I_{Spline}(\tau_0(k), n_{Int}) \quad (5.17)$$

The lag of the new ‘tracked peak’ of the cross-correlogram which maintains continuity with the previous estimates denoted by $\tau_0(k)$ is the minimum element of $M(k)$ given as:

$$\tau_0(k) = \min\{M(k)\} \quad (5.18)$$

where $\tau_0(k) \in \{-N \dots N\} \subseteq \mathbb{Z}$, $\tau_0^l(k) \in [-N, N] \subseteq \mathbb{R}$.

This procedure essentially performs a local maxima search of the cross-correlogram within the neighbourhood of lags around the previously estimated lag (figure 5.13). Since elements of $M(k)$ are drawn from $X_{Sorted}(m)$, this guarantees that the lag returned by (5.18) corresponds to the highest peak within the search neighbourhood. This discrete lag returned by (5.18) is then refined further by sub-sample interpolation using (5.17). The size of the search neighbourhood is decided by the value selected for $\Delta_{Tolerance}$.

The lower bound for $\Delta_{Tolerance}$ is greater than or equal to the maximum possible lag in the sample domain corresponding to variation of angles and distances within the duration between two estimation steps (one schedule slot) based on the relative angular and linear velocities between the observer and the sender. This can be expressed as follows:

$$\Delta_{Tolerance} \geq \frac{|\omega_{max}| f_s t_{TS}}{v} \quad (5.19)$$

where t_{TS} is the duration of a schedule slot, f_s is the sampling frequency, v is the speed of sound in water and ω_{max} is a placeholder for maximum relative velocity between the observer and the sender¹. The underlying assumption is that the position variations maintain continuity between estimation steps within the tolerance bounds. Since $\Delta_{Tolerance}$ is defined for one schedule slot and the localisation system operates at minimum granularity of t_{TS} , irregular update rates in localising a particular sender can be accommodated by modifying (5.16) as:

$$M(k) = \{m \in \{-N \dots N\} \text{ s.t. } |m - \tau_0^l(k-1)| < j \Delta_{Tolerance}\} \quad (5.20)$$

where j is the number of schedule slots (multiples of t_{TS}) since the particular sender was previously localised. For the experiments presented in chapters 6 and 7 which involved only one sender, this value remains at $j = 1$.

¹. See appendix C for derivation of lower bounds of $\Delta_{Tolerance}$ for maximum angular and linear relative velocities.

The motivation behind the implementation described above which involves sorting the elements of the cross-correlogram, was to provide a facility to dynamically limit the search domain for lags to some $N_{Restricted} \leq N$ by restricting minimum $y(m)$ to some y_{min} in (5.16) (which in turn violates the bijectivity condition between $X(n)$ and $X_{Sorted}(m)$). This condition is stated as follows:

$$\forall(m, y(m)) \in X_{Sorted}(m), y(m) \geq y_{min} \quad (5.21)$$

This would specify a lower bound to the peak magnitude in the cross-correlogram which can correspond to the lag returned by (5.18). As a consequence of the violation of the bijectivity condition, there could be situations where $M(k) = \{ \}$ ¹. Therefore (5.18) needs to be reformulated as:

$$\tau_0(k) = \begin{cases} \min\{M(k)\}, M(k) \neq \{ \} \\ \tau_0^*, M(k) = \{ \} \end{cases} \quad (5.22)$$

The value for τ_0^* can either represent a constant position model or a constant velocity model by returning the previous lag $\tau_0^l(k-1)$ or $\tau_0^l(k-1)(1 + \nabla\tau_0^l(k-1))$ where $\nabla\tau_0^l(k-1)$ is the sample domain gradient of lags at the previous estimation step. While this choice depends on the application, for the experimental evaluation of the system presented in chapters 6 and 7, the constant velocity model was used.

The parameter y_{min} can be used to control the behaviour of the peak tracking system in the face of low received signal levels. As shown in chapter 3, for MLS signals, the peak height of cross-correlograms reduce as the SNR deteriorates. By having empirical knowledge of the peak heights caused by cross-correlation of background ambient noise in the absence of a source signal, the relative localisation system can be prevented from erroneously tracking noise sources as the signal source moves beyond the maximum sensing range of the receivers. This methodology was implicitly implemented for range estimation using the **range tracking** scheme introduced later in section 5.5.1 for the long range experiments presented in chapter 7.

Implementation

As depicted in the block diagram in figure 5.1, there are multiple cross-correlations per estimation step which results in multiple sets for $M(k)$ used for estimating the intermediate quantities r_{11} , r_{12} , r_{21} , r_{22} , θ_1 , θ_2 , φ_1 and φ_2 . For each of these quantities, there is a corresponding tolerance value $\Delta_{Tolerance}$ calculated using the maximum possible variation (constrained by the physical capabilities of the Serafina Mk II AUV/experimental setup) of the lags in the sample domain corresponding to variation of angles and distances within a schedule slot as mentioned

¹. This could also be caused by a $\Delta_{Tolerance}$ value which is smaller than the lower bound stated earlier.

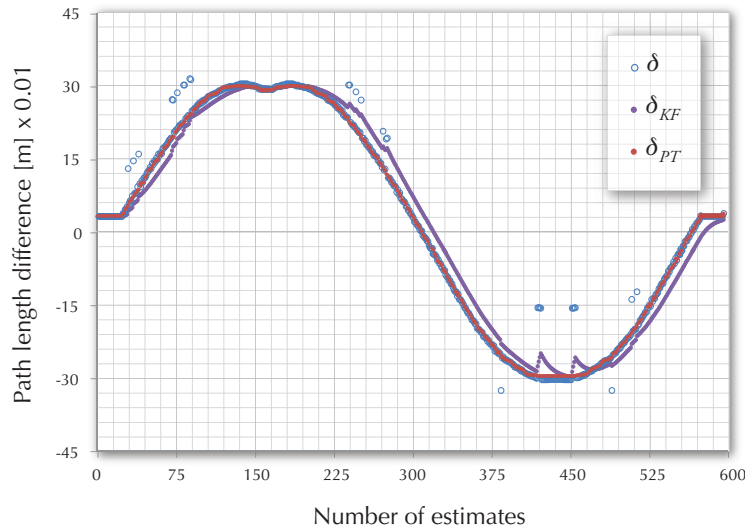


Figure 5.14: Comparison of raw measurements for acoustic path length difference δ with the output of a simple Kalman filter δ_{KF} and peak tracking δ_{PT} where δ varies smoothly. The relatively few outliers appear mostly in consecutive segments.

earlier. As a ‘boot-strapping’ technique, initially peak tracking is disabled and (4.9) is used to find the lags corresponding to the maximum magnitude peak in the cross-correlogram as no prior estimate is available at initialization. Once the position of the peak stabilises (*e.g.* detected by a result sequence which can be explained by the maximal relative speeds of the vehicles, *i.e.* no discontinuities over a certain number of estimation steps), peak tracking is enabled.

As explained later in section 7.2, this peak tracking scheme operating at an early stage in the estimation process is extremely effective in eliminating outliers and heavily contributes towards minimising estimation errors. However, it is not effective in dealing with outliers arising from the numerical structure of the formulae used for calculating secondary estimates such as the alternate range. These are handled by the **threshold bounding** process discussed in section 5.4.2.

Comparison of peak tracking with a simple Kalman filter

In order to justify the effectiveness of the simple peak tracking scheme, the output is compared with that of a simple Kalman filter (Welch and Bishop, 1995). Acoustic path length differences corresponding to cross-correlogram peak positions are plotted in figures 5.14, 5.16 and 5.15. Sample space lags corresponding to the peak position in a cross-correlogram are related to the acoustic path length differences as given by (4.12) and (4.37) (for sub-azimuth and sub-reverse azimuth estimations respectively). Each example plot was chosen to represent different degrees of outliers, patterns of occurrence and different time evolution patterns of the raw measurement. Plots in figure 5.14 represents a variation of path length difference in sub-azimuth induced by an azimuth variation of $\theta : 0^\circ \rightarrow -90^\circ \rightarrow 0^\circ \rightarrow 90^\circ \rightarrow 0^\circ$ over 600 estimation steps. The ‘raw measurements’ (highest peak positions in cross-correlograms) δ are plotted along with the

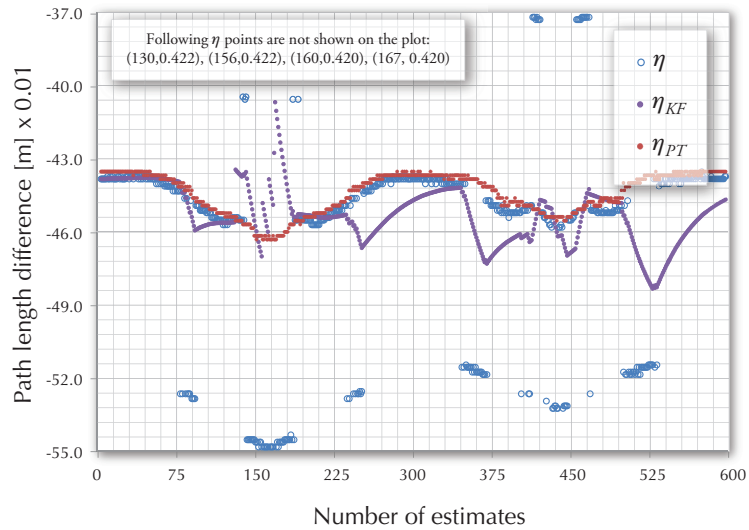


Figure 5.16: Comparison of raw measurements for acoustic path length difference η with the output of a simple Kalman filter η_{KF} and peak tracking η_{PT} over 600 estimates. The variation of η is relatively smooth with a larger number of outliers. The outliers appear mostly in consecutive segments.

outputs of a simple Kalman filter δ_{KF} and outputs of peak tracking δ_{PT} . The nominal angular velocity during the variation was 6.0° s^{-1} and $\Delta_{Tolerance} = 0.67$ was used for peak tracking corresponding to a maximum relative angular velocity of approximately 10° s^{-1} . For the Kalman filter, the initial process noise covariance was set to 1.56×10^{-4} which was empirically calculated. The initial measurement noise covariance was set to 2.25×10^{-2} which converged to 1.8×10^{-3} within 50 estimates and remained stable. As can be seen from the plots, the Kalman filter output shows a slightly delayed response compared to that of the peak tracking.

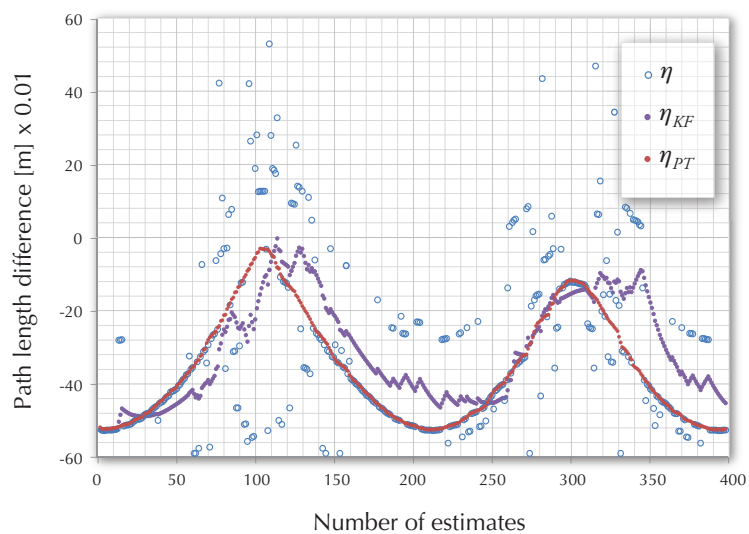


Figure 5.15: Comparison of raw measurements for acoustic path length difference η with the output of a simple Kalman filter η_{KF} and peak tracking η_{PT} . A large number of spurious outliers appear alongside the 'noisy' raw measurements of η .

Plots in figure 5.16 represents a variation of path length difference in sub-reverse azimuth induced by the same azimuth variation as the previous case over 600 estimation steps. The ‘raw measurements’ η are plotted along with the outputs of a simple Kalman filter η_{KF} and outputs of peak tracking η_{PT} . The same $\Delta_{Tolerance}$ value as earlier was used for peak tracking. For the Kalman filter, the initial process noise covariance was set to 3.90×10^{-5} which was again empirically calculated. The initial measurement noise covariance was set to 6.25×10^{-2} which converged to 1.55×10^{-3} within 90 estimates and remained stable. Unlike the previous case, this variation includes many outliers which diverge from the true positions. The plots show that the peak tracking output performs better than the Kalman filter output and stays with the raw measurements while recovering the true position when outliers are present. However, a slight quantization effect can be noticed on the peak tracked output which is due to the finite segment size of the sub-sample interpolation. For all experiments, the number of interpolation segments (n_{Int}) was 10 giving a granularity of 0.1 samples for the peak tracked output.

Plots in figure 5.15 represents a variation of path length difference in sub-reverse azimuth induced by a heading variation of $\alpha : -120^\circ \rightarrow 180^\circ \rightarrow 60^\circ \rightarrow 180^\circ \rightarrow -120^\circ$ over 400 estimation steps. Once again, the ‘raw measurements’ η are plotted along with the outputs of a simple Kalman filter η_{KF} and outputs of peak tracking η_{PT} . The nominal angular velocity during the variation was 4.5° s^{-1} and $\Delta_{Tolerance} = 0.62$ was used for peak tracking corresponding to a maximum relative angular velocity of approximately 10° s^{-1} . For the Kalman filter, the initial process noise covariance was set to 2.44×10^{-4} which was empirically calculated. The initial measurement noise covariance was set to 6.25×10^{-2} which converged to 3.8×10^{-3} within 50 estimates and remained stable. The number of outliers in this variation is much higher than the previous examples and the pattern of occurrence is different as well. The delayed response of the Kalman filter output is evident from the plot while the peak tracked output recovers the true peak positions accurately.

Attributes and limitations of peak tracking

From the examples shown in the earlier subsection it is evident that the simple peak tracking scheme introduced earlier is remarkably well suited for the application at hand. When combined with the nature of raw measurements (cross-correlogram peak positions) and the underlying sub-sample interpolation scheme, this strategy contributes to effectively handle outliers induced by interference. This is achieved without any prior knowledge of an explicit sensor model or a motion model. Peak tracking also handles non-linear motion and seamlessly adapts to changing time evolution patterns of the measurements. As explained earlier using (5.20), this scheme can also be used under changing update rates. This is an important feature as the update rates at which a particular sender is localised can vary depending upon the evolving structure of the local sending schedules.

The success of this method greatly depends on the value chosen for the parameter $\Delta_{Tolerance}$. A lower bound for this parameter was defined in terms of maximum relative velocities between senders and observers, it is difficult to pick an optimal value without empirical measurements conducted in the operational environment to gauge the level of interference present. As $\Delta_{Tolerance}$ is increased, the ability of the system to recover true peak positions from nearby spurious outlier peaks would decrease. In this context, an upper bound for $\Delta_{Tolerance}$ can be specified as follows:

$$\Delta_{Tolerance} \leq t_{PT} f_s \quad (5.23)$$

where spurious peaks (higher than the peak due to the true position) due to multipath arrivals after t_{PT} seconds of the direct path arrival are guaranteed to be handled by the peak tracking system. Multipath signals arriving before t_{PT} seconds have lapsed since the direct path arrival (tolerance interval) does not affect the estimation system as long as the corresponding peak heights are lower than the peak due to the direct path signal, which usually is the case¹.

In the event of sustained occurrence of spurious peaks with higher peak amplitude than the true peak within the tolerance interval, the peak tracking scheme is susceptible to ‘latch on’ and keep tracking the outlier peaks. In such a scenario, if the $\Delta_{Tolerance}$ value is selected too low, the tracking system could start wandering without being able to find the true peak. This would require a restart of the peak tracking system by reverting to a simple maxima search until the peak position stabilises and then re-enable peak tracking. However, for an appropriately selected $\Delta_{Tolerance}$ value, the tracking scheme would recover within a few estimation steps and continue to track the ‘true’ peak².

5.4.2 Threshold bounding

Earlier in this chapter, the quantities produced by the relative localisation system were categorised as primary and secondary estimates. The primary estimates (azimuth, range and alternative heading) are kept within bounds by restricting the extremums of lags produced by the relevant cross-correlations. As mentioned in the previous section, the cross-correlation lags for sub-azimuths and sub-reverse-azimuths are restricted in sample space between $-f_s d/v$, $f_s d/v$ and $-f_s l/v$, $f_s l/v$ respectively. According to (4.31) and (4.38), this limits sub-azimuths and sub-reverse azimuths to -90° , 90° and 0° , 180° respectively, considering the extremes imposed by the physical dimensions which separate the hydrophones and projectors. The matched filter cross-correlations for measuring sub-ranges are limited to sample domain lags of $-N$, N corresponding to the size of the channel window, which in turn reflects the maximum effective range

¹ Except in situations where reflected signals can appear louder than the direct path signal due to the non-omnidirectional directivity pattern of the receivers used.

² An example of self recovery can be seen in the second experiment discussed in section 7.2 of chapter 7.

of the localisation system r_{max} . This scheme guarantees that the localisation system does not produce out of bound primary estimates.

The secondary estimates (heading and alternative range) which are calculated using the primary estimates can potentially produce out of bound values due to the numerical structure of the formulae used. However the adjustment function given by (4.32) ensures that heading estimates produced by (4.36) are always within bounds of $-180^\circ, 180^\circ$. The outliers in alternate range estimation are handled by a combination of range checking and validation against gradients defined by maximum relative velocities. The threshold used for validating the alternate range estimate is r_{max} (since $r' > 0$ according to (4.42)). For gradient validation *a priori* knowledge of the maximum possible linear relative velocities between the AUVs are used.

The procedure is as follows; if the position gradient induced by the current secondary estimate is greater than the gradient permitted by the maximum relative velocity, the estimate is replaced either by the previous estimate (constant position model) or an extrapolated value based on the gradient associated with the previous value (constant velocity model). As with the previously explained peak tracking scheme, the choice is dependant on the application. A constant velocity model was used in the range variation experiments presented in chapter 7. The second validation involves a range check to see if the secondary estimates (including those corrected by the gradient validation) are within the absolute threshold of r_{max} mentioned earlier. If the range check fails, the estimate is replaced by the threshold itself. If both gradient and range checks fails, the pose vector assembly module is meant to flag the estimate as invalid. The effects of these threshold bounding techniques are visible in the experimental results presented in chapter 7¹.

5.5 Computational complexity

Considering the processing chains depicted by the block diagram in figure 5.1, the data acquisition and analogue to digital conversion can be assumed to be done using a dedicated hardware module producing real-time output. The channel windowing module has a constant complexity $\mathcal{O}(1)$ and the filtering using an FFT would be $\mathcal{O}(N \log N)$ where N is the truncated channel length resulting from windowing as described in section 5.3.

Out of the three parallel cross-correlation operations, the one depicted on the top row, corresponding to matched filtering for direct range estimation has the highest complexity of $\mathcal{O}(N^2)$ while the other two have constant complexities of $\mathcal{O}(1)$ each. This is due to the cross-correlation shifts for azimuth and reverse azimuth being always limited to $(2f_s d/v) + 1$ and $(2f_s l/v) + 1$ respectively with d and l being the relevant base distances, regardless of the channel length N . All the subsequent modules have constant complexity of $\mathcal{O}(1)$.

¹. The 'clipping' of the alternate range estimates presented in section 7.3.3 and section 7.4.2 are examples.

As the channel length N is related to the maximum sensing range r_{max} as given in (5.1), the cross-correlations to estimate range takes longer as the range increases with the $\mathcal{O}(N^2)$ complexity. Considering the two multiplications within the inner loop of the cross-correlation routine for a maximum range of 5.0m, the total number of multiplications for processing one sending event is $4 \times 2.0 \times 10^5$ with the actual number of times the inner loop is executed being $N(N+1)/2$. In the case of 10.0m the number is $4 \times 5.9 \times 10^5$. The $4 \times$ in each of these cases refer to the four separate cross-correlations for the estimation of intermediate ranges r_{11} , r_{12} , r_{21} and r_{22} needed for calculating the final range estimate as depicted at the beginning of this chapter in figure 5.1. However, if implemented using hardware capable of parallel processing, these cross-correlations can be done in parallel. As suggested by the three parallel chains of processing depicted in the middle section of the block diagram in figure 5.1, the processor intensive calculations needed for the estimations accommodate parallel processing by the design of the system.

5.5.1 Range tracking

As mentioned above, the length of cross-correlations used for direct range estimation scales up with increasing range and proves to be computationally costly for longer ranges. A **range tracking** scheme is proposed to overcome this problem. In this scheme, the truncated window of the received hydrophone channels are further cropped using information based on the time-history of range estimates. The length of this secondary crop window N_{RT} is based on the maximum relative velocities of the submersible being localised and the time duration since the last localisation of the said submersible. The crop window is centred at r_{prev}^i which would be the estimated range of the sender (with node ID i) during the previous sending event initiated by the same sender. As discussed earlier, depending on the structure of the local communication schedule, a particular node may trigger multiple sending events within a given local schedule run. Apart from addressing the issue of high computational cost, the secondary crop window implicitly implements search space restriction in peak tracking related to range estimation. In this regard, the length of the secondary crop window N_{RT} is equivalent to $N_{Restricted}$ mentioned in section 5.4.1.

With range tracking enabled, once the start of a sending event is triggered, the sample counter on the observer resets and starts counting until $r_{prev}^i f_s / v - N_{RT} / 2$ and then starts assembling the first cropped channel window segment of length N_{RT} . The beginning of the second segment is aligned with sample $(r_{prev}^i f_s / v - N_{RT} / 2) + t_{FB} f_s + l_{MLS}$. As a consequence, the constraint on the maximum effective range given by (5.7) based on the delay t_{FB} no longer applies and defaults to the constraint given by (5.3) which is based on the duration of a scheduling time-step t_{TS} .

This scheme greatly reduces the computational cost of the range estimation for longer ranges by transforming the computational complexity from $\mathcal{O}(N^2)$ to $\mathcal{O}(1)$ since the cross-correlation

length N_{RT} no longer scales up with N due to increasing r_{max} . However, this simple tracking scheme's effectiveness relies heavily on the accuracy of the previous range estimates. As a consequence, it is preferably used only when the local swarm configuration is stable with relatively slow changes in position. The effectiveness of this range tracking scheme was experimentally evaluated for long range ($r > 10\text{m}$) estimations and the results are presented and analysed in section 7.5 of chapter 7.

5.6 Discussion

The basic structural overview of the relative localisation system with regard to information flow between different components and modules was presented and explained at the beginning of this chapter. Later on, the way in which the relative localisation system operating on individual vehicles contribute towards realising a distributed relative localisation solution in a swarm was discussed. The relationship between the relative localisation system and the underlying communication and scheduling system was explained by discussing how the local communication schedules are utilised as a basis for organising the acoustical sending events in a local neighbourhood. As a consequence, it was explained how the update rates at which observers localise a particular sender depends on the structure of the communication schedule. The low level update rate, which is how often a given observer localise senders, was explained in terms of various parameters used by the relative localisation system including the channel window size and effective sensing range.

In this chapter several different forms of interference caused by reverberation (delayed multipath arrivals), cross-talk and extraneous noise sources were identified. Subsequently the effect of aforementioned interferences on the performance of the relative localisation system was extensively discussed. The effect of cross-talk induced by multiple nodes sending simultaneously within the 1-hop neighbourhood of an observer was simulated experimentally. The results were then used to discuss how the relative localisation system behaves under such circumstances. It was shown that causality and relative spatial separation of acoustic sources mitigates most of the potentially detrimental effects of cross-talk. Furthermore, a strategy of incorporating geometrical information to resolve ambiguities arising due to cross-talk under specific conditions was presented.

Handling of outliers were introduced in terms of peak tracking and threshold bounding strategies. The described peak tracking mechanism operates at an early stage of processing of the localisation system and effectively handles position tracking in the face of interference due to delayed multipath arrivals. While this relatively simple approach cannot be directly compared to filtering schemes used by cooperative multi-robot localisation schemes in the literature which operate at a much higher abstraction level, it does not assume linear motion nor require information about the sensor models or motion dynamics. The key parameter used in this method is based upon

a priori information of maximum relative velocities between the platforms and upper and lower bounds for it is presented. Further more, how peak tracking can adapt to changing update rates was also discussed. The output of this outlier handling strategy was compared to the performance of a simple Kalman filter under different motion outlier evolution conditions. The three experimental examples presented showed clearly that peak tracking performs better with regard to peak position recovery in the face of outliers. How tracking performance is affected by the value chosen for the tolerance parameter is discussed later along with perceived limitations of this approach.

Additionally, the computational complexity of the system and its affect on longer range estimates were discussed and a **range tracking** scheme was proposed to overcome the problem of increasing computational cost as the effective sensing range increases. Results of the experimental evaluation of this strategy along with further analysis of the peak tracking performance are presented later in chapter 7.

The following chapter describes the configuration, apparatus and procedure used for the experimental evaluation of the relative localisation system developed and explained throughout this chapter. The experiments are aimed at gauging the accuracy and precision of the estimates produced under operational conditions, the angular and radial sensing limits of the system and the overall suitability of the approach to solve the task of relative localisation for small AUVs.

Chapter 6

Experiments

The relative localisation system described in chapter 5 was implemented to carry out a series of experiments to test its performance. These experiments were aimed at gauging the accuracy and precision of the estimates under operational conditions, angular and radial sensing limits of the system and the overall suitability of the approach to solve the task of relative localisation for small AUVs. Most of the experiments were carried out at the ANU test tank¹ while other experiments were carried out at Lake Burley Griffin². The experimental setup, its implementation and the experimental procedure are explained in the following sections. Also discussed is how experimental ground truth is established and the ensuing estimation errors are defined.

6.1 Experimental setup

The main relative localisation system software was executed on a laptop computer running a standard non-real-time desktop operating system. The projectors and hydrophones were mounted on mock-up hulls based on the dimensions of the Serafina Mk II prototype AUV. The

¹ *Cylindrical tank with corrugated metal walls filled with tap water. Diameter 4.2m, depth 1.5m.*

² *Lake Burley Griffin has an approximate surface area of 6.64km² situated in the centre of Canberra, ACT, Australia.*

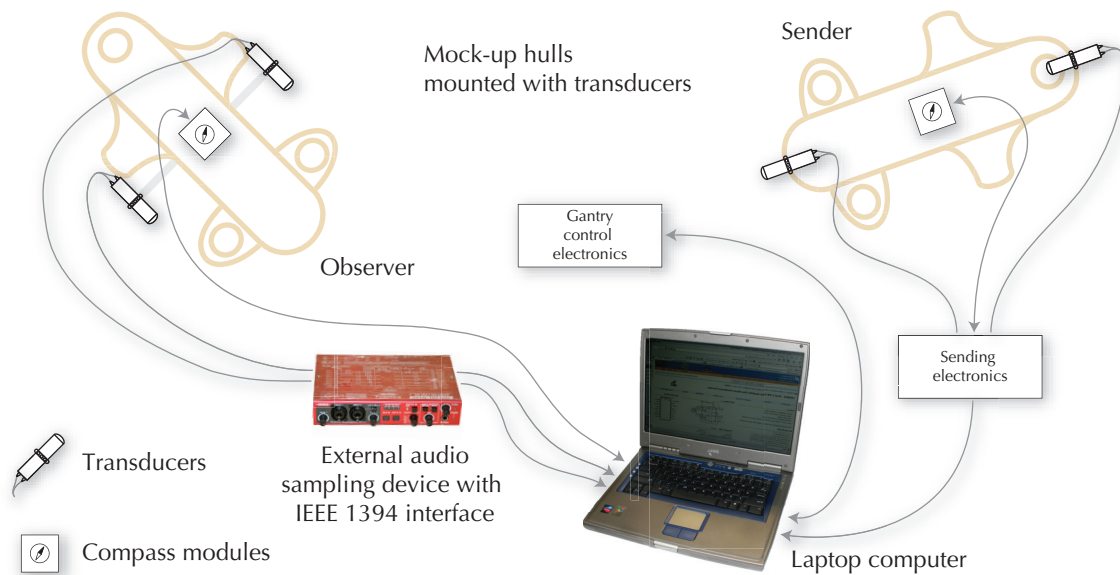


Figure 6.1: The main components of the experimental setup showing data and control flows between them.

signals received by the hydrophone pair were fed through to the computer from an external sampling device via the IEEE 1394 (firewire) bus. The sender-observer synchronisation which is meant to be provided by the long-wave radio communication system in the final implementation (as depicted in figure 5.1 in the previous chapter), was replaced by the sending electronics module signalling the start of sending events via the serial port¹. Two mock-up hull rigs (observer and sender) fitted with hydrophones and projectors (figure 6.3) and mounted at the end of shafts were moved relative to each other with the use of a robotic gantry placed on top of the test tank (for test tank experiments), mounted on the side of a pier (for lake experiments) or by attaching one rig to a boat (for long range lake experiments). The connectivity of this setup is depicted in figure 6.1. The relative localisation system produces the relevant pose vectors on-line corresponding to each time step during the experiments. The raw audio data is stored on the computer for later off-line processing. The results obtained during the experiments and from subsequent off-line processing is presented and analysed later in chapter 7.

6.1.1 Software modules

The software involved with the experimental setup can be divided into a number of modules as depicted in figure 6.2. The main external inputs are the live audio stream received via the external audio sampling device and the sending event signalling received via the sending electronics module. The gantry control module takes the experimental procedure as an *a priori* input which is then converted into a series of motion commands for the gantry as the experiment proceeds.

¹ Explained further in section 6.2.

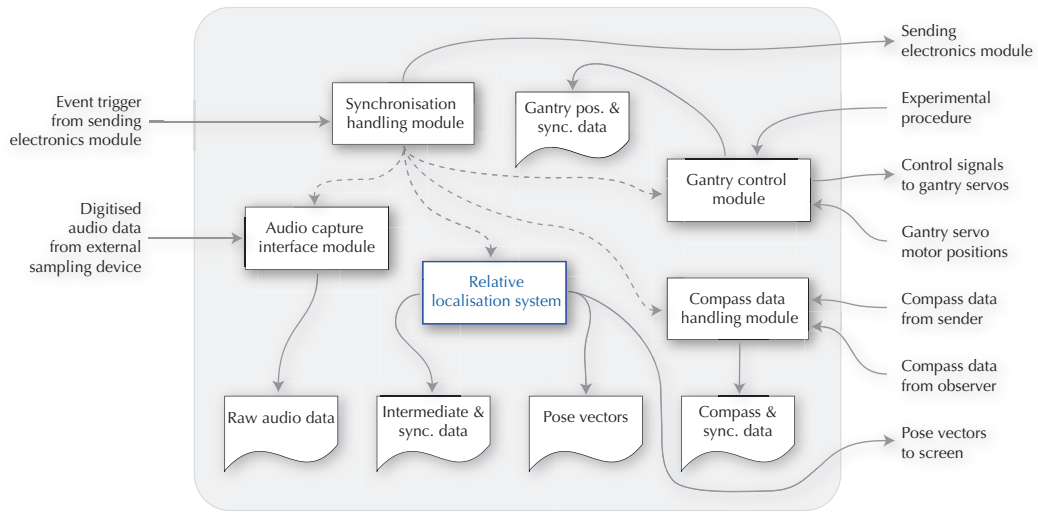


Figure 6.2: The software modules being executed on the laptop computer during an experiment along with the data flows and data stores.

The compass modules attached to both the sender and observer hulls return heading data via the serial ports. The raw audio data, the pose vectors, gantry positions, compass data and intermediate values along with the synchronisation time stamps are stored in disk files.

All these modules are implemented in ADA¹ except for the audio capture interface which is implemented with Visual C++ and linked to the rest of the system as a dynamic library. The disk files created during the live experiment are later used as inputs for an off-line version of the relative localisation system software. The time stamps in each of the files associated with the data records are used to reconstruct the synchronisation. Gantry positions and compass readings are used as “ground truths” when analysing and evaluating the pose vectors produced by the system. The following sub-sections describe the functionality of each of the modules.

Relative localisation system

The main module consists of the relative localisation system which was described in detail in the previous chapter. This module calculates the pose vectors on-line, displays the data on the screen while storing the same on a disk file along with synchronisation time stamps and intermediate values resulting from the multiple cross-correlations for later debugging and analysis.

An identical module is later used for offline processing where the raw audio data stored in the disk file during the ‘live’ experiment is used to provide the main input. The synchronisation is reconstructed from the time-stamps stored in the disk files. During the offline processing, the ground truth is derived from gantry positions and compass readings read from the disk files.

¹. ADA is a high integrity programming language (ISO/IEC 8652:1995/Amd 1:2007).

Audio capture interface

The software module which interfaces with the external audio sampling device via the IEEE 1394 bus stores the raw audio data in a disk file for later off-line processing while transferring the live dual channel audio stream to the relative localisation system.

Synchronisation handling

This module waits for a sending event signal from the sending electronics module via the serial port. Once the signal is received it creates a time stamp and triggers all other modules indicating the start of a sending event. It also retrieves the send counter value (logical time) from the received signal packet. This information is used to attribute the final pose vector estimates. In addition, this module indicates the start and stop of an experimental run by sending bit patterns via the serial port to the sending electronics module, initiating and terminating the sending process.

Gantry control

The gantry cart is controlled via this module which takes the experimental procedure as an *a priori* input, converts it in to a series of motion commands which are then sent to the gantry electronics module. The gantry motion is in the form of translations and rotations controlled via two servo motors. This module also reads the gantry servo motor positions (position feedback) in synchrony with the event triggers described earlier. The step sizes for linear and angular

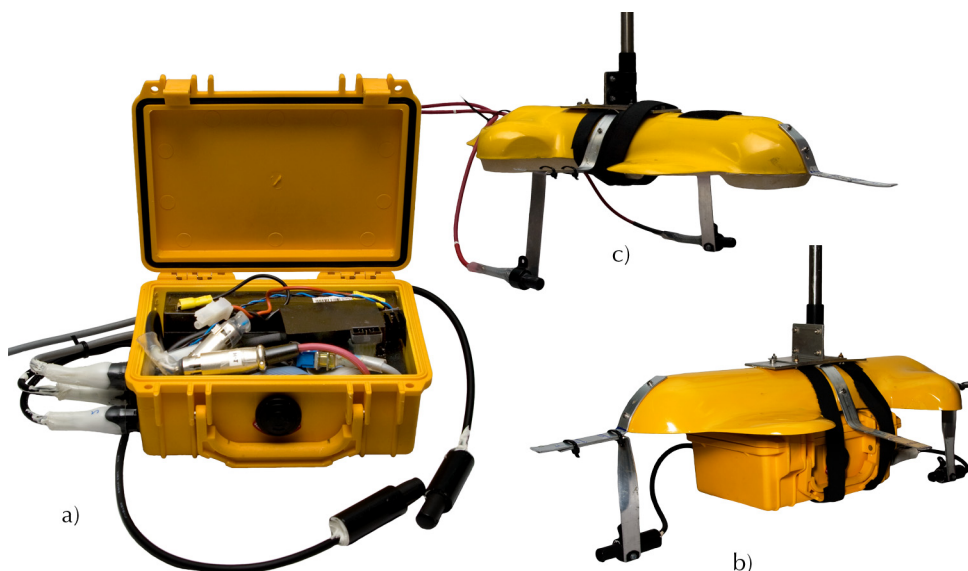


Figure 6.3: a) Waterproof Pelican box housing the sending electronics to which the two projectors are connected, b) Sender rig with the Pelican box strapped to its belly and projectors fixed to the mounting points and c) Observer rig with the two hydrophones fixed to the mounting points and the compass module strapped to its belly.

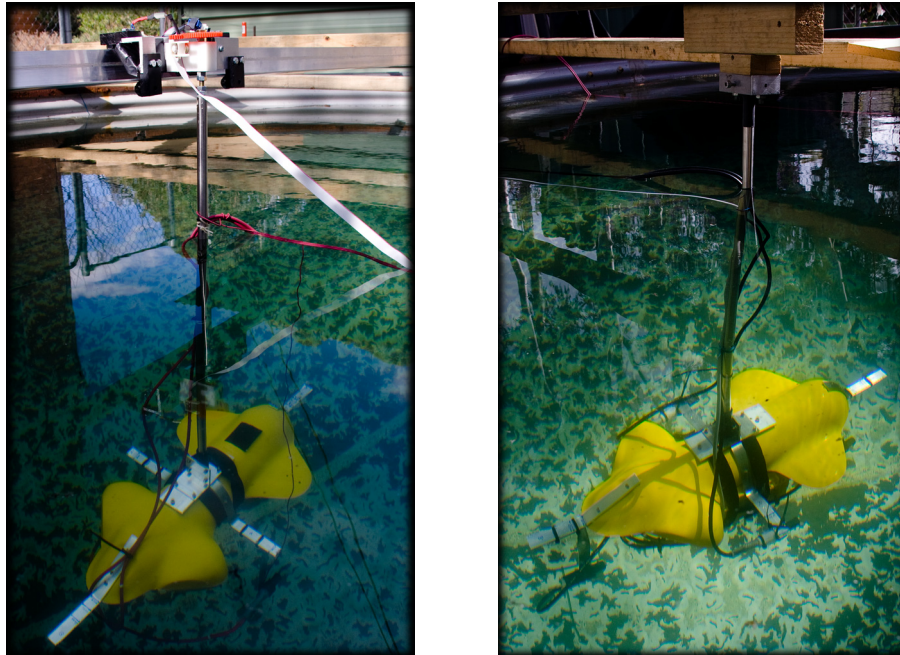


Figure 6.4: The observer rig [left] and sender rig [right] connected to the gantry frame. The observer rig is attached to the gantry cart which can move along a rail, whose position is controlled according to the experimental procedure.

motion as well as the speed of movement is included in the experimental procedure input. The gantry positions at each time-step is stored in a disk file along with the time stamps.

Compass data handling

The compass data handling module, which is again synchronised with the sending event signalling, reads in data returned by the 3-axis magnetometers attached to both the sender and observer rigs. The data from the sender rig mounted compass module is received along with the event signal data packets as described in the following sub-sections while the compass module on the observer rig is queried for data by the compass data handling module at the onset of each sending event. The received magnetometer outputs are converted to compass readings and stored in a disk file for later analysis along with time stamps.

6.1.2 Electromechanical apparatus and firmware

Each electronic hardware module controlling the sending events and reading the magnetometers has its own microcontroller. The data communication between these modules and the laptop computer is via multiple serial ports and in the case of the external sampling device, through the IEEE 1394 bus. The serial port connection to the electronics module including the compass on the sending rig is either the wired RS-232 bus or interfaced wirelessly using XBee RF modules (Digi International, 2008) and connected to the computer via the USB when used during the

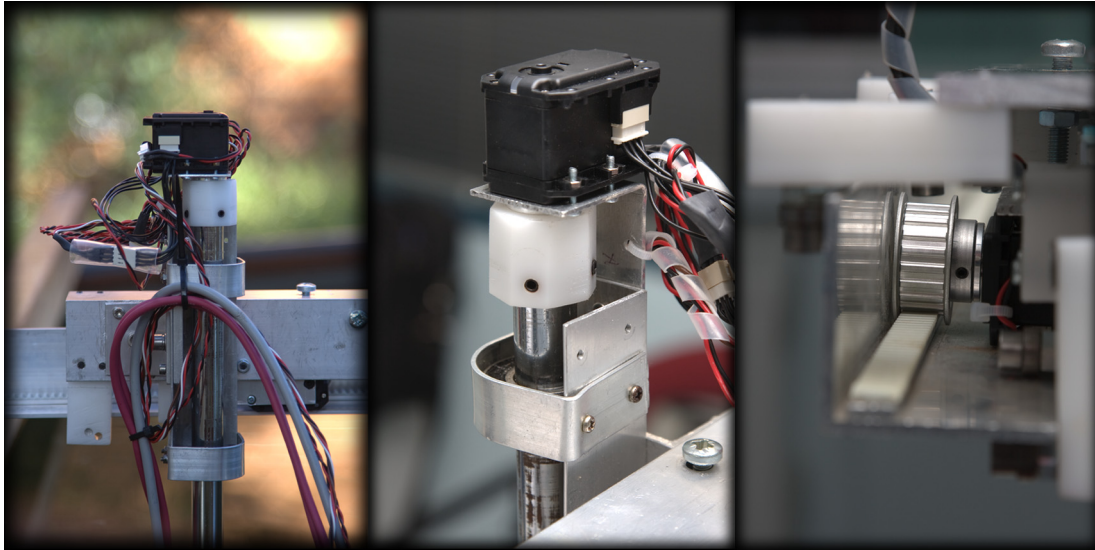


Figure 6.5: Three views of the robotic gantry cart. The cart mounted on the rail during an experiment [left], servo motor controlling rotary motion and shaft coupling [center] and servo motor controlling translatory motion with attached timing pulley running on toothed belt affixed to the gantry rail [right].

[PHOTOGRAPHY BY HIMADHU KOTTEGE]

long range boat experiments. The compass module on the observer was connected via the wired RS-232 bus. The gantry control module communicated with servo motors via a USB/RS-422 adapter device (Robotis, 2007).

Sending electronics and compass modules

The sender electronics module is housed in a waterproof Pelican box as shown in figure 6.3.a. The box holds a lead-acid battery, an Atmel ATmega32 microcontroller and serial line-driver which is used to communicate with the computer, a dual channel cascaded step-up converter

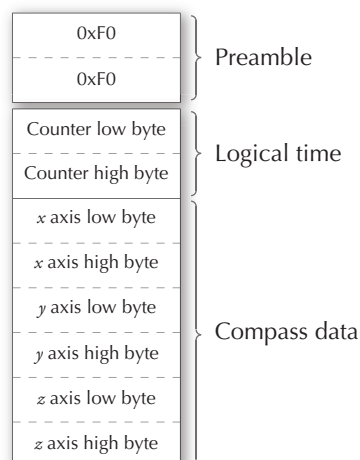


Figure 6.6: Structure of a 10byte data packet sent from the sending electronics module to the computer signalling the start of a sending event.

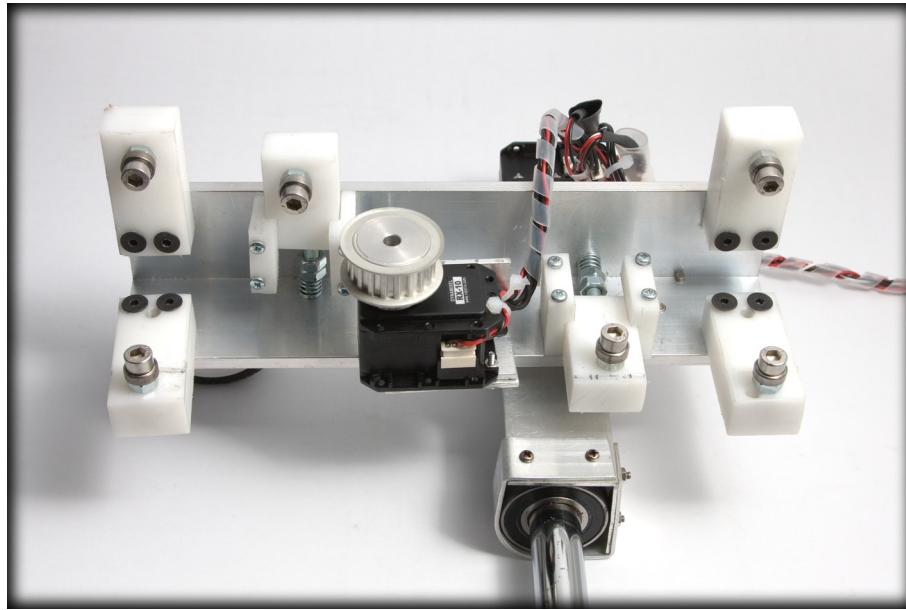


Figure 6.7: View of the robotic gantry cart showing the translatory motion servo motor with the timing pulley. The image also shows the six small rolling-element bearings mounted on plastic blocks which run on the gantry rail and one of the two larger rolling-element bearings holding the shaft.

with a MOSFET driver based stage and a line-driver transformer based stage which drives two Benthos AQ-2000 hydrophones (Benthos, 2001) which are used as projectors and a PNI MicroMag3 3-axis magnetometer (PNI, 2006). The Pelican box is strapped to the hull on the sender rig as shown in figure 6.3.b.

A timer routine on the microcontroller mimics the synchronisation meant to be provided by the long-wave radio communication module and the omnicast scheduling system. Once a ‘start’ signal is received via the serial port from the computer, the timer routine starts and triggers a sending event every 200 ms (t_{TS}) while signalling its start to the relative localisation system running on the computer (via the same serial port). This period governs the update rate of the experimental system with one sender and one observer.

At the onset of each time-step, the following sequence of events take place. First, the microcontroller queries the magnetometer interfaced via the SPI bus and temporarily stores returned values. Then a 16 bit counter is incremented whose value represents logical time. A 10 byte data packet is assembled consisting of a 2 byte preamble, the counter value and 6 bytes comprising the stored magnetometer values (figure 6.6). This data packet is written to the UART with a non-blocking call signalling the start of a sending event to the synchronisation handling module on the computer. Immediately afterwards the MLS sending routine is called. Then a ping consisting of the stored MLS signal¹ is driven to the first projector (P_1) through a general purpose I/O pin

¹. An MLS of length 127 is stored on the microcontroller memory in binary form.



Figure 6.8: Sender and observer rigs attached to the gantry frame placed on top of the test tank. The 3.0m rail and the gantry cart can be seen on the top left side of the image.

via the step-up converter stages and after a ‘front-back’ delay of 50 ms (t_{FB}) another ping is driven to the second projector (P_2). This sequence of events repeat until a ‘stop’ signal is received indicating the termination of an experimental run.

Observer electronics

The observer rig is mounted with two Benthos AQ-2000 hydrophones as shown in figure 6.3.c. The hydrophone outputs are then connected to an Edirol FA-101 sampling device (Roland, 2004) as indicated in figure 6.1. The two analogue audio input channels are pre-amplified and converted to a digital stream with its 96 000 Hz, 24 bit analogue to digital converter. The output is connected to the computer via the IEEE 1394 bus. A separate waterproof enclosure holds the compass module with a PNI MicroMag3 3-axis magnetometer connected to an Atmel ATmega32 microcontroller with a serial line-driver. Data queries from the compass data handling module are received and magnetometer readings are returned to the computer via the same RS-232 serial bus.

Gantry electromechanics

The mechanical apparatus used in the experiments include the two rigs with transducers mounted on shafts and the gantry to which they are connected. The two hulls are submerged by approximately 0.75 m below the water surface. Figure 6.8 shows the wooden frame of the gantry and the aluminium rail on which the robotic gantry cart moves, placed on top of the test tank with the two rigs attached to it. Figure 6.4 shows the observer and sender rigs separately, while figures 6.5 and 6.7 shows multiple views of the gantry cart. Figure 6.9 shows the experimental setup at the lake with the gantry rail attached alongside a pier.

The gantry cart is actuated with two Dynamixel RX-10 servo motors (Robotis, 2008), one each for the rotary and translatory motion. The motion commands are sent and position feedback is received via a USB/RS-422 adapter device (Robotis, 2007). The gantry control module on the computer uses the received position feedback¹ of the two servos to maintain a log of linear and angular gantry cart positions which are later used as ground truth for the experiments along with the compass headings.

The rotary motion servo motor is directly coupled with the rig shaft (figure 6.5 [center]) held in place by two large rolling-element bearings. This minimises any undesirable backlash or sway effects which would influence the ground truth reference of the angular position. The translatory motion servo motor is directly coupled with a timing pulley with 20 teeth which runs on an open ended timing belt (figure 6.5 [right]) affixed to a 3.0m long aluminium gantry rail. Both the pulley and the belt has a pitch of 5.0mm. The six small rolling-element bearings (including two on spring mounted blocks) ensures the cart moves smoothly along the rail without detaching. The translatory motion servo itself is spring mounted to ensure constant coupling between the pulley and the belt. These design features prevent any slippage during translatory motion of the cart which could potentially influence the ground truth reference of the linear position.



Figure 6.9: The experimental setup at the lake with the gantry attached to a pier giving a maximum range of 10m between the sender and observer rigs. [PHOTOGRAPHY BY UWE R. ZIMMER]

¹. The position feedback of the servo motors used is limited to 300° and for translatory motion involving complete rotations (continuous rotation mode of the RX-10), interpolation is used to compensate for the 'missing' 60° .



Figure 6.10: A pedal kayak used during the long range experiments with the sender rig mounted on the side of the vessel. The elevated housing of the GPS module, the data logger and the wireless communication module can also be seen in this image. [PHOTOGRAPHY BY HIMADHU KOTTEGE]

During the experiments, either the sender rig or the observer rig is kept stationary with a predefined heading direction for the hull while only one rig attached to the gantry cart is moved. For some experiments, the sender rig is affixed to the gantry cart while for others the observer rig takes its place. The maximum linear travel distance of the gantry cart is limited by the length of the 3.0 m rail. The angular motion is restricted to $\pm 150^\circ$ about the zero position (clockwise or counter-clockwise). The maximum linear speed of the gantry cart under load (when attached with the observer rig, with the hull submerged 0.75 m below the water surface) is 0.14 ms^{-1} and the maximum angular speed is 300° s^{-1} . However, during most of the experiments, the speeds used are much slower than the maximum possible values to observe the resolution limits of the relative localisation system.

Long range experiments

During the long range experiments conducted at the lake, the sender rig was mounted on the side of a pedal kayak (figure 6.10) such that the sender hull was submerged by approximately 1.5 m beneath the water surface. As mentioned earlier, the serial link between the sender electronics and the computer was maintained via XBee RF modules (Digi International, 2008) which operate in the 2.4 GHz wireless band. The observer rig was mounted on the gantry frame attached to a pier and kept stationary during the experiments. The kayak travelled at a nominal speed of $1.0\text{-}1.5 \text{ ms}^{-1}$ during these experiments.

GPS modules¹ connected to data loggers with a wireless interface² were used to provide the required ground truth reference during these experiments. One GPS module provided the stationary position of the observer rig while the other provided the position of the kayak as it navigated in a predetermined motion pattern on the lake. The GPS position update rate was 5 Hz.

6.2 Synchronisation

In the final deployable implementation of the relative localisation system, the sender-observer synchronisation is intended to be provided by the underlying communication and scheduling system as detailed in the previous chapter. However, during the experiments presented in this thesis, this synchronisation was replaced by the sender electronics module signalling the relative localisation system with a ‘sync’ signal indicating the start of a sending event. The structure of this sync signal and how it is synthesised was explained in a previous section describing the sending electronics module. Since a non-real-time full-featured processing environment was chosen to conduct the experiments to allow maximum flexibility in evaluating the system, the sync signal reception was affected by latency variations typical of input/output operations in such environments. The resulting synchronisation timing jitter experienced during the experiments is compared with that expected from the communication and scheduling system in the following sub-sections.

Synchronisation timing jitter

During this signalling process, the main parameter which has an impact on the performance of the relative localisation scheme, namely the synchronisation timing jitter was compared with the specifications of the long-wave radio communication module (Schill, 2007, pp. 66-69). The carrier frequency of the long-wave radio communication module is 122880 Hz while sampling is done at 32000 Hz. The data rate is specified at 8192 bps. Given these parameters, an upper bound for synchronisation timing jitter arising from variation in detection latency due to bit alignment errors can be specified as 0.12×10^{-3} s. The latency mentioned here is equivalent to the synchronisation latency t_L defined in section 4.2.1 of chapter 4. Therefore, the synchronisation timing jitter mentioned here is equivalent to Δt_L .

Measured time-slot durations

The duration of a time-slot (the perceived duration of a sending event), t_{TS} is measured as the duration between two consecutive sync signals received by the synchronisation handling module.

¹. LS20031 smart antenna modules (Locosys Technology, 2006)

². Seagull wireless dashboard telemetry and data recorders (Eagle Tree Systems, 2008) used with GPS expander V3 modules (Eagle Tree Systems, 2005).

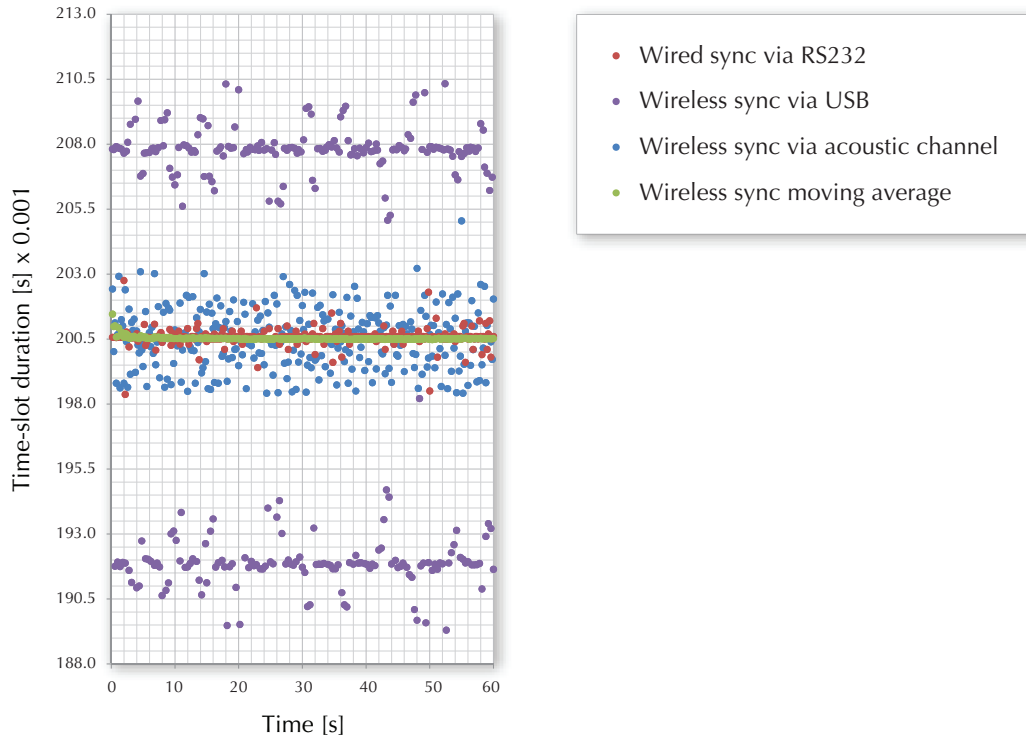


Figure 6.11: Durations between two consecutive sending event signals received by the synchronisation handling module measured over 60s (300 sending events).

These durations were measured to analyse how they were affected by the behavior of the non-realtime operating system running on the computer which was used during the experiments. The durations measured with sync signals received via the wired RS-232 port were compared with those measured with sync signals received via the USB port when using the XBee RF modules. The wired connection had a relatively low average deviation of 0.17×10^{-3} s from the mean while the USB/XBee combination had a relatively high average deviation of 8.03×10^{-3} s from the mean. Furthermore, the deviations of the latter combination was not uniformly distributed but was centred around $\pm 8.0 \times 10^{-3}$ s of the mean. To isolate the timing jitter introduced to the USB by the operating system and the timing jitter caused by the XBee RF transmission, the TTL

Direct sync via acoustic channel	Wired sync via RS232	Wireless sync via USB	Wireless sync via acoustic channel	Wireless sync moving average
$\sigma_{t_{TS}} = 4.57 \times 10^{-6}$ s	$\sigma_{t_{TS}} = 0.34 \times 10^{-3}$ s	$\sigma_{t_{TS}} = 8.21 \times 10^{-3}$ s	$\sigma_{t_{TS}} = 1.14 \times 10^{-3}$ s	$\sigma_{t_{TS}} = 0.08 \times 10^{-3}$ s
$\mu_{t_{TS}} = 200.53 \times 10^{-3}$ s	$\mu_{t_{TS}} = 200.57 \times 10^{-3}$ s	$\mu_{t_{TS}} = 200.62 \times 10^{-3}$ s	$\mu_{t_{TS}} = 200.51 \times 10^{-3}$ s	$\mu_{t_{TS}} = 200.53 \times 10^{-3}$ s
$\overline{\Delta t_{TS}} = 4.00 \times 10^{-6}$ s	$\overline{\Delta t_{TS}} = 0.17 \times 10^{-3}$ s	$\overline{\Delta t_{TS}} = 8.03 \times 10^{-3}$ s	$\overline{\Delta t_{TS}} = 0.92 \times 10^{-3}$ s	$\overline{\Delta t_{TS}} = 0.03 \times 10^{-3}$ s

Table 6.1: Comparison of time-slot durations according to the 'sync' signal received by the synchronisation handling module under different circumstances.

output of the wireless receiver module was connected to an input channel of the sampling device. The duration between sync signals was measured using leading edge detection of the received audio channel considering the bit pattern of the preamble bytes of the sync signal packet. This measurement showed a uniformly distributed average deviation of 0.92×10^{-3} s suggesting that the $\pm 8.0 \times 10^{-3}$ s jitter was due to the operating system/USB combination. A 25 point moving average was applied to the wireless sync received via the acoustic channel which reduced the average deviation to 0.03×10^{-3} s. These four different time-slot durations measured over 60s (300 sending events) under different circumstances are depicted in figure 6.11. For reference, the acoustic output of the sender was directly coupled to the sampling device to measure the actual duration of a sending event¹. The average deviation of the actual sending event duration was 4.0×10^{-6} s from the mean which was 200.53×10^{-3} s. The standard deviations, means and the average deviations of these measurements are presented in table 6.1 for comparison. It must be noted that the shorter duration time-slots depicted in figure 6.11 are due to communication latencies causing the previous time-slot to appear longer. As evident from the extremely low average deviation of the actual sending event duration, the sending electronics module maintains a fairly constant² period between sending events.

The average deviation of the duration from its mean value can be considered the synchronisation timing jitter in the experimental setup and can be denoted by Δt_{TS} . These timing jitter values can be compared with those associated with the long-wave radio communication system.

6.3 Experimental procedure

A series of experiments were conducted to evaluate the performance of the relative localisation system. Within the constraints of the directionality of the transducers used, experiments attempted to cover the full angular range for azimuth and heading estimates. This was achieved by rotating the shafts attached to the rigs by 180° using the gantry cart. The maximum distance measured at the tank was 2.25 m with a translation of 1.5 m of the cart while the maximum distance measured at the lake was 10.0 m with a translation of 2.0 m. The possible variations of the three parameters, azimuth (θ), heading (α) and range (r) using the experimental setup is shown in figure 6.12. The long range experiments where the sender rig was attached to a kayak involved distances beyond 90 m.

¹. Once directly coupled with the output of the sender, the duration between pings were measured by simple threshold detection on the received acoustic channels.

². A 4.0×10^{-6} s variation contributes to a $\pm 6.0 \times 10^{-3}$ m variation in range estimation which can be considered negligible.

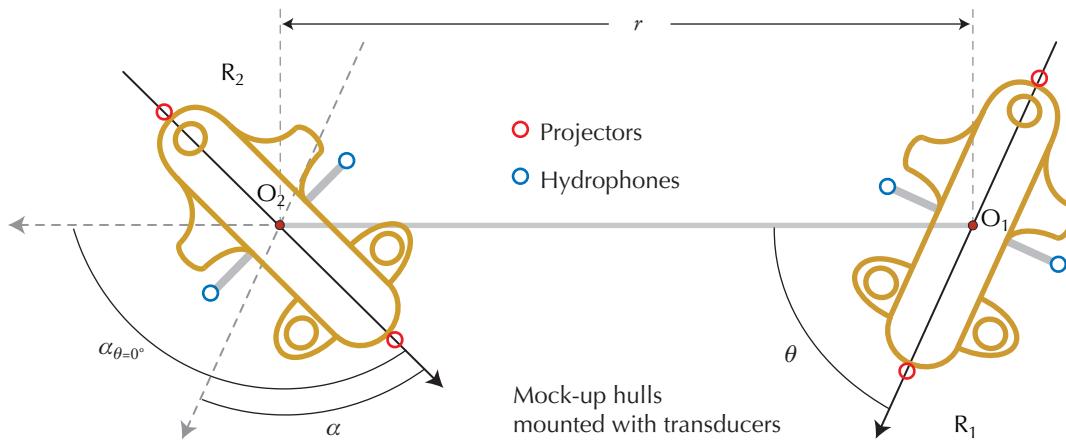


Figure 6.12: Possible variations in the experimental setup. The mock-up hulls with the transducers attached to the rigs can be rotated to vary the azimuth (θ) and heading (α) and the range (r) can be varied by moving the rigs along the rail on the gantry.

6.3.1 Variation of azimuth

With the sender hull stationary at a distance r from the observer, rotating the observer hull clockwise by 180° about its central vertical axis is equivalent to the sender hull making a semi-circular arc of radius r around the observer counter-clockwise. A number of experiments were conducted where the observer hull was rotated clockwise such that the azimuth of the sender relative to the observer varied as: $-90^\circ \rightarrow 0^\circ \rightarrow 90^\circ$ and rotated counter-clockwise such that the azimuth varied as: $90^\circ \rightarrow 0^\circ \rightarrow -90^\circ$. The distance between the central vertical axes of the hulls remained unchanged at r . During these rotations, the heading of the sender hull relative to the observer varied as well. The relationship between the variation of azimuth and heading is as follows:

$$\alpha = [\alpha_{\theta=0^\circ} - \theta]_{adj} \quad (6.1)$$

where the adjustment function $[\]_{adj}$ is defined as in (4.32) and $\alpha_{\theta=0^\circ}$ is the heading of the sender hull when its azimuth is 0° relative to the observer hull.

6.3.2 Variation of heading

As explained in the previous section, the relative heading varied during the azimuth variation. However, the heading can be explicitly varied by keeping the observer hull stationary and rotating the sender hull about its central vertical axis. The azimuth remains constant at θ which is the angle between the gantry rail and the center line of the observer hull (figure 6.12) and so does the range r . Depending on the mounting direction of the projectors, the sender hull is rotated

about its central vertical axis to vary the relative heading as either $-90^\circ + \theta \rightarrow \theta \rightarrow 90^\circ + \theta$ or $-90^\circ + \theta \rightarrow 180^\circ + \theta \rightarrow 90^\circ + \theta$.

6.3.3 Variation of range

While the range remained constant during variations of azimuth and heading, the latter parameters remains constant during variations of range. Translation of the gantry cart along the rail, with either of the two rigs attached, results in a variation of the relative distance between the sender and observer hulls. During the experiments conducted, a range variation was incorporated as the initial phase before the rotations of the rigs to either vary the azimuth or the heading. While one rig was attached to the gantry cart, the other rig was not necessarily mounted exactly at the end of the rail. The gantry frame could be adjusted such that the rig is mounted some distance r_g away from the end of the rail as can be seen in figures 6.8 and 6.9. Then r_g is the minimum range between the sender and the observer during the experiment while the maximum range is $(r_g + r_r)$ where r_r denotes the length along which the gantry cart moves and this quantity has a maximum of 3.0m in the current setup.

6.4 Calibration of experimental apparatus

Apart from the errors discussed in chapter 4 which affect the components of the estimated pose vector, there are errors which could potentially arise due to the configuration of the experimental setup. The following sections describe the sources of these errors, methods of calibrating the experimental setup and presents corrections which are applied to the estimates produced by the relative localisation system.

Alignment of sender and observer rigs with the rail

For both tank and lake experiments, a number of distance measurements are made while setting up the gantry frame using a standard measuring tape. These values are used to accurately align the experimental rigs. Figure 6.13 shows the measurements made during the gantry frame setup procedure before a series of tank experiments. A, B and D represents wooden beams of equal length (4.5m) and C represents the aluminium gantry rail (3.0m). One rig (R_2) is mounted at the mid point of beam D while the other rig (R_1) is mounted to the robotic gantry cart running on the rail. The two ends of the rail are clamped to the mid points of beams A and B. The gantry frame made up by the three beams and the rail is placed on top of the tank as shown in the figure with the two rigs submerged. First, beams A and B are adjusted such that $a = a'$, $b = b'$ and $c = c'$ ensuring that the beams are parallel and the rail is perpendicular to the beams while placing the rail along a diameter of the circular tank. Next, beam D is adjusted such that $b = b'$ and $e = e'$. This ensures that the two central vertical axes (rig shafts going through O_1 and O_2) of

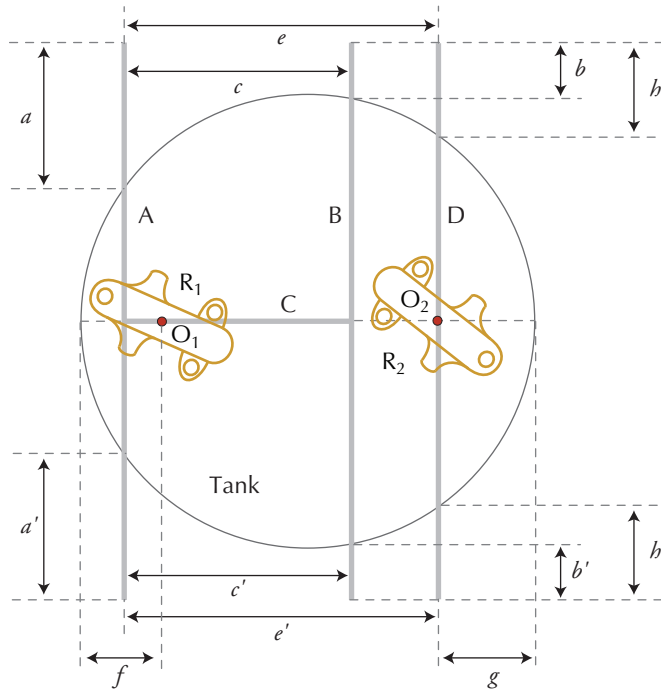


Figure 6.13: Measurements made during the gantry setup and calibration process for tank experiments.

the rigs are aligned with the rail. The starting distance (r_s) between the two rigs for a particular series of experiment is related to f and g as:

$$r_s = d_{tank} - (f + g) \tag{6.2}$$

where d_{tank} is the diameter of the tank (4.2 m). A value for g is selected when beam D is initially placed such that $e = e' > r_s$. Later, f is adjusted by moving R_1 along the rail using direct control¹ of the translatory motion servo motor on the gantry cart until (6.2) is satisfied. Once the adjustments are made, the three beams are clamped to the rim of the tank to prevent further movement throughout the series of experiments.

Figure 6.14 shows the measurements made during the gantry frame setup procedure before a series of lake experiments. The gantry rail C is clamped to the beams A and B such that $a = a'$ and rig R_2 is attached to beam D such that $a'' = a'$. All three beams are placed across the breadth of the pier such that $c = c'$ and $b = b'$ while the gantry rail is along side the pier. As before, if r_s is the starting distance between the rigs for a series of experiments, the beams are placed such that $b = b' > r_s$. Later, f is adjusted as in the previous case such that:

$$r_s = b - f \tag{6.3}$$

¹. Using the ‘Dynamixel Manager’ software provided with the USB2Dynamixel adapter (Robotis, 2007).

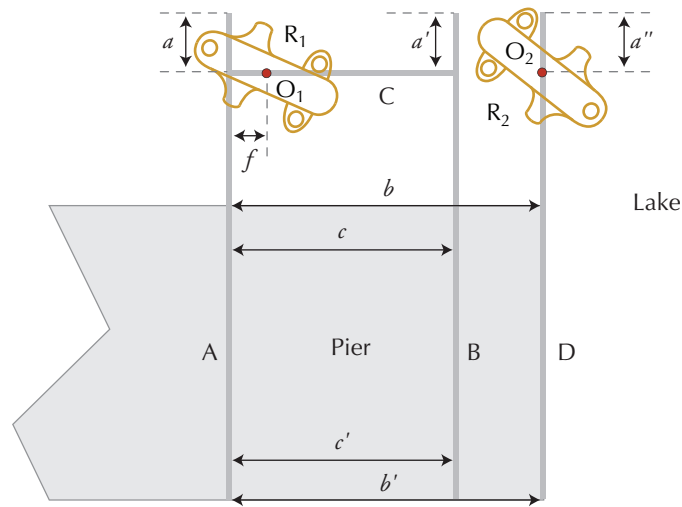


Figure 6.14: Measurements made during the gantry setup and calibration process for lake experiments.

Once the adjustments to f are made and measured, the whole frame is pushed out while still maintaining the separation between the beams. The ends of the beams are lined up with one edge of the pier while the rail is parallel to the opposite edge of the pier as shown in the figure and clamped to prevent further movement. This ensures that the central vertical axes (rig shafts going through O_1 and O_2) of the two rigs are aligned with the rail throughout the series of experiments. In both setup procedures, it is assumed that the beams are straight within reasonable bounds and additionally for the lake experiments, it is assumed that the sides of the pier are straight and the corner angles are 90° .

Compass calibration

Once O_1 and O_2 are aligned with the gantry rail, for calibration of the compass heading readings, both rigs are rotated clockwise and counter-clockwise by 180° . Rig R_1 is rotated using direct control of the rotational motion servo motor of the gantry cart while rig R_2 is rotated manually.

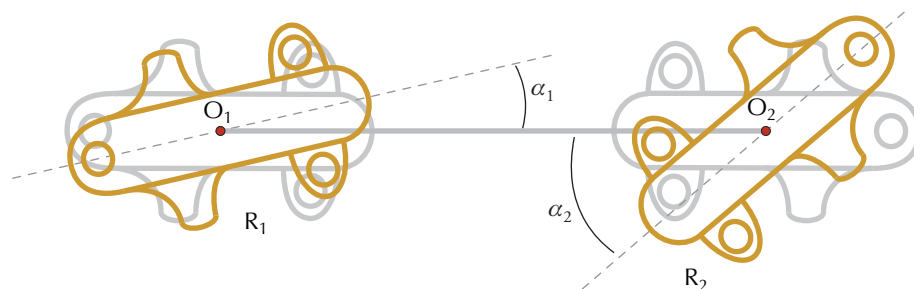


Figure 6.15: Angular offsets of sender and observer rigs before angular calibration.

Calibration of the compass modules was performed as described in the multipoint calibration primer application note (PNI, 2004).

Angular calibration of the rigs

The two rigs need to be calibrated such that the relative rotation between the two mock-up hulls is zero and the poles of the two body-fixed coordinate frames are aligned with each other and the rail. Rig R_1 is initially attached to the gantry cart oriented in a way that the mock-up hull would be parallel to the gantry rail with the rotational servo motor at its zero position (figure 6.15). Assuming this orientation is accurate once the servo motor is brought to its zero position after the compass calibration procedure, R_2 is manually rotated until the relative rotation between the two rigs is zero with the aid of the compass module on each rig. The calibration software module used for this process outputs the two compass headings (which have been calibrated as described in the previous sub-section) and the sub-azimuth estimates produced by the relative localisation system. A relative offset of 180° between the compass headings indicates that the two poles of the coordinate frames are parallel to each other ($\alpha_1 = \alpha_2$) but are not necessarily aligned with the rail. Minor angular adjustments are made to both R_1 and R_2 (via the rotational motion servo motor for R_1 and manually for R_2) until the relative offset of compass headings is 180° and both sub-azimuth estimates return 0° . Once these are achieved ($\alpha_1 = \alpha_2 = 0^\circ$), the current angular position of the rotational motion servo motor of the gantry cart is used as a starting angular offset for rotations of R_1 during the ensuing experimental procedures. The angular scale affixed to beam D (figures 6.13 and 6.14) at the mounting point of the shaft of R_2 is read and its value is used as an angular offset for rotations during the experiments. Once this calibration is done, R_2

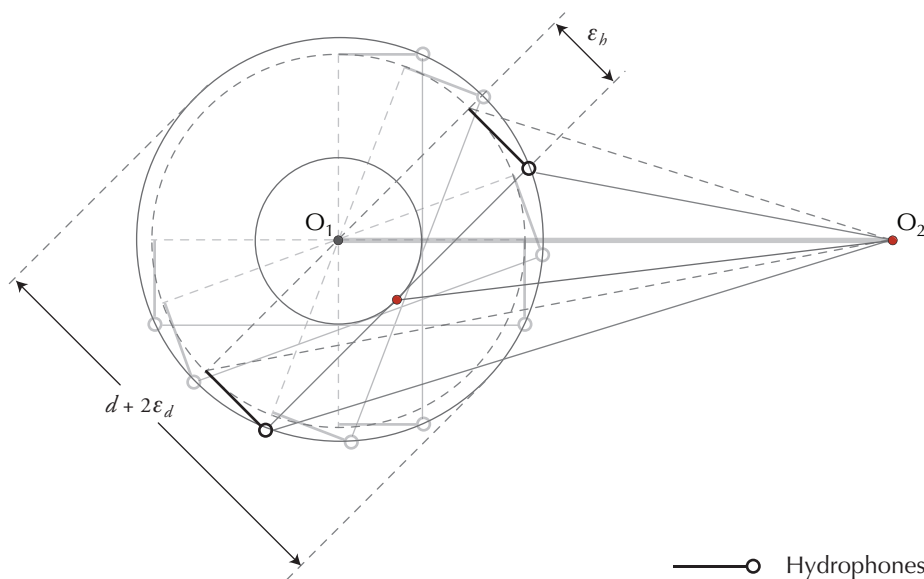


Figure 6.16: Experimental errors introduced by the positioning of the hydrophones on the observer rig.

is rotated to a predefined angle to represent either an initial azimuth (for heading variations) or a heading (for azimuth variations) in preparation of the experiments.

Errors due to hydrophone position on observer hull

The line joining the receiving surfaces of the two hydrophones is meant to intersect the pole (O_1) of the coordinate frame attached to the observer hull. However, due to the finite protrusions on the mounting points on the rig, the receiving surfaces of the hydrophones protrude by ε_b , as illustrated in figure 6.16. The quantity ε_d mentioned in the figure is related to ε_b as follows:

$$\varepsilon_d = \frac{\sqrt{d^2 + 4\varepsilon_b^2} - d}{2} \quad (6.4)$$

where d has the usual meaning of being the base distance between the hydrophones. The angle and distance dependant azimuth correction required is:

$$\varepsilon_{\theta_b} = \tan^{-1}\left(\frac{\varepsilon_b \sin \theta_0}{r_0 - \varepsilon_b \cos \theta_0}\right) \quad (6.5)$$

Where θ_0 and r_0 are the ground truth azimuth and range derived from the position of the gantry cart and the initial positions of the rigs. The distance and angle dependant correction required for the range due to this is:

$$\varepsilon_{r_b} = \varepsilon_b \cos(\theta_0 + \varepsilon_{\theta_b}) \quad (6.6)$$

Errors due to projector position on sender hull

The mid-point of the line joining the transmitting surfaces of the two projectors is meant to coincide with the pole (O_2) of the coordinate frame fixed on the sender hull. As with the hydrophones on the observer hull, these too have finite protrusions due to the mounting points on the rig. As depicted in figure 6.17, this necessitates corrections for both azimuth and range and these quantities are as follows:

$$\varepsilon_{\theta_p} = \tan^{-1}\left(\frac{\varepsilon_p \sin(\theta_0 + \alpha_0)}{r_0 + \varepsilon_p \cos(\theta_0 + \alpha_0)}\right) \quad (6.7)$$

$$\varepsilon_{r_p} = \varepsilon_p \cos(\theta_0 + \alpha_0 - \varepsilon_{\theta_p}) \quad (6.8)$$

While these corrections are distance and angle dependant, the quantities θ_0 , r_0 and α_0 are ground truth azimuth, range and heading derived from the linear and angular position of the gantry cart and the initial positions of the rigs.

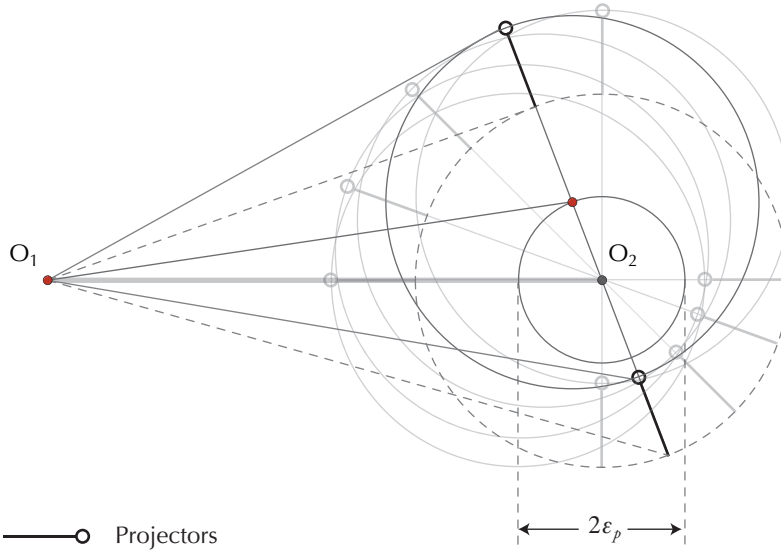


Figure 6.17: Experimental errors introduced by the positioning of the projectors on the sender rig.

Correction of experimental errors

Considering all the errors and their corresponding corrections mentioned earlier, the compound corrections for azimuth, range and heading can be expressed as follows:

$$\varepsilon_{\theta} = \varepsilon_{\theta_b} + \varepsilon_{\theta_p} \quad (6.9)$$

$$\varepsilon_r = \varepsilon_{r_b} + \varepsilon_{r_p} \quad (6.10)$$

$$\varepsilon_{\alpha} = \varepsilon_{\theta} \quad (6.11)$$

These corrections are applied to the pose vector components output by the relative localisation system before the values are compared with the ground truth quantities for calculation of experimental errors as defined in section 6.5.1. The compound corrections are applied as follows:

$$\theta = \theta_{raw} - \varepsilon_{\theta} \quad (6.12)$$

$$r = r_{raw} - \varepsilon_r \quad (6.13)$$

$$\alpha = \alpha_{raw} - \varepsilon_{\alpha} \quad (6.14)$$

$$r' = r'_{raw} - \varepsilon_r \quad (6.15)$$

$$\alpha' = \alpha'_{raw} - \varepsilon_{\alpha} \quad (6.16)$$

where θ_{raw} , r_{raw} , α_{raw} , r'_{raw} and α'_{raw} are the uncorrected estimates produced by the relative localisation system while θ , r , α , r' and α' are the respective corrected quantities. In the

subsequent sections, the output of the relative localisation system during the experimental evaluation of the system refers to these corrected quantities.

6.5 Establishing ground truth

The heading readings of the two compass modules attached to the rigs and the linear position of the gantry cart were used to derive ground truth references for the estimated quantities. While the linear positions were validated by actually measuring the initial and final positions of the gantry cart along the rail, the relative shifts of the compass heading readings were validated against the angular positions returned by the rotational motion servo motor on the gantry cart.

If r_s is the starting distance between the sender and the observer rigs for a particular experiment and the linear position returned by the gantry cart is r_g , then the ground truth for range is given by:

$$r_0 = r_s - r_g \quad (6.17)$$

Since the compass readings are absolute heading angles relative to magnetic North, the relative angular positions were calculated by considering absolute headings from both the compass modules attached to the sender and the observer. If the absolute compass headings from the modules attached to the sender and observer rigs are denoted by α_{sender} and $\alpha_{observer}$, then the relative variation of azimuth induced by a rotation of the observer defined as the azimuth ground truth is given by:

$$\theta_0 = [\alpha_{observer} - \alpha_{sender}]_{adj} \quad (6.18)$$

and the relative variation of heading induced by a rotation of the sender defined as the heading ground truth is given by:

$$\alpha_0 = [\alpha_{sender} - \alpha_{observer}]_{adj} \quad (6.19)$$

where the adjustment function $[]_{adj}$ is defined as in (4.32) in both instances.

During the long range experiments on the lake where one rig was mounted to a kayak, the derivation of ground truth for the relative position of the sender is different to the procedure explained above. All three parameters, azimuth, range and heading vary independent of each other through the course of these experiments. While the ground truth for the relative heading as given by (6.19) is still applicable, this relies on a reliable communication channel between the sender rig mounted to the kayak and the computer on the pier. As mentioned earlier, wireless serial communication was established with XBee RF modules during these experiments. The azimuth and range ground truths were derived from the positions of the kayak recorded via the GPS

module and data logger (Eagle Tree Systems, 2005; Eagle Tree Systems, 2008). For these experiments, at each time-step, the ground truth for range is

$$r_0 = r_{GPS} - r_{offset} \quad (6.20)$$

where r_{GPS} is the GPS distance returned by the data logger on the kayak while r_{offset} is the starting distance between the mounting points of the observer rig attached to the pier and the sender rig mounted to the kayak. The ground truth for azimuth is calculated using the longitude and latitude returned by the GPS data logger as follows:

$$\theta_0 = \tan^{-1}\left(\frac{x_{sender} - x_{observer}}{y_{sender} - y_{observer}}\right) - 90^\circ + \theta_{offset} \quad (6.21)$$

where x_{sender} , y_{sender} are the longitude, latitude coordinates returned by the GPS data logger on the kayak and $x_{observer}$, $y_{observer}$ are the longitude, latitude coordinates of the mounting point of the observer rig. The θ_{offset} represents the correction for the relative rotation between the coordinate frame fixed on the observer hull and the longitude, latitude coordinate system (based on true North).

6.5.1 Definition of estimation errors

Apart from the errors potentially arising due to the configuration of the experimental setup as mentioned in the earlier sections, the deviations of pose vector components from their respective ground truth values are considered estimation errors. Formulae are derived to analyse the statistical behaviour of these deviations. In the following derivations, ϕ is used as a placeholder for θ , r , α , r' and α' . Therefore, the deviation of estimates with bias is given by:

$$\Delta\phi_i^{biased} = \phi_i - \phi_{0_i} \quad (6.22)$$

where ϕ_i is the estimate and ϕ_{0_i} the corresponding ground truth value at estimation step i . The mean $\mu_{\Delta\phi}$ of the estimation error for m estimation steps is

$$\mu_{\Delta\phi} = \frac{\sum_{i=1}^m (\phi_i - \phi_{0_i})}{m} \quad (6.23)$$

and the standard deviation $\sigma_{\Delta\phi}$ of the estimation error for m estimation steps is

$$\sigma_{\Delta\phi} = \sqrt{\frac{\sum_{i=1}^m (\Delta\phi_i^{biased} - \mu_{\Delta\phi})^2}{m}} \quad (6.24)$$

The unbiased root squared errors (RSE) of the estimate would then be given by:

$$\Delta\phi_i = \sqrt{(\Delta\phi_i^{biased} - \mu_{\Delta\phi})^2} \quad (6.25)$$

The average deviation of the unbiased root squared error (*i.e.* mean of RSE) of the azimuth estimates is given by:

$$\overline{\Delta\phi} = \frac{\sum_{i=1}^m \Delta\phi_i}{m} \quad (6.26)$$

where m is the number of estimation steps. Since there are no assumptions regarding the form of estimation error distribution, rather than the standard deviation given by (6.24), the average deviation given by (6.26) is considered to be a better indication of the behaviour of the estimation error being a more direct representation of empirical data.

The next chapter contains experimental results of azimuth, range and heading variations and corresponding plots showing the RSE of each of these quantities with respect to the relevant ground truth measurements. These include results obtained by experiments conducted both at the test tank and the lake. In addition, the biased deviations are also presented to illustrate the spread of estimation errors.

6.6 Measuring Signal-to-Noise Ratio

As an additional performance parameter, the signal-to-noise ratio (SNR) of the acoustic pings received by the relative localisation system was measured. While elucidating the difficulties in accurately estimating SNR in practice, Bosworth et al. (2008) presents a method to do so for an underwater acoustic waveform received by two hydrophones. This method was of particular interest since it is specified for conditions very similar to those of the relative localisation system, where the two hydrophones are sufficiently close spatially such that the attenuation or propagation loss of the signal is common to both receivers. Additionally this method uses the normalised cross-correlation coefficients produced by cross-correlating the two received signal channels to derive the SNR. They contend that

$$S/N = \rho / (1 - \rho) \quad (6.27)$$

where S denotes the total power of the signal and $N_1 = N_2 \equiv N$ denotes the noise power (N_1 and N_2 being the noise powers present on the two received hydrophone channels) and ρ being the normalised cross-correlation coefficient evaluated at a given time delay between the channels.

Despite the attractiveness of this method, one of the assumptions¹ do not hold in practice (as admitted by the authors) in the face of correlated background noise when the signal power of the source drops significantly. Under such conditions, the cross-correlation coefficients represent peaks due to correlated noise instead of the signal, resulting in falsely elevated SNRs.

In order to overcome this problem, a different procedure was followed to calculate an approximate value for SNR at each estimation step during offline processing. Since the onsets of sending events were known *a priori* and the continuous recorded raw audio data was available during offline processing, a finite segment of the received channels *before* the start of each sending event was used to calculate the noise power. This was with the knowledge that since the pings have not yet been emitted for that particular time-slot, this received channel segment does not contain the signal but only ‘noise’². The root mean squared value of this channel segment is considered to be representative of the noise power. Similarly, the full length of the channel window *after* the start of a sending event is processed to calculate the signal power. Since the onset of the signal within this windowed channel segment is not known without explicit information about the source position, it can only be assumed that the signal is contained within this segment. The main drawback of this approach is that this segment would also contain background noise and delayed multipath arrivals of the signal, in addition to the direct path signal. However, the results from this approach agreed with those achieved by the method suggested by Bosworth et al. (2008) when the signal power was significantly higher than the background noise power (SNR > 0dB). The latter method was used to estimate the SNR for the long range experiments presented in section 7.5.

6.7 Discussion

The experimental setup and procedure used to evaluate the performance of the relative localisation system was presented in this chapter. Additionally, the calibration process of the experimental setup was described along with derivations of corrections for errors arising due to the configuration of the apparatus. This chapter also presented how ground truth was established for the experiments.

As stated initially, the experiments were aimed at evaluating the relative localisation system in terms of accuracy and precision of the estimates produced and to find out the angular and radial sensing limits of the system. Experiments are conducted under operational conditions which are as close as possible to the conditions faced by a final implementation deployed on autonomous submersibles such that the overall suitability of the system to solve the task of relative localisation for small AUVs can be examined. With this in mind, the parameters governed by devices used

¹ Noise on the two received channels are uncorrelated.

² This segment can however contain decayed remnants of the pings emitted in the previous sending event.

as part of the experimental setup were checked against availability, performance and power consumption of integrated components that could be used in a final hardware implementation of a deployable system. An integral component of the experimental setup was the external sampling device which provided pre-amplification and analogue to digital conversion of the hydrophone channels. This has a specified dynamic range of 108 dB, sampling rate of 96 000 Hz with a resolution of 24 bits. These parameters can be substituted with integrated components which are commercially available¹.

The sender-observer synchronisation provided through direct signalling by the sending electronics module is meant to be provided by the underlying communication and scheduling scheme. The key parameter related to synchronisation which has an impact on the precision of range estimates is the synchronisation timing jitter. According to parameters and specifications of the long-wave radio module (Schill, 2007, pp. 66-69), it was contended in section 6.2 that 0.12×10^{-3} s is a reasonable upper bound for synchronisation timing jitter due to specified frequencies and data rates. Later in that section, it was shown that the synchronisation timing jitter due to the wired serial links between the computer and the sending electronics module was nominally higher (0.17×10^{-3} s) than the aforementioned value while the timing jitter due to the wireless serial link² was much greater (0.92×10^{-3} s). Therefore, since the synchronisation timing jitter experienced by the experimental setup is greater than the upper bound suggested by the long-wave radio communication system, it can be safely assumed that a final implementation of the system would perform better than the experimentally evaluated system with regard to range estimation precision.

The design features of the gantry cart and rail such as the use of timing belts, pulleys and spring mounted stabilising bearings for translatory motion and direct coupling of the servo motor with the rig shaft for rotational motion virtually eliminated experimental errors due to wheel slippage and backlash of coupling gears. This coupled with the careful calibration on the gantry frame before each experimental run ensured that the actual gantry motion was as close as possible to that intended by the experimental procedure. Additionally, by using the compass modules which were submerged and placed coaxial with the central vertical axes of the rigs for deriving angular ground truth, these values were closely representative of the actual motion of the rigs as experienced by the transducers themselves. All these factors attribute a high degree of confidence on the experimental apparatus used for evaluating the relative localisation system. This confidence

¹. The ADA4692-2 from Analog Devices (2009) is an example of a suitable single supply low power, low noise, wideband Op-Amp for pre-amplifying the hydrophone channels while the AD1974 from Analog Devices (2007) is an example of a single supply four channel 8 - 192 kHz 24 bit A/D converter with a specified dynamic range of 107 dB.

². Interfaced with the relative localisation system via an acoustic channel on the sampling device - this method was used during the long range experiments carried out on the lake, using a wireless sync signal between the sending rig attached to the kayak and the computer on the pier.

significantly contributes to the interpretation and analysis of the experimental results presented in the following chapter.

The results of selected short, medium and long range experiments are presented in detail in the next chapter. The estimation errors defined in this chapter are used in analysing the performance of the localisation system in terms of accuracy, precision while the angular and radial sensing ranges of the system are evaluated with respect to SNR of the received hydrophone channels as well.

Chapter 7

Results and analysis

Out of the many experiments carried out using the setup described in the previous chapter, results of selected short, medium and long range experiments are presented in detail in this chapter. In these experiments, the main constituents of the pose vector, azimuth, range and heading were explicitly varied using the experimental setup and the resulting pose vectors estimated by the relative localisation system were recorded.

The first sections presents the effects of filtering and peak tracking on the experimental data. As explained in chapter 3, filtering of the signals is done in order to compensate for the frequency response characteristics of the Benthos AQ-2000 hydrophones prior to cross-correlation of the channels, while the peak tracking algorithm operates on the cross-correlograms as explained in chapter 5. The main experimental results are presented in the subsequent sections with plots and statistical quantities describing the deviation of estimates from their respective ground truth references. The behaviour of errors are further analysed with composite error plots derived from multiple experiments under different conditions (experimental configurations and operational environments) and validated against theoretical error models derived earlier in chapter 4.

The performance of the localisation system is analysed in terms of accuracy and precision while the angular and radial sensing ranges of the system are evaluated with respect to signal-to-noise

ratios (SNR) of the received hydrophone channels and position errors resulting from pose vector estimates. Experimental data is also used to demonstrate how the system recovers from degradation of position estimation accuracy.

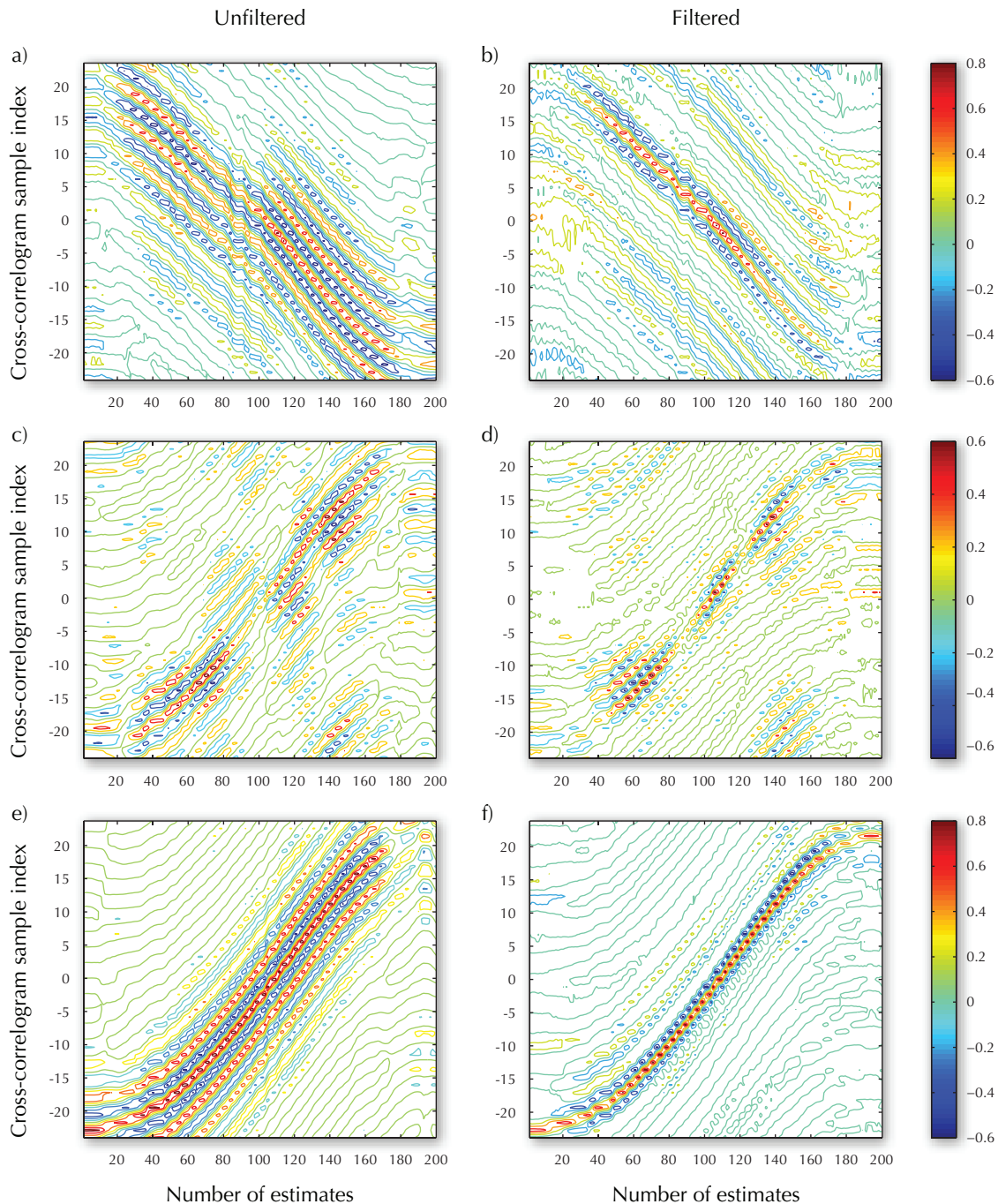


Figure 7.1: Contour plots show a series of cross-correlograms resulting from three different experimental runs given on three rows. The left column is obtained with no filtering of the input channels while the right column is obtained by filtering input channels with the inverse frequency response filter of the hydrophones. The first row represents results from an experiment where the gantry rotation corresponded to an azimuth variation of $\theta: 90^\circ \rightarrow 0^\circ \rightarrow -90^\circ$ while the next two rows represent results from rotations with $\theta: -90^\circ \rightarrow 0^\circ \rightarrow 90^\circ$.

7.1 Effects of filtering

To analyse the effect of filtering the audio stream with the inverse frequency response filter of the hydrophones, the offline relative localisation system was fed with the filtered and unfiltered versions of the raw audio data captured during experiments. Figure 7.1 shows contour plots of normalised cross-correlograms resulting from cross-correlating the two hydrophone channels corresponding to the MLS pings emitted by the bow projector P_1 , which are used to estimate θ_1 , the azimuth of the bow end of the sender. The three rows shows three different experimental runs while the first column is without any filtering and the second column is with the inverse frequency response filter applied.

In each of the contour plots, each vertical ‘slice’ is a normalised cross-correlogram with the peaks moving from top to bottom (first row) or vice versa (second and third row) as the experiment proceeds with increasing estimates. For clarity, two cross-correlograms representing two ‘slices’ from plots a) and b) of figure 7.1 are presented in plots a) and b) of figure 7.2.

The three different experiments whose results are depicted in figure 7.1 were selected to show varying levels of effectiveness and necessity of the filter being applied. The instance shown in plot a) has at least three adjacent peaks competing for prominence characterised by red parallel ‘ridges’ continuing diagonally across the plot. This is due to the dominant frequency component introduced by the resonance of the transducers as explained in section 3.3.3. This behaviour of the cross-correlogram peaks causes the precision of the relative localisation system estimates to decrease (the standard deviation of errors increase). As a result of the filter, the side lobe peaks in the cross-correlograms subsides leaving only the main ridge of peaks as shown in plot b).

Plot c) depicts an experiment where the peaks of the cross-correlograms were affected by actual reflected signals (off the test tank walls) apart from the multiple adjacent peaks due to resonance

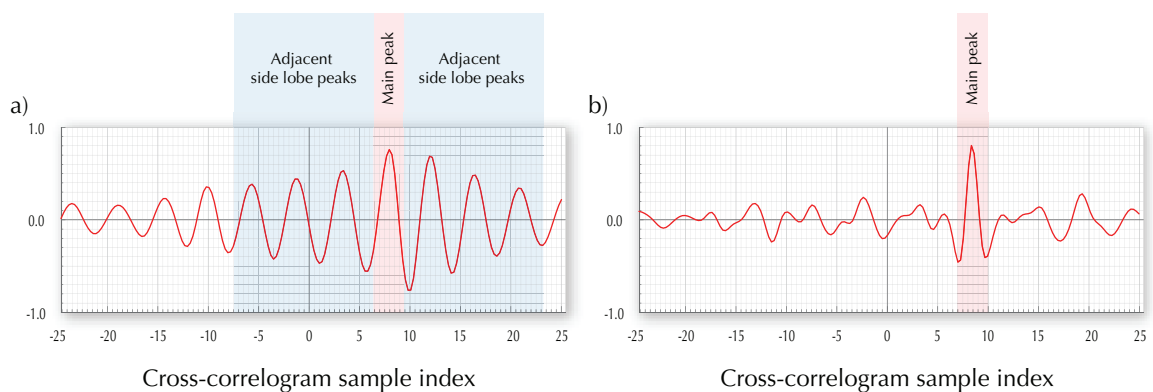


Figure 7.2: Cross-correlogram plots resulting from a) unfiltered signal channels and b) filtered signal channels, showing the main peak and adjacent side lobe peaks caused by the resonance frequency of the transducers. The *y-axes* on these plots represents the normalised amplitude. Vertical slices of the contour plots in figure 7.1 consists of cross-correlograms such as these.

as in the previous case. In the first instance of reflection between estimates 80 to 100, the peaks are lost while in the second instance between estimates 140 to 160, a series of outlier peaks appear further away from the continuing ridge of peaks. As a result of the filter, the adjacent peaks subside leaving the main ridge as before but the outlier peaks still remain as seen from plot d).

In plot e), though there are multiple ridges flanking the main ridge caused by adjacent side lobe peaks in the cross-correlograms, the main ridge is continuously higher than its flanks. As expected, the filtered signals causes the side lobe peaks to subside leaving only the prominent main ridge shown in plot f).

The experiment represented in the first row clearly benefits from the filtering scheme as it helps to subdue unwanted side lobe peaks. In the experiment shown in the third row, due to the height of the main ridge compared to its flanks, filtering does not necessarily introduce any improvement to the estimates even though the side lobe peaks are suppressed in the process. In the experiment depicted in the second row, while filtering contributes to reducing the standard deviation of estimation errors, it does not improve performance in areas affected by reflections (i.e. peak drop-offs and outliers). Such situations necessitate the peak tracking algorithm described in detail previously in chapter 5. The effect of applying peak tracking to cross-correlograms is described and illustrated in the following section.

7.2 Effects of peak tracking

The scheme used for measuring the acoustic path length difference corresponding to a particular TDOA between two channels by cross-correlation was introduced in chapter 4 and elaborated under section 4.1. The simple search used to locate the peak only considered the amplitude of the cross-correlogram. Sub-sample interpolation was then used to refine the position of the peak in the sample domain. With peak tracking, the history of the previous peak positions is incorporated in to the search parameters and a higher prominence is given to the position rather than the amplitude of the peak. Peak positions estimated in this manner are refined as before using the sub-sample interpolation. Details about this scheme was elaborated previously in chapter 5 under section 5.4.1. Two experimental runs¹ are used to analyse the effects of peak tracking on the different pose vector components when combined with filtering described in the previous section.

¹. A series of azimuth variations depicted in figure 7.3 and a series of heading variations depicted in figure 7.4.

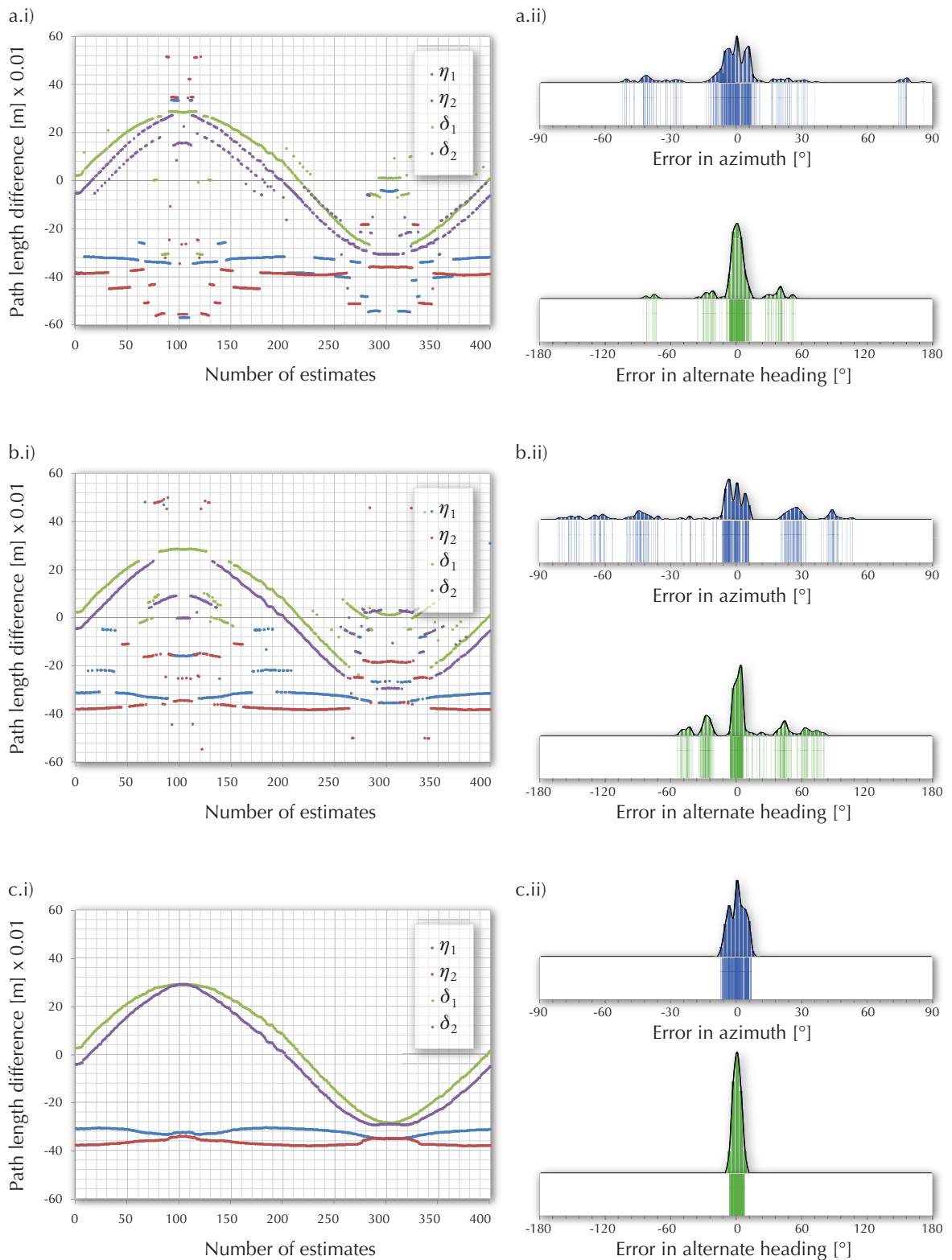


Figure 7.3: The intermediate values produced by the relative localisation system which consists of the acoustic path length differences are plotted along with the errors of azimuth and alternate heading which are calculated using these values. The first row is with no filtering, the second row is with inverse frequency response filtering applied to the hydrophone channels which are inputs to the cross-correlation. The third row is with filtering applied and with peak tracking on the cross-correlograms enabled.

Azimuth and alternate heading

The first column of figure 7.3 contains plots of δ_1 , δ_2 , η_1 and η_2 produced during an experiment. These acoustic path length differences derived from the position of the peak in the cross-correlograms using (4.11) are intermediate values produced by the relative localisation system. The bow and stern azimuths θ_1 and θ_2 are calculated using δ_1 and δ_2 as explained in section 4.4.3, while the reverse azimuths φ_1 and φ_2 used for reverse hyperbolic localisation uses η_1 and η_2 as explained in section 4.4.4.

In the experiment depicted in figure 7.3, the gantry was used to rotate the observer such that the azimuth ground truth varied as $\theta_0 : 0^\circ \rightarrow -90^\circ \rightarrow 0^\circ \rightarrow 90^\circ \rightarrow 0^\circ$, while the sender was kept stationary with $\alpha_{\theta=0^\circ} = 100^\circ$ and $r_0 = 1.5\text{ m}$. Plot a.i) was obtained using unfiltered hydrophone channels as the inputs to the cross-correlation with no peak tracking on the cross-correlograms, plot b.i) was with the inverse frequency response filter applied but without any peak tracking while plot c.i) was with the filter applied and with peak tracking enabled. Plot a.i) shows the effects of the adjacent side lobe peaks which causes the outliers on either side of the main path length differences. The η_1 and η_2 estimates are worse affected than the δ_1 and δ_2 estimates at this stage. When the filter is applied, a deterioration of the values around 100 and 300 estimates is clearly noticeable. These areas correspond to azimuths of -90° and 90° where the hydrophones on the observer are pointed in a direction almost perpendicular to projectors on the sender. Due to the directivity pattern of the AQ-2000 hydrophones which are non-omni-directional, the direct-path signals that are received in these regions would carry most of their energy in frequencies within a narrow bandwidth centred at the resonance frequency of the transducers. The filtering process which aims to ‘smoothen out’ the received frequency spectrum by attenuating spikes caused by resonance contributes to further reduce the energy of the direct-path signals. Under these circumstances the signals reflected off the curved metal walls of the test

	No filtering and no peak tracking	Filtered with no peak tracking	Filtered with peak tracking
Std. dev. of azimuth error ($\sigma_{\Delta\theta}$)	20.38° (4.43°)	30.06° (2.12°)	3.55° (1.79°)
Mean of azimuth error ($\mu_{\Delta\theta}$)	-0.73° (-4.40°)	-5.47° (-4.20°)	0.04° (-3.91°)
Avg. dev. of azimuth error ($\overline{\Delta\theta}$)	11.49° (3.46°)	21.46° (1.58°)	2.96° (1.43°)
Std. dev. of alt. heading error ($\sigma_{\Delta\alpha'}$)	20.62° (4.41°)	30.19° (2.09°)	3.54° (1.77°)
Mean of alt. heading error ($\mu_{\Delta\alpha'}$)	0.37° (4.31°)	4.50° (3.61°)	-0.22° (3.63°)
Avg. dev. of alt. heading error ($\overline{\Delta\alpha'}$)	11.57° (3.47°)	21.43° (1.56°)	2.94° (1.41°)

Table 7.1: Comparison of standard deviations, means and average deviations of errors associated with azimuth and alternate heading estimates corresponding to the intermediate values plotted in figure 7.3. The quantities within brackets correspond to the region between 150 and 250 estimates.

tank, which impinge on the hydrophones from the front, tend to carry more energy than the direct-path signals. Hence the cross-correlogram peaks due to reflections tends to have a higher amplitude than those due to direct-path signals in these regions causing the performance of the estimation system to deteriorate when the filter is applied. However, peaks caused by direct-path signals occur *before* the peaks caused by reflected signals albeit with much lower amplitude as explained in section 5.3.1. The peak tracking algorithm exploits this fact and manages to retrieve the peaks caused by direct path signals by considering peak positions in previous estimates. The results can be seen by comparing plot b.i) and c.i) where applying filtering and peak tracking (with $\Delta_{Tolerance} = 0.65$ for each of the four cross-correlations) completely eliminates outliers in the path length difference measurements which are subsequently used for the angular estimations.

The second column in figure 7.3 shows the errors in the azimuth and alternate heading, which are primary estimates directly dependant on the path length differences δ_1 , δ_2 , η_1 and η_2 plotted in the first column. These are plotted as combinations of conventional error histograms and band plots which show the actual spread of the deviations of the estimate from the ground truth reference. These novel band plot representations overcome the quantization effect of histograms caused by binning and each line represents an actual estimate¹. The height of the histogram at a given point can be seen as a function of the unit line density of the corresponding band plot around that point.

As observed from these plots, filtering has clearly different effects on different regions of variation. The deterioration in filtered performance affects the overall error when the sender reaches the sensing limits of the hydrophones on the observer giving prominence to peaks caused by signals reflected off the tank walls. This results in the error histograms showing more spread than in the unfiltered case. However, there is a marked improvement when peak tracking is enabled. Consequently, the performance of region between 150 and 250 estimates which is not affected by the aforementioned deterioration actually improves with filtering. The standard deviation, mean and average deviations of these errors are compared in table 7.1 under the different filtering and peak tracking regimes on different regions. The first quantity corresponds to the overall run of 400 estimates while the quantity within brackets correspond to the 100 estimates in the mid-region unaffected by the source reaching the sensing limits of the receivers. The overall performance degrades (signified by the increased average deviation of error) with filtering enabled and shows significant improvement with peak tracking enabled. However, the mid-region performance actually shows a marked improvement with filtering while the performance gain when peak tracking is enabled is minimal. This effect is common to both the angular estimates of azimuth and alternate heading.

¹. These band plots are used in the following sections to illustrate the estimation errors in place of error histograms.

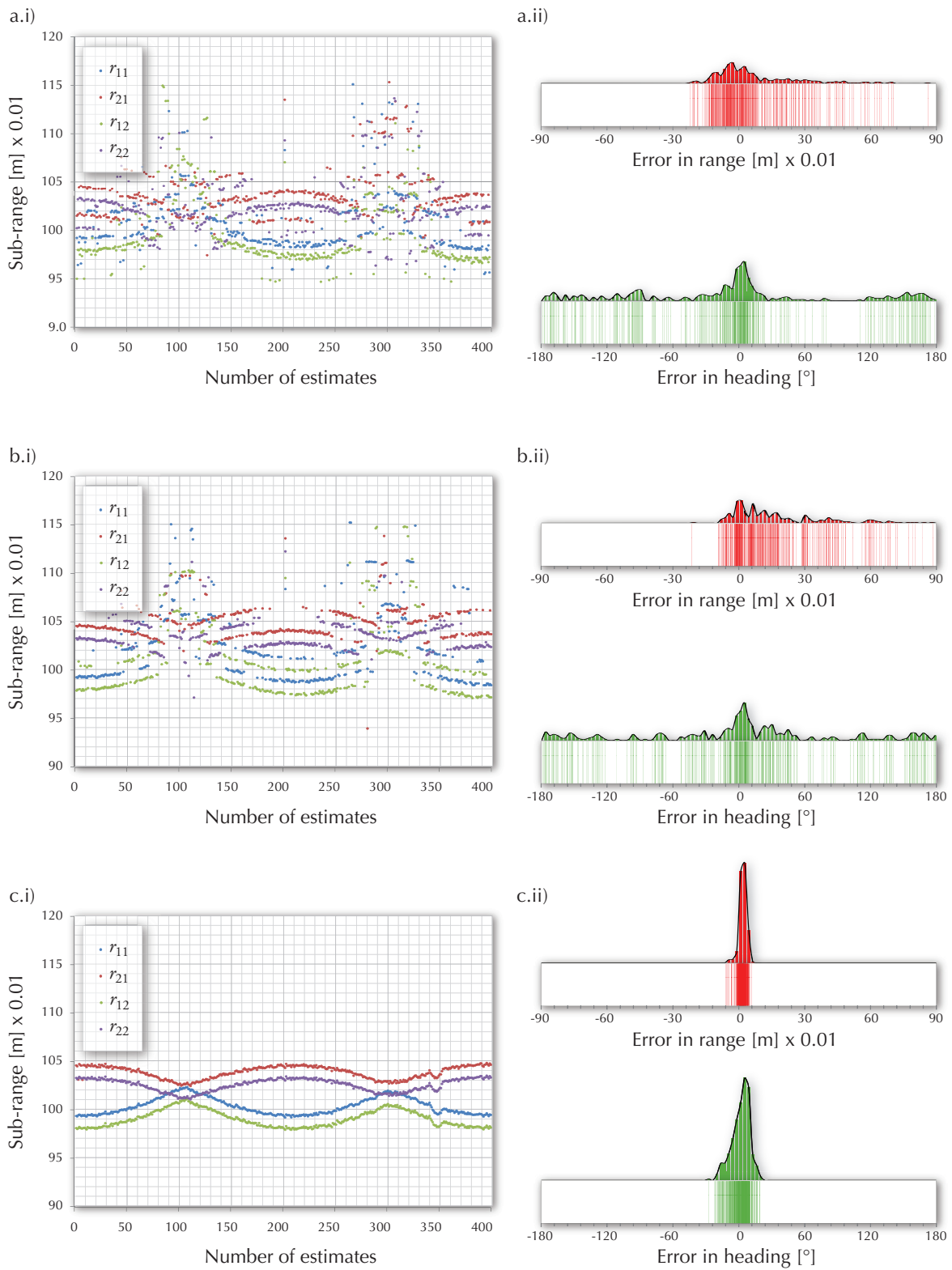


Figure 7.4: The intermediate values of sub-ranges produced by the relative localisation system are plotted along with the errors of the final range and heading estimates which are calculated using these values. The first row is with no filtering, the second row is with inverse frequency response filtering applied. The third row is with filtering applied and peak tracking enabled.

Range and heading

The first column of figure 7.4 contains plots of intermediate sub-ranges r_{11} , r_{21} , r_{12} and r_{22} produced by matched filter processing during an experiment. These sub-ranges derived from the position of the peak in the cross-correlograms using (4.17) are used to calculate the final range estimate r and (together with sub azimuths θ_1 and θ_2) the heading estimate α . These derivations are explained in section 4.4.3.

In the experiment depicted in figure 7.4, the gantry was used to rotate the sender such that the heading ground truth varied as $\alpha_0 : 150^\circ \rightarrow 60^\circ \rightarrow 180^\circ \rightarrow -60^\circ \rightarrow -180^\circ \rightarrow 150^\circ$, while the observer was stationary with $\theta_0 = -30^\circ$ and $r_0 = 10.0\text{m}$. As before, plot a.i) was obtained using unfiltered hydrophone channels as the inputs to the cross-correlation with no peak tracking on the cross-correlograms, plot b.i) with the inverse frequency response filter applied but without any peak tracking while plot c.i) was with the filter applied and with peak tracking enabled. Once again in the plots a.i) and b.i) the two regions around estimate 100 and estimate 300 where the projectors on the sender pointed in a direction perpendicular to the hydrophones on the observer (heading reaching 60° and -60° with azimuth at -30°), the estimation performance visibly deteriorates. In this experiment which was conducted in the lake, the delayed multi-path arrivals due to surface and bottom reflections are present throughout the experimental run. When the source reaches the limits of the sensing range of the receivers, the peaks due to delayed multipath arrivals takes prominence over the peak attributed to the direct-path signal. Enabling peak tracking (with $\Delta_{Tolerance} = 1.55$ for each of the four cross-correlations) results in virtually all ‘true’ peaks being recovered from amongst the outliers as seen by plot c.i). The region near estimate 350 is an example of peak tracking latching on to a spurious peak¹ and ‘wandering’ for a few consecutive estimation steps. However, the scheme recovers within 10 estimation steps to continue tracking the ‘true’ peak.

	No filtering and no peak tracking	Filtered with no peak tracking	Filtered with peak tracking
Std. dev. of range error ($\sigma_{\Delta r}$)	$112.6 \times 10^{-2}\text{m}$ ($10.7 \times 10^{-2}\text{m}$)	$130.0 \times 10^{-2}\text{m}$ ($11.8 \times 10^{-2}\text{m}$)	$1.6 \times 10^{-2}\text{m}$ ($0.9 \times 10^{-2}\text{m}$)
Mean of range error ($\mu_{\Delta r}$)	$-7.1 \times 10^{-2}\text{m}$ ($4.4 \times 10^{-2}\text{m}$)	$-2.0 \times 10^{-2}\text{m}$ ($3.9 \times 10^{-2}\text{m}$)	$1.0 \times 10^{-2}\text{m}$ ($0.2 \times 10^{-2}\text{m}$)
Avg. dev. of azimuth error ($\overline{\Delta r}$)	$29.0 \times 10^{-2}\text{m}$ ($5.4 \times 10^{-2}\text{m}$)	$34.6 \times 10^{-2}\text{m}$ ($7.2 \times 10^{-2}\text{m}$)	$1.2 \times 10^{-2}\text{m}$ ($0.7 \times 10^{-2}\text{m}$)
Std. dev. of heading error ($\sigma_{\Delta \alpha}$)	73.21° (51.13°)	68.76° (16.30°)	4.56° (1.88°)
Mean of heading error ($\mu_{\Delta \alpha}$)	2.07° (1.47°)	-1.62° (-0.27°)	0.05° (-3.05°)
Avg. dev. of heading error ($\overline{\Delta \alpha}$)	52.37° (38.60°)	45.35° (9.69°)	3.89° (1.53°)

Table 7.2: Comparison of standard deviations, means and average deviations of errors associated with range and heading estimates corresponding to the intermediate values plotted in figure 7.4. The quantities within brackets correspond to the region between 150 and 250 estimates.

Plots a.ii), b.ii) and c.ii) show the combined histogram and band plots which depicts the spread of errors in range and heading estimates derived from the intermediate sub-ranges. The standard deviation, mean and average deviations of these errors are compared in table 7.1 under the different filtering and peak tracking regimes on different regions. As before, the first quantity corresponds to the overall run of 400 estimates while the quantity within brackets correspond to the 100 estimates in the mid-region (between estimates 150 and 250) unaffected by the source reaching the sensing limits of the receivers. A relatively small increase in average deviation of range error signifies a performance degradation with filtering enabled overall as well as in the mid-region unlike in the previous case. A significant improvement in range estimation can only be seen once peak tracking is enabled. On the other hand, heading performance improves both overall (nominally) and mid-region (significantly) as filtering is enabled. Both regions show marked improvement in heading estimation when peak tracking is enabled.

The two experimental runs whose results were presented first with no filtering or peak tracking, with filtering only and then with both filtering and peak tracking enabled, briefly illustrates the effect these schemes have on the final estimates of the relative localisation system under different configurations and different operating environments. Detailed results of selected individual experiments where both filtering and peak tracking was enabled in producing the final pose vector components are presented throughout the next sections. The values of the peak tracking parameter $\Delta_{Tolerance}$ used during these experiments are tabulated in appendix C.2.

7.3 Results and errors of short range experiments

The following sections present results obtained from experiments conducted in the test tank with the relative localisation system using the procedure and setup described in the previous chapter. The main components of the pose vector being estimates for azimuth, range and heading along with alternate estimates for heading and range calculated using reverse hyperbolic localisation as described in section 4.4.4 in chapter 4 are plotted as the two experimental rigs are moved relative to each other to induce variations of these different quantities. The deviation of these quantities from the respective ground truth values are also presented as estimation errors of the system. These deviations and their statistical behaviour is calculated as described previously in section 6.5.1. The gantry motion speeds for the variations azimuth, range and heading were 4.0°s^{-1} , 0.05ms^{-1} and 5.5°s^{-1} respectively.

¹. A spurious peak occurring within the tolerance interval as explained under 'Attributes and limitation of peak tracking' in section 5.4.1.

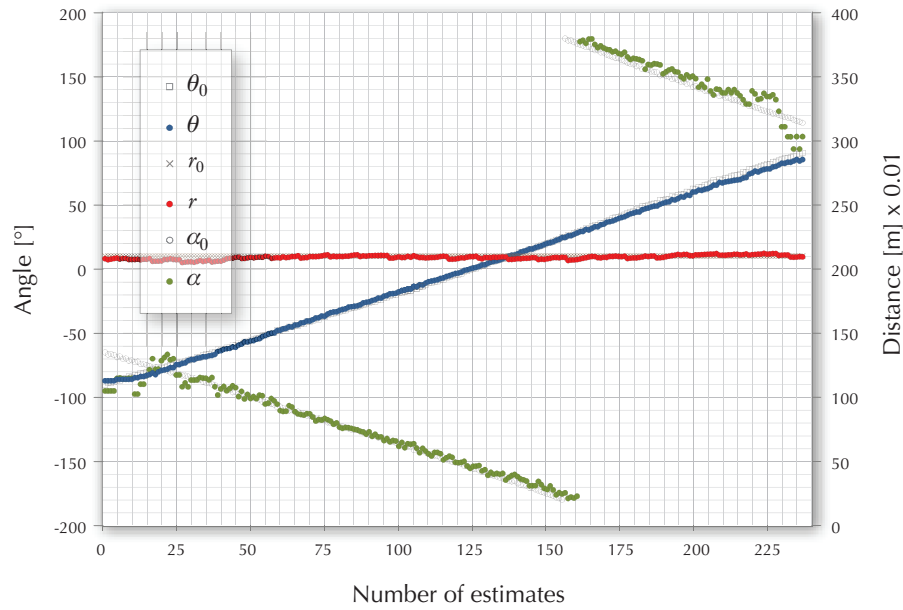


Figure 7.5: Estimates for azimuth θ , range r and heading α produced by the relative localisation system for an explicit azimuth variation of $\theta_0: -90^\circ \rightarrow 0^\circ \rightarrow 90^\circ$ with $\alpha_{\theta=0^\circ} = -150^\circ$ and $r_0 = 2.1\text{m}$.

7.3.1 Variation of azimuth

The azimuth was varied as described by the procedure given in section 6.3.1. Figure 7.5 plots the azimuth θ , range r and heading α of the sender relative to the observer as estimated by the relative localisation system along with the corresponding ground truth values.

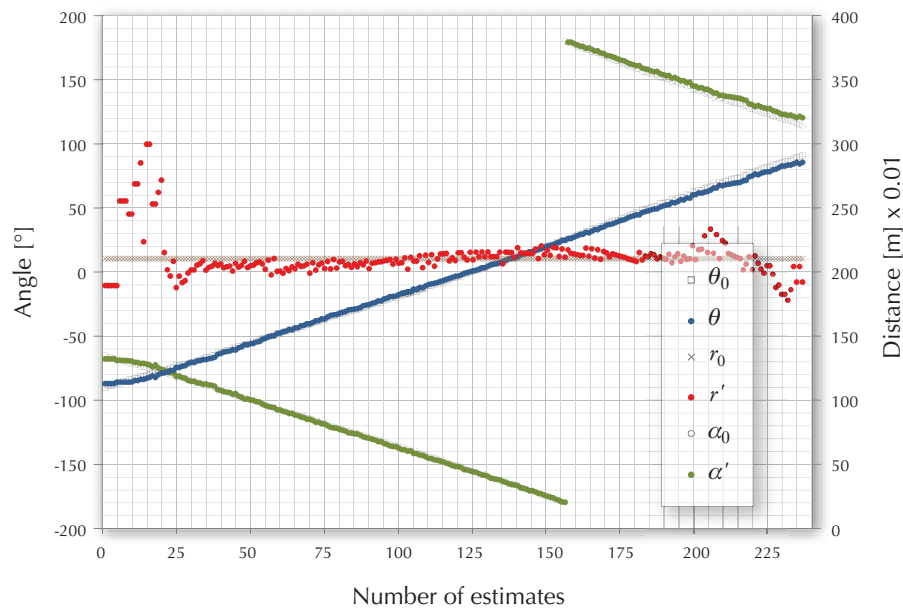


Figure 7.6: Azimuth θ , alternate range r' and alternate heading α' estimated by the relative localisation system for an explicit azimuth variation of $\theta_0: -90^\circ \rightarrow 0^\circ \rightarrow 90^\circ$ with $\alpha_{\theta=0^\circ} = -150^\circ$ and $r_0 = 2.1\text{m}$.

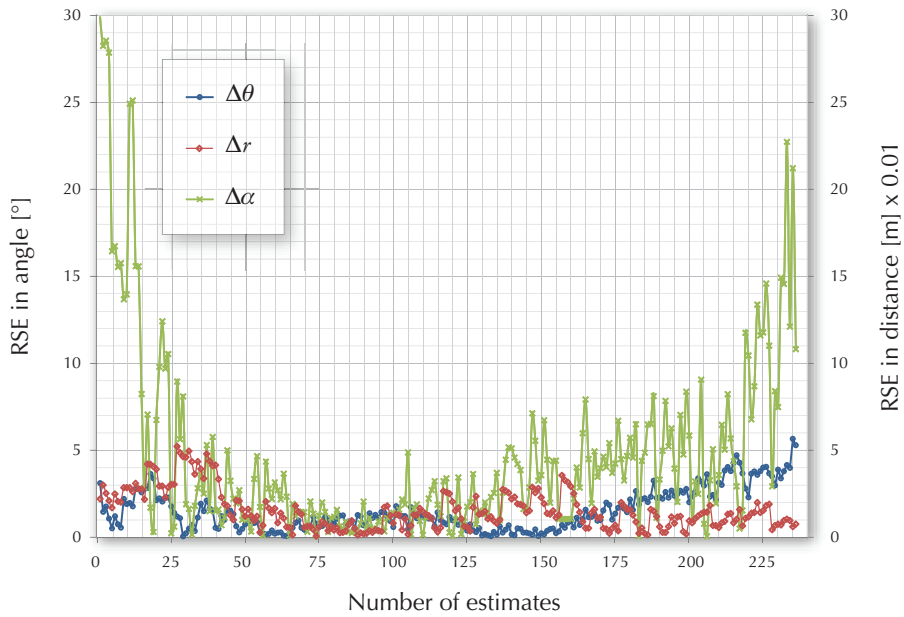


Figure 7.7: Unbiased root squared errors (RSE) in estimates for azimuth θ , range r and heading α corresponding to the variation of azimuth plotted in figure 7.6.

The heading also varies as the azimuth changes according to (6.1). Figure 7.6 plots the alternate range r' and alternate heading α' for the same variation of azimuth.

Plots in figures 7.7 and 7.8 shows the root squared errors (RSE) of azimuth, range, heading and their alternate counterparts. The RSE are calculated according to (6.25).

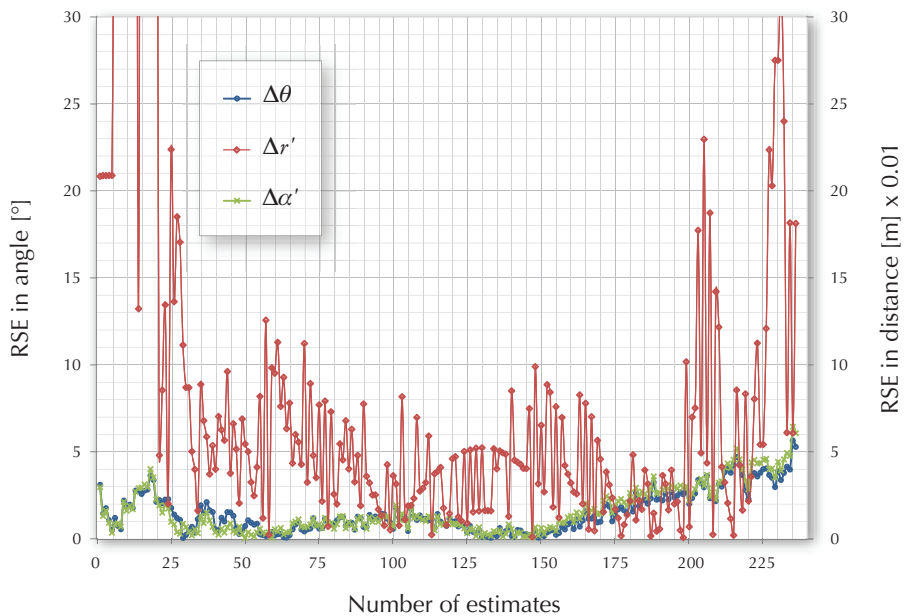


Figure 7.8: Unbiased root squared errors (RSE) in estimates for azimuth θ , alternate range r' and alternate heading α' corresponding to the variation of azimuth plotted in figure 7.7.

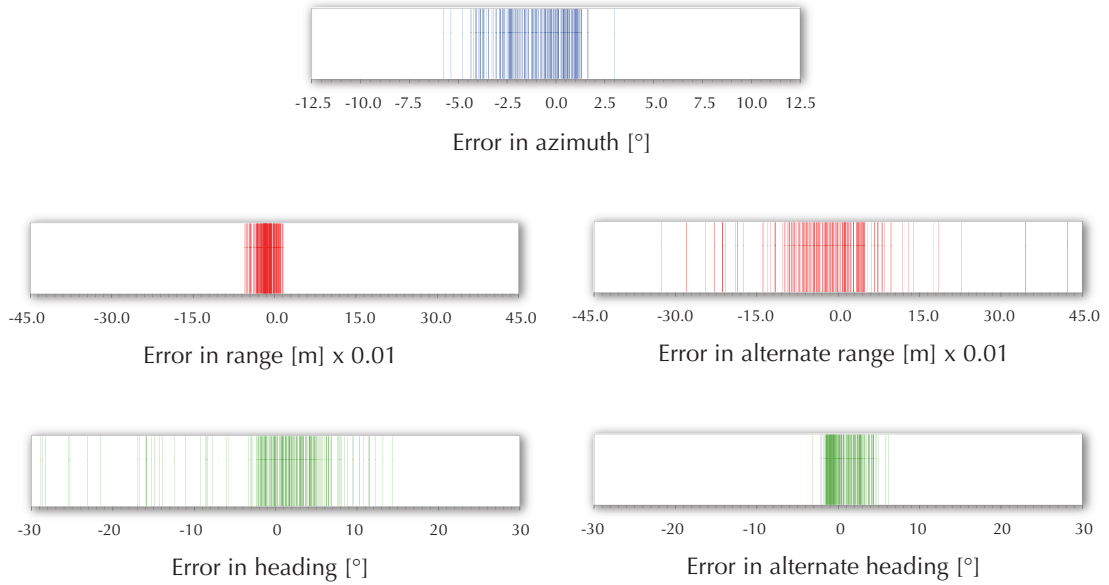


Figure 7.9: Estimate errors with bias for azimuth, range, heading and their alternate counterparts corresponding to the azimuth variation depicted in figures 7.5. and 7.6.

Estimate errors with bias, calculated according to (6.22), are shown in figure 7.9 which illustrates the actual spread of the deviations. Table 7.3 gives the statistical quantities which describe the behaviour of these errors.

Error in azimuth	Error in range	Error in alternate range	Error in heading	Error in alternate heading
$\sigma_{\Delta\theta} = 1.68^\circ$	$\sigma_{\Delta r} = 15.27 \times 10^{-3} \text{ m}$	$\sigma_{\Delta r'} = 162.29 \times 10^{-3} \text{ m}$	$\sigma_{\Delta\alpha} = 7.27^\circ$	$\sigma_{\Delta\alpha'} = 1.87^\circ$
$\mu_{\Delta\theta} = -0.87^\circ$	$\mu_{\Delta r} = -11.34 \times 10^{-3} \text{ m}$	$\mu_{\Delta r'} = 12.42 \times 10^{-3} \text{ m}$	$\mu_{\Delta\alpha} = 0.51^\circ$	$\mu_{\Delta\alpha'} = 0.91^\circ$
$\overline{\Delta\theta} = 1.43^\circ$	$\overline{\Delta r} = 12.06 \times 10^{-3} \text{ m}$	$\overline{\Delta r'} = 90.86 \times 10^{-3} \text{ m}$	$\overline{\Delta\alpha} = 4.58^\circ$	$\overline{\Delta\alpha'} = 1.60^\circ$

Table 7.3: Comparison of standard deviations, means and average deviations of errors associated with azimuth, range and heading estimates corresponding to variation of azimuth depicted in figures 7.5. and 7.6.

7.3.2 Variation of range

The observer rig was moved along the gantry rail towards the sender rig inducing a variation of range as described in 6.3.3. The components of the pose vector estimates produced by the relative localisation system during this variation are plotted in figure 7.10. The alternate estimates for range and heading during the same variation are plotted in figure 7.11. The azimuth and heading of the sender remains constant with respect to the observer during this variation of range, where the observer moves directly towards the sender.

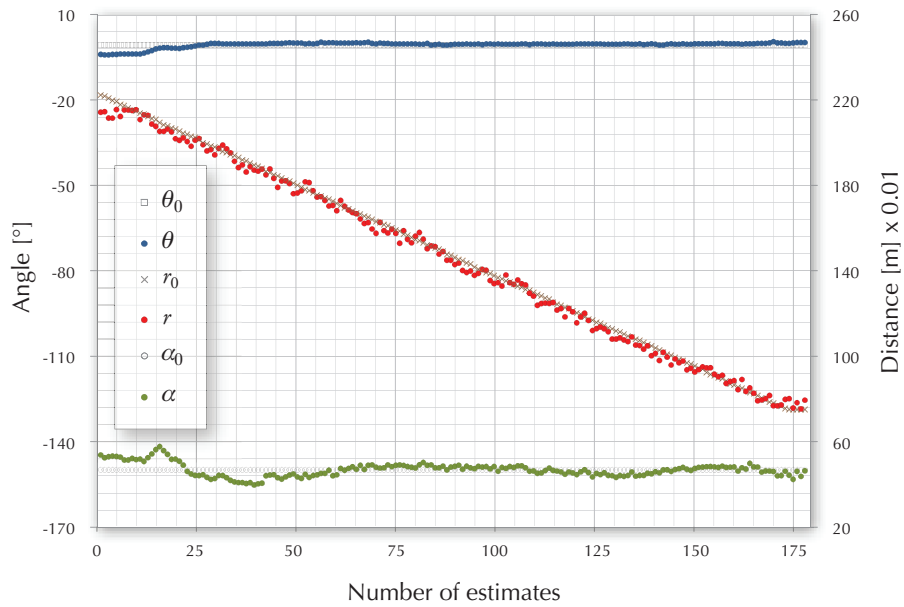


Figure 7.10: Estimates for azimuth θ , range r and heading α produced by the relative localisation system for a range variation of $r_0 : 2.25\text{m} \rightarrow 0.75\text{m}$ with $\alpha_0 = -150^\circ$ and $\theta_0 = 0^\circ$.

The RSE corresponding to these estimates are plotted in figures 7.12 and 7.13. The errors in direct range estimation is comparable with the previous case despite the range being explicitly varied in this case. However, the error in alternate range estimation increased with range as predicted in section 4.4.5.

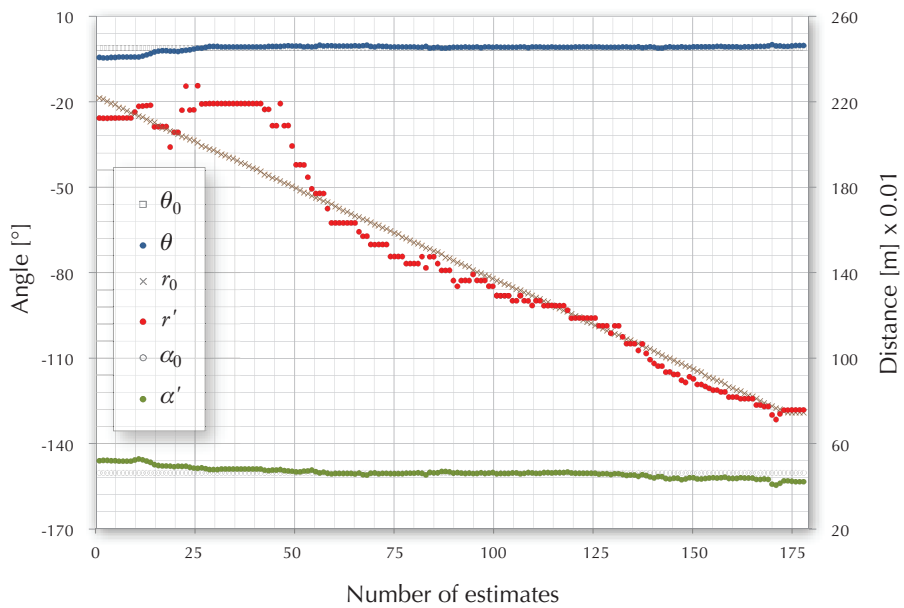


Figure 7.11: Estimates for azimuth θ , alternate range r' and alternate heading α' produced by the relative localisation system for a range variation of $r_0 : 2.25\text{m} \rightarrow 0.75\text{m}$ with $\alpha_0 = -150^\circ$ and $\theta_0 = 0^\circ$.

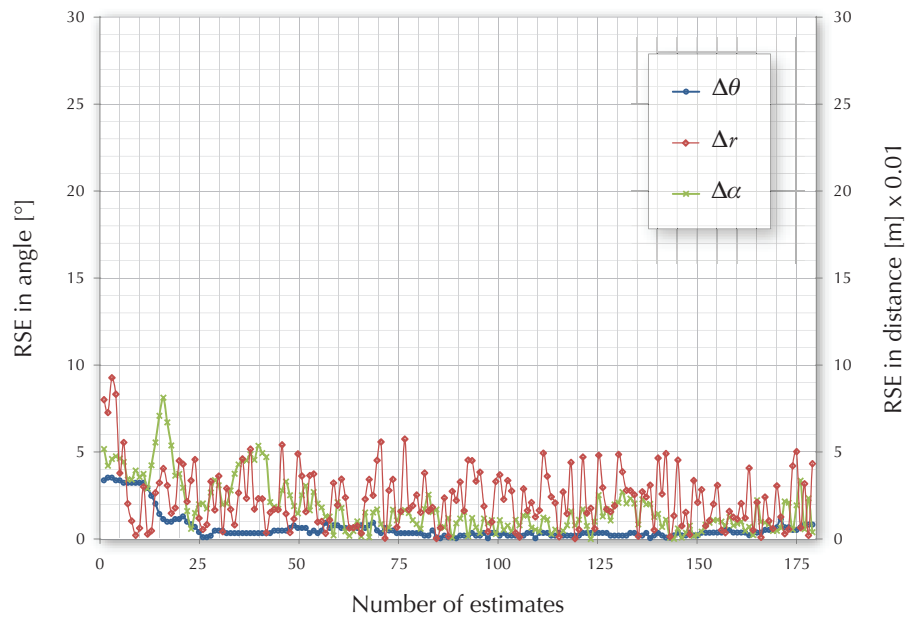


Figure 7.12: Unbiased root squared errors (RSE) in estimates for azimuth θ , range r and heading α corresponding to the variation of range plotted in figure 7.10.

The biased estimation errors for the range varying experiment is plotted in figure 7.14. The spread of azimuth and direct heading estimation errors are lower compared to those during the previous experiment as the relative azimuth and heading remained constant during the range variation.

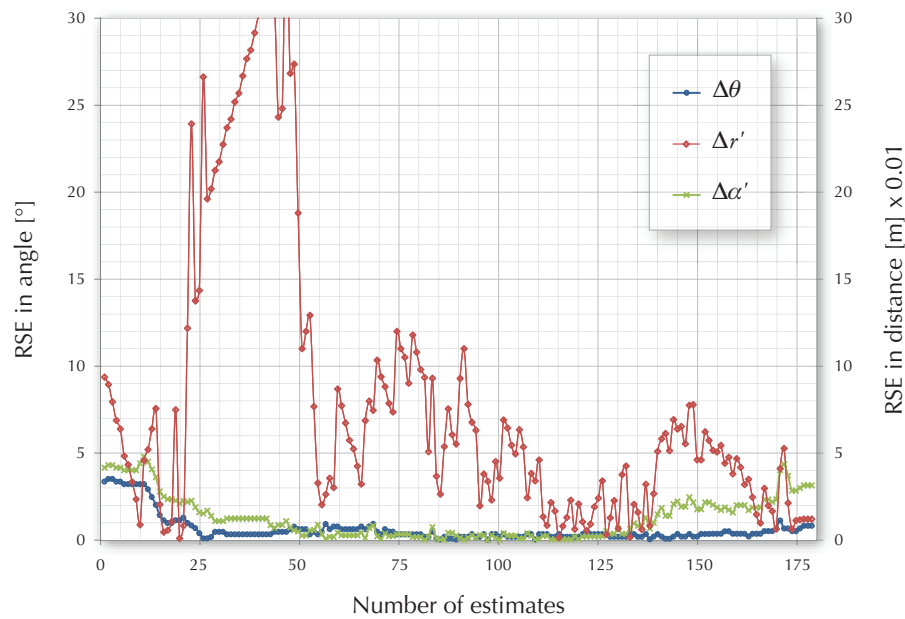


Figure 7.13: Unbiased root squared errors (RSE) in estimates for azimuth θ , alternate range r' and alternate heading α' corresponding to the variation of azimuth plotted in figure 7.11.

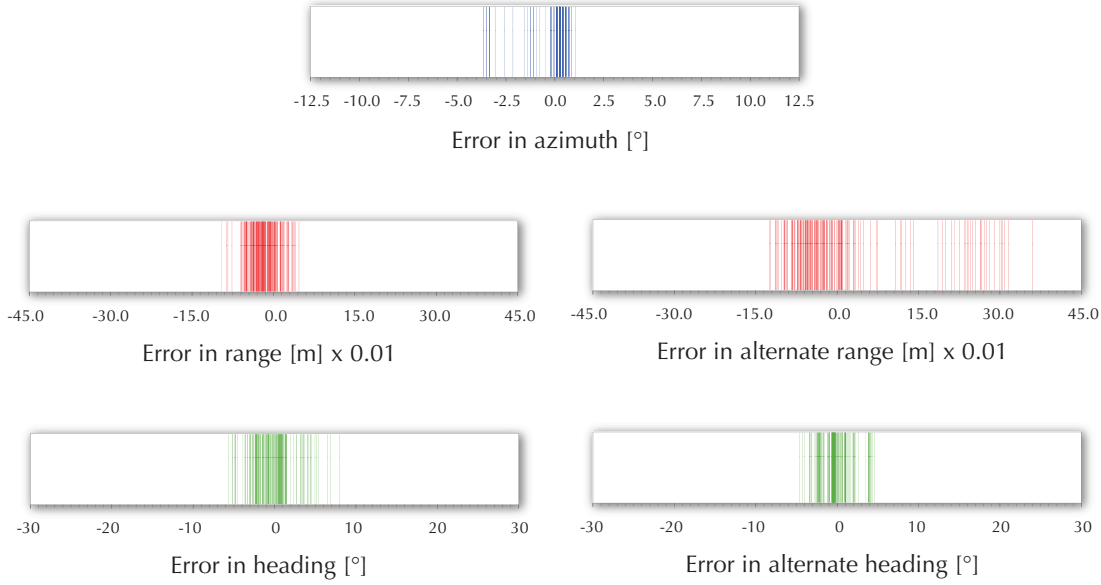


Figure 7.14: Estimate errors with bias for azimuth, range, heading and their alternate counterparts corresponding to the range variation depicted in figures 7.10. and 7.11.

The statistical quantities related to the evolution of errors related to this range variation are given below in table 7.4.

Error in azimuth	Error in range	Error in alternate range	Error in heading	Error in alternate heading
$\sigma_{\Delta\theta} = 1.01^\circ$	$\sigma_{\Delta r} = 25.47 \times 10^{-3} \text{ m}$	$\sigma_{\Delta r'} = 114.12 \times 10^{-3} \text{ m}$	$\sigma_{\Delta\alpha} = 2.37^\circ$	$\sigma_{\Delta\alpha'} = 1.80^\circ$
$\mu_{\Delta\theta} = 0.01^\circ$	$\mu_{\Delta r} = -14.4 \times 10^{-3} \text{ m}$	$\mu_{\Delta r'} = 13.7 \times 10^{-3} \text{ m}$	$\mu_{\Delta\alpha} = -0.02^\circ$	$\mu_{\Delta\alpha'} = 0.01^\circ$
$\overline{\Delta\theta} = 0.63^\circ$	$\overline{\Delta r} = 20.03 \times 10^{-3} \text{ m}$	$\overline{\Delta r'} = 84.25 \times 10^{-3} \text{ m}$	$\overline{\Delta\alpha} = 1.82^\circ$	$\overline{\Delta\alpha'} = 1.29^\circ$

Table 7.4: Comparison of standard deviations, means and average deviations of errors associated with azimuth, range and heading estimates corresponding to variation of range depicted in figures 7.10. and 7.11.

7.3.3 Variation of heading

By keeping the observer rig stationary while the sender was rotated about its central vertical axis, the relative heading was varied explicitly as described in section 6.3.2. The observer was positioned such that the relative azimuth remained constant at $\theta_0 = -30^\circ$ during the experiment. A heading variation of $\alpha_0 : -150^\circ \rightarrow 180^\circ \rightarrow 60^\circ \rightarrow 180^\circ \rightarrow -150^\circ$ was induced by the experiment. Estimates produced by the relative localisation system for this variation of heading is plotted in figures 7.15 and 7.16 depicting the azimuth estimates along with both direct and alternate estimates for range and heading. As predicted in section 4.4.5, whenever $|\theta + \alpha| \approx 90^\circ$, the

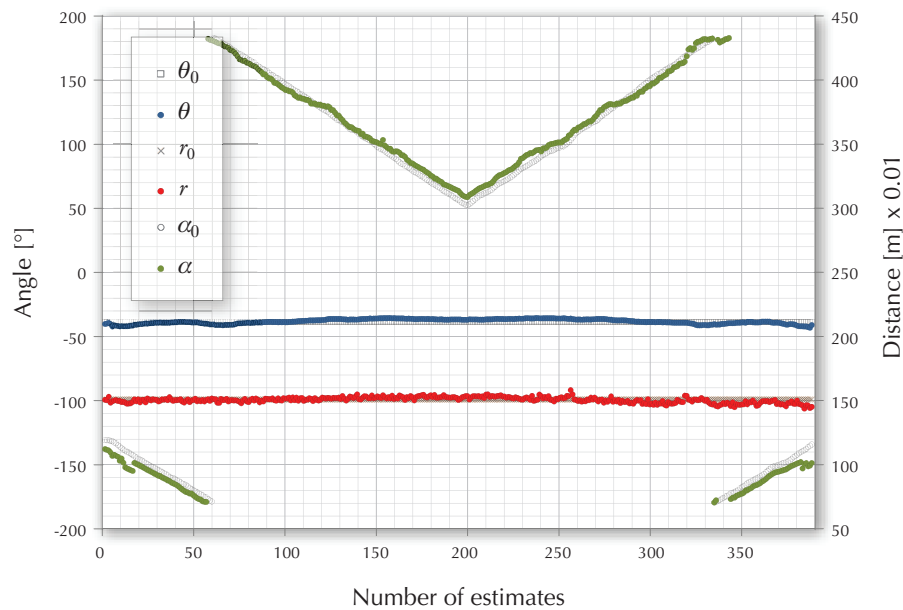


Figure 7.15: Estimates for azimuth θ , range r and heading α produced by the relative localisation system for an explicit heading variation of $\alpha_0 : -130^\circ \rightarrow 180^\circ \rightarrow 50^\circ \rightarrow 180^\circ \rightarrow -130^\circ$ with $\theta_0 = -30^\circ$ and $r = 1.5\text{m}$.

alternate range estimates based on reverse hyperbolic localisation tend to have larger errors. As observed in figure 7.16, the alternate range estimates are affected by larger deviations in the vicinity of estimate numbers 115 and 285 which corresponds to the earlier condition being fulfilled by the values of θ and α . However, the alternate heading estimates are not severely affected as

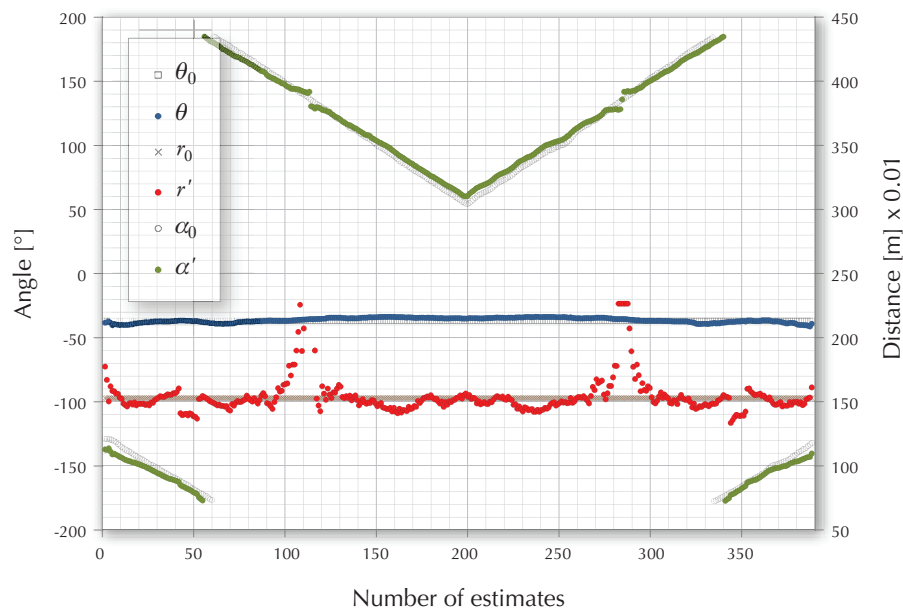


Figure 7.16: Azimuth θ , alternate range r' and alternate heading α' estimated by the relative localisation system for an explicit heading variation of $\alpha_0 : -130^\circ \rightarrow 180^\circ \rightarrow 50^\circ \rightarrow 180^\circ \rightarrow -130^\circ$ where $\theta_0 = -30^\circ$ and $r_0 = 1.5\text{m}$ remained constant.

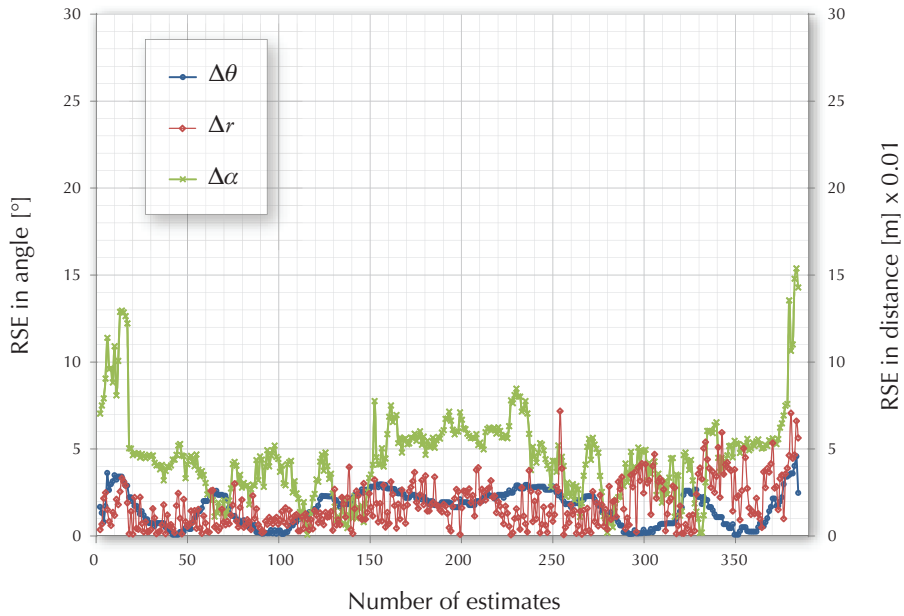


Figure 7.17: Unbiased root squared errors (RSE) in estimates for azimuth θ , range r and heading α corresponding to the variation of heading plotted in figure 7.15.

predicted when the condition $|\theta + \alpha| \approx 0^\circ, 180^\circ$ is satisfied. The clipping effect of alternate range estimates as the deviations increase is explained in section 7.6.1. The RSE associated with this experiment are plotted in figures 7.17 and 7.18. Apart from the large deviations in alternate range estimates described earlier, the direct range error variations are comparable with the previous case when the range was varied while azimuth and heading remained constant.

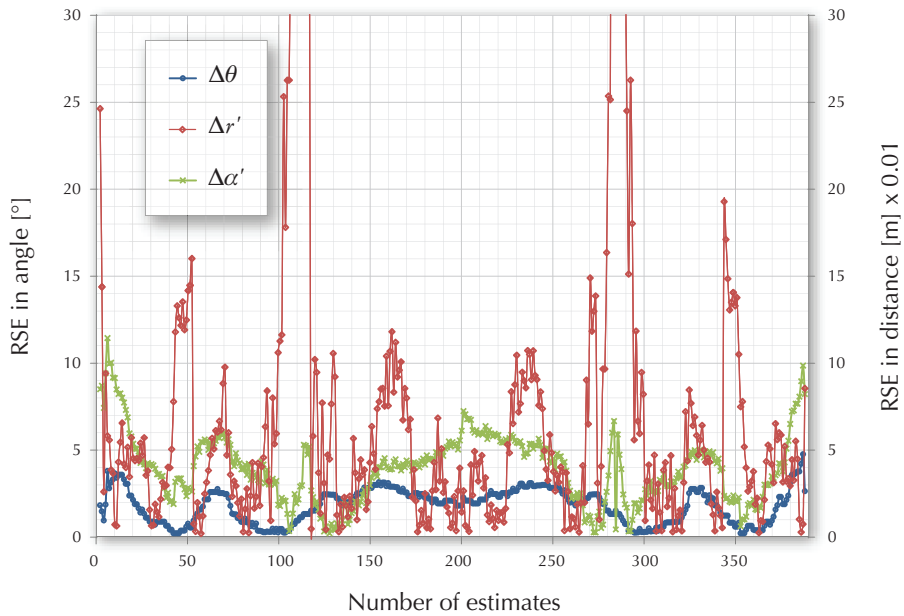


Figure 7.18: Unbiased root squared errors (RSE) in estimates for azimuth θ , alternate range r' and alternate heading α' corresponding to the variation of range plotted in figure 7.16.

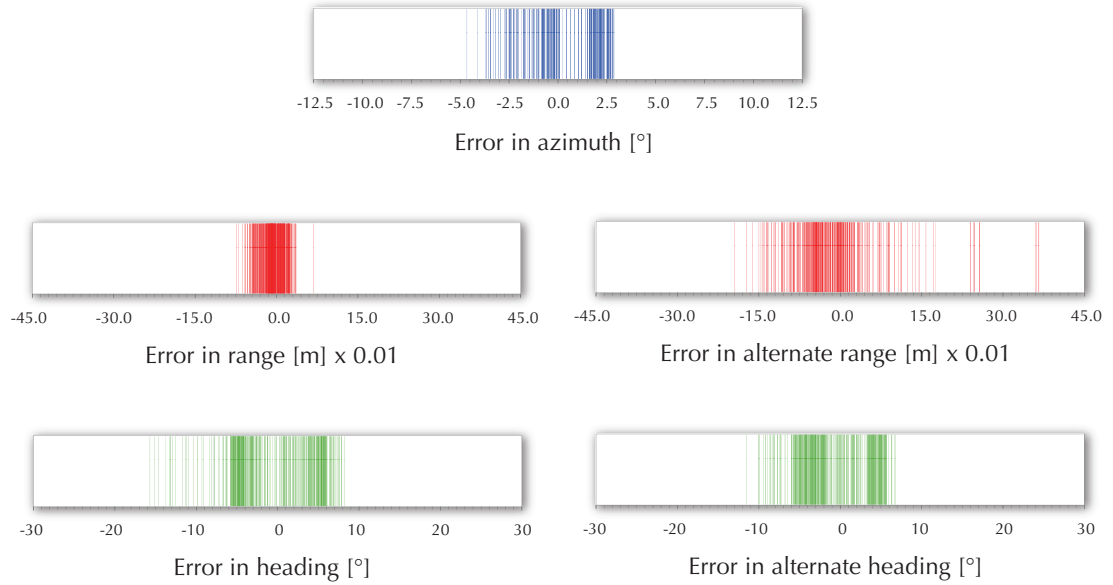


Figure 7.19: Estimate errors with bias for azimuth, range, heading and their alternate counterparts corresponding to the heading variation depicted in figures 7.15. and 7.16.

The biased estimation errors corresponding to the variation of heading is shown in figure 7.19. Table 7.5 gives the statistical quantities associated with these errors. The errors related to this explicit variation of heading can be compared with the errors associated with the variation of heading induced during the azimuth variation experiment presented earlier. In this instance, the direct heading estimation error is smaller than the alternate heading estimation error.

Error in azimuth	Error in range	Error in alternate range	Error in heading	Error in alternate heading
$\sigma_{\Delta\theta} = 1.82^\circ$	$\sigma_{\Delta r} = 21.43 \times 10^{-3} \text{ m}$	$\sigma_{\Delta r'} = 163.79 \times 10^{-3} \text{ m}$	$\sigma_{\Delta\alpha} = 5.13^\circ$	$\sigma_{\Delta\alpha'} = 4.19^\circ$
$\mu_{\Delta\theta} = 0.38^\circ$	$\mu_{\Delta r} = -3.49 \times 10^{-3} \text{ m}$	$\mu_{\Delta r'} = 19.85 \times 10^{-3} \text{ m}$	$\mu_{\Delta\alpha} = -0.42^\circ$	$\mu_{\Delta\alpha'} = -0.60^\circ$
$\overline{\Delta\theta} = 1.60^\circ$	$\overline{\Delta r} = 16.98 \times 10^{-3} \text{ m}$	$\overline{\Delta r'} = 88.91 \times 10^{-3} \text{ m}$	$\overline{\Delta\alpha} = 4.52^\circ$	$\overline{\Delta\alpha'} = 3.67^\circ$

Table 7.5: Comparison of standard deviations, means and average deviations of errors associated with azimuth, range and heading estimates corresponding to variation of heading depicted in figures 7.15. and 7.16.

7.4 Results and errors of medium range experiments

For comparison, the following sections present results obtained from experiments conducted at the lake (see figure 6.9) where the sender and receiver rigs were placed further apart than in the tank experiments presented earlier. The experiments were conducted approximately 15m from the bank of the lake where the maximum depth was 2.25m and the minimum 1.80m with a gentle gradient in between. The lake bottom consisted of soft sediment and had moderate

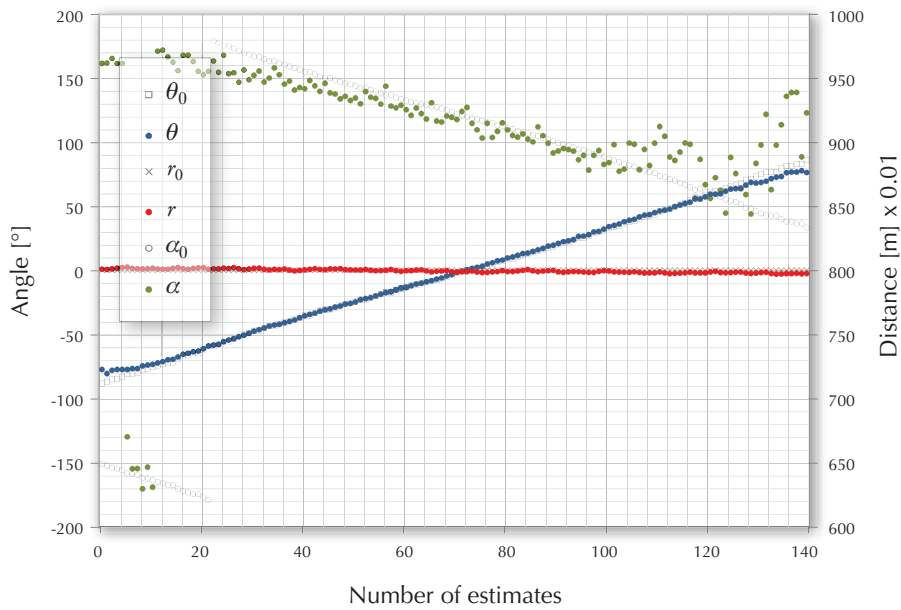


Figure 7.20: Estimates for azimuth θ , range r and heading α produced by the relative localisation system for an explicit azimuth variation of $\theta_0: -90^\circ \rightarrow 0^\circ \rightarrow 90^\circ$ with $\alpha_{\theta=0^\circ} = 120^\circ$ and $r_0 = 8.0\text{m}$.

underwater vegetation in the vicinity where the experiment was conducted. As with the experiments conducted in the test tank, the azimuth, range and heading of the sender was varied relative to the observer. The gantry motion speeds for the three variations were 6.5°s^{-1} , 0.07ms^{-1} and 4.5°s^{-1} respectively. The resulting estimates accompanied by the relevant errors obtained during the experiments are presented in the following sections.

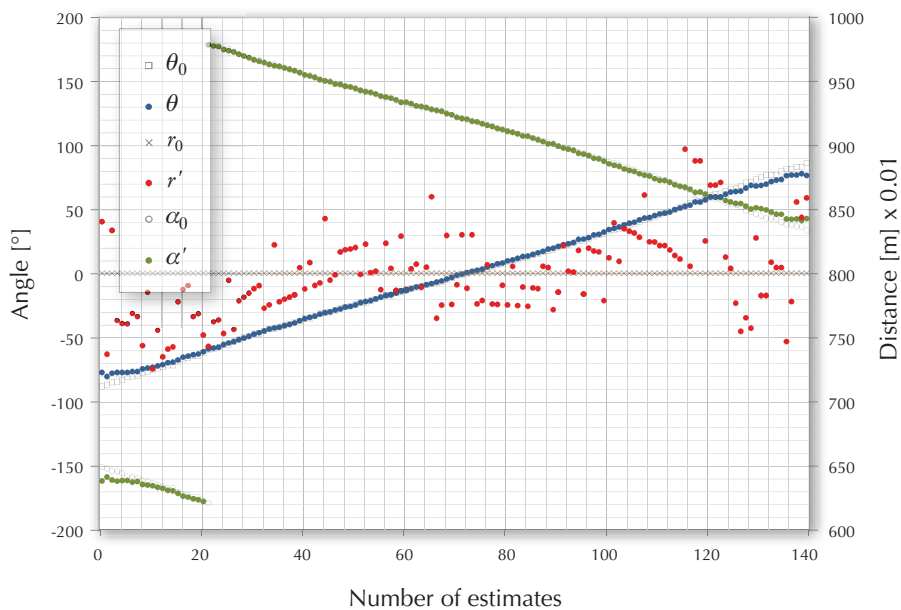


Figure 7.21: Azimuth θ , alternate range r' and alternate heading α' estimated by the relative localisation system for an explicit azimuth variation of $\theta_0: -90^\circ \rightarrow 0^\circ \rightarrow 90^\circ$ with $\alpha_{\theta=0^\circ} = 120^\circ$ and $r_0 = 8.0\text{m}$.

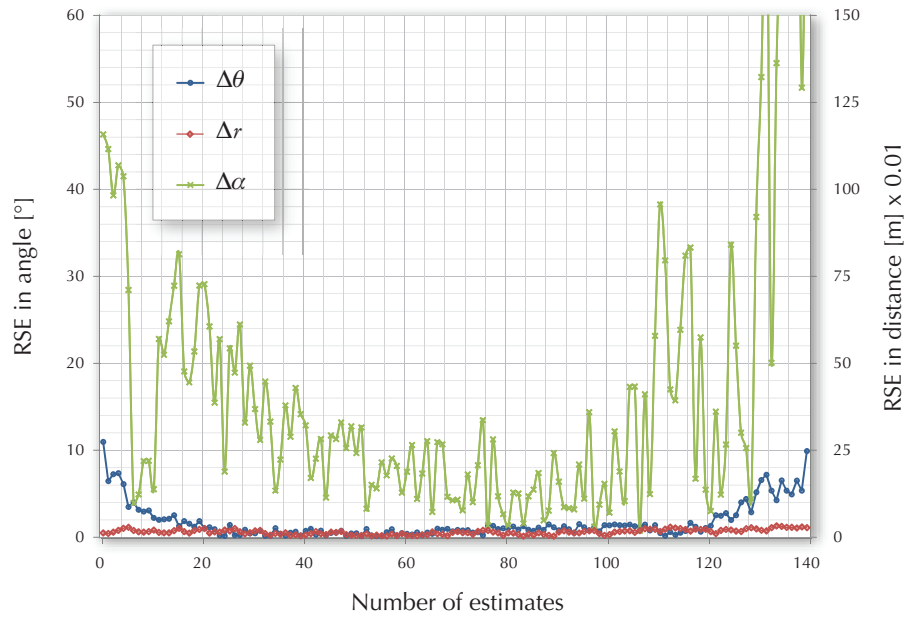


Figure 7.22: Unbiased root squared errors (RSE) in estimates for azimuth θ , range r and heading α corresponding to the variation of azimuth plotted in figure 7.20.

7.4.1 Variation of azimuth

The azimuth was varied as described in section 6.3.1. Figure 7.20 plots the azimuth θ , range r and heading α of the sender relative to the observer as estimated by the relative localisation system along with the corresponding ground truth value while figure 7.21 plots the azimuth θ , alternate range r' and alternate heading α' along with the ground truth values as before. The

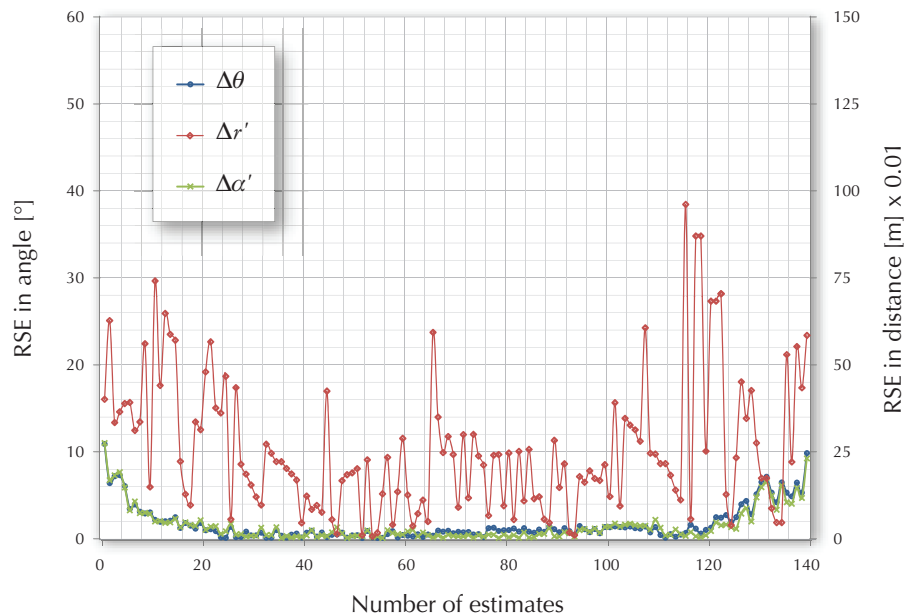


Figure 7.23: Unbiased root squared errors (RSE) in estimates for azimuth θ , alternate range r' and alternate heading α' corresponding to the variation of azimuth plotted in figure 7.21.

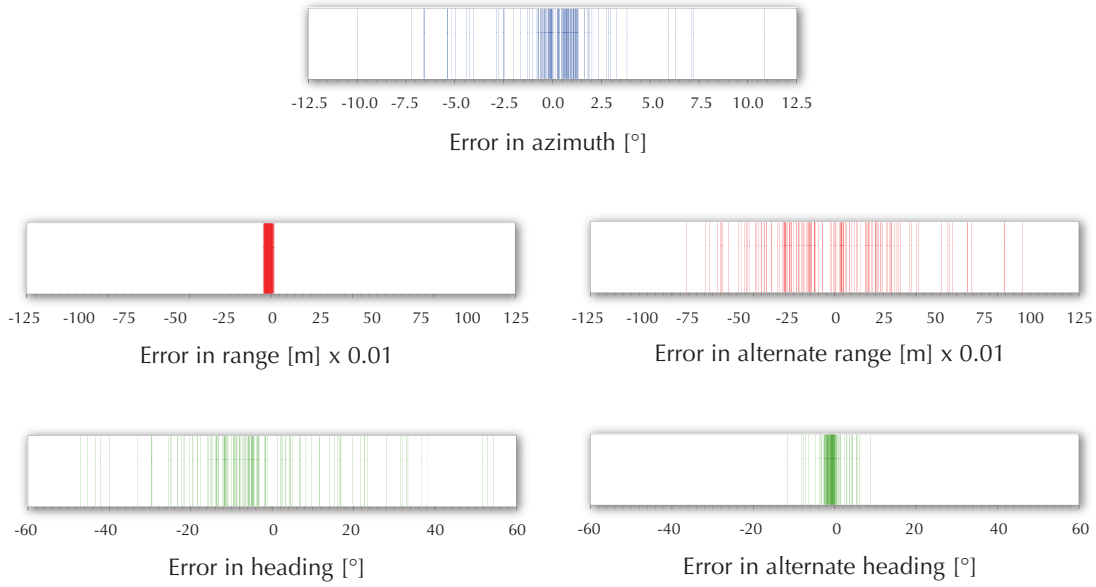


Figure 7.24: Estimate errors with bias for azimuth, range, heading and their alternate counterparts corresponding to the azimuth variation depicted in figures 7.20. and 7.21.

RSE for each of the above experiments are plotted in figures 7.22 and 7.23 respectively. Errors with bias are plotted in figure 7.24 while table 7.6 gives the statistical quantities derived from the errors. As expected, the errors for the direct heading estimation had increased with the increase in range in comparison to the shorter range used earlier in the tank. Due to this, the angular scales on the heading error plots extend to 60° instead of 30° used for earlier error plots. However, the alternate heading estimation errors remain much lower than the direct counterpart, at a level comparable to previous experiments. As predicted by the error model, the alternate range error had risen with increased range compared to the tank experiments and the scales of the range error plots are expanded accordingly. The scale is increased to 150.0×10^{-2} m from the usual 30.0×10^{-2} m for the RSE plots and to $\pm 125.0 \times 10^{-2}$ m from the usual $\pm 45.0 \times 10^{-2}$ m for the biased error plots. However, the direct range estimation error is comparable to those arising during tank experiments and behaves as predicted by not scaling up with range.

Error in azimuth	Error in range	Error in alternate range	Error in heading	Error in alternate heading
$\sigma_{\Delta\theta} = 2.59^\circ$	$\sigma_{\Delta r} = 13.85 \times 10^{-3}$ m	$\sigma_{\Delta r'} = 327.62 \times 10^{-3}$ m	$\sigma_{\Delta\alpha} = 26.23^\circ$	$\sigma_{\Delta\alpha'} = 2.44^\circ$
$\mu_{\Delta\theta} = 0.15^\circ$	$\mu_{\Delta r} = -3.46 \times 10^{-3}$ m	$\mu_{\Delta r'} = -17.4 \times 10^{-3}$ m	$\mu_{\Delta\alpha} = 0.45^\circ$	$\mu_{\Delta\alpha'} = -0.26^\circ$
$\overline{\Delta\theta} = 1.59^\circ$	$\overline{\Delta r} = 11.94 \times 10^{-3}$ m	$\overline{\Delta r'} = 260.72 \times 10^{-3}$ m	$\overline{\Delta\alpha} = 17.64^\circ$	$\overline{\Delta\alpha'} = 1.43^\circ$

Table 7.6: Comparison of standard deviations, means and average deviations of errors associated with azimuth, range and heading estimates corresponding to variation of azimuth depicted in figures 7.20. and 7.21.

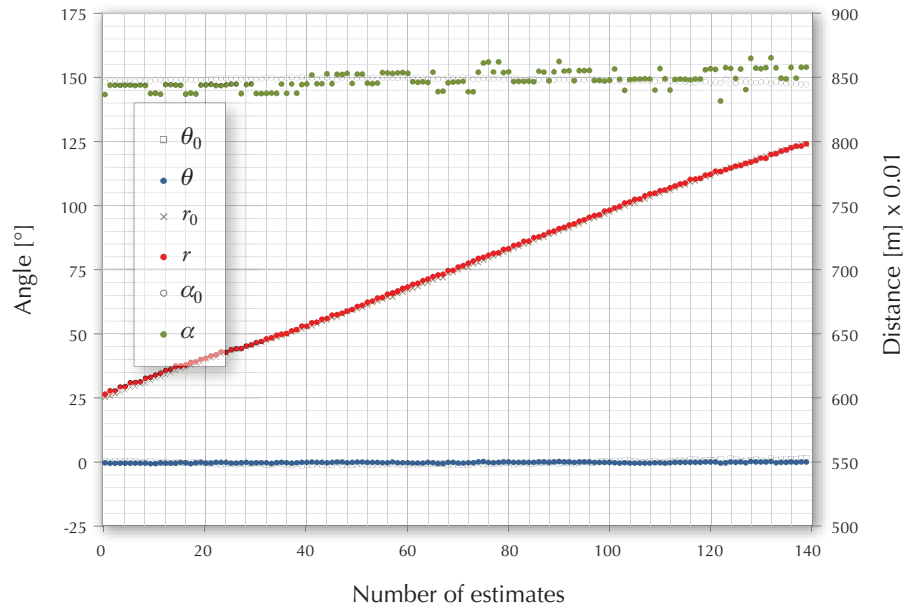


Figure 7.25: Estimates for azimuth θ , range r and heading α produced by the relative localisation system for a range variation of $r_0:6.0\text{m} \rightarrow 8.0\text{m}$ with $\alpha_0 = 150^\circ$ and $\theta_0 = 0^\circ$.

7.4.2 Variation of range

The relative distance between the sender and observer rigs were made to vary by 2.0m from 6.0m to 8.0m as described in the procedure given in section 6.3.3. The estimated quantities for azimuth, range and heading and the alternate estimates for range and heading along with ground truth reference values are plotted in figures 7.25 and 7.26.

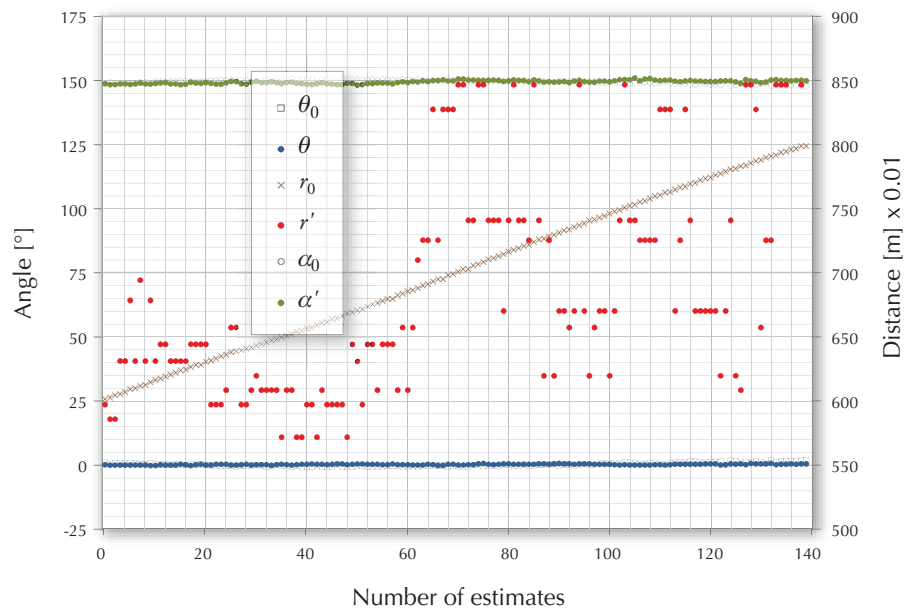


Figure 7.26: Estimates for azimuth θ , alternate range r' and alternate heading α' produced by the relative localisation system for a range variation of $r_0:6.0\text{m} \rightarrow 8.0\text{m}$ with $\alpha_0 = 150^\circ$ and $\theta_0 = 0^\circ$.

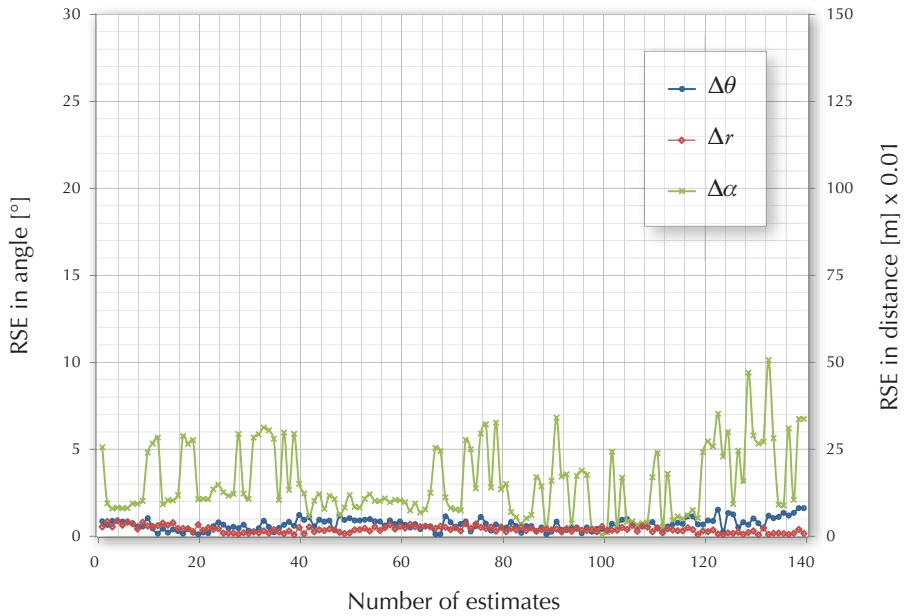


Figure 7.27: Unbiased root squared errors (RSE) in estimates for azimuth θ , range r and heading α corresponding to the variation of range plotted in figure 7.25.

The RSE associated with the estimated quantities are plotted in figures 7.27 and 7.28. The errors with bias are depicted in figure 7.29 while the statistical quantities attached to the errors are tabulated in table 7.7.

During the experiment the azimuth and direct and alternate heading estimates remained constant and displayed relatively low errors. This includes the direct heading estimate which in the

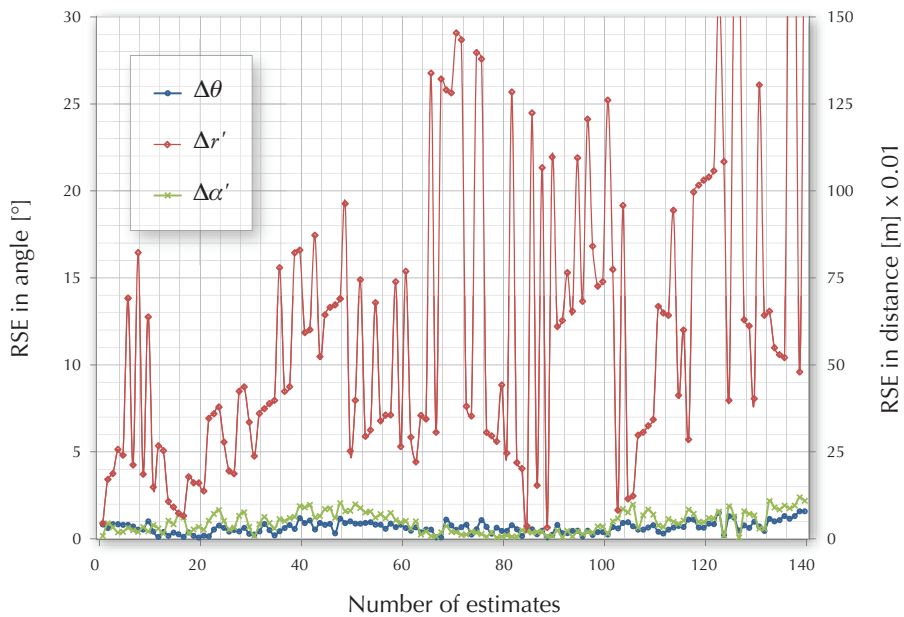


Figure 7.28: Unbiased root squared errors (RSE) in estimates for azimuth θ , alternate range r' and alternate heading α' corresponding to the variation of range plotted in figure 7.26.

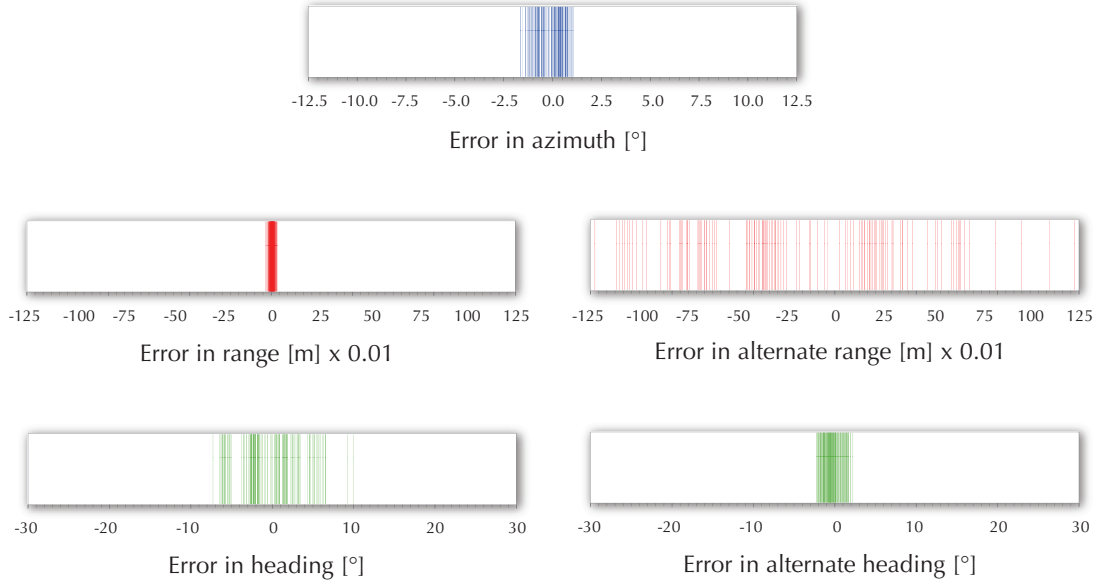


Figure 7.29: Estimate errors with bias for azimuth, range, heading and their alternate counterparts corresponding to the range variation depicted in figures 7.25. and 7.26.

previous experiment (section 7.4.1) showed much larger errors. However, the alternate range estimates showed substantial instability in this orientation and produced out of bound outliers. These were handled by the threshold bounding scheme presented in section 5.4.2. A maximum effective range of $r_{max} = 8.5$ m was enforced during these experiments. While the error model for alternate range predicts increased errors as the range increases, it also predicts additional uncertainties when reverse sub-azimuths φ_1 and φ_2 reach 0° or 180° . The experimental configuration which had $\alpha = 150^\circ$ and $\theta = 0^\circ$ operates near this region leading to the observed instability in the alternate range estimates.

To accommodate the larger variations, the scales of the plots related to errors in range are maintained at 150.0×10^{-2} m for the RSE plots and the $\pm 125.0 \times 10^{-2}$ m for the biased error plots. The angular error plot scales are maintained at the usual values of 30° for RSE plots and biased error plots for heading and 12.5° for the biased error plot for azimuth.

Error in azimuth	Error in range	Error in alternate range	Error in heading	Error in alternate heading
$\sigma_{\Delta\theta} = 0.68^\circ$	$\sigma_{\Delta r} = 10.84 \times 10^{-3}$ m	$\sigma_{\Delta r'} = 756.37 \times 10^{-3}$ m	$\sigma_{\Delta\alpha} = 3.65^\circ$	$\sigma_{\Delta\alpha'} = 1.07^\circ$
$\mu_{\Delta\theta} = 0.00^\circ$	$\mu_{\Delta r} = 14.32 \times 10^{-3}$ m	$\mu_{\Delta r'} = -89.74 \times 10^{-3}$ m	$\mu_{\Delta\alpha} = -0.04^\circ$	$\mu_{\Delta\alpha'} = -0.09^\circ$
$\overline{\Delta\theta} = 0.60^\circ$	$\overline{\Delta r} = 8.47 \times 10^{-3}$ m	$\overline{\Delta r'} = 604.74 \times 10^{-3}$ m	$\overline{\Delta\alpha} = 3.03^\circ$	$\overline{\Delta\alpha'} = 0.88^\circ$

Table 7.7: Comparison of standard deviations, means and average deviations of errors associated with azimuth, range and heading estimates corresponding to variation of range depicted in figures 7.25. and 7.26.

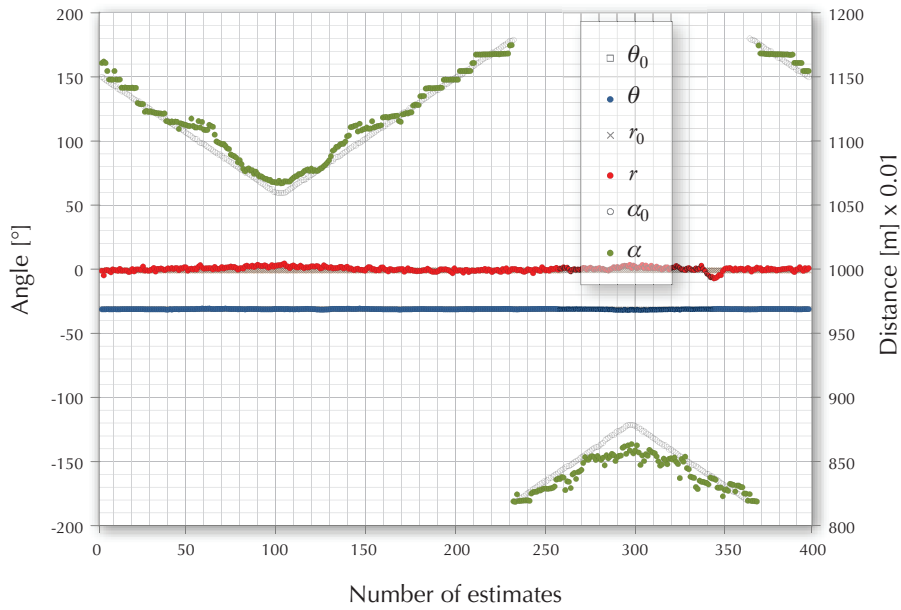


Figure 7.30: Azimuth θ , range r and heading α estimated by the relative localisation system for an explicit heading variation of $\alpha_0 : 150^\circ \rightarrow 60^\circ \rightarrow 180^\circ \rightarrow -60^\circ \rightarrow 150^\circ$ where $\theta_0 = -30^\circ$ and $r_0 = 10.0\text{m}$ remained constant.

7.4.3 Variation of heading

As explained in section 6.3.2, the relative heading was explicitly varied by rotating the sender rig while keeping the observer rig stationary. The resulting estimates for azimuth, range and heading are plotted in figure 7.30 while those for alternate range and heading are plotted in figure 7.31.

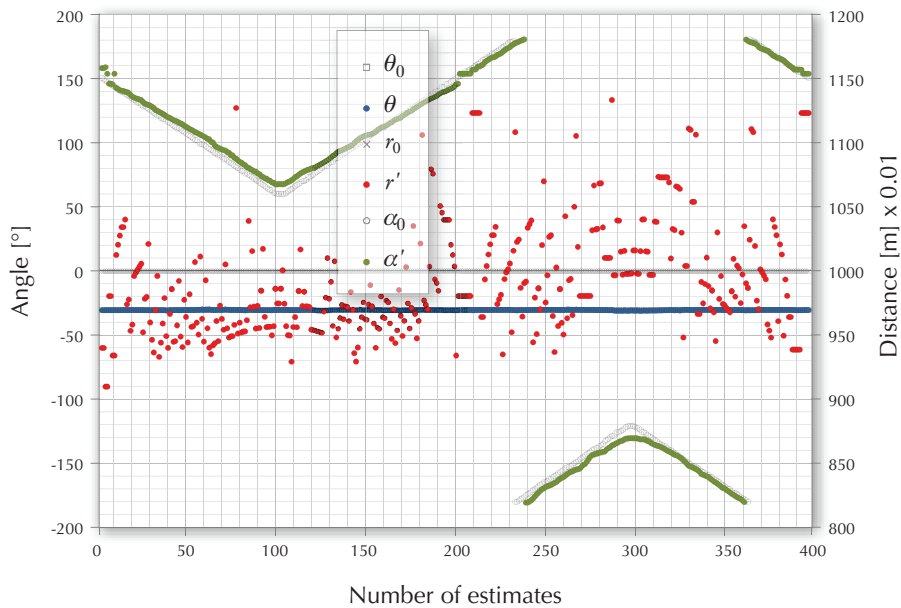


Figure 7.31: Azimuth θ , alternate range r' and alternate heading α' estimated by the relative localisation system for an explicit heading variation of $\alpha_0 : 150^\circ \rightarrow 60^\circ \rightarrow 180^\circ \rightarrow -60^\circ \rightarrow 150^\circ$ where $\theta_0 = -30^\circ$ and $r_0 = 10.0\text{m}$ remained constant.

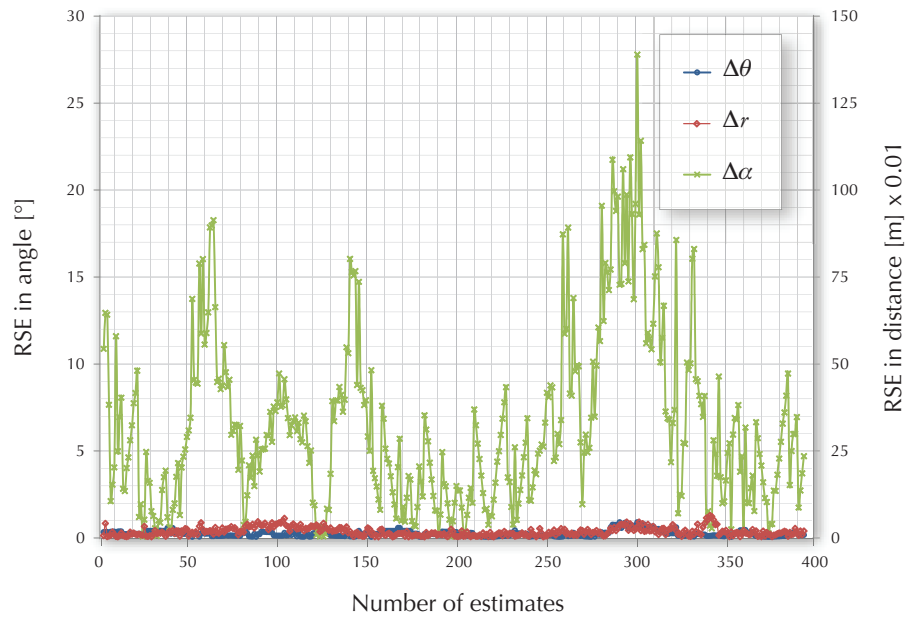


Figure 7.32: Unbiased root squared errors (RSE) in estimates for azimuth θ , range r and heading α corresponding to the variation of azimuth plotted in figure 7.30.

The RSE associated with the estimates are given by plots in figures 7.32 and 7.33 while the biased errors are plotted in figure 7.34. The statistical quantities derived from the errors are tabulated in table 7.8. The scales of the plots related to errors in range are maintained at 150.0×10^{-2} m and $\pm 125.0 \times 10^{-2}$ m for the RSE and biased error plots respectively. The angular error plot scales

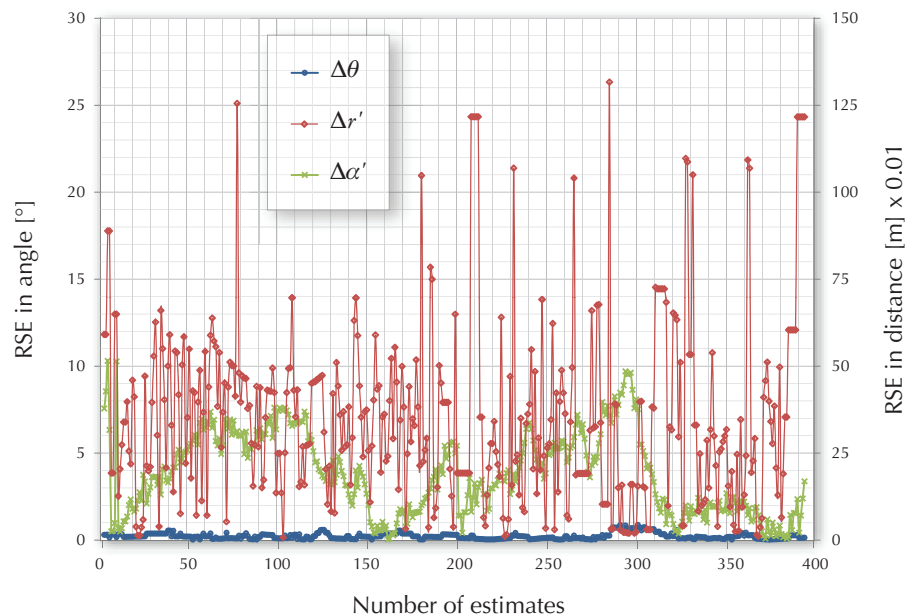


Figure 7.33: Unbiased root squared errors (RSE) in estimates for azimuth θ , alternate range r' and alternate heading α' corresponding to the variation of azimuth plotted in figure 7.31.

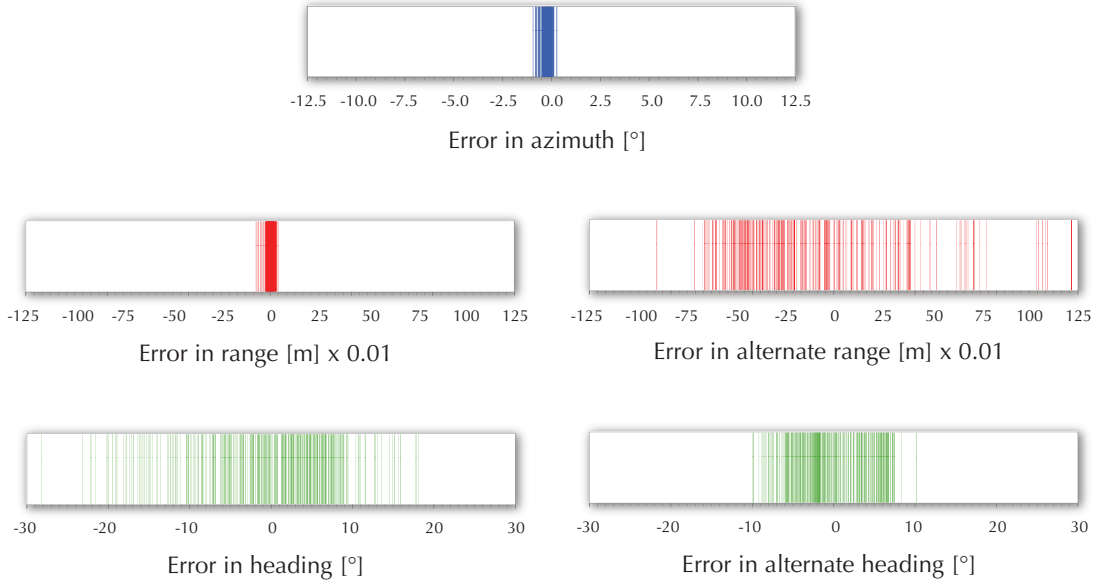


Figure 7.34: Estimate errors with bias for azimuth, range, heading and their alternate counterparts corresponding to the heading variation depicted in figures 7.30. and 7.31.

are maintained at the usual values since the error magnitudes are comparable to those arising during the tank experiments. However, the direct heading caused larger errors than the alternate counterpart in conformance with the error model.

Error in azimuth	Error in range	Error in alternate range	Error in heading	Error in alternate heading
$\sigma_{\Delta\theta} = 0.22^\circ$	$\sigma_{\Delta r} = 16.09 \times 10^{-3} \text{ m}$	$\sigma_{\Delta r'} = 442.79 \times 10^{-3} \text{ m}$	$\sigma_{\Delta\alpha} = 8.18^\circ$	$\sigma_{\Delta\alpha'} = 4.51^\circ$
$\mu_{\Delta\theta} = -0.15^\circ$	$\mu_{\Delta r} = 10.70 \times 10^{-3} \text{ m}$	$\mu_{\Delta r'} = -74.84 \times 10^{-3} \text{ m}$	$\mu_{\Delta\alpha} = -0.03^\circ$	$\mu_{\Delta\alpha'} = -0.03^\circ$
$\overline{\Delta\theta} = 0.17^\circ$	$\overline{\Delta r} = 11.84 \times 10^{-3} \text{ m}$	$\overline{\Delta r'} = 342.44 \times 10^{-3} \text{ m}$	$\overline{\Delta\alpha} = 6.47^\circ$	$\overline{\Delta\alpha'} = 3.84^\circ$

Table 7.8: Comparison of standard deviations, means and average deviations of errors associated with azimuth, range and heading estimates corresponding to variation of heading depicted in figures 7.30. and 7.31.

7.5 Results and errors of long range experiments

The azimuth and range estimates produced during the first 200s of a long range experiment along with the ground truth values are presented in figure 7.35. The observer rig was mounted on the gantry frame attached to the pier while the sender rig was mounted to a kayak. The kayak was navigated along a predetermined path on the lake. Range tracking (section 5.5.1) was enabled¹ during processing of results to overcome the range limitation constraints and to reduce

¹. $N_{RT} = 768$ corresponding to a spatial window length of 10m according to (5.1).

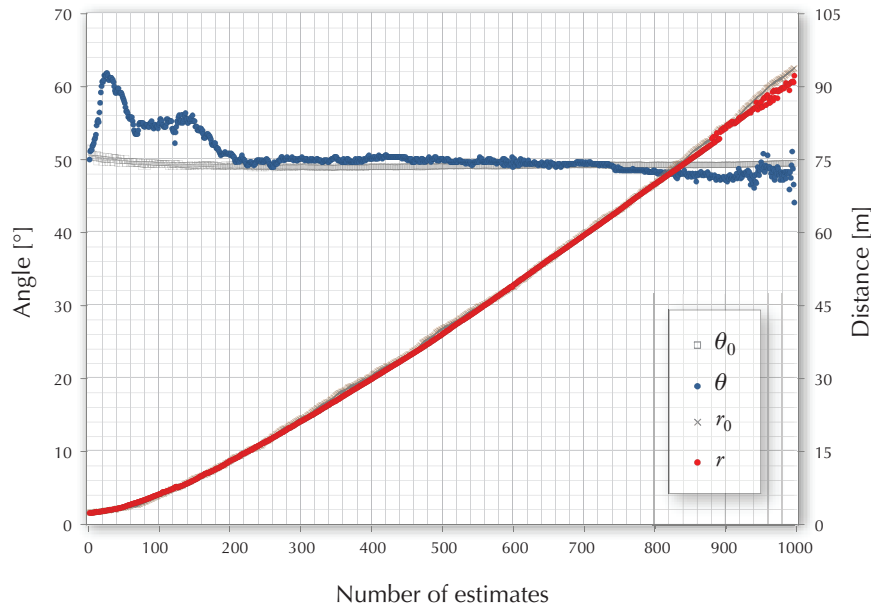


Figure 7.35: Estimates for azimuth θ and range r produced during the first 200s of a long range experiment along with the associated ground truth quantities.

computational cost. Ground truth reference for this experiment was provided via the GPS module and data logger on board the kayak as explained previously in chapter 6. As a result, the ground truth during these experiments were coarser and less precise than in the previous short and medium range experiments conducted utilising the gantry. Additionally, the relative velocities between the sender and observer rigs were considerably higher than in the previous experiments with the kayak maintaining a nominal speed of $1.0\text{-}1.5\text{ms}^{-1}$ (as measured via the GPS

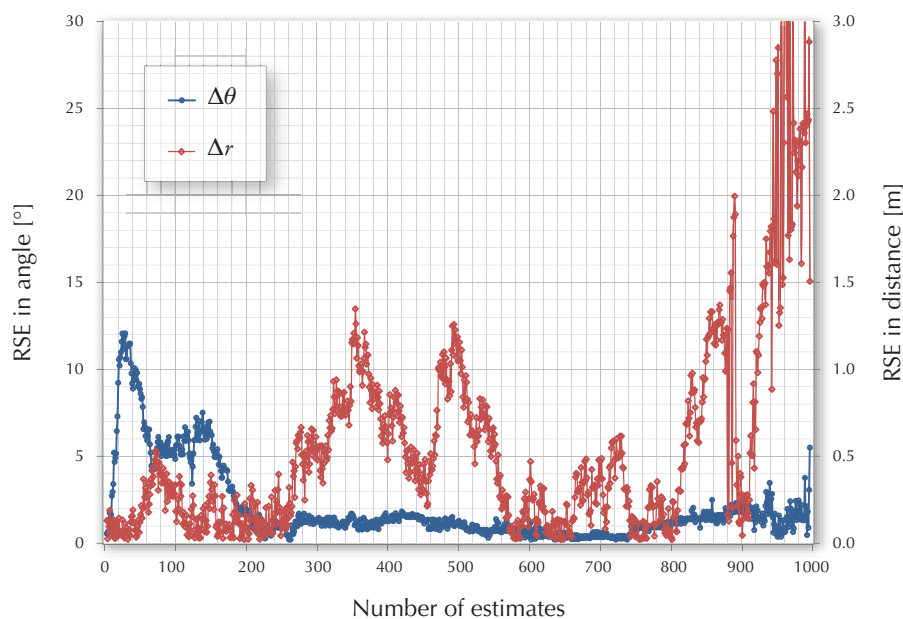


Figure 7.36: Unbiased root squared errors corresponding to the variations plotted in figure 7.35.

data logger). Due to these factors, the RSE associated with the estimated quantities (plotted in figure 7.36), especially the range estimates were significantly higher. However, since the ground truth acquisition methodology and the precision is different to the previous cases, these errors cannot be directly compared to those obtained in the previously presented experiments. While heading estimates were produced by the relative localisation system, reliable and consistent ground truth reference for heading could not be obtained during this experiment. Therefore, the heading estimates are not discussed as they cannot be evaluated against ground truth. The statistical quantities related to the distribution of azimuth and range errors related to this experiment are given below in table 7.9.

Error in azimuth	Error in range
$\sigma_{\Delta\theta} = 1.35^\circ$	$\sigma_{\Delta r} = 62.2 \times 10^{-2} \text{ m}$
$\mu_{\Delta\theta} = -0.73^\circ$	$\mu_{\Delta r} = 33.1 \times 10^{-2} \text{ m}$
$\overline{\Delta\theta} = 1.01^\circ$	$\overline{\Delta r} = 47.4 \times 10^{-2} \text{ m}$

Table 7.9: Comparison of standard deviations, means and average deviations of errors associated with azimuth and range estimates corresponding to the estimates depicted in figures 7.35.

7.6 Analysis

A large number of experiments were conducted throughout the development process of the relative localisation system with different configurations of the setup in order to evaluate its

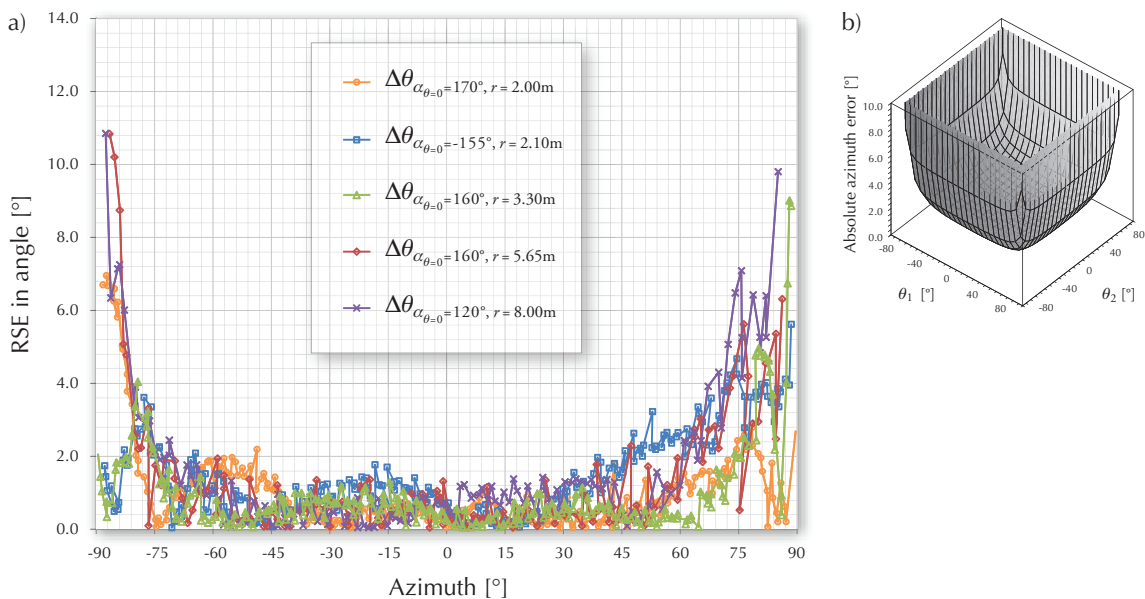


Figure 7.37: Azimuth estimate errors associated with five azimuth variation experiments with different initial heading and range configurations are plotted in a) and the corresponding error model is shown in b).

performance. Out of these, three experiments conducted at the test tank and another three conducted at the lake were presented in detail in the previous section in addition to one long range experiment. These were meant to represent the general characteristics of the results obtained in different experimental environments and to gauge the angular and radial sensing range of the system.

7.6.1 Behaviour of errors

Aggregate RSE plots of azimuth, heading, alternate heading, range and alternate range derived from multiple experiments¹ are used to analyse the behaviour of estimation errors under different experimental conditions in the following sections.

Azimuth estimation errors

RSE of azimuth estimates obtained during five different experiments are plotted in figure 7.37.a. The azimuth was varied as $\theta_0 : -90^\circ \rightarrow 0^\circ \rightarrow 90^\circ$ during these experiments which had different initial heading ($\alpha_{\theta=0^\circ}$) and range (r_0) combinations. The RSE are plotted against the ground truth azimuth θ_0 for comparison instead of the estimate numbers as done in the previous section. As depicted in these plots, the overall trend of the unbiased root squared errors remains consistent and the shape conforms to that presented in section 4.3 for the absolute angular error (except for a 90° offset along the x -axis due to the adjustments introduced in section 4.4.3) calculated based on the general error propagation formula. The different plots also correspond to multiple cross sections of the absolute azimuth error plot given section 4.4.5 (reproduced in figure 7.37.b) with different relationships between the sub-azimuths θ_1 and θ_2 depending on the initial heading $\alpha_{\theta=0^\circ}$. The actual azimuth variations which these error plots relate to are given in appendix A.

Error in azimuth ($\alpha_{\theta=0^\circ} = 170^\circ$) ($r = 2.0\text{m}$)	Error in azimuth ($\alpha_{\theta=0^\circ} = -155^\circ$) ($r = 2.1\text{m}$)	Error in azimuth ($\alpha_{\theta=0^\circ} = 160^\circ$) ($r = 3.3\text{m}$)	Error in azimuth ($\alpha_{\theta=0^\circ} = 160^\circ$) ($r = 6.0\text{m}$)	Error in azimuth ($\alpha_{\theta=0^\circ} = 120^\circ$) ($r = 8.0\text{m}$)
$\sigma_{\Delta\theta} = 1.63^\circ$	$\sigma_{\Delta\theta} = 1.68^\circ$	$\sigma_{\Delta\theta} = 1.51^\circ$	$\sigma_{\Delta\theta} = 2.25^\circ$	$\sigma_{\Delta\theta} = 2.59^\circ$
$\mu_{\Delta\theta} = -0.13^\circ$	$\mu_{\Delta\theta} = -0.87^\circ$	$\mu_{\Delta\theta} = 0.05^\circ$	$\mu_{\Delta\theta} = -0.24^\circ$	$\mu_{\Delta\theta} = 0.15^\circ$
$\overline{\Delta\theta} = 1.02^\circ$	$\overline{\Delta\theta} = 1.43^\circ$	$\overline{\Delta\theta} = 0.92^\circ$	$\overline{\Delta\theta} = 1.30^\circ$	$\overline{\Delta\theta} = 1.59^\circ$

Table 7.10: Comparison of standard deviations, means and average deviations of errors associated with azimuth variations plotted in figure A.2 and whose RSE are shown in figure 7.37.

¹. These results were drawn from multiple experiments conducted over a 24 month period during 2007 and 2008.

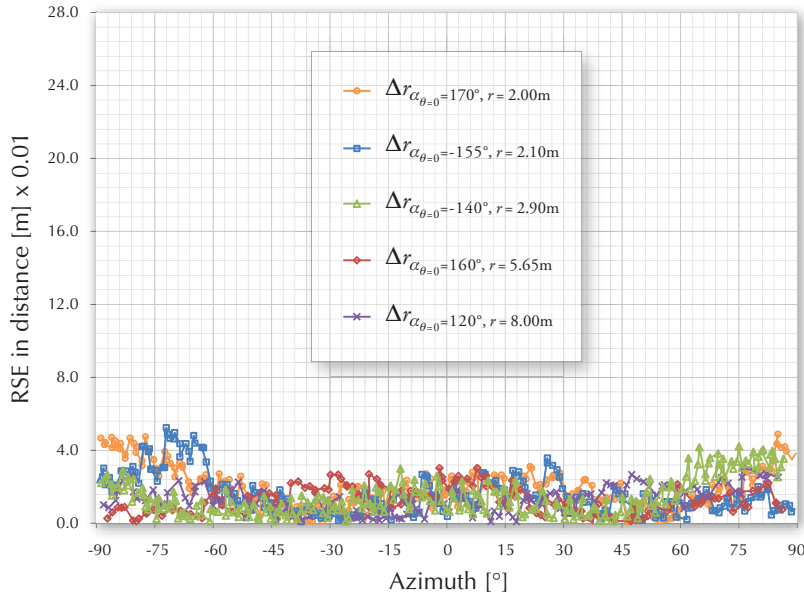


Figure 7.38: Range estimate errors associated with five azimuth variation experiments with different initial heading and range configurations.

While the shape of the error distributions are consistent, it must be noted that the errors in the experimental case remain finite in the vicinity where azimuth approaches $\pm 90^\circ$ despite a significant increase as opposed to tending towards infinity as predicted by the theoretical error model. This behaviour of the error model can be explained by the perceived ambiguities arising due to degenerative cosine terms in (4.45) as the sub-azimuths approach $\pm 90^\circ$. However, the use of non-omnidirectional hydrophones in the experimental case avoids these ambiguities and the increase of errors in this region can be attributed to the decrease in angular resolution as predicted by (4.28). The errors due to loss of SNR as the source reaches the sensing limits of the receivers as the azimuth approaches $\pm 90^\circ$ are effectively handled by the peak tracking scheme as discussed at the beginning of this chapter. Table 7.10 lists the means, standard deviations and average deviations of the errors for the five experiments depicted in figure 7.37. The consistency

Error in range ($\alpha_{\theta=0^\circ} = 170^\circ$) ($r = 2.0\text{m}$)	Error in range ($\alpha_{\theta=0^\circ} = -155^\circ$) ($r = 2.1\text{m}$)	Error in range ($\alpha_{\theta=0^\circ} = -140^\circ$) ($r = 2.9\text{m}$)	Error in range ($\alpha_{\theta=0^\circ} = 160^\circ$) ($r = 6.0\text{m}$)	Error in range ($\alpha_{\theta=0^\circ} = 120^\circ$) ($r = 8.0\text{m}$)
$\sigma_{\Delta r} = 21.90 \times 10^{-3} \text{ m}$	$\sigma_{\Delta r} = 15.27 \times 10^{-3} \text{ m}$	$\sigma_{\Delta r} = 16.82 \times 10^{-3} \text{ m}$	$\sigma_{\Delta r} = 12.62 \times 10^{-3} \text{ m}$	$\sigma_{\Delta r} = 13.85 \times 10^{-3} \text{ m}$
$\mu_{\Delta r} = 4.02 \times 10^{-3} \text{ m}$	$\mu_{\Delta r} = -11.34 \times 10^{-3} \text{ m}$	$\mu_{\Delta r} = 2.87 \times 10^{-3} \text{ m}$	$\mu_{\Delta r} = -7.12 \times 10^{-3} \text{ m}$	$\mu_{\Delta r} = -3.46 \times 10^{-3} \text{ m}$
$\overline{\Delta r} = 19.26 \times 10^{-3} \text{ m}$	$\overline{\Delta r} = 12.06 \times 10^{-3} \text{ m}$	$\overline{\Delta r} = 14.06 \times 10^{-3} \text{ m}$	$\overline{\Delta r} = 10.58 \times 10^{-3} \text{ m}$	$\overline{\Delta r} = 11.93 \times 10^{-3} \text{ m}$

Table 7.11: Comparison of standard deviations, means and average deviations related to different sets of RSE of range estimates shown in figure 7.38.

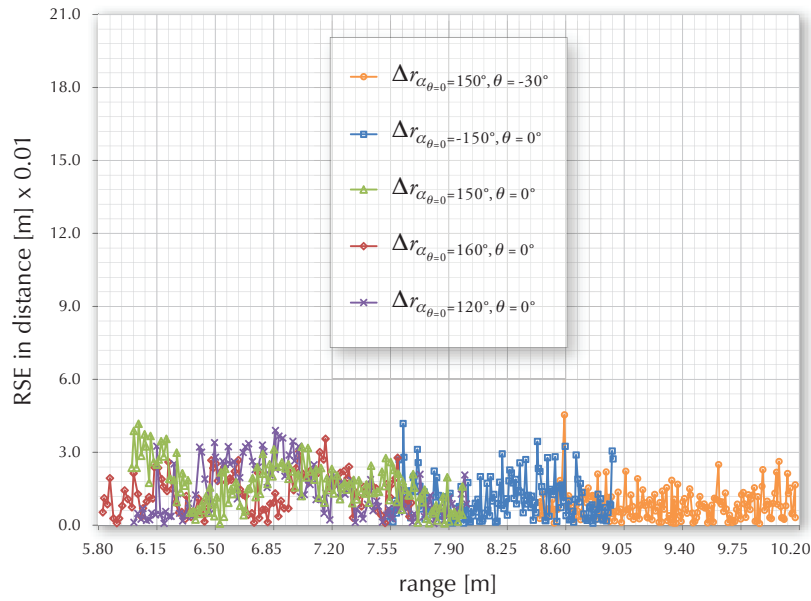


Figure 7.39: Range estimate errors associated with five range variation experiments with different heading and azimuth configurations.

of azimuth estimation error behaviour across these different experiments become evident by observing these tabulated error statistics.

Range estimation errors

Figure 7.38 plots range estimate errors associated with five azimuth variation experiments conducted under different conditions. Figure 7.39 plots range estimate errors associated with five different range variation experiments under different angular configurations where the range is varied between 5.8m and 10.2m collectively.

These experimental results are consistent with the error model given by (4.47) which predicts that the range error remains invariant as the azimuth and range varies. However, the range estimate errors show a very slight increase as the azimuth approaches $\pm 90^\circ$, during three (short

Error in range ($\alpha_{\theta=0^\circ} = 150^\circ$) ($\theta = -30^\circ$)	Error in range ($\alpha_{\theta=0^\circ} = -150^\circ$) ($\theta = 0^\circ$)	Error in range ($\alpha_{\theta=0^\circ} = 150^\circ$) ($\theta = 0^\circ$)	Error in range ($\alpha_{\theta=0^\circ} = 160^\circ$) ($\theta = 0^\circ$)	Error in range ($\alpha_{\theta=0^\circ} = 120^\circ$) ($\theta = 0^\circ$)
$\sigma_{\Delta r} = 9.82 \times 10^{-3} \text{ m}$	$\sigma_{\Delta r} = 11.39 \times 10^{-3} \text{ m}$	$\sigma_{\Delta r} = 10.85 \times 10^{-3} \text{ m}$	$\sigma_{\Delta r} = 13.95 \times 10^{-3} \text{ m}$	$\sigma_{\Delta r} = 16.11 \times 10^{-3} \text{ m}$
$\mu_{\Delta r} = -0.73 \times 10^{-3} \text{ m}$	$\mu_{\Delta r} = 6.61 \times 10^{-3} \text{ m}$	$\mu_{\Delta r} = 14.32 \times 10^{-3} \text{ m}$	$\mu_{\Delta r} = 6.36 \times 10^{-3} \text{ m}$	$\mu_{\Delta r} = -6.66 \times 10^{-3} \text{ m}$
$\overline{\Delta r} = 7.71 \times 10^{-3} \text{ m}$	$\overline{\Delta r} = 8.76 \times 10^{-3} \text{ m}$	$\overline{\Delta r} = 8.47 \times 10^{-3} \text{ m}$	$\overline{\Delta r} = 11.18 \times 10^{-3} \text{ m}$	$\overline{\Delta r} = 13.76 \times 10^{-3} \text{ m}$

Table 7.12: Comparison of standard deviations, means and average deviations related to different sets of RSE of range estimates shown in figure 7.39.

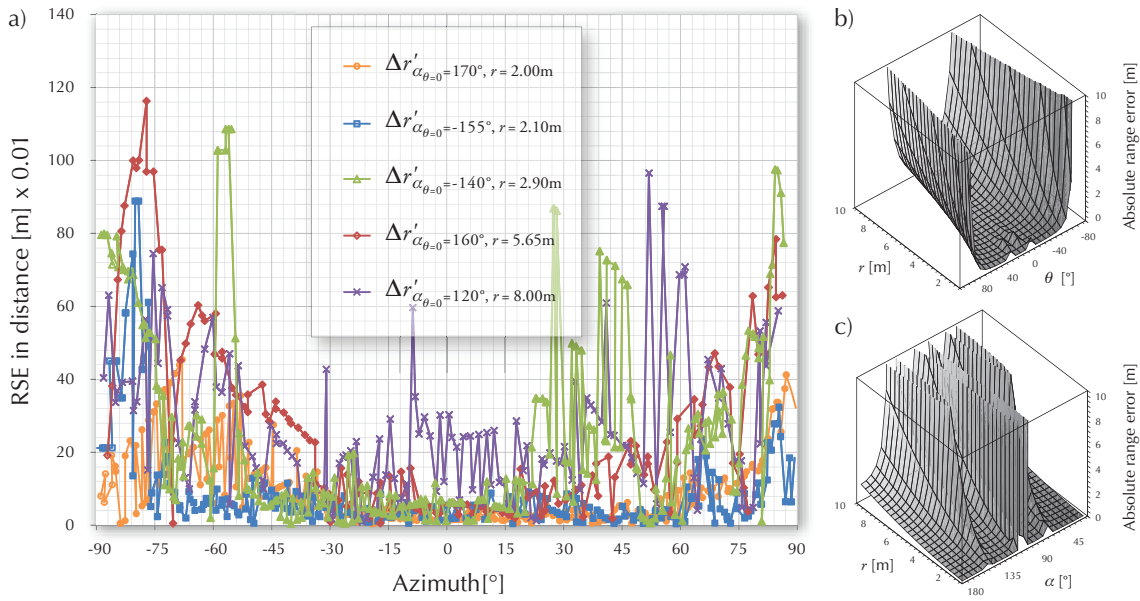


Figure 7.40: Alternate range estimate errors associated with five azimuth variation experiments with different initial heading and range configurations are plotted in a) while the error models are plotted in b) and c).

range) experiments conducted in the test tank, which can be traced to the influence of delayed multipath arrivals of the signal as the source reaches the sensing limits of the receivers which was discussed at the beginning of this chapter. Furthermore, according to figure 7.39, the range

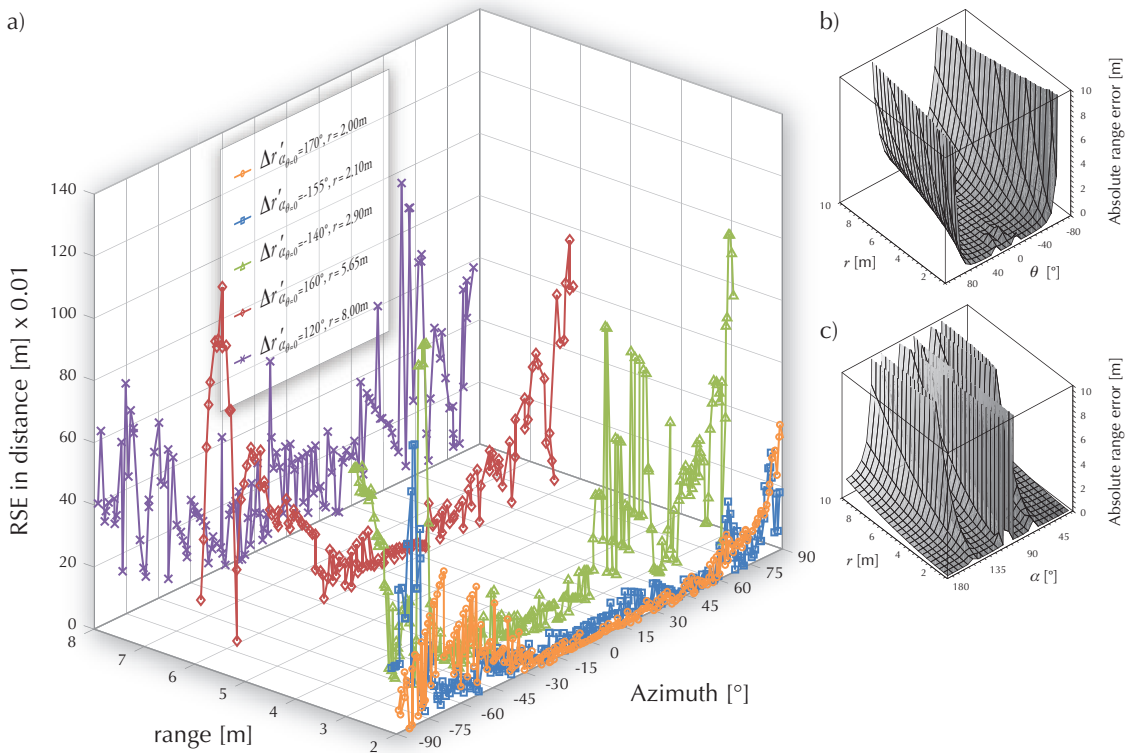


Figure 7.41: Plots shown in figure 7.40.a with a rotated 3-dimensional projection.

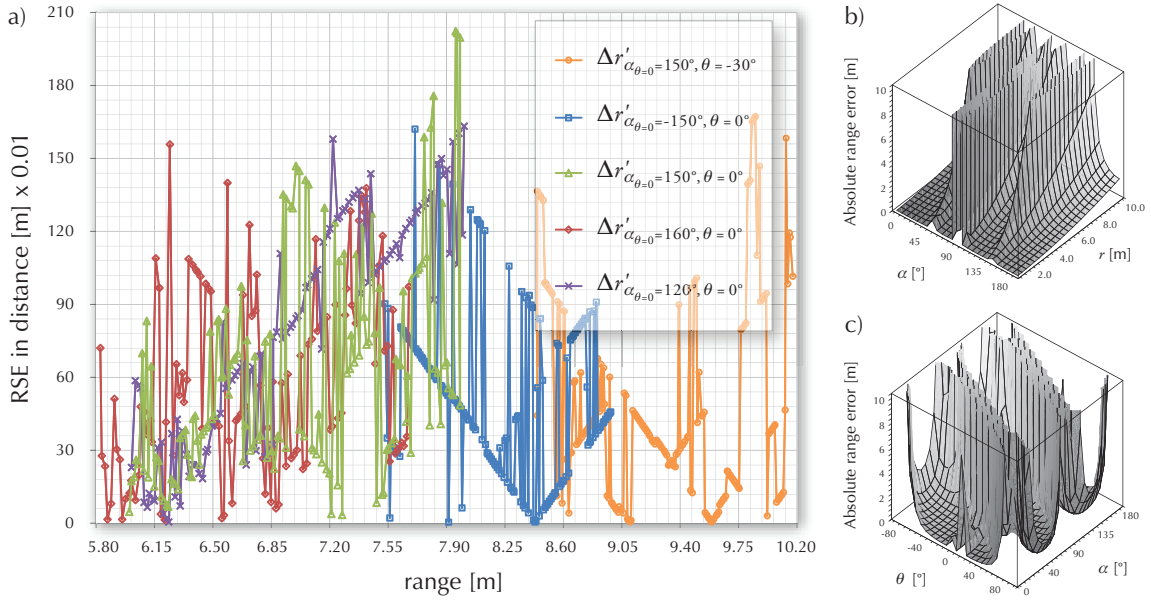


Figure 7.42: Alternate range estimate errors associated with five azimuth variation experiments with different heading and azimuth configurations are plotted in a) while the error models are plotted in b) and c).

estimation error slightly *decreases* for the medium range experiments conducted in the lake compared to the short range experiments conducted in the test tank. This effect can be attributed to the prevalence of multipath arrivals of the signal in the reverberant environment of the enclosed test tank compared to the lake environment. Additionally, the range error remains well below the theoretical upper bound depicted in figure 4.17. Table 7.11 lists the means, standard deviations and average deviations of the errors for the five azimuth variation experiments depicted in figure 7.38. Table 7.12 lists those quantities corresponding to the five range variation experiments depicted in figure 7.39. Inspection of these tabulated values show the consistency of range estimation error behaviour under multiple experimental configurations and environmental conditions. Figure 7.40.a and figure 7.42.a plots alternate range estimates corresponding to five

Error in alternate range ($\alpha_{\theta=0^\circ} = 170^\circ$) ($r = 2.0\text{m}$)	Error in alternate range ($\alpha_{\theta=0^\circ} = -155^\circ$) ($r = 2.1\text{m}$)	Error in alternate range ($\alpha_{\theta=0^\circ} = -140^\circ$) ($r = 2.9\text{m}$)	Error in alternate range ($\alpha_{\theta=0^\circ} = 160^\circ$) ($r = 6.0\text{m}$)	Error in alternate range ($\alpha_{\theta=0^\circ} = 120^\circ$) ($r = 8.0\text{m}$)
$\sigma_{\Delta r'} = 145.02 \times 10^{-3} \text{m}$	$\sigma_{\Delta r'} = 162.29 \times 10^{-3} \text{m}$	$\sigma_{\Delta r'} = 366.59 \times 10^{-3} \text{m}$	$\sigma_{\Delta r'} = 284.95 \times 10^{-3} \text{m}$	$\sigma_{\Delta r'} = 327.62 \times 10^{-3} \text{m}$
$\mu_{\Delta r'} = 20.98 \times 10^{-3} \text{m}$	$\mu_{\Delta r'} = 12.42 \times 10^{-3} \text{m}$	$\mu_{\Delta r'} = -50.43 \times 10^{-3} \text{m}$	$\mu_{\Delta r'} = -228.56 \times 10^{-3} \text{m}$	$\mu_{\Delta r'} = -17.45 \times 10^{-3} \text{m}$
$\overline{\Delta r'} = 101.63 \times 10^{-3} \text{m}$	$\overline{\Delta r'} = 90.86 \times 10^{-3} \text{m}$	$\overline{\Delta r'} = 250.11 \times 10^{-3} \text{m}$	$\overline{\Delta r'} = 224.83 \times 10^{-3} \text{m}$	$\overline{\Delta r'} = 260.72 \times 10^{-3} \text{m}$

Table 7.13: Comparison of standard deviations, means and average deviations related to different sets of RSE of alternate range estimates shown in figure 7.40.

azimuth variation experiments and five range variation experiments (same experiments used to analyse range estimate errors earlier) conducted under different conditions. The corresponding error model plots are reproduced from section 4.4.5 alongside these aggregate error plots for comparison. Unlike the direct counterpart, alternate range estimate error magnitudes vary with changing range, azimuth as well as heading according to the error model given by (4.50). Figure 7.41.a shows a rotated 3-dimensional projection of the plots depicted in figure 7.40.a. This view shows the conformity of the experimental data with the error model in plot b) where the error magnitude increases with increasing range and as the azimuth approaches $\pm 90^\circ$. The intermediate variations conform to the variations in error with changing heading as predicted by the error model in plot c). The errors associated with the range variation experiments depicted in figure 7.42.a shows a trend of increase up to 8.0m beyond which there is no clear trend. It appears that the numerical instability of the formulae used for deriving alternate range estimates under certain azimuth and heading combinations (when $|\theta + \alpha| \approx 90^\circ$ or $\varphi_1, \varphi_2 \rightarrow 0^\circ, 180^\circ$) contribute towards the loss of estimation accuracy as the range increases. Therefore, the errors associated with alternate range estimates are much higher than those associated with direct range estimates which were analysed earlier.

Tables 7.13 and 7.14 tabulate the standard deviations, means and average deviations of the two sets of experiments with regard to errors associated with alternate range estimates. While the error performance of these alternate range estimates conform to the theoretical error models, due to the high error magnitudes, this form of range estimates is useful only for short ranges where accurate direct range estimates are not available.

Heading estimation errors

Figure 7.43.a plots the errors associated with heading estimates for five experiments where the azimuth was varied as $\theta_0 : -90^\circ \rightarrow 0^\circ \rightarrow 90^\circ$. These experiments were conducted under

Error in alternate range ($\alpha_{\theta=0^\circ} = 150^\circ$) ($\theta = -30^\circ$)	Error in alternate range ($\alpha_{\theta=0^\circ} = -150^\circ$) ($\theta = 0^\circ$)	Error in alternate range ($\alpha_{\theta=0^\circ} = 150^\circ$) ($\theta = 0^\circ$)	Error in alternate range ($\alpha_{\theta=0^\circ} = 160^\circ$) ($\theta = 0^\circ$)	Error in alternate range ($\alpha_{\theta=0^\circ} = 120^\circ$) ($\theta = 0^\circ$)
$\sigma_{\Delta r'} = 636.24 \times 10^{-3} \text{ m}$	$\sigma_{\Delta r'} = 568.68 \times 10^{-3} \text{ m}$	$\sigma_{\Delta r'} = 756.38 \times 10^{-3} \text{ m}$	$\sigma_{\Delta r'} = 684.92 \times 10^{-3} \text{ m}$	$\sigma_{\Delta r'} = 568.42 \times 10^{-3} \text{ m}$
$\mu_{\Delta r'} = -97.23 \times 10^{-3} \text{ m}$	$\mu_{\Delta r'} = 218.35 \times 10^{-3} \text{ m}$	$\mu_{\Delta r'} = -89.74 \times 10^{-3} \text{ m}$	$\mu_{\Delta r'} = -166.43 \times 10^{-3} \text{ m}$	$\mu_{\Delta r'} = -735.37 \times 10^{-3} \text{ m}$
$\overline{\Delta r'} = 490.52 \times 10^{-3} \text{ m}$	$\overline{\Delta r'} = 470.54 \times 10^{-3} \text{ m}$	$\overline{\Delta r'} = 604.75 \times 10^{-3} \text{ m}$	$\overline{\Delta r'} = 563.28 \times 10^{-3} \text{ m}$	$\overline{\Delta r'} = 480.71 \times 10^{-3} \text{ m}$

Table 7.14: Comparison of standard deviations, means and average deviations related to different sets of RSE of alternate range estimates shown in figure 7.42.

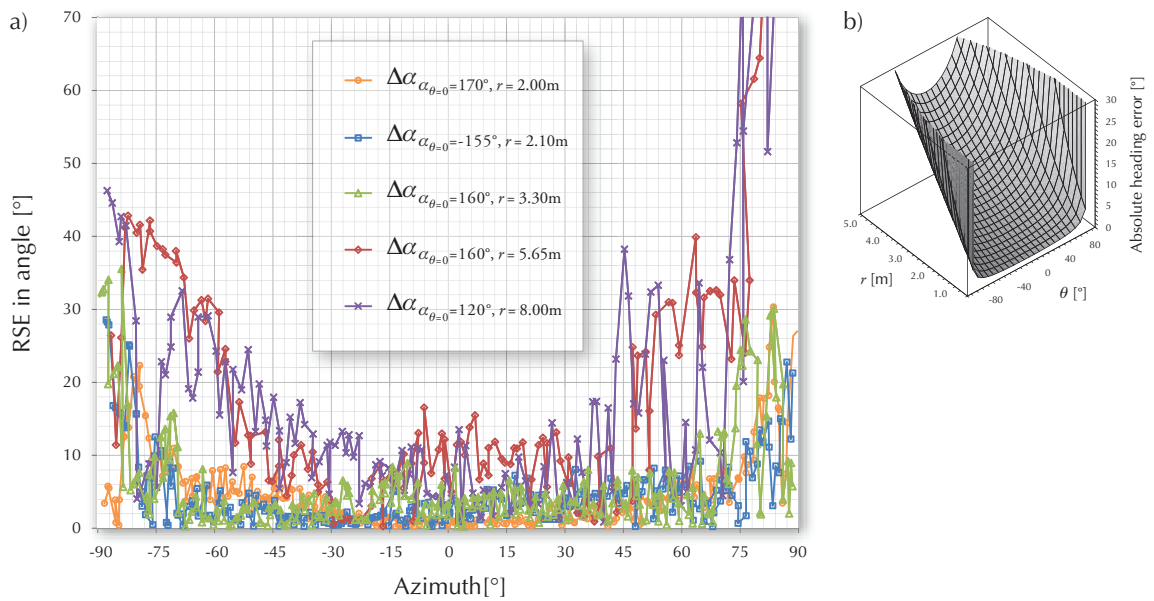


Figure 7.43: Heading estimate errors associated with five azimuth variation experiments with different initial heading and range configurations are plotted in a) and the corresponding error model is shown in b).

different initial headings and ranges both in the test tank as well as in the lake. Since heading is a secondary estimate calculated using sub-azimuths and sub-ranges, the performance of heading estimate errors depend on the error performance of azimuth and range estimates as well. This is affirmed by the theoretical error model given by (4.48). The error model plot showing the

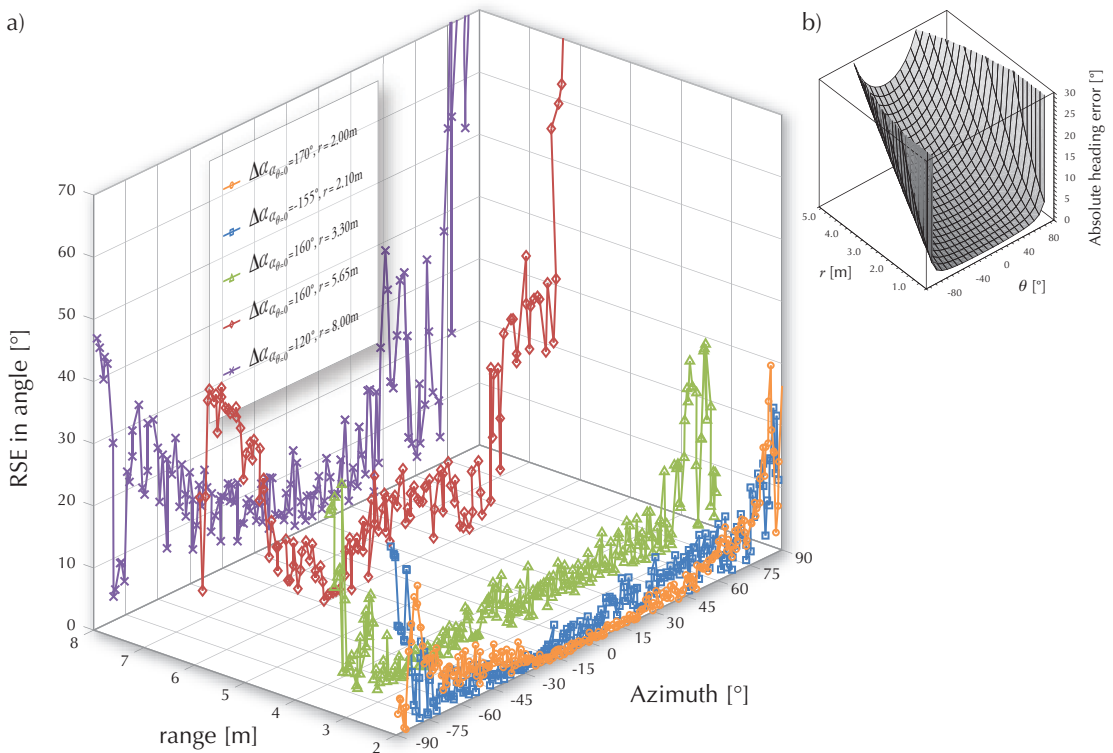


Figure 7.44: Plots shown in figure 7.43.a with a rotated 3-dimensional projection.

variation of heading error as range and azimuth varies is reproduced from section 4.4.5 and shown in figure 7.43.b. The rotated 3-dimensional projection of the plots in figure 7.43.a is given in figure 7.44.a showing the conformity of the shape of error evolution with that depicted by the error model in plot b). As predicted by the model, the estimate errors associated with the presented experiments increase in magnitude with increasing range as well as when the azimuth approaches $\pm 90^\circ$. However, the magnitude of these experimental estimation errors are mostly less than those depicted on the error model plot. Table 7.15 lists the means, standard deviations and average deviations of the errors for the five experiments depicted in figure 7.43. The actual heading estimates which these error plots relate to are given in appendix A.

Figure 7.45.a plots alternate heading estimate errors associated with five azimuth variation experiments discussed above. The error model given by (4.49) suggests that unlike the direct counterpart, the alternate heading estimate errors are invariant with range. The error model plot showing the error variation with varying azimuth and range is reproduced from section 4.4.5 in Figure 7.45.b. Comparisons of the plots show that the estimation errors of alternate heading conforms to the theoretical model. The error magnitudes remain invariant with increasing range while increasing only when the azimuth approaches $\pm 90^\circ$. Table 7.16 lists the means, standard deviations and average deviations of the errors for the five experiments depicted in figure 7.45. Inspecting these tabulated values show that the error performance of the alternate heading estimates remain consistent under different experimental configurations and operational environments. The actual alternate heading estimates which the error plots in figure 7.45 relate to are given in appendix A.

7.6.2 System performance

The performance of the relative localisation system is analysed in terms of accuracy, precision, sensing limits and how the system recovers from degradation of position estimation accuracy. The following sections will use experimental data obtained from multiple short, medium and long range experiments presented in this chapter to evaluate these performance characteristics.

Error in heading ($\alpha_{\theta=0^\circ} = 170^\circ$) ($r = 2.0\text{m}$)	Error in heading ($\alpha_{\theta=0^\circ} = -155^\circ$) ($r = 2.1\text{m}$)	Error in heading ($\alpha_{\theta=0^\circ} = 160^\circ$) ($r = 3.3\text{m}$)	Error in heading ($\alpha_{\theta=0^\circ} = 160^\circ$) ($r = 6.0\text{m}$)	Error in heading ($\alpha_{\theta=0^\circ} = 120^\circ$) ($r = 8.0\text{m}$)
$\sigma_{\Delta\alpha} = 7.21^\circ$	$\sigma_{\Delta\alpha} = 7.27^\circ$	$\sigma_{\Delta\alpha} = 8.91^\circ$	$\sigma_{\Delta\alpha} = 27.31^\circ$	$\sigma_{\Delta\alpha} = 26.23^\circ$
$\mu_{\Delta\alpha} = 0.74^\circ$	$\mu_{\Delta\alpha} = 0.51^\circ$	$\mu_{\Delta\alpha} = -0.42^\circ$	$\mu_{\Delta\alpha} = -0.63^\circ$	$\mu_{\Delta\alpha} = 0.45^\circ$
$\overline{\Delta\alpha} = 4.82^\circ$	$\overline{\Delta\alpha} = 4.58^\circ$	$\overline{\Delta\alpha} = 5.57^\circ$	$\overline{\Delta\alpha} = 19.11^\circ$	$\overline{\Delta\alpha} = 17.63^\circ$

Table 7.15: Comparison of standard deviations, means and average deviations related to different sets of RSE of heading estimates shown in figure 7.43.

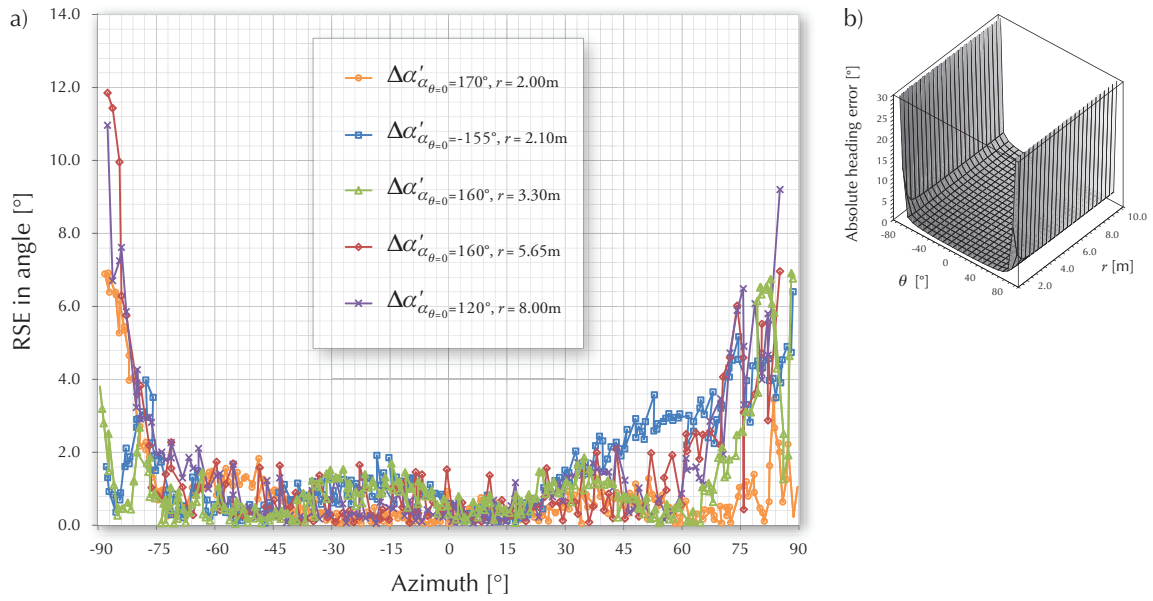


Figure 7.45: Alternate heading estimate errors associated with five azimuth variation experiments with different initial heading and range configurations are plotted in a) and the corresponding error model is shown in b).

Accuracy and precision of estimates

The accuracy and precision of the estimates produced by the relative localisation system can be inferred by observing the results and associated errors. The mean and average deviation of error can be considered as performance parameters for each of the different pose vector components.

For all experiments presented, in the test tank as well as in the lake, including the variations shown in figure 7.37, the mean error for azimuth remained less than 1.0° and the average deviations were under 2.0° . Estimation errors near the limits of $\pm 90^\circ$ remained well below 12.0° .

As mentioned in section 4.3.2, the resolving power of the estimation system improved with sub-sample interpolation of the cross-correlation peak. With the number of sub-sample segments

Error in alternate heading ($\alpha_{\theta=0^\circ} = 170^\circ$) ($r = 2.0\text{m}$)	Error in alternate heading ($\alpha_{\theta=0^\circ} = -155^\circ$) ($r = 2.1\text{m}$)	Error in alternate heading ($\alpha_{\theta=0^\circ} = 160^\circ$) ($r = 3.3\text{m}$)	Error in alternate heading ($\alpha_{\theta=0^\circ} = 160^\circ$) ($r = 6.0\text{m}$)	Error in alternate heading ($\alpha_{\theta=0^\circ} = 120^\circ$) ($r = 8.0\text{m}$)
$\sigma_{\Delta\alpha} = 1.50^\circ$	$\sigma_{\Delta\alpha} = 1.87^\circ$	$\sigma_{\Delta\alpha} = 1.65^\circ$	$\sigma_{\Delta\alpha} = 2.50^\circ$	$\sigma_{\Delta\alpha} = 2.44^\circ$
$\mu_{\Delta\alpha} = -0.33^\circ$	$\mu_{\Delta\alpha} = 0.91^\circ$	$\mu_{\Delta\alpha} = -0.29^\circ$	$\mu_{\Delta\alpha} = -0.06^\circ$	$\mu_{\Delta\alpha} = -0.26^\circ$
$\overline{\Delta\alpha} = 0.90^\circ$	$\overline{\Delta\alpha} = 1.61^\circ$	$\overline{\Delta\alpha} = 1.10^\circ$	$\overline{\Delta\alpha} = 1.42^\circ$	$\overline{\Delta\alpha} = 1.43^\circ$

Table 7.16: Comparison of standard deviations, means and average deviations related to different sets of RSE of alternate heading estimates shown in figure 7.45.

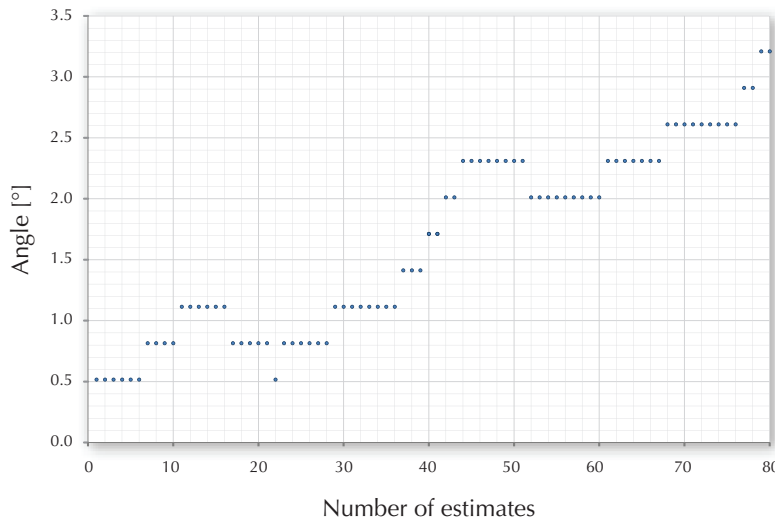


Figure 7.46: Estimates for sub-azimuth θ_1 plotted against the number of estimates.

$n_{int} = 10$, figure 7.46 shows a plot of sub-azimuth θ_1 as the observer was rotated with a low angular speed of $0.15^\circ \text{ s}^{-1}$ causing the azimuth to vary in the vicinity of 0° . As the plot shows, the minimum resolvable angle is near the theoretically predicted value of 0.29° mentioned in section 4.3.2. causing a visible quantization effect.

For direct estimation of range, the absolute mean error remained below $1.5 \times 10^{-2} \text{ m}$ while the average deviation was at most $2.0 \times 10^{-2} \text{ m}$ during the presented short (test tank) and medium range (lake) experiments including the variations represented in figures 7.38 and 7.39. The plot in figure 7.47 shows the variation of direct sub-range r_1 as the observer gantry was linearly

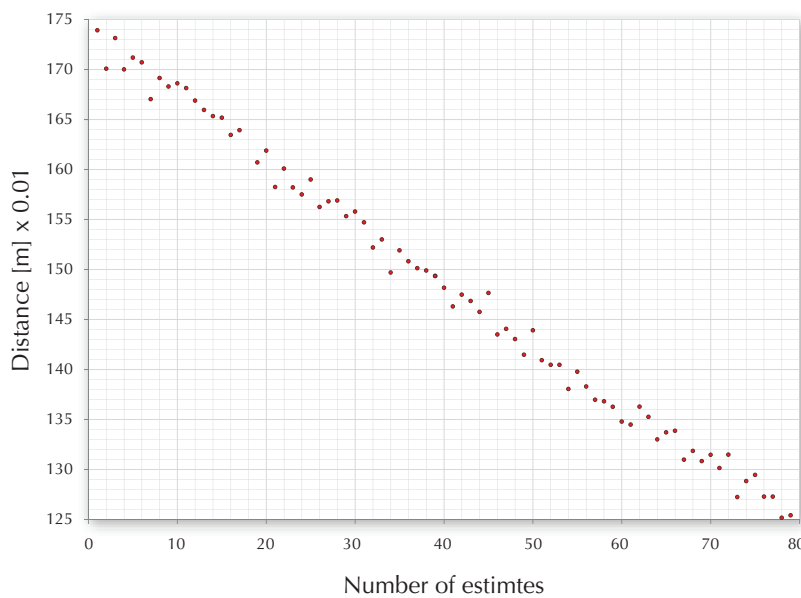


Figure 7.47: Estimates for sub-range r_1 plotted against the number of estimates.

translated at a speed of 0.03ms^{-1} along the gantry rail. Though not clearly noticeable as with the azimuth estimates earlier, the minimum resolvable distance of around $3.2 \times 10^{-3}\text{m}$ as predicted in section 4.3.2 can be observed. When considering the long range experiments, as mentioned in section 7.5, the errors do not warrant direct comparison with the short and medium range experiments due to the difference in precision of ground truth references. However, a maximum percentage error defined as $(\max(\text{Average deviation of RSE})/\max(\text{Range})) \times 100$ can be calculated for a series of range estimation experiments. This value is 0.2% for short and medium range experiments (up to 10m of separation between sender and observer) and 0.55% for long range experiments (up to 90m of separation between sender and observer).

The accuracy and precision for alternate range estimates were substantially lower compared to the direct range estimates as observed from error behaviour analysis in the previous section, especially as the range increases. For short range experiments, the absolute mean deviation of alternate range estimates was below $2.0 \times 10^{-2}\text{m}$ and maximum average deviation remained below $10.0 \times 10^{-2}\text{m}$. This gives a relatively high maximum percentage error of 3.03% for alternate range estimates during short range experiments of up to 3.3m of separation between sender and observer.

During all the presented experiments, including the variations shown in figure 7.43, the mean error for heading estimates remained less than 1.0° and the average deviation is under 20.0° . Comparatively, the alternate heading estimates (including the variations represented by figure 7.45) were considerably more precise with a maximum average deviation remaining below 4.0° . Estimation errors for alternate heading remain below 12.0° in all instances of short and medium range experiments.

Angular and radial sensing limits

The angular sensing range (of azimuth estimation) is limited by the directivity of the hydrophones. While the experiments presented covered the full range of $-90^\circ \rightarrow 90^\circ$ the estimation errors which remained relatively stable below $\pm 3.0^\circ$ within $-75^\circ \rightarrow 75^\circ$ tend to increase beyond that range as seen from the plot comparison in figure 7.37. As a measure to validate these angular sensing limits, a ‘position error’ quantity associated with a position (r, θ) where r and θ are the estimated relative range and azimuth can be defined as:

$$\Delta p = \sqrt{|r^2 + r_0^2 - 2rr_0 \cos(\theta - \theta_0)|} \quad (7.1)$$

where r_0 and θ_0 are the range and azimuth ground truth references associated with the estimated quantities. Position estimates produced by four azimuth variation experiments conducted at different ranges¹ are plotted on the polar plot in figure 7.48 with circles centred at (r, θ) . The radii of the circles and the colour represents the magnitude of the position error associated with

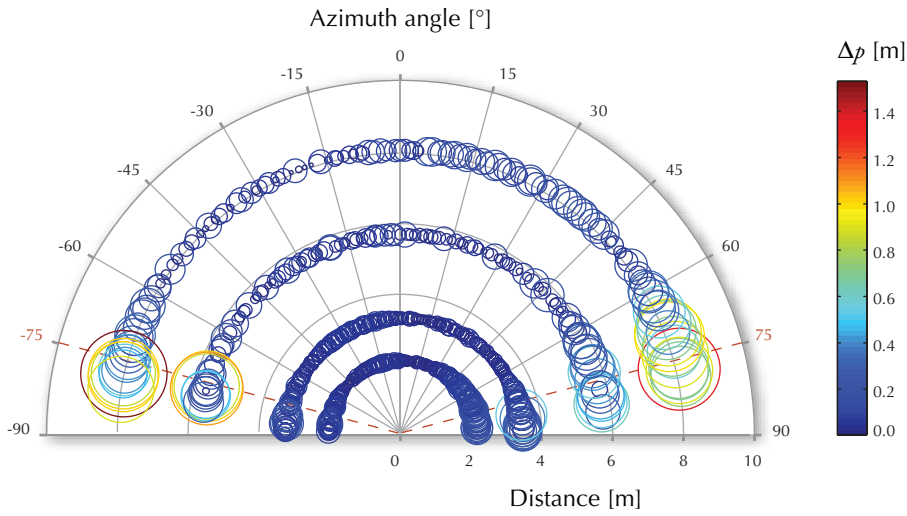


Figure 7.48: Position estimates produced by four azimuth variation experiments plotted with circles of radius Δp centred at (r, θ) . The colour represents the magnitude of position error Δp along with the radii.

each position. According to these plots the position error remains below 0.5 m within $-75^\circ \rightarrow 75^\circ$ which can be considered as the angular sensing limits of the relative localisation system being evaluated, where accurate and precise position estimates are produced.

Despite the azimuth and range estimation error behaviour discussed earlier in section 7.6.1 (supported by the formulae given in section 4.4.5 suggesting invariance with increasing range), the effectiveness of the estimation system deteriorates as the SNR drops. Therefore, as another measure to establish sensing limits of the system, SNR is calculated for each estimation step as

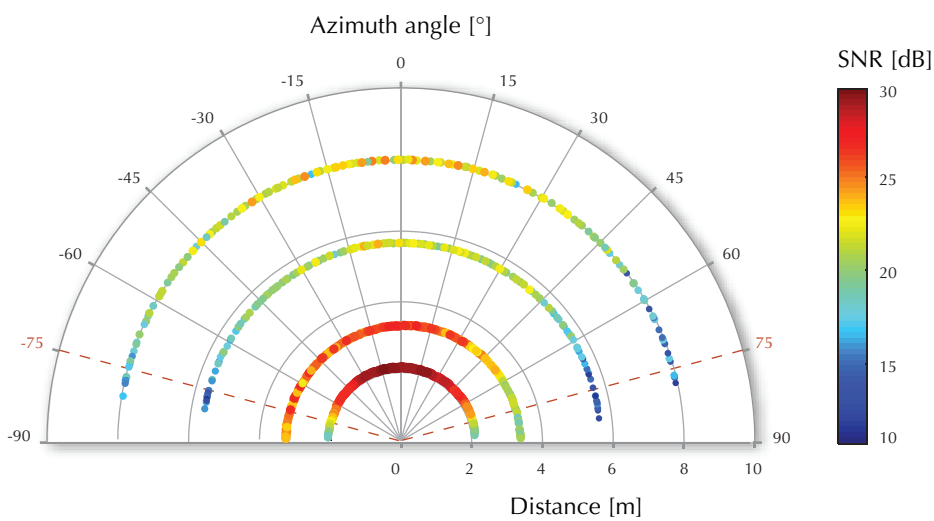


Figure 7.49: Position estimates produced by four azimuth variation experiments plotted with the colour representing the SNR of the received hydrophone channels.

¹: Distance between sender and observer at 2.00 m, 3.30 m, 5.65 m and 8.00 m

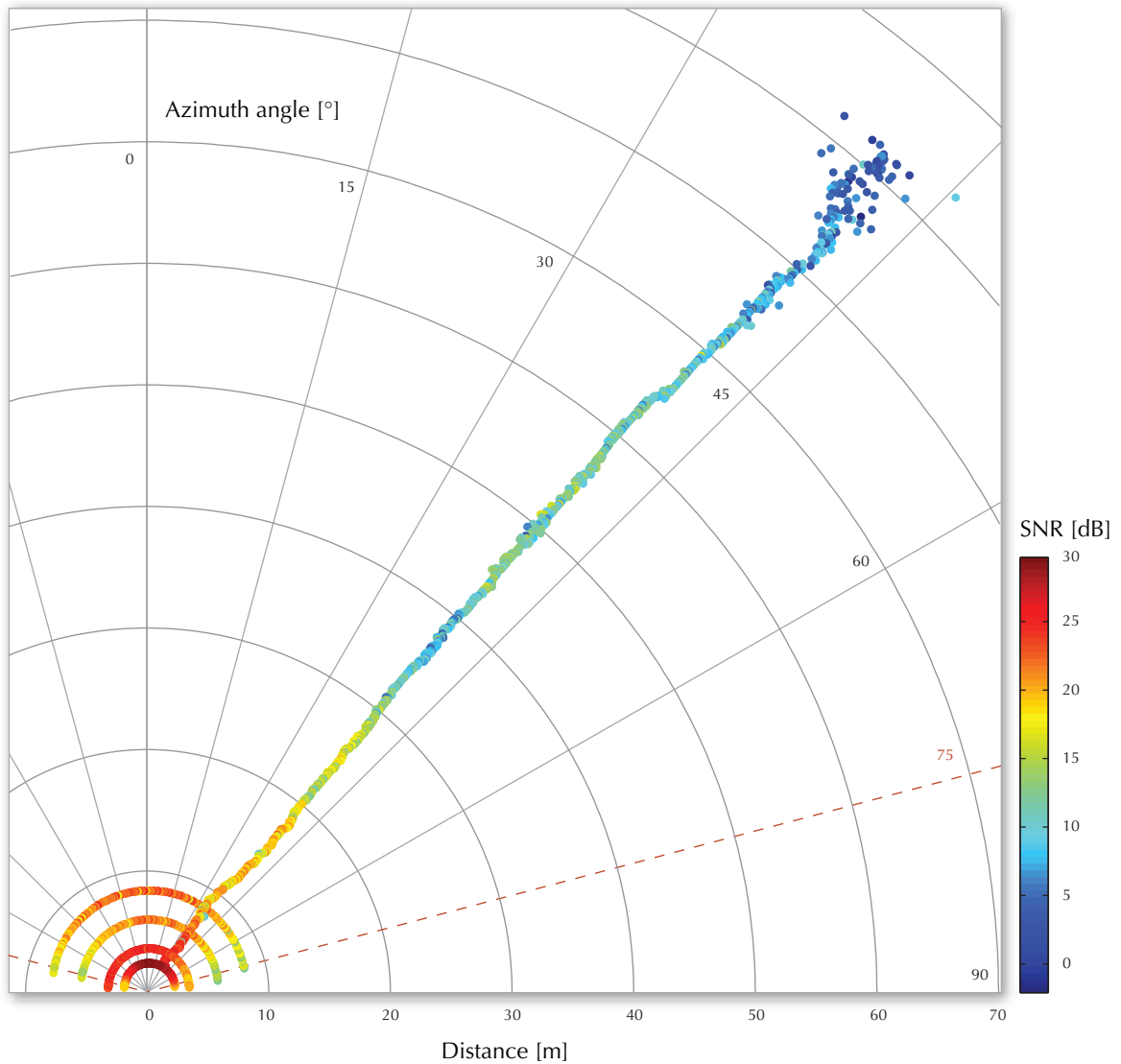


Figure 7.50: Position estimates produced by a long range experiment and four azimuth variation experiments plotted with the colour representing the SNR of the received hydrophone channels.

elaborated in section 6.6. Figure 7.49 plots the estimated positions produced by the same four azimuth variation experiments plotted earlier in figure 7.48 with the colour representing the calculated SNR at each estimation step. The SNR remains above 10dB within the angular range $-75^\circ \rightarrow 75^\circ$ reaffirming the earlier stated angular sensing limits for the system.

The primary purpose of the long range experiments were to gauge the maximum radial sensing range of the relative localisation system with regard to loss of SNR and deterioration of estimation accuracy. Figure 7.50 adds position estimates produced by a long range experiment to the previous plots depicted in figure 7.49. As seen by the plot, the SNR of received channels drop below 10dB beyond a range of 75m. Scattering of the estimated positions beyond a range of 80m suggests an increase in position error, hence a deterioration of position estimation accuracy.

Therefore, the radial sensing limit of the evaluated experimental implementation of the relative localisation system can be stated as 75 m, within which sufficiently accurate and precise position estimates are produced.

In order to establish an empirical relationship between the SNR and ensuing position error, these quantities were plotted against each other for six different short and medium range experiments in figure 7.51. However, it is difficult to establish an exact SNR threshold beyond which estimates are deemed inaccurate. This is partly due to the inexact measurements of SNR as described in section 6.6., and the influence of the peak tracking scheme. Additionally, the sensing limits also depends on the hardware used by the system and the transmission power utilised. As an example, the plot in figure 7.52 plots the variation of the average deviation of the azimuth error (with and without peak tracking enabled) when the bit resolution of the analogue to digital converter was varied between 8 to 24 bits with increments of 4 bits. This also depicts the variation of the theoretical SNR calculated¹ based on the bit resolution of the analogue to digital converter which serves as an absolute upper bound to the actual SNR. The 24 bit converter used during the experiments was specified to have a maximum SNR of 108 dB (Roland, 2004). However, this value is far less than the ‘real’ SNR as it does not account for signal propagation through the underwater medium, where it is affected by environmental noise and attenuation due to scattering and fading effects inherent to this channel.

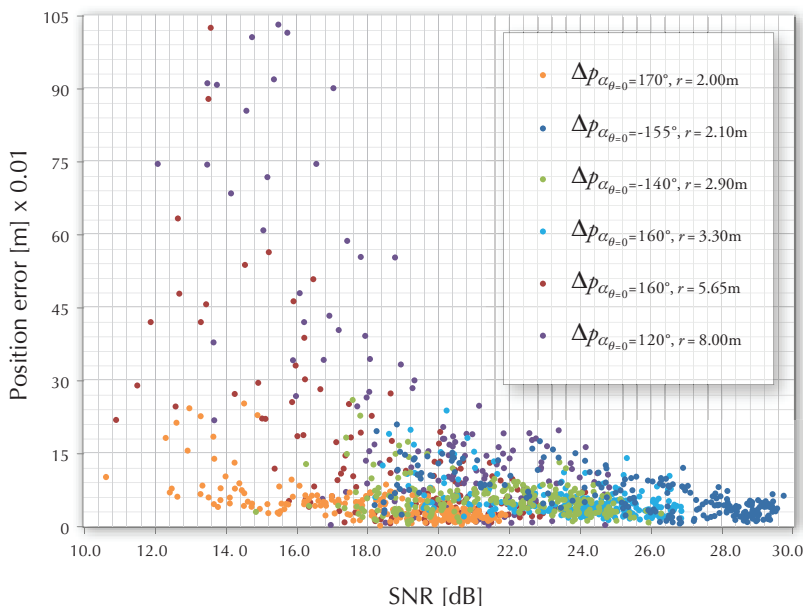


Figure 7.51: Empirical relationship between position error and SNR for six short and medium range experiments with different configurations.

¹. $SNR(dB) \approx 20 \log_{10}(2^n \sqrt{2/3})$ where n is the number of bits.

System recovery

Azimuth and range estimates obtained during the full 15 minute duration of a long range experiment is plotted along with measured SNR in figure 7.53. The SNR continues to drop with increasing range and drops below 0 dB as the range estimates reach 125 m. For the same experiment, it was earlier shown that position errors start to increase as SNR drops below 10 dB which corresponds to a range of approximately 75 m.

Even as the SNR drops below 0 dB intermittently up to about 1300 estimates, the azimuth estimates remain relatively stable due to peak tracking. However, as the SNR further deteriorates beyond 1300 estimates, the azimuth estimation gradually approaches 0° as the cross-correlograms used for TDOA estimation returns a peak corresponding to the weakly correlated ambient noise instead of the weak signal (as explained in section 4.3 under ‘Errors due to low SNR’). The gradual approach instead of an abrupt change is due to peak tracking which attempts to maintain a trend in peak positions based on the current and previous estimates. The range estimate errors are bounded by a combination of peak tracking and range tracking ($N_{RT} = 768$ corresponding to a spatial window length of 10 m). The range estimation is unaffected by correlated ambient noise and will return random errors within the bounds defined by the channel window size when the signal is no longer producing a discernible peak in the cross-correlogram output by matched filter processing. Additionally, unlike the azimuth estimation, the range estimation responds

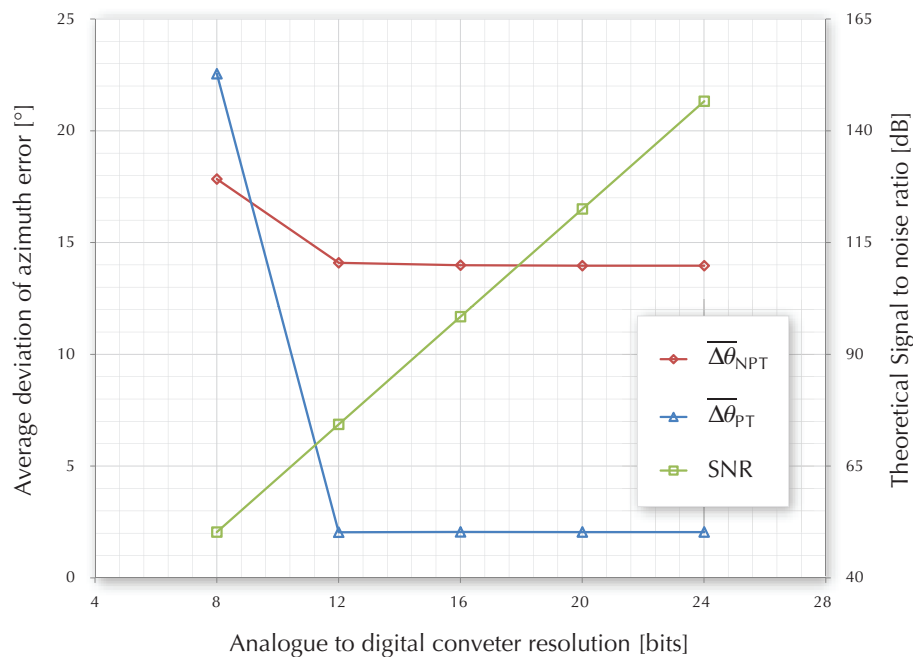


Figure 7.52: The variation of average deviation for azimuth error is plotted as the bit resolution of the analogue to digital converter is varied. $\overline{\Delta\theta_{PT}}$ and $\overline{\Delta\theta_{NPT}}$ denotes average deviations for azimuth error with and without peak tracking enabled. The variation of the theoretical upper bound for SNR is also plotted against the bit resolution of the converter.

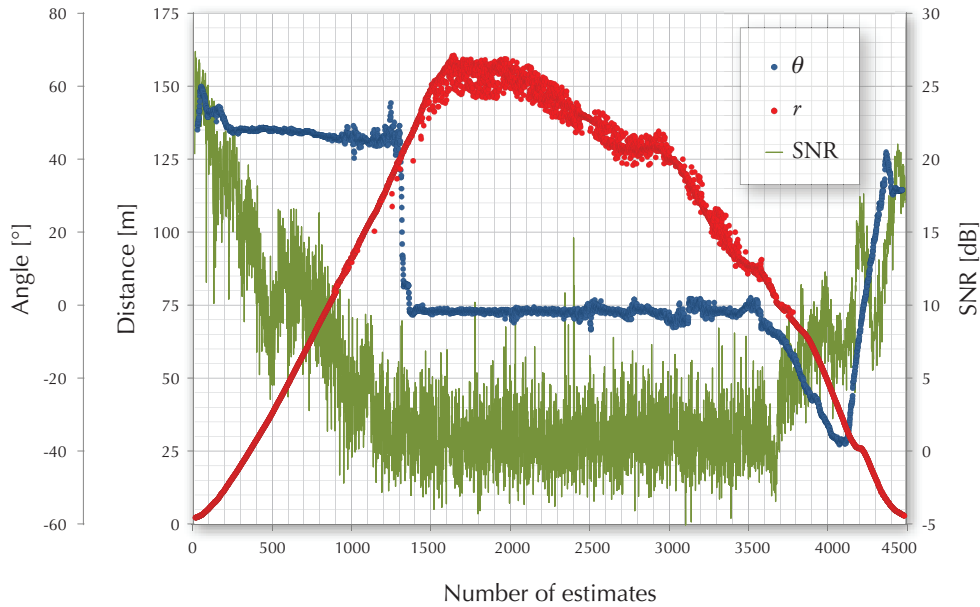


Figure 7.53: Azimuth and range estimates obtained during the full duration of the long range experiment plotted with the corresponding SNR of received hydrophone channels at each estimation step.

quickly when SNR improves even for a few estimates as seen by the plot - especially near 2500 estimates. When the range decreased (kayak/sender approaching the pier/observer) causing the SNR to increase beyond 0dB, both the azimuth and range estimates regain accuracy and continues to track the path of the sender. This ‘self recovery’ by the peak tracking scheme, facilitated by appropriate selection of the tolerance parameter is explained in section 5.4.1 under ‘Attributes and limitations of peak tracking’. The track of the kayak/sender relative to the observer consisting of positions estimated at a rate of 5.0Hz during this long range experiment is plotted in figure 7.54 against a background image showing the actual location of the experiment at Lake Burley Griffin. The gradual ‘wandering’ of the estimated track due to the azimuth estimate approaching 0° can be seen in this plot. Only a segment of the GPS track¹ up to a range of 95m was used as the ground truth.

7.7 Discussion

This chapter presented results of a number of experiments used to experimentally evaluate the performance of the relative localisation system being presented in this thesis. Detailed results of quantities estimated by the system along with associated errors were presented for short, medium and long range experiments. Furthermore, the effects of techniques such as inverse frequency

¹: GPS positions received beyond 300s of initiating the experiment were affected by large drifts (Wing et al., 2005). Therefore, the ‘ground truth’ reference beyond that was deemed unreliable.

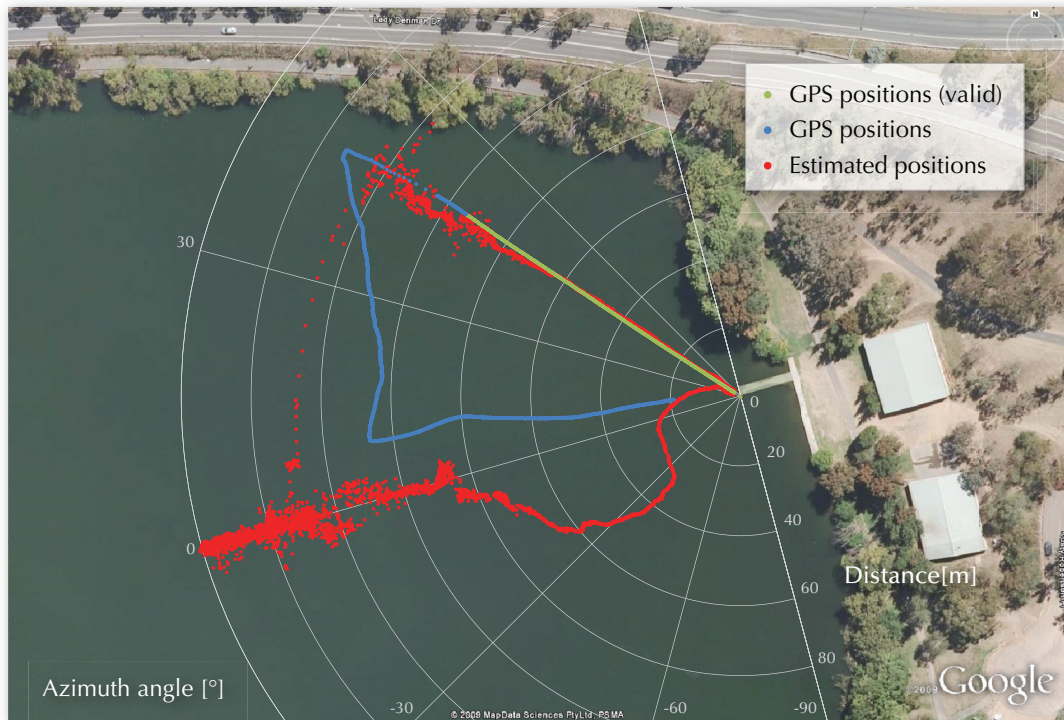


Figure 7.54: Estimated sender positions obtained during a long range experiment plotted with the GPS ‘ground truth’ track. The ‘valid’ segment of the GPS track used for ground truth based error calculations is shown in green. GPS coordinates of the pole (position of the observer) of the coordinate system is $35^{\circ}17'10''$ S, $149^{\circ}05'58''$ E. The polar axis has a 13° counter-clockwise rotation from true North.

[BACKGROUND IMAGE COURTESY GOOGLE, © 2009 MAPDATA SCIENCE PTY LTD.]

filtering (introduced in section 3.3.3) and peak tracking (introduced in section 5.4.1) on the experimental data and their contribution towards improving estimation accuracy and precision was discussed at the beginning of the chapter.

The analysis of estimation errors in section 7.6.1 attempted to establish how the accuracy and precision of the localisation estimates behave under different conditions, *i.e.* different experimental configurations and different operating environments. Errors of the estimated quantities such as the azimuth, range and alternate heading which are integral in fixing position and orientation were shown to be invariant with increasing range (up to sensing limits) and within bounds defined by the theoretical error models with the use of aggregate error plots derived from multiple experiments. Additionally, these errors were shown to be sufficiently low (average deviations for azimuth error and alternate heading error being less than 2.0° and 4.0° respectively and range error less than 0.55%) within the sensing range of the localisation system as discussed in section 7.6.2. The sensing range was established empirically using position error and SNR as measures with regard to angular and radial limits ($-75^{\circ} \rightarrow 75^{\circ}$ and up to 75 m) within which the evaluated experimental implementation of the relative localisation system provide accurate

and precise estimates. Finally, a long range experiment was used to demonstrate how the relative localisation system behaves at the limits of the sensing range with the contribution of the peak tracking and range tracking schemes and how the estimation system recovers from performance degradation.

The results, errors and performance measures evaluated in this chapter will be used later in chapter 9 in discussing the overall suitability of the approach developed throughout this thesis to solve the task of relative localisation for small AUVs.

Chapter 8

Towards 3D source localisation

The localisation system discussed throughout this thesis focuses on 2-dimensional or planar localisation, where the localised position is expressed in polar coordinates¹ with an angle (azimuth) and a distance (range). As mentioned in section 4.1.1, the source to be localised (neighbouring AUV in a swarm) is assumed to be on the same plane containing the two receivers (hydrophones) and their main axes of directivity. The azimuth angle was defined on this aforementioned plane, which will be referred to as the **hydrophone plane** in the subsequent sections. When the source leaves the hydrophone plane, the range estimation r remains valid but the estimated angle θ is no longer contained within the plane for which the azimuth was defined. Instead, the estimated angle is on a plane containing the two hydrophones and the source position, which will be referred to as the **source plane**. The true azimuth is the projection of the estimated angle on to the hydrophone plane. By denoting this true azimuth as ϕ and defining the inclination of the source plane with respect to the hydrophone plane as the true elevation denoted by γ , the source position in 3-dimensional space can be expressed in spherical polar coordinates as (r, ϕ, γ) . Additional information about the source position needs to be

¹. A slightly modified version of polar coordinates are used with the azimuth angle measured positive clockwise and negative counter-clockwise as explained in section 4.4.1.

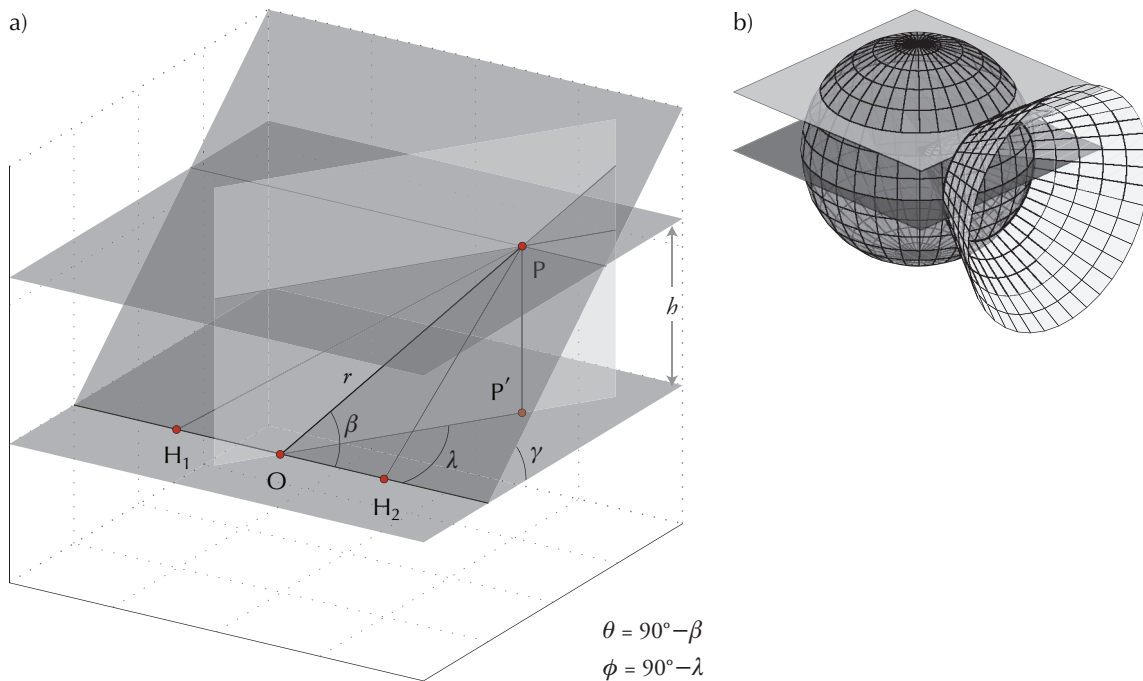


Figure 8.1: Incorporating the relative depth h to localise the source P in 3-dimensions with two hydrophones at H₁ and H₂. a) Geometrical and spatial relationship between the source plane and the hydrophone plane. b) The underlying spatial structure.

incorporated with the estimated r and θ quantities to produce the true azimuth and elevation angles. The following sections propose several strategies to obtain the required information.

8.1 Incorporating relative depth information

Most modern submersibles, including the Serafina class AUVs are outfitted with pressure sensors which in turn provides an accurate depth measurement. Bahr and Leonard (2008) describes a cooperative localisation system where the depth of the submersible to be localised¹ and the depth of the observing vehicle is used to calculate the relative depth between them, thereby reducing the relative localisation problem to 2-dimensions. Bellingham et al. (1992) presents a similar approach to self-localisation of multiple AUVs in 3-dimensions with respect to multiple acoustic beacons at known locations. In work presented by Vaganay et al. (2000), the depth of an acoustic beacon is assumed to be known by the AUV, converting the 3-dimensional homing problem into a 2-dimensional one. Extending this work, Baccou et al. (2001) presents a leader-follower scheme for AUVs where the depth of the leader vehicle is assumed to be known (communicated via an acoustic communication link) by the followers, thus converting the localisation problem into 2-dimensions. Cheng et al. (2008) suggests a similar approach using depth information

¹ Received by the observer via the acoustic communication system using WHOI acoustic modem (Freitag et al., 2005)

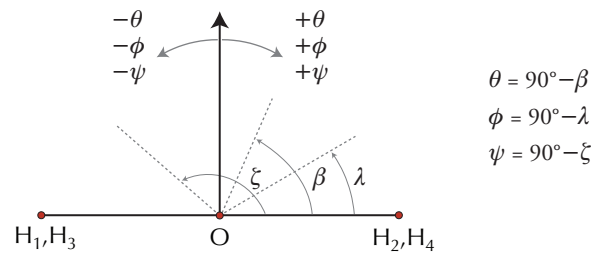


Figure 8.2: Measuring convention used for angular estimations. The angles β , ζ and λ are measured positive counter-clockwise while θ , ψ and ϕ are zero-centred with a 90° offset and measured negative counter-clockwise and positive-clockwise.

with regard to 3-dimensional localisation in underwater acoustic sensor networks (UWASN) while Bahr and Leonard (2008) uses relative depth information conveyed via acoustic communication links to reduce the problem of cooperative localisation for AUVs in to 2-dimensions.

Figure 8.1 shows the geometrical and spatial relationship between the planes when the source P lies outside the hydrophone plane. In the usual notation, H_1 and H_2 are the hydrophone positions. Without loss of generality, for clarity of the diagram, P is representative of projector positions P_1 and P_2 used in the relative localisation system¹. The source plane contains H_1 , H_2 and P while the hydrophone plane contains H_1 , H_2 and P' . The plane containing the pole O (the midpoint between H_1 and H_2), P and P' is orthogonal to the hydrophone plane. Another plane, denoted as the **depth plane**, contains P and is parallel to the hydrophone plane with a separation of h - the relative depth between the sender and the observer.

As derived in chapter 4, in the 2-dimensional case, the estimated range restricts the position of the signal source to a circle and the estimated azimuth placed the signal source on a branch of an asymptote of a hyperbola. In the 3-dimensional case, the line and circle creates a cone with its apex at O and a sphere centred at O respectively. The solid angle of the apex of the cone is $(180^\circ - 2\theta)$ and the radius of the sphere is r . This spatial structure is depicted in figure 8.2b. The source position P is no longer a point but a circle which is created by the intersection of the hollow sphere and cone². The depth plane which is defined by the relative depth h intersects this circle at (maximally) two points. These points lie either side of a plane (**symmetry plane**) orthogonal to the hydrophone plane, intersecting it along the line containing H_1 and H_2 . As with the 2-dimensional case mentioned in section 4.1.1, this *front-back ambiguity* can be resolved by the use of non-omnidirectional hydrophones as in the discussed relative localisation system which reduces the sensing volume to a semi-hemisphere instead of a complete sphere.

¹ Depending in the spatial orientation of the sending vehicle, P_1 and P_2 could either belong to a single source plane or define two unique source planes.

² Uncertainties associated with the quantities makes this a torus with a finite cross-sectional area instead of a circle.

The measuring conventions of the angular quantities are shown in figure 8.2 while the additional information given by the relative depth h can be incorporated with the estimated azimuth θ and the range r to produce the true elevation γ and the true azimuth ϕ as follows:

$$\gamma = \tan^{-1}\left(\frac{h}{\sqrt{r^2 \cos^2 \theta - h^2}}\right) \quad (8.1)$$

$$\phi = \tan^{-1}\left(\frac{r \sin \theta}{\sqrt{r^2 \cos^2 \theta - h^2}}\right) \quad (8.2)$$

According to the geometry depicted in figure 8.1, the relative depth is bounded as $-r \leq h \leq r$ with ranges of the true azimuth and elevation given by $-180^\circ < \gamma \leq 180^\circ$ and $-180^\circ < \phi \leq 180^\circ$. However, when the sensing volume is limited to a semi-hemisphere as mentioned earlier, these angular quantities are bounded by $-90^\circ, 90^\circ$. As expected, according to (8.1) and (8.2), when the relative depth $h \rightarrow 0$, the true elevation $\gamma \rightarrow 0$ and the true azimuth $\phi \rightarrow \theta$.

The 3-dimensional localisation strategy outlined above is based on the following assumptions:

- 1) The underlying communication system delivers the absolute depth of the sending vehicle at each sending event, which is combined with the absolute depth of the observing vehicle to estimate the relative depth.
- 2) Absolute depths of the observing and sending vehicles are measured with respect to a common reference plane (water surface).
- 3) The observing vehicle is oriented such that the hydrophone plane is parallel to the aforementioned common reference plane.
- 4) During a sending event, the sending vehicle is spatially oriented such that the line containing P_1 and P_2 does not intersect the hydrophone plane (*i.e.* either parallel or skew to a line on the hydrophone plane).

With regard to the Serafina class AUVs¹ and the swarm communication system that has been developed, the first assumption holds true. The second assumption is valid under most operating environments except in rough sea states. Validity of this assumption affects the accuracy of the relative depth estimation. The third and fourth assumptions are valid if the observing vehicle is roll neutral and the sending vehicle is pitch neutral during a sending event respectively. These rules can be incorporated in to the vehicle control system. However, the formulae to calculate the elevation and the true azimuth can be modified to cope with situations where the actual orientations of the vehicles, provided by the inertial measurement units are used as parameters.

¹. Serafina Mk I AUVs already have a pressure sensor included in its sensor suite while the Mk II AUVs will include same.

With the current form of (8.1) and (8.2), violation of the third and fourth assumptions will, in the worst case, result in a maximum error of ± 0.15 m and ± 0.25 m respectively in the estimation of the relative depth h according to the physical dimensions of a Serafina Mk II AUV upon which the relative localisation system is based on.

If omnidirectional hydrophones are used in order to extend the sensing volume to a sphere, a third hydrophone H_3 would need to be introduced to the system at a position not lying on the symmetry plane in order to resolve the *front-back ambiguity* mentioned earlier. A 3-dimensional localisation strategy involving additional hydrophones is described in the following section.

8.2 Using additional hydrophones

Another popular approach is to have multiple receiver pairs, forming an array, to extract additional information for localising a signal source lying outside of the hydrophone plane. Minimally two pairs - four hydrophones are needed to resolve the *up-down ambiguity* and the *front-back ambiguity* in a spherical sensing volume. Though three are sufficient for a semi-hemispherical sensing volume, additional measurements by a fourth sensor provides robustness to the position estimation when dealing with noisy measurements in real environments.

Giraudet and Glotin (2006) describes the use of a sparse array of five hydrophones to localise and track marine mammals with multiple TDOA measurements. Dudek et al. (2007) describes a square planar four hydrophone array used for localising the AQUA robot with multiple TDOA measurements in a semi-hemispherical sensing volume. Experiments with this system is described in detail by Liu and Milios (2005). The concepts used in 3-dimensional underwater localisation with multiple transponders in general, from traditional long baseline (LBL) navigation to more recent localisation in underwater acoustic sensor networks (UWASN) are broadly given in chapter 2.

The geometrical and spatial relationship between a source, the primary hydrophone plane (for hydrophones H_1 and H_2) and a secondary hydrophone plane (for additional hydrophones H_3 and H_4) is shown in figure 8.3. In this proposed hydrophone configuration, the secondary hydrophone plane is orthogonal to the primary hydrophone plane, intersecting each other along lines perpendicular to the baselines containing the hydrophone positions, while bisecting these baselines. The baseline for the primary hydrophone plane is H_1H_2 while for the secondary hydrophone plane it is H_3H_4 . The addition of the hydrophone pair also results in another source plane. As in the previous section, the primary source plane contains P , H_1 and H_2 while the secondary source plane contains P , H_3 and H_4 .

Figure 8.3.b shows the spatial structure related to this hydrophone configuration where two cones intersect a sphere. The sphere and the cone with its axis along the primary hydrophone plane are as described in the previous section. The sphere centred at O has a radius of r and the

apex of the cone at O has a solid angle of $(180^\circ - 2\theta)$ corresponding to the estimated range and azimuth by the relative localisation system. With the additional hydrophone pair H_3 and H_4 , the sample procedure described in section 4.1.1 to estimate β can be applied to estimate the angular quantity ζ and apply measuring conventions shown in figure 8.2 (as done in section 4.4.3 to derive azimuth θ from β) to estimate the elevation angle ψ . Therefore, the second cone with its axis perpendicular to the primary hydrophone plane has solid apex angle of $(180^\circ - 2\psi)$. This cone intersects with the sphere along a circle. The two circles created by the two cones intersecting the sphere lie on orthogonal planes and intersect each other at (maximally) two points, representing the position of the signal source P. The two positions lie either side of the symmetry plane containing H_1, H_2, H_3 and H_4 representing a front-back ambiguity when omnidirectional hydrophones are used. In the case of non-omnidirectional hydrophones such as those used in the experimental evaluation of the relative localisation system, the sensing volume is reduced to a semi-hemisphere where this ambiguity does not arise.

The azimuth θ estimated by the relative localisation system can be incorporated with the angular quantity ψ described above to derive the true elevation γ and the true azimuth ϕ as follows:

$$\gamma = \tan^{-1}\left(\frac{\sin\psi}{\sqrt{\cos^2\theta - \sin^2\psi}}\right) \quad (8.3)$$

$$\phi = \tan^{-1}\left(\frac{\sin\theta}{\sqrt{\cos^2\theta - \sin^2\psi}}\right) \quad (8.4)$$

These quantities can be used to construct the spherical coordinate (r, ϕ, γ) of the source position in 3-dimensions. Comparing the above formulae with (8.1) and (8.2) derived earlier, it can be noted that the quantities γ and ϕ does not depend on the range estimate r in this instance. Unlike in the previous strategy, additional assumptions about the spatial orientation of the sending and observing vehicles are not needed in this case. As expected, according to (8.3) and (8.4), when $\psi \rightarrow 0$, the true elevation $\gamma \rightarrow 0$ and the true azimuth $\phi \rightarrow \theta$.

If omnidirectional hydrophones are used in order to extend the sending volume to a sphere, the front-back ambiguity mentioned earlier can be resolved by placing the hydrophones H_3 and H_4 outside of the symmetry plane (which is orthogonal to the primary hydrophone plane) such that the lines H_1H_2 and H_3H_4 does not intersect. This ‘symmetry breaking’ will require modifications to the formulae used to calculate γ and ϕ . The exact modification will depend on the choice of positioning of H_3 and H_4 which does not necessarily have to be on a plane orthogonal to the primary hydrophone plane. The placement would be governed by the physical dimensions and the design of the AUV on which this system would be used.

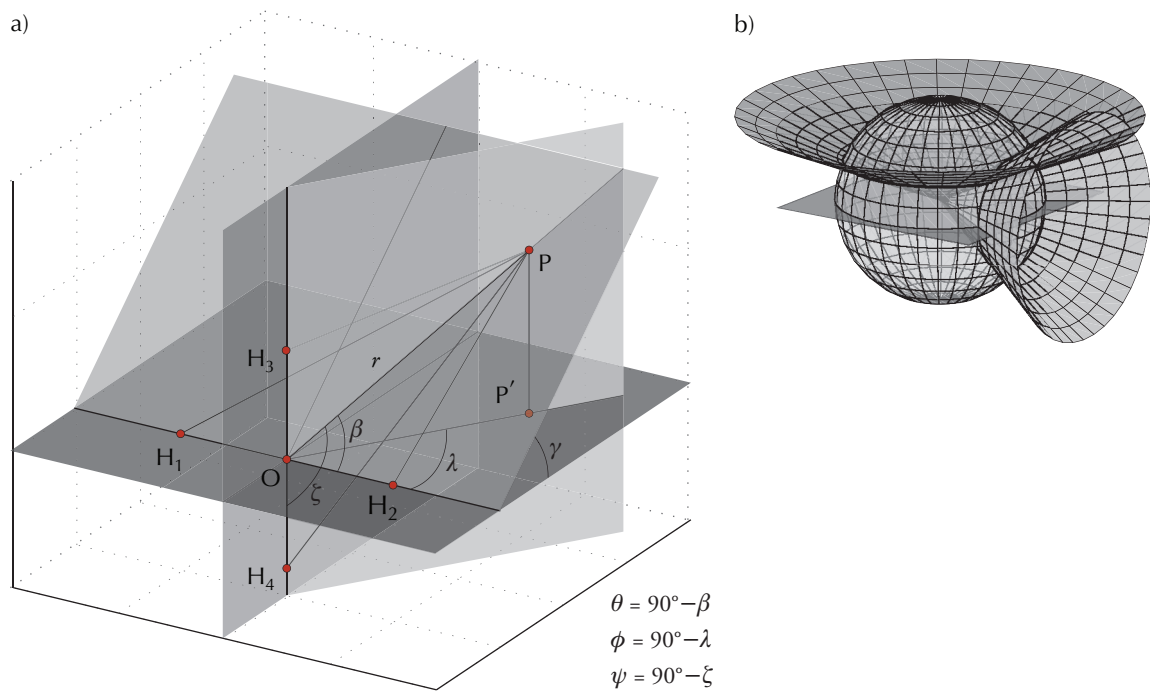


Figure 8.3: Addition of hydrophones at H_3 and H_4 to localise the source P in 3-dimensions. a) Geometrical and spatial relationship between the source plane and the two hydrophone planes. b) The underlying spatial structure.

8.2.1 Vehicle motion to emulate additional hydrophones

On a platform with only one pair of receivers, the manoeuvring capability of the platform itself can be exploited to emulate multiple receivers. Among the multiple possible configurations, two are proposed in this section which uses vehicle motion to estimate the 3-dimensional position of a sending submersible. These two strategies are meant to specifically exploit the manoeuvring capabilities of the Serafina class AUVs.

As described in section 4.4.2, the two hydrophones are to be placed on a baseline along the pitch axis (and across the roll axis) of the Serafina Mk II AUVs. With its thruster configuration and hull design, unlike torpedo style AUVs, the Serafina AUVs demonstrate very high roll rates (up to 360°s^{-1} for Serafina Mk I AUVs), it is possible to perform a 90° roll manoeuvre on several sending events in the schedule to receive the MLS pings with the hydrophone plane orthogonal to its usual orientation. Though it would not provide an instantaneous update as in the strategy discussed in the previous section, it would be able to simulate the same condition without actually adding more hydrophones. Using the time history of previous angular estimates for the particular sending vehicle, the same formulae given previously in (8.3) and (8.4) can be used to calculate the true azimuth and elevation and localise the sending vehicle in 3-dimensions. This method would however be less accurate due to the temporal separation between the two estimation instances where the sending vehicle can move.

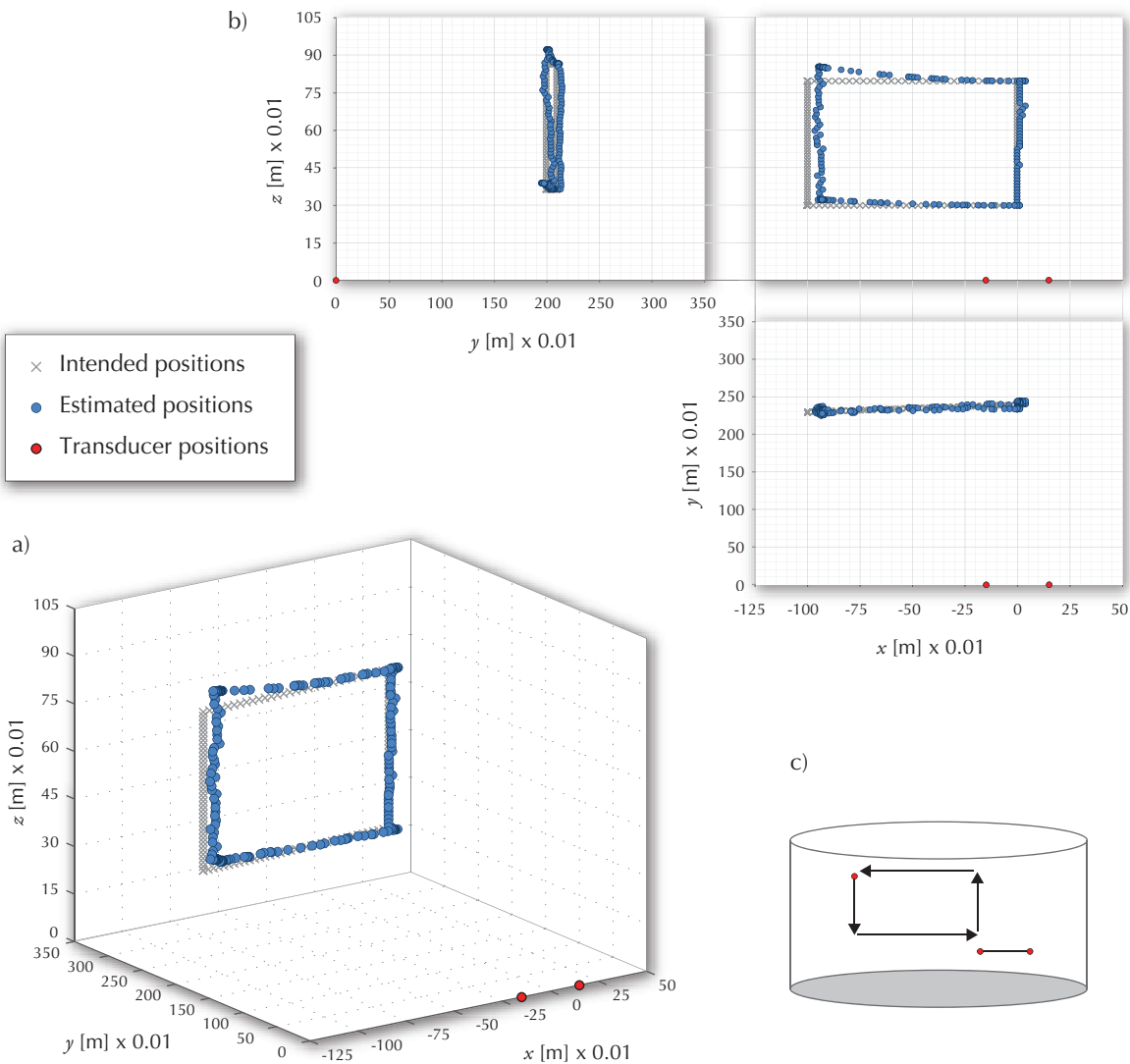


Figure 8.4: a) and b) shows experimental results of 3D source localisation by incorporating relative depth information while c) shows the approximate positions and motion of transducers during the experiment.

Another similar strategy would be for the AUV to make a heave (vertical) manoeuvre (maximum vertical speed is 0.5ms^{-1} for Serafina Mk I AUVs) on several sending events of the schedule to receive the MLS pings from a different parallel hydrophone plane. The vertical distance travelled (calculated using the pressure sensor readings) combined with range and azimuth estimates from the two planes can be used to localise the sending vehicle in 3-dimensions. This method too have the same problem as the previous one where the sending vehicle can move during the two estimation instances. Apart from the inaccuracies introduced by the motion of the sending vehicle, constant use of thrusters for these localisation manoeuvres would strain the already tight power budget of the AUV. These methods might be suited for situations where a relative depth information of the sender nor additional hydrophones are available to enable the strategies described

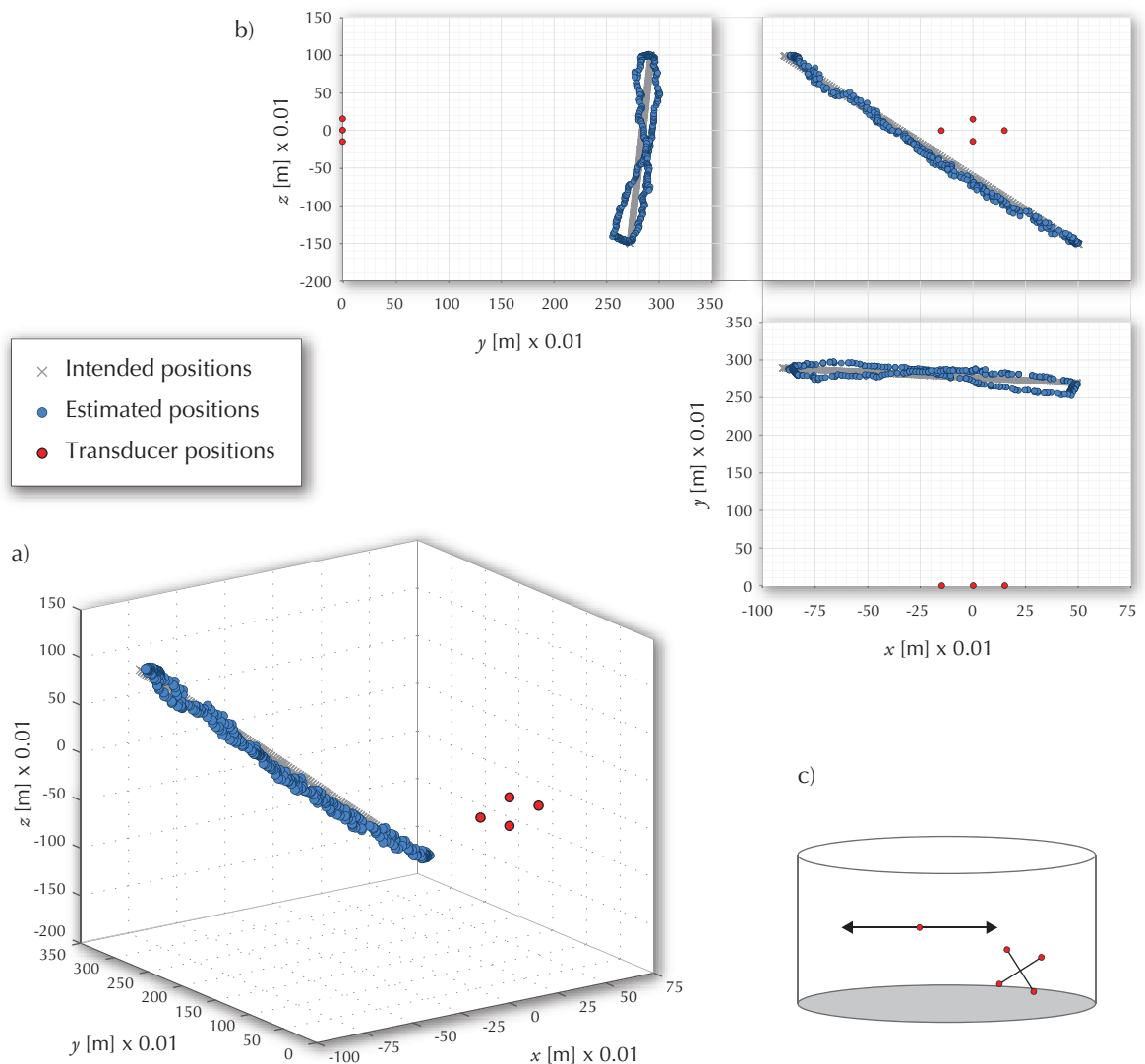


Figure 8.5: a) and b) shows experimental results of 3D source localisation by using additional hydrophones while c) shows the approximate positions and motion of transducers during the experiment.

in sections 8.1 and 8.2 given that the relative motion between the swarm members are slow and an infrequent update of the elevation angle of the localised submersibles is sufficient for overall swarm behaviour.

8.3 Source localisation experiments in 3D

The strategies discussed in the previous sections were experimentally tested using the relative localisation system which is being presented and evaluated in this thesis. This was done to ascertain the feasibility of extending the 2-dimensional localisation capability in to 3-dimensions when the signal source lie outside the hydrophone plane. Therefore, the experiments were geared more towards feasibility testing rather than a rigorous experimental evaluation, hence was carried

out with coarse ground truth. The experiments were carried out in the ANU test tank with the experimental apparatus described in chapter 6 with slight modifications.

Incorporating relative depth information

As depicted in figure 8.4.c, the acoustic source¹ (projector) attached to a gantry mounted shaft was moved in a vertical rectangular pattern with dimensions 0.5 m × 1.0 m approximately 3.0 m in front of the receivers (hydrophones). The motion of the source was manually conducted with distances and depths measured with a standard measuring tape which gave coarse ground truth. The source was held stationary at each of the vertices of the rectangle for 10 s. As in the experiments described in chapter 6, the base distance between the hydrophones were 0.3 m.

The relative depth information of the source was constructed using a uniform velocity model² for the motion and the measured depth with a 0.2 s time resolution to match the 5.0 Hz update rate of the relative localisation system. During offline processing, the azimuth θ and range r estimates output by the localisation system along with the constructed relative depth h was used as inputs to produce estimates for the true azimuth and elevation angles using the formulae given in (8.1) and (8.2). The 3-dimensional spherical polar coordinates expressed by (r, ϕ, γ) are converted in to 3-dimensional cartesian coordinates for ease of plotting using following transformations:

$$x = r \cos \gamma \sin \phi \quad (8.5)$$

$$y = r \cos \gamma \cos \phi \quad (8.6)$$

$$z = r \sin \gamma \quad (8.7)$$

These 3-dimensional cartesian coordinates of the localised source positions are shown by plots a) and b) in figure 8.4. The ‘intended positions’ plotted on those same plots are based on the constructed relative depth information and the measured distance between the receivers and the gantry mounted acoustic source.

Using additional hydrophones

A secondary hydrophone pair with the same base distance of 0.3 m was mechanically attached to the primary hydrophone pair such that the two hydrophones planes were orthogonal - similar to the primary and secondary hydrophone planes described in section 8.2 using figure 8.3. Due to the depth limitation of the test tank (1.5 m), the hydrophone assembly was tilted such that the angle between the secondary hydrophone plane and the vertical plane was 30°. The relative

¹ The sending rig used in experiments described in chapter 6, emitting MLS signal pings every 0.2 s. For these experiments, the source localisation was performed only with respect to the ‘front’ ping.

² This model only provides coarse accuracy since the motion was conducted manually.

orientation between the two hydrophone planes remained unchanged. The acoustic source (projector) was the same as used in the previous experiments. As shown in figure 8.5.c, the gantry mounted shaft was moved along a horizontal line segment with a displacement of 1.4m to either side of the initial position. This motion was equivalent to a diagonal movement of the source if the hydrophone assembly remained un-tilted. As with the previous experiment, the motion was done manually in this instance as well, with a pause of 10s at each end of the line segment. The distances were measured with a measuring tape and the motion was assumed to be uniform, providing coarse ground truth.

During the experiment, the four audio channels corresponding to the four hydrophones were recorded simultaneously and stored for offline processing. Channel pairs corresponding to the primary and secondary hydrophone pairs were processed in two separate runs by the relative localisation system software, each run producing an azimuth and a range estimate. The azimuth and range corresponding to the primary hydrophone pair are denoted by θ and r_θ while those corresponding to the secondary hydrophone pair are denoted by ψ and r_ψ . substituting the angular quantities in (8.3) and (8.4) provides the true azimuth and elevation angles of the source while the range r is calculated as follows:

$$r = \frac{\sqrt{r_\theta^2 + r_\psi^2}}{2} \quad (8.8)$$

These quantities yield the 3-dimensional spherical polar coordinate of the estimated source location as (r, ϕ, γ) and as with the previous case, the transformations given by (8.5), (8.6) and (8.7) are used to derive the 3-dimensional cartesian coordinates for plotting. The estimated source positions and the ‘intended positions’ are plotted in a) and b) of figure 8.5.

8.4 Discussion

This chapter proposed strategies for localising a signal source lying outside of the hydrophone plane of the relative localisation system and later utilised the same localisation system to implement those strategies. The experimental results presented, though with coarse ground truth, validates the feasibility of the relative localisation system in handling 3-dimensional localisation, either with additional information (relative depth) or additional sensors without further modification of the sensing and processing methodologies described in detail throughout this thesis. As discussed in sections 8.1 and 8.2, the sensing was limited to a semi-hemisphere due to the use of non-omnidirectional transducers, hence the *front-back ambiguity* did not arise during the experiments. As future considerations, further experiments are suggested with the use of a modified setup capable of producing more accurate ground truth for 3-dimensional localisation experiments. This would facilitate detailed error analysis and provide insights in to how the

accuracy and precision of additional information such as the relative depth information affects the final position estimates.

The two main strategies discussed (apart from those involving vehicle motion) for localising a signal source lying outside of the hydrophone plane of the relative localisation system can broadly be applied for many different underwater platforms including underwater acoustic sensor networks, which are not necessarily AUVs.

Chapter 9

Conclusions

The research conducted in developing this thesis was motivated by the challenging problem of facilitating swarming for autonomous submersibles. As elaborated in the introduction, relative position sensing capability amongst neighbouring robots is a prerequisite for the successful implementation of the swarming paradigm. The work presented focused on designing, developing and experimentally evaluating a relative localisation system which enable vehicles to sense the positions of its near neighbours. The main requirements and constraints were derived based on a fully embodied implementation which could facilitate swarming of Serafina class AUVs.

The underwater environment itself posed a number of challenges by precluding access to sensing and communication modalities commonly used by in-air applications. A survey of underwater localisation techniques revealed that acoustics was considered the method of choice in this domain albeit with multipath propagation and fading effects. A further review of literature addressing the problem of multi-AUV navigation revealed that most of the approaches are extensions of beacon based single AUV localisation methods which does not scale well with an increasing number of vehicles. The state of the art multi-AUV localisation implementations rely on underwater acoustic modems capable of inter-node ranging and communication. In the context of swarming Serafina class AUVs, the small size of the vehicles places constraints on the available

power budget as well as in-hull space. The agility and manoeuvrability of the AUVs require a high degree of accuracy and precision in addition to a reasonably fast update rate from the localisation system. Moreover, a fully decentralised and distributed solution which scales efficiently with an increasing number of members is desired to realise the full potential of the swarming paradigm. As discussed in chapter 2, the existing techniques and approaches does not adequately address these requirements nor adhere to the constraints.

9.1 The relative localisation system

To address the localisation requirements of Serafina class AUVs to operate as a swarm, a fully decentralised relative localisation system comprising of a ‘localisation sensor’ capable of producing relative estimates for range, azimuth and heading of neighbouring AUVs was developed and experimentally evaluated. The choice of a short duration acoustically transmitted Maximum Length Sequence (MLS) ping as the source signal helped to mitigate some of the detrimental characteristics of the underwater acoustic channel. Its statistical properties led to better cross-correlation performance in the presence of multipath propagation and interference compared to other candidate waveforms as described in chapter 3.

The system was designed to exploit the underlying communication scheduling system developed by Schill (2007). By synchronising the emission of the acoustic pings with long-wave radio broadcasts within a local neighbourhood, each observing vehicle could measure ranges to the sender using the arrival time difference between the electromagnetic and acoustic signals based on spherical localisation concepts. The azimuth estimations were done using hyperbolic localisation methods while the heading estimate was derived from the intermediate angular and radial measurements. In addition, an alternate method utilising a reverse hyperbolic localisation scheme based on transducer geometry was used to calculate the heading and range independent of the earlier estimations and the afore mentioned synchronisation adding redundancy to the position estimation and improving reliability. The detailed measurement methodology, the configuration of the transducers and their geometrical relationships were elaborated in chapter 4.

The decentralised spatially distributed routing algorithm used by the underlying communication system provides locally collision free schedules for the acoustic ‘sending events’ which minimises localisation performance degradation due to cross-talk. With swarm members each equipped with the proposed ‘localisation sensor’, they are able to localise the positions of all other members within their local neighbourhood per schedule run without the position information being explicitly exchanged using the communication system (*i.e.* for a given position sensing instance, the communication system is only used to derive implicit synchronisation between a sender and observers). By design, the relative localisation system is intended to integrate with the existing long-wave radio communication and scheduling system to provide a swarm wide

distributed decentralised localisation solution which scales efficiently with an increasing number of members as described in section 5.2.

The way in which characteristics of MLS signals coupled with channel windowing methods are used to handle different forms of interference along with how thresholding and peak tracking schemes are used to handle ensuing outliers are described and analysed in chapter 5. These techniques along with the pre-cross-correlation inverse frequency response filtering (chapter 3) and post-cross-correlation sub-sample interpolation scheme (chapter 4) directly contributed to the high degree of accuracy and precision of the position estimates obtained during the experimental evaluation of the system as demonstrated in chapter 7.

The use of relatively short duration pings, the efficient localisation routines which can be processed in parallel (section 5.1), the aforementioned channel windowing and the range tracking scheme (section 5.5) lead to an update rate of 5.0Hz during the experimental evaluation of the localisation system which can reliably cope with relatively fast angular and linear motions of both the sender and the observer. This rate can be further increased up to 9.74Hz with the use of a dedicated microprocessor without changing any other system parameter.

9.1.1 Accuracy and precision of position estimates

Evaluation of the relative localisation system was conducted by an experimental implementation whose estimation results and associated errors were scrutinized. A sender rig mounted with two projectors and an observer rig mounted with two hydrophones were mounted on a gantry and moved relative to each other to establish how the accuracy and precision of the localisation estimates behave under different experimental configurations and different operating environments (test tank and lake) as described in chapter 6. In the ensuing short, medium and long range experiments the two rigs were rotated to produce a relative azimuth range of $-90^\circ \rightarrow 90^\circ$ and a

	Error in azimuth	Error in range	Error in heading
Short range experiments (up to 3.5 m)	$\mu_{\Delta\theta} = -0.87^\circ$ $\overline{\Delta\theta} = 1.60^\circ$	$\mu_{\Delta r} = -1.4 \times 10^{-2} \text{ m}$ $\overline{\Delta r} = 2.0 \times 10^{-2} \text{ m}$	$\mu_{\Delta\alpha} = 0.91^\circ$ $\overline{\Delta\alpha} = 3.67^\circ$
Medium range experiments (up to 10 m)	$\mu_{\Delta\theta} = 0.15^\circ$ $\overline{\Delta\theta} = 1.59^\circ$	$\mu_{\Delta r} = 1.4 \times 10^{-2} \text{ m}$ $\overline{\Delta r} = 1.2 \times 10^{-2} \text{ m}$	$\mu_{\Delta\alpha} = -0.26^\circ$ $\overline{\Delta\alpha} = 3.84^\circ$
Long range experiments (up to 90 m)	$\mu_{\Delta\theta} = -0.73^\circ$ $\overline{\Delta\theta} = 1.01^\circ$	$\mu_{\Delta r} = 33.1 \times 10^{-2} \text{ m}$ $\overline{\Delta r} = 47.4 \times 10^{-2} \text{ m}$	n/a

Table 9.1: Comparison of maximum means and average deviations of errors associated with azimuth, range and heading estimates produced across all the experiments presented in chapter 7.

relative heading range of $-180^\circ \rightarrow 180^\circ$ while the distance between the rigs were varied up to and beyond 90 m.

Table 9.1 gives a summary of the maximum means and average deviations of errors associated with each of the pose vector components¹ obtained during all the experiments presented in chapter 7. As seen from the tabulated quantities, throughout the experiments conducted, the absolute mean error for azimuth estimation remained less than 1.0° and the average deviation was less than 2.0° . For heading estimation, the absolute mean error was less than 1.0° in all instances while the average deviation remained below 4.0° considering alternate heading estimates. For short and medium range experiments where the distances varied up to 10 m, the absolute mean error remained well below 1.5×10^{-2} m while the average deviation was at most 2.0×10^{-2} m for range estimates. For long range experiments² where the range varied up to 90 m, the mean error was less than 35.0×10^{-2} m while the average deviation was at most 47.4×10^{-2} m.

With regard to range estimation, the maximum percentage error (described in section 7.6.2) is 0.2% for short and medium range experiments and 0.55% for long range experiments. The best azimuth resolution of 0.29° was achieved near relative azimuth estimates of 0° and the best range resolution for range estimates greater than 0.5 m was 3.2×10^{-3} m. Accordingly, the behaviour of errors associated with the estimates produced by the relative localisation system exhibit a high degree of accuracy and precision as demonstrated by the quantities stated above. Moreover, errors associated with azimuth, range and alternate heading estimates which are integral in fixing position and orientation were shown to be invariant with increasing range in section 7.6.1. Empirical results also show that they remain within bounds defined by the theoretical error models derived earlier in section 4.4.5.

9.1.2 Can the localisation system support swarming?

As explained previously in section 9.1, the strategy of localisation utilising the communication and scheduling system adequately addresses the problem of setting up a scalable and fully decentralised localisation solution for swarming. The ‘localisation sensor’ performance with regard to position estimation accuracy and precision was experimentally evaluated and analysed in chapter 7 and summarised in the previous section. Compared to the state of the art implementations of multi-AUV localisation schemes reviewed in chapter 2, the position errors of the system evaluated in this thesis are much lower in magnitude. However, it must be noted that due to the varied spatial scales of operation and performance metrics used in different implementations, the results

¹ The quantities corresponding to range are from the direct estimation scheme while those for heading are from the alternate estimation scheme. Both these estimation schemes performed consistently better than their counterparts as discussed in section 7.6.2.

² The errors associated with long range experiments cannot be directly compared to those associated with short and medium range experiments due to the difference in precision of ground truth references as mentioned in section 7.5.

summarised in table 2.1 in chapter 2 cannot be qualitatively compared to those shown in table 9.1. However, the update rate of 5.0 Hz used during the experimental evaluation of the presented relative localisation system is much higher than 0.1 Hz (Bahr and Leonard, 2008) and 0.5 Hz (Corke et al., 2007) used in the reviewed implementations where only one AUV was localised with respect to either mobile communication and navigation aids (CNAs) or static sensor nodes. Upon the premise that the systems reviewed in the literature can support multi-robot navigation, it can be argued that the presented relative localisation system with its better accuracy and higher update rate can indeed provide a position fixing solution for swarming of AUVs in general.

The sensing range of the experimental implementation of relative localisation system that was evaluated was established empirically using position error and SNR as measures in section 7.6.2. The use of two non-omnidirectional hydrophones as receivers yielded an angular sensing range of $-75^\circ \rightarrow 75^\circ$ and a radial sensing limit of 75 m where the position errors remained below 0.5 m (azimuth error below $\pm 3.0^\circ$) and SNR was above 10 dB. The relevant plots were shown in figures 7.48, 7.49 and 7.50. The detailed experimentation and evaluation of the system concentrated on localising signal sources within the plane containing the directivity axes of the hydrophones (sensor plane). This approach is supported by a large body of literature addressing underwater localisation spanning from the early work of Bellingham et al. (1992) to more recent work of Bahr and Leonard (2008) where the problem is reduced to 2-dimensions with availability of accurate depth information derived from pressure sensor measurements.

Chapter 8 was dedicated to discussing and demonstrating means to extend the relative localisation system to cope with signal sources lying outside the sensor plane, *i.e.* to perform 3-dimensional localisation. These included empirical feasibility testing of incorporating relative depth information (section 8.1) as well as using an additional hydrophone pair (section 8.2). In both cases, the use of non-omnidirectional hydrophones such as the Benthos AQ-2000 transducers would yield a semi-hemispherical (radius of 75 m) sensing volume truncated by a solid cone (with a solid angle of 150°) with its axis lying on the sensor plane. Based on this evidence, it can be postulated that the use of an omnidirectional pair of hydrophones (with an additional hydrophone for *front-back ambiguity* resolution¹) for the ‘localisation sensor’ can cover the complete spherical operational volume by incorporating relative depth information by including an elevation estimate in addition to the range and azimuth already produced. In the absence of relative depth information, two pairs of omnidirectional hydrophones can achieve the spherical volume coverage required as discussed in section 8.2.

Apart from the sensing volume limitations imposed by the choice of transducers, the relative localisation system comprising of a ‘localisation sensor’ capable of producing relative azimuth, range and heading estimates which was developed and evaluated in this thesis adequately

¹. An ambiguity about the plane containing the three hydrophones does not arise when relative depth information is available.

addresses the problem of providing accurate, precise and robust relative localisation to support swarming of small agile autonomous submersibles. The system efficiently scales up with increasing swarm size and is independent of pre-deployed beacon networks providing a fully decentralised and distributed solution. As discussed in chapter 6, considering the hardware devices used during the evaluation of the experimental implementation, the relative localisation system can be ported to a ‘deployment-ready’ implementation with an embedded microprocessor and other relevant components which comply with the space constraints of Serafina Mk II AUVs. Due to the use of short duration pings, the total acoustic transmission time is 13 milliseconds for every second, resulting in a duty cycle of 1.3%. Therefore, the power consumption of the proposed system can be adequately accommodated within the available power budget of the AUVs.

9.2 Key contributions

The review of existing approaches in addressing relative localisation for multi-robot setups in the underwater domain revealed an increasing reliance on inter-vehicle communication channels and explicit synchronised clock or round-trip time based ranging methods (Curcio et al., 2005b; Bahr and Leonard, 2008; Eustice et al., 2007; Corke et al., 2007). ‘Robot sensors’ or ‘localisation sensors’ such as those mentioned in the land based multi-robot literature (Fox et al., 2000; Rekleitis, 2003; Howard et al., 2003) which provides relative estimates for range, azimuth and heading of another robot based on observation and sensing have not been implemented in underwater robotics to address the problem of relative localisation to support swarming.

The relative localisation strategy proposed and designed in this thesis represents a novel approach which has no precedent in surveyed underwater robotics literature. The experimentally implemented and evaluated ‘localisation sensor’ is capable of producing instantaneous estimates of relative azimuth, range and heading of a neighbouring submersible without relying on integration of multiple (angle only or range only) observations to estimate position and heading as done in target motion analysis literature (Farina, 1999; Ristic et al., 2002). Moreover, the position estimates produced by the relative localisation system demonstrates a higher degree of accuracy and precision when compared to the state of the art in addressing the problem of localisation for multiple AUV navigation including those reviewed in chapter 2¹. This is especially significant when considering the low power requirements, higher update rates, low cost, small size and fully decentralised and distributed implementation possibilities of the system in the context of the small and agile Serafina class AUVs which motivated the research.

While the requirements and constraints were derived based on the concept of swarming Serafina class AUVs, the relative localisation methodology (chapter 4) and innovative strategies developed

¹. By quantitative comparison of position errors summarised in table 2.1 and table 9.1.

throughout this thesis can be utilised to implement ‘localisation sensors’ to be used in many other underwater applications which are not limited to small AUV swarms (*e.g.* underwater sensor network localisation, tracking of underwater life forms *etc.*). The detailed experimental results and analyses which were presented herein contributes to the growing field of acoustic localisation in the context of understanding limitations and opportunities presented by underwater environments (chapter 7). Furthermore, the choice of signal waveform (chapter 3) and techniques of handling interference and outliers (chapter 5) can be extended beyond underwater robotics applications and can potentially be transferred to other application domains (*e.g.* aerial robotics, sensor networks) with minimal modifications to serve localisation requirements.

The effectiveness and accuracy of the presented system can be attributed to a number of design strategies and characteristics such as the choice of acoustical MLS signals as the source waveform, exploiting the long-wave radio communication system to achieve sender-observer synchronisation, inverse frequency filtering to compensate for transducer response nonlinearities, sub-sample interpolation to increase resolution, the novel use of reverse hyperbolic localisation and the peak-tracking scheme which handles outliers.

Use of MLS signals

As it was elaborated in section 3.2, MLS signals provided a source waveform with many desirable characteristics. Prominent among those were the extremely high robustness against spurious and environmental noise and the uniqueness of the peak in the cross-correlogram. MLS signals proved to be a viable alternative to chirps and other pseudo-noise waveforms when considering the SNR and cross-correlation peak resolution.

Pre-cross-correlation inverse frequency filtering

As it is difficult to find small low cost hydrophones and projectors which would faithfully reproduce broadband acoustic signals, an inverse frequency response filtering was used to compensate for the frequency filtering behaviour of the transducers due to resonance. This scheme introduced in section 3.3.3 contributed in recovering the uniqueness of the cross-correlation peak by suppressing adjacent side-lobes when applied to the incoming hydrophone signal channels as demonstrated in section 7.1.

Post-cross-correlation sub-sample interpolation

Given the relatively short base distance of 0.3m separating the hydrophones, the maximum achievable resolution of the estimates were limited. While the base distance was constrained by the physical size of the Serafina Mk II AUVs, the estimation resolution was improved by using sub-sample interpolation to locate the peak of the cross-correlograms. As explained in section

4.3.2, this had an effect similar to increasing the sampling frequency of the analogue to digital converters albeit without the additional processing overhead.

Reverse hyperbolic localisation

Conventional hyperbolic localisation involves one signal source and multiple receivers or multiple synchronised signal sources with one receiver. By combining these concepts and using two synchronised sources on the sender vehicle and two receivers on the observer vehicle, the relative localisation system manages to estimate relative heading and range (distance) between the two vehicles. As explained in section 4.4.4, these alternate heading and range measurements are independent of the sender-observer synchronisation provided by the communication scheduling scheme. This provides robustness against possible timing drifts in the scheduling scheme which otherwise would adversely effect the accuracy of the estimates. Additionally, as mentioned in section 4.4.5 and demonstrated in section 7.6.1, the errors associated with alternate heading estimates are independent of the distance between the vehicles and does not deteriorate with increasing range.

Peak tracking

The outlier handling scheme introduced in section 5.4.1 and demonstrated in section 7.2 uses the time history of previous measurements for relevant time of flights and time difference of arrivals to find the next peak position on the cross-correlograms. This framework was based on enforcing the continuity assumptions of the estimated quantities. As a result of peak tracking, according to the results presented in table 7.1, the average deviation of errors associated with azimuth estimates were reduced by 86% ($21.46^\circ \rightarrow 2.96^\circ$) and alternate heading estimates by 86% ($21.43^\circ \rightarrow 2.94^\circ$). According to results presented in table 7.2, the average deviation of errors associated with range estimates were reduced by 96% ($34.6 \times 10^{-2} \text{ m} \rightarrow 1.2 \times 10^{-2} \text{ m}$) and heading estimates by 91% ($45.35^\circ \rightarrow 3.89^\circ$). These improvements were major contributing factors for the high degree of accuracy and precision of the pose vector estimates produced by the novel ‘localisation sensor’ incorporated with the relative localisation system presented in this thesis.

9.2.1 Summary of contributions

The work presented in this thesis proposed a novel distributed relative localisation strategy to be used in underwater multi-robot setups with an emphasis on providing swarming capability to small agile AUVs. This strategy was implemented and demonstrated with an acoustic relative localisation system comprising of a ‘localisation sensor’ capable of producing estimates for azimuth, range and heading of neighbouring vehicles. This approach is unprecedented in the

underwater domain as such a position sensing method capable of producing azimuth, range and heading has not been utilised in existing underwater robotics literature. In addition to the novelty of this implementation, the position estimates produced by this system are of higher quality when compared with the state of the art techniques which address the problem of simultaneous navigation of multiple AUVs.

Despite the implementation characteristics focusing on the Serafina AUVs, the relative localisation strategy and innovative methodologies developed in this research have a wider scope to be utilised in implementing ‘localisation sensors’ for many other applications. Examples are underwater sensor network localisation and position tracking of underwater life forms which are in addition to position tracking of underwater vehicles. The decentralised nature of the approach allows implementations where position tracking is required for one or many nodes.

The experimental results and analyses presented in this thesis contributes to the growing field of underwater localisation. These especially contribute to understanding limitations and opportunities presented by underwater environments in the context of using acoustical methods for localisation. Aspects such as the choice of signal waveform and techniques of handling interference and outliers developed herein have potential applications transcending underwater robotics. They can be transferred with minimal modifications to serve localisation requirements in other application domains. One such example is the proposed localisation scheme for highly agile small unmanned helicopters as mentioned in the following section.

9.3 Future considerations

Drawing on the insights gained while conducting this research, a number of future possibilities can be identified. Immediate considerations include porting the relative localisation system software on to an embedded hardware platform. With the many choices presented by the current developments in low power embedded processor technology, a suitable platform needs to be selected after considering aspects such as power consumption, speed, availability of suitable input/ output interfaces and cost. A parallel extension would also be to conduct experiments with multiple mobile sender/ observer rigs as opposed to the two vehicle configuration used in the experiments described in this text. This would provide an opportunity to evaluate the local neighbourhood map building characteristics of the higher level swarming and navigation modules which receive inputs from the relative localisation system. Once the system is ported to an embedded solution, a subsequent step would be to deploy the system on actual Serafina Mk II AUVs and to conduct experiments to evaluate the performance of the system.

Another aspect under consideration is to extend the MLS signal based short-range relative localisation concept to the aerial domain. While GPS based solutions have been used in almost all outdoor above water localisation applications, apart from the use of differential GPS systems, the

temporal and spatial resolution of the localisation fixes have been somewhat limited. This is especially true in application domains such as short-range localisation of highly agile unmanned aerial vehicles (UAVs), for example, small helicopters. In line with an ongoing project at The Australian National University with regard to autonomous flight of small helicopters, there is an intention to adapt the concepts developed through the research presented in this text to implement an aerial short-range relative localisation system based on acoustical MLS pings. Despite the fact that propagation speeds, transmission characteristics, transducers as well as the types and modes of interference are different to those encountered in the underwater domain with regard to the acoustic signals, most of the key concepts mentioned earlier in section 9.2, the power consumption requirements, sensing range and size of the vehicles still remain valid and applicable in the aerial domain in the context of small helicopter UAVs.

Appendix A

A.1 Source signals before and after filtering

The source signals used to demonstrate the inverse frequency response filtering described in chapter 3 (section 3.3.3) are shown below in figure A.1.

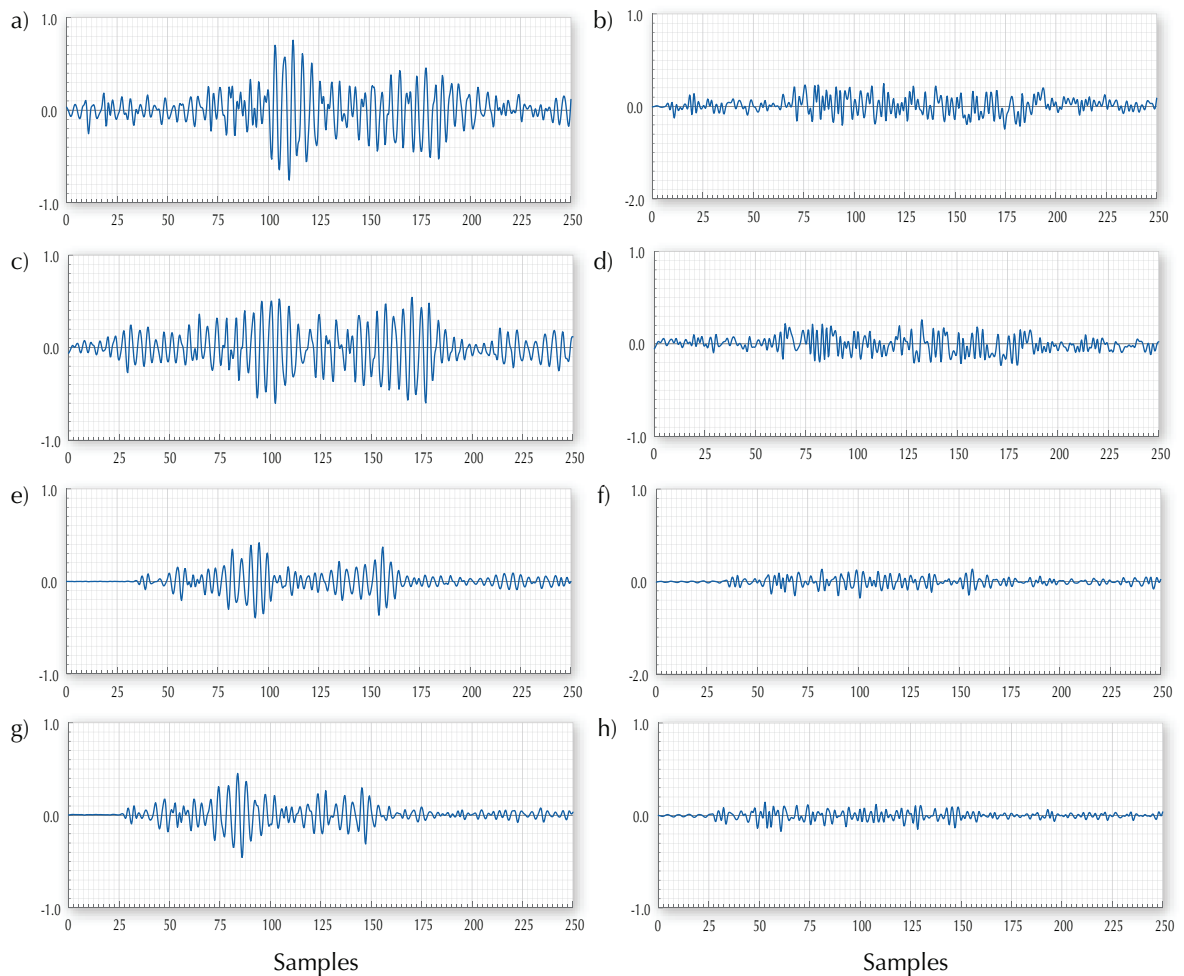


Figure A.1: Simulated source signal channels; a) and c) before and b) and d) after applying the filter along with real source signal channels; e) and g) before and f) and h) after applying the filter.

A.2 Azimuth variations for error comparison

The actual azimuth variations from which the error variations compared in section 7.6 (figure 7.37) are derived from, are shown below in figure A.2.

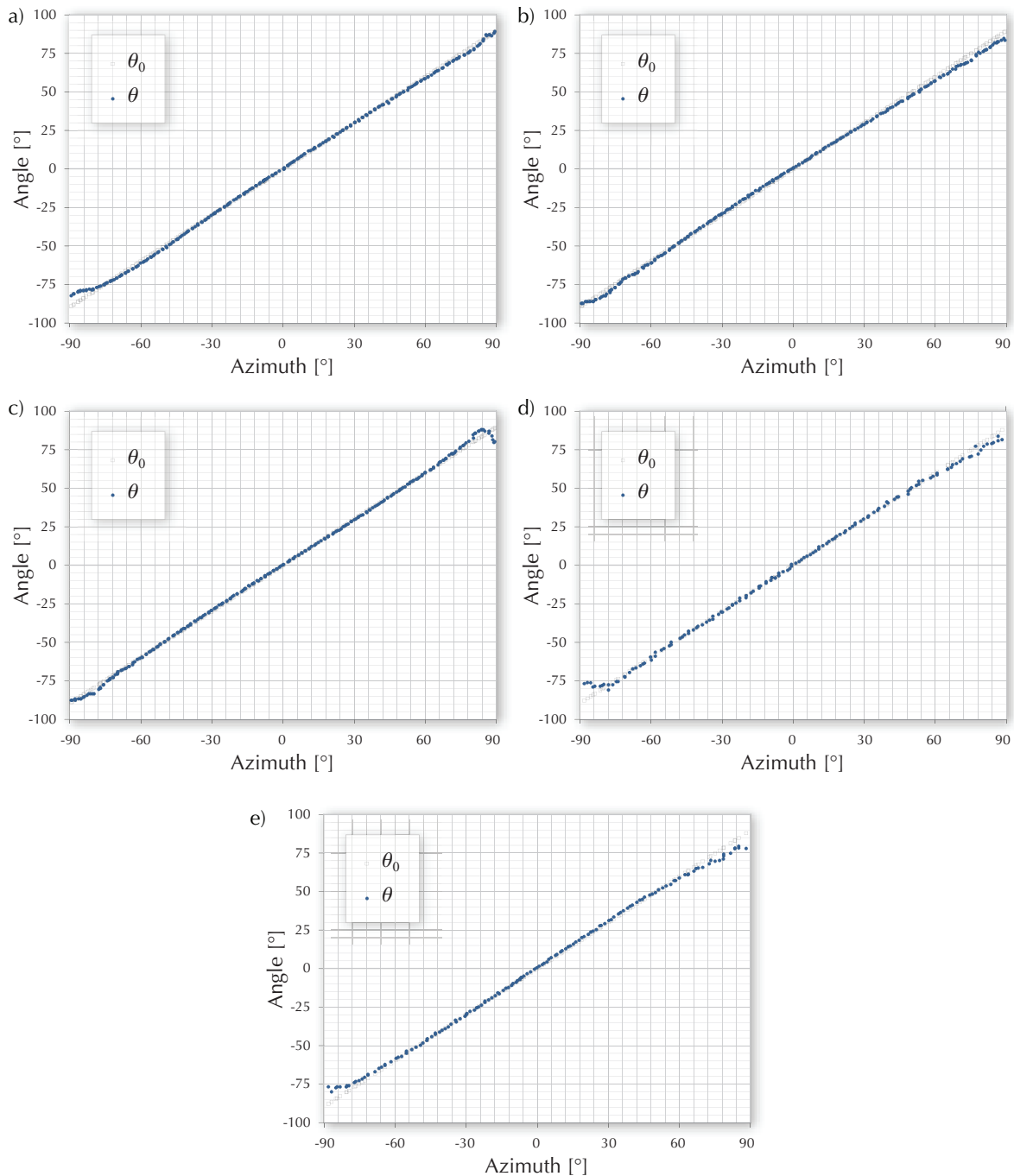


Figure A.2: Plots showing azimuth variations from which the RSE shown in figure 7.37 were derived. The parameters of $\alpha_{\theta=0^\circ}$ and r for each of the plots are as follows; a) $\alpha_{\theta=0^\circ} = 170^\circ$, $r = 2.0\text{m}$, b) $\alpha_{\theta=0^\circ} = -155^\circ$, $r = 2.1\text{m}$, c) $\alpha_{\theta=0^\circ} = 160^\circ$, $r = 3.3\text{m}$, d) $\alpha_{\theta=0^\circ} = 160^\circ$, $r = 5.65\text{m}$ and e) $\alpha_{\theta=0^\circ} = 120^\circ$, $r = 8.0\text{m}$.

A.3 Heading variations for error comparison

The actual heading and alternate heading variations from which the error variations compared in section 7.6 (figures 7.43 and 7.45) are derived from, are shown in figures A.3 and A.4.

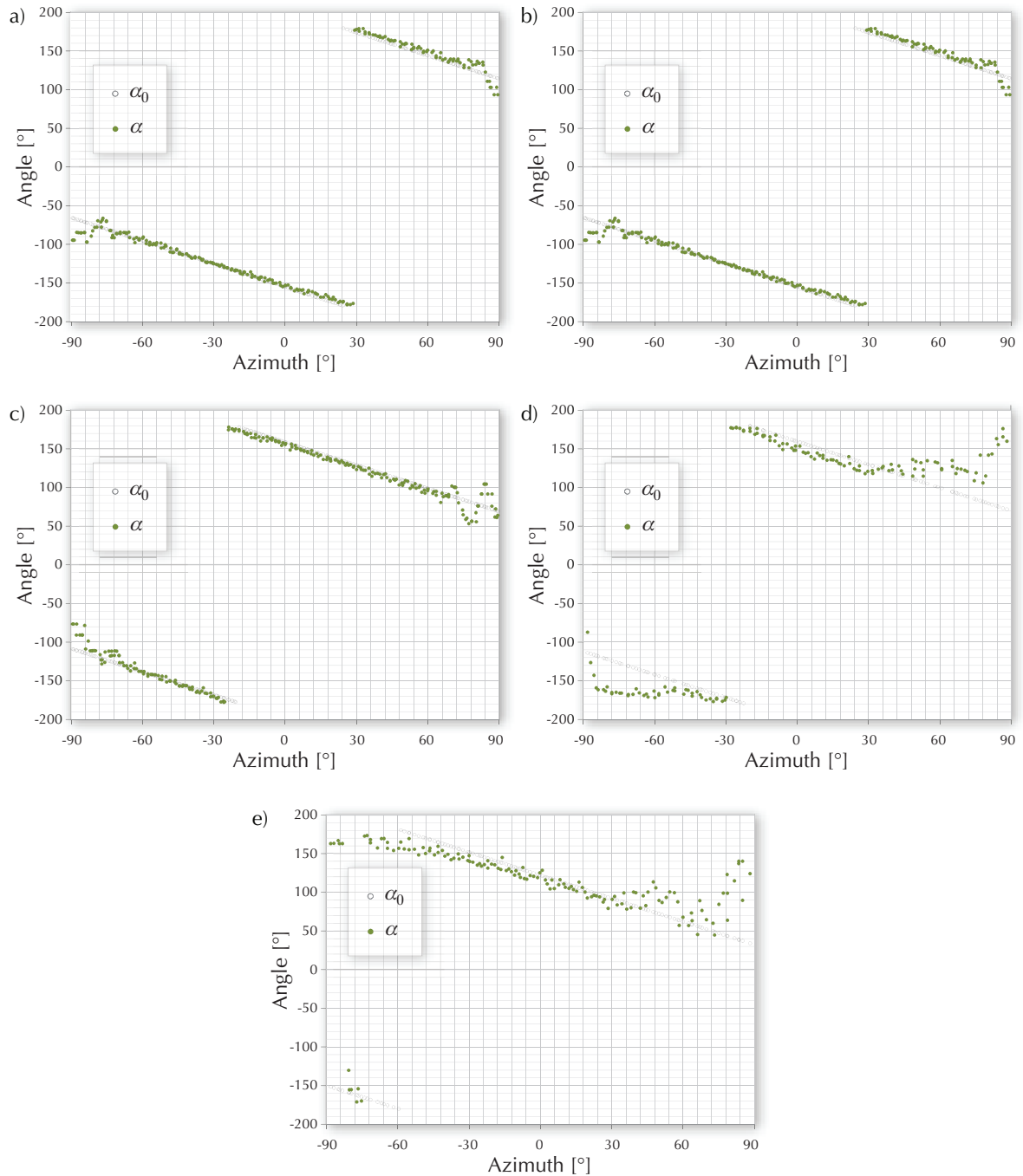


Figure A.3: Plots showing heading variations from which the RSE shown in figure 7.43 were derived. The parameters of $\alpha_{\theta=0^\circ}$ and r for each of the plots are as follows; a) $\alpha_{\theta=0^\circ} = 170^\circ$, $r = 2.0\text{m}$, b) $\alpha_{\theta=0^\circ} = -155^\circ$, $r = 2.1\text{m}$, c) $\alpha_{\theta=0^\circ} = 160^\circ$, $r = 3.3\text{m}$, d) $\alpha_{\theta=0^\circ} = 160^\circ$, $r = 5.65\text{m}$ and e) $\alpha_{\theta=0^\circ} = 120^\circ$, $r = 8.0\text{m}$.

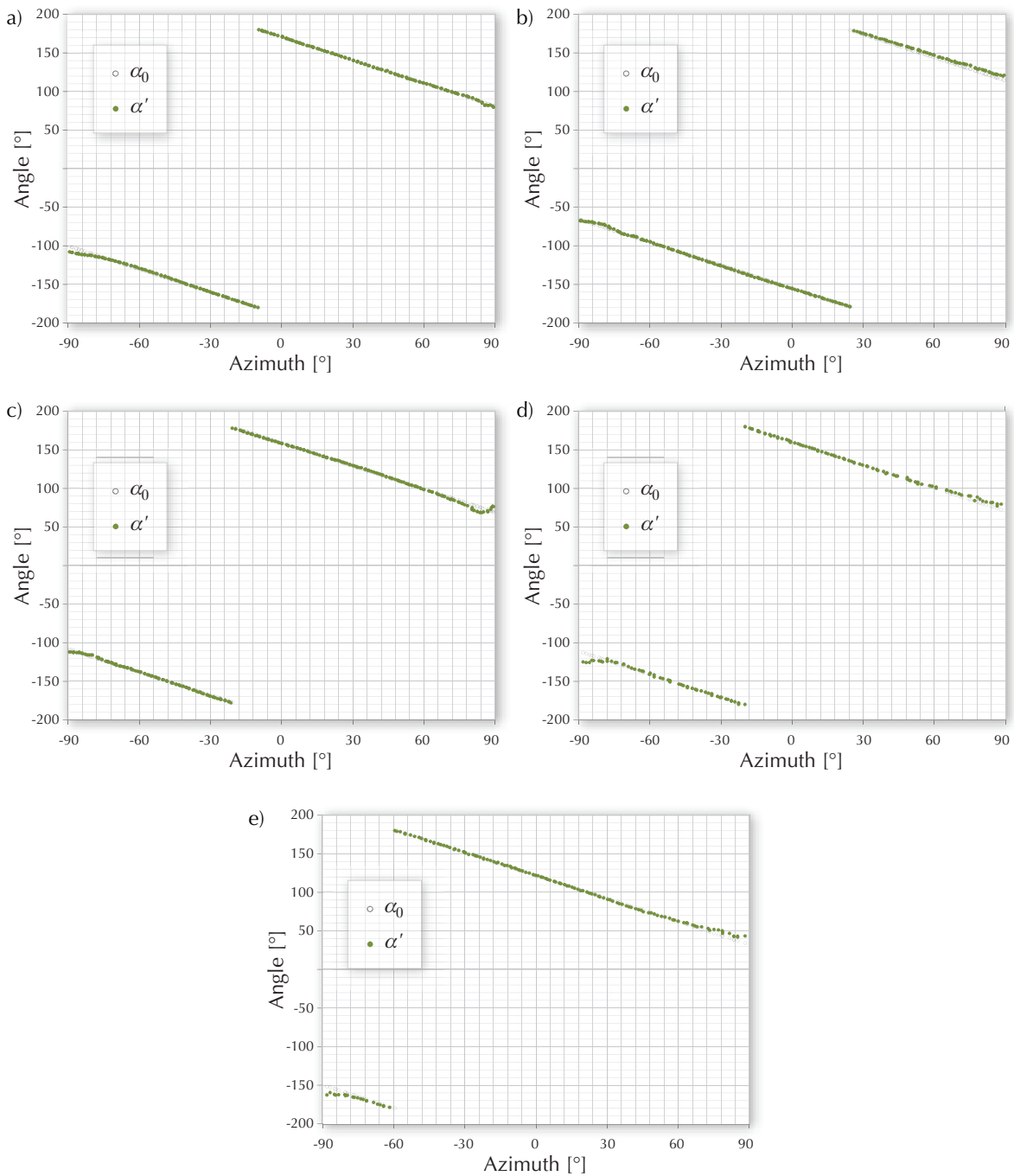


Figure A.4: Plots showing alternate heading variations from which the RSE shown in figure 7.45 were derived. The parameters of $\alpha_{\theta=0^\circ}$ and r for each of the plots are as follows; a) $\alpha_{\theta=0^\circ} = 170^\circ$, $r = 2.0\text{m}$, b) $\alpha_{\theta=0^\circ} = -155^\circ$, $r = 2.1\text{m}$, c) $\alpha_{\theta=0^\circ} = 160^\circ$, $r = 3.3\text{m}$, d) $\alpha_{\theta=0^\circ} = 160^\circ$, $r = 5.65\text{m}$ and e) $\alpha_{\theta=0^\circ} = 120^\circ$, $r = 8.0\text{m}$.

Appendix B

B.1 MLS generation routine

The following algorithm was used to pre-generate the Maximum Length Sequence signals which were used as the source signals during the experiments presented in this thesis. The ADA source code given below was written and tested by Uwe R. Zimmer.

```
-- Description : MLS Generator
-- Author      :Uwe Zimmer
-- Created On  : Mon Dec 12 14:48:23 2005
generic
    Degree : in Natural;
    -- a degree of n will result in an MLS lengths of 2**(n+1)-1
package MLS_Generator is
    type Primitive_Polynom is array (0..Degree) of Boolean;
    type MLS_Signal is array (1..2**(Degree+1)-1) of Boolean;
    type Polynom_ListT is array (Positive range <>) of Primitive_Polynom;
    type MLS_ListT is array (Positive range <>) of MLS_Signal;

    function Generator (Polynom : in Primitive_Polynom) return MLS_Signal;
    function Test_Polynom (Polynom : in Primitive_Polynom) return Boolean;
    function NoOf_Primitive_Polynoms return Natural;
    function Primitive_Polynoms return Polynom_ListT;
    function MLSs return MLS_ListT;
end MLS_Generator;

package body MLS_Generator is
    NoOf_Polynoms : Natural := 0;
    procedure Generate_And_Test (Polynom : in Primitive_Polynom;
                                MLS : out MLS_Signal;
                                Primitive : out Boolean) is
        Generated_MLS : MLS_Signal;
        Register : Primitive_Polynom := Polynom;
```

```

    NewBit : Boolean;
    Store_Registers : array (MLS'Range) of Primitive_Polynom;
begin
    Primitive := True;
    for I in MLS'Range loop
        Store_Registers (I) := Register;
        for J in 1 .. I-1 loop
            if Store_Registers (I) = Store_Registers (J) then
                Primitive := False;
                exit;
            end if;
        end loop;
        Generated_MLS (I) := Register (Register'First);
        NewBit := False;
        for Bit in Register'First .. Register'Last loop
            if Polynom (Bit) then
                NewBit := NewBit xor Register (Bit);
            end if;
        end loop;
        for Bit in Register'First .. Register'Last - 1 loop
            Register (Bit) := Register (Bit+1);
        end loop;
        Register (Register'Last) := NewBit;
    end loop;
    MLS := Generated_MLS;
end Generate_And_Test;

function Generator (Polynom : in Primitive_Polynom) return MLS_Signal is
    MLS : MLS_Signal;
    Primitive : Boolean;
begin
    Generate_And_Test (Polynom, MLS, Primitive);
    return (MLS);
end Generator;

function Test_Polynom (Polynom : in Primitive_Polynom) return Boolean is
    MLS : MLS_Signal;
    Primitive : Boolean;
begin
    Generate_And_Test (Polynom, MLS, Primitive);
    return (Primitive);
end Test_Polynom;

function NoOf_Primitive_Polynoms return Natural is
    Polynom_Candidate : Primitive_Polynom;
    Poly_Counter : Natural := 0;
begin
    if NoOf_Polynoms = 0 then
        for I in 0 .. 2**Polynom_Candidate'Length-1 loop
            for Bit in 0..Polynom_Candidate'Length-1 loop
                Polynom_Candidate (Bit) := (I / 2**(Bit)) mod 2 = 0;
            end loop;
            if Test_Polynom (Polynom_Candidate) then
                Poly_Counter := Poly_Counter + 1;
            end if;
        end loop;
    end if;
end NoOf_Primitive_Polynoms;

```

```

        end loop;
        NoOf_Polynoms := Poly_Counter;
    end if;
    return (NoOf_Polynoms);
end NoOf_Primitive_Polynoms;

function Primitive_Polynoms return Polynom_ListT is
    Polynom_Candidate : Primitive_Polynom;
    Poly_Counter      : Natural := 0;
begin
    declare
        Polynom_List : Polynom_ListT (1..NoOf_Primitive_Polynoms);
    begin
        Poly_Counter := 0;
        for I in 0 .. 2**Polynom_Candidate'Length-1 loop
            for Bit in 0..Polynom_Candidate'Length-1 loop
                Polynom_Candidate (Bit) := (I / 2**(Bit)) mod 2 = 0;
            end loop;
            if Test_Polynom (Polynom_Candidate) then
                Poly_Counter := Poly_Counter + 1;
                Polynom_List (Poly_Counter) := Polynom_Candidate;
            end if;
        end loop;
        return (Polynom_List);
    end;
end Primitive_Polynoms;

function MLSs return MLS_ListT is
    Polynom_Candidate : Primitive_Polynom;
    Poly_Counter      : Natural := 0;
begin
    declare
        MLS_List : MLS_ListT (1..NoOf_Primitive_Polynoms);
    begin
        Poly_Counter := 0;
        for I in 0 .. 2**Polynom_Candidate'Length-1 loop
            for Bit in 0..Polynom_Candidate'Length-1 loop
                Polynom_Candidate (Bit) := (I / 2**(Bit)) mod 2 = 0;
            end loop;
            if Test_Polynom (Polynom_Candidate) then
                Poly_Counter := Poly_Counter + 1;
                MLS_List (Poly_Counter) := Generator (Polynom_Candidate);
            end if;
        end loop;
        return (MLS_List);
    end;
end MLSs;
end MLS_Generator;

```


Appendix C

C.1 Lower bound for peak tracking parameters

The lower bound for $\Delta_{Tolerance}$ used in peak tracking is stated as follows:

$$\Delta_{Tolerance} \geq \frac{|\omega_{max}| f_s t_{TS}}{v} \quad (C.1)$$

where ω_{max} is a placeholder for maximum relative velocity between the observer and the sender. With usual notations, f_s represents the sampling frequency, t_{TS} the duration of a time-step and v is the speed of sound underwater.

Range estimation

For estimating the intermediate quantities r_{11} , r_{12} , r_{21} and r_{22} used to calculate the direct range estimate, the relevant value for ω_{max} is equal to the maximum linear relative velocity denoted by ω_r and given in meters per second. Relative angular velocity is ignored in this context since the effect of pure rotational motion on the final range estimate r is negligible.

Azimuth estimation

For estimating θ_1 and θ_2 used for calculating the azimuth estimate, the relevant value for ω_{max} is a combination of maximum relative linear and angular velocities. First, the maximum linear velocity induced by a particular angular velocity needs to be derived. The formula for calculating the azimuth θ is given as:

$$\theta = \tan^{-1}\left(\frac{\sqrt{d^2 - \delta^2}}{\delta}\right) \quad (C.2)$$

where d is the base distance between the hydrophones and δ is the acoustic path length difference associated with the time delay between the hydrophone channels. Due to geometric constraints, the condition $\delta \leq d$ is satisfied by the quantities.

By differentiating (C.2) with respect to time, the following can be obtained:

$$\frac{d\theta}{dt} = \frac{d}{dt} \tan^{-1} \left(\frac{\sqrt{d^2 - \delta^2}}{\delta} \right) \quad (\text{C.3})$$

$$\frac{d\theta}{dt} = \frac{-1}{\sqrt{d^2 - \delta^2}} \frac{d\delta}{dt} \quad (\text{C.4})$$

If the relative angular velocity is denoted by ω_θ and the induced linear velocity by ω , then they are related as follows:

$$|\omega| = |\omega_\theta| \sqrt{d^2 - \delta^2} \quad (\text{C.5})$$

where

$$\omega_\theta = \frac{d\theta}{dt} \text{ and } \omega = \frac{d\delta}{dt} \quad (\text{C.6})$$

Therefore, the magnitude of the maximum linear velocity induced by a given angular velocity ω_θ is given by:

$$|\omega|_{max} = |\omega_\theta| d \quad (\text{C.7})$$

The maximum relative velocity to calculate the lower bound of $\Delta_{Tolerance}$ is given by:

$$|\omega_{max}| = |\omega_\theta| d + |\omega_r| \quad (\text{C.8})$$

where the relative angular velocity ω_θ should be given in radian per second.

Reverse azimuth estimation

For estimating φ_1 and φ_2 used for calculating the reverse azimuth estimate, as in the previous case, the relevant value for ω_{max} is a combination of maximum linear and angular relative velocities. The formula for calculating the reverse azimuth φ is given as:

$$\varphi = \tan^{-1} \left(\frac{\sqrt{l^2 - \eta^2}}{\eta} \right) \quad (\text{C.9})$$

where l is the separation between projectors and η is the associated acoustic path length difference. By differentiating (C.9) as done previously for the azimuth estimate, the relationship between the angular velocity ω_φ and the induced linear velocity ω can be stated as follows:

$$|\omega| = |\omega_\varphi| \sqrt{l^2 - \eta^2} \quad (\text{C.10})$$

where

$$\frac{d\varphi}{dt} = \omega_\varphi \text{ and } \frac{d\eta}{dt} = \omega \quad (\text{C.11})$$

Therefore, the magnitude of the maximum linear velocity induced by a given angular velocity ω_φ is given by:

$$|\omega|_{max} = |\omega_\varphi|l \quad (\text{C.12})$$

The maximum relative velocity to calculate the lower bound of $\Delta_{Tolerance}$ is given by:

$$|\omega_{max}| = |\omega_\varphi|d + |\omega_r| \quad (\text{C.13})$$

where the relative angular velocity ω_φ should be given in radian per second.

C.2 Values of peak tracking parameters used

The following table gives the different values for $\Delta_{Tolerance}$ used during the experiments presented in chapter 7.

Type	Variation	Value of $\Delta_{Tolerance}$		
		For path-length differences δ_1, δ_2	For path-length differences η_1, η_2	For intermediate sub-ranges $r_{11}, r_{21}, r_{12}, r_{22}$
Tank tank experiments	Azimuth	0.65	0.65	2.50
	Range	0.70	0.70	3.00
	Heading	0.62	0.62	1.00
Lake experiments	Azimuth	1.00	1.50	3.50
	Range	1.00	1.50	2.50
	Heading	0.65	0.65	1.55
Long range (kayak) experiments	(combined)	1.50	1.50	15.5

Table C.1: Values used for the peak tracking parameter $\Delta_{Tolerance}$ during different experiments, of which results are presented in chapter 7.

Bibliography

- Aidala, V. J. and Hammel, S. E. (1983) Utilization of modified polar coordinates for bearings-only tracking; *IEEE Transactions on Automatic Control*, **28**(3), pp. 283-294.
- Aguirre, G. K. and Kerr, W. (2009) *Creating M-sequences*,
http://cfn.upenn.edu/aguirre/wiki/doku.php?id=m_sequences
- Ajdler, T., Kozintsev, I., Lienhart, R. and Vetterli, M. (2004) Acoustic source localization in distributed sensor networks; *In proceedings of the 38th IEEE Asilomar Conference on Signals, Systems and Computers, 2004*, Monterey, CA, USA, November 2004, pp. 1328-1332.
- Alcocer, A., Oliveira, P. and Pascoal, A. (2006) Underwater acoustic positioning system based on buoys with GPS; *In proceedings of the European Conference on Underwater Acoustics 2006 (ECUA 2006)*, Carvoeiro, Portugal, June 2006.
- Allen, B., Vorus, W. S. and Prestero, T. (2000) Propulsion system performance enhancements on REMUS AUVs; *In proceedings of the MTS/IEEE Oceans 2000*, Providence, RI, USA, pp. 1869-1873.
- Altes, R. A. (1979) Target position estimation in radar and sonar, and generalized ambiguity analysis for maximum likelihood parameter estimation; *Proceedings of the IEEE*, **67**(6), pp. 920-930.
- Analog Devices (2007), *AD1974 Datasheet*, Revision: April 2007, <http://www.analog.com/en/analog-to-digital-converters/audio-ad-converters/ad1974/products/product.html>
- Analog Devices (2009), *ADA4692-2 Datasheet*, Revision: April 2009,
<http://www.analog.com/en/amplifiers-and-comparators/operational-amplifiers-op-amps/ada4692-2/products/product.html>
- Arulampalam, M. S., Ristic, B., Gordon, N. J. and Mansell, T. (2004) Bearings-only tracking of manoeuvring targets using particle filters; *EURASIP Journal on Applied Signal Processing*, **2004**(15), pp. 2351-2365.
- Atwood, D. K., Leonard, J. J., Bellingham, J. G. and Moran, B. A. (1995) An acoustic navigation system for multi-vehicle operations; *In proceedings of the International Symposium on Unmanned Untethered Submersible Technology 1995*, NH, USA, September 1995, pp. 202-208.

- Baccou, P., Jouvencel, B., Creuze, V. and Rabaud, C. (2001) Cooperative positioning and navigation for multiple AUV operations; *In proceedings of the MTS/IEEE Oceans 2001*, Honolulu, HI, USA, November 2001, pp. 1816-1821.
- Bachmayer, R., Leonard, N. E., Graver, J. G., Fiorelli, E., Bhatta, P. and Paley, D. A. (2004) Underwater gliders: Recent developments and future applications; *In proceedings of the IEEE International Symposium on Underwater Technology 2004 (UT '04)*, Taipei, April 2004, pp. 195-200.
- Baggeroer, A. B., Kuperman, W. A. and Mikhalevsky, P. N. (1993) An overview of matched field methods in ocean acoustics; *IEEE Journal of Oceanic Engineering*, **18**(4), pp. 401-424.
- Bahr, A. and Leonard, J. J. (2008) Cooperative localization for autonomous underwater vehicles, in Khatib, O., Kumar, V. and Rus, D. (Eds.) *Experimental robotics*. Berlin; Heidelberg, Springer, pp. 387-395.
- Baker, B. N., Odell, D. L., Anderson, M. J., Bean, T. A. and Edwards, D. B. (2005a) Performance of a two-hydrophone heading sensor and AUV formation flying controller; *In proceedings of the International Symposium of Unmanned Untethered Submersible Technology 2005*, Durham, NH, USA, August 2005.
- Baker, B. N., Odell, D. L., Anderson, M. J., Bean, T. A. and Edwards, D. B. (2005b) A new procedure for simultaneous navigations of multiple AUVs; *In proceedings of the MTS/IEEE Oceans 2005*, Washington, DC, USA, September 2005.
- Balakrishnan, H., Baliga, R., Curtis, D., Goraczko, M., Miu, A., Priyantha, N. B., Smith, A., Steele, K., Teller, S. and Wang, K. (2003) *Lessons from developing and deploying the cricket indoor location system*; Technical report, CSAIL, MIT, Boston, MA, USA.
- Bellingham, J. G., Consi, T. R., Tedrow, U. and Massa, D. D. (1992) Hyperbolic acoustic navigation for underwater vehicles: Implementation and demonstration; *In proceedings of the IEEE Symposium on Autonomous Underwater Vehicle Technology 1992 (AUV '92)*, Washington, DC, USA, June 1992.
- Bellingham, J. G., Goudey, C. A., Consi, T. R., Bales, J. W., Atwood, D. K., Leonard, J. J. and Chryssostomidis, C. (1994) A second generation survey AUV; *In proceedings of the IEEE Symposium on Autonomous Underwater Vehicle Technology 1994 (AUV '94)*, Cambridge, MA, USA, July 1994, pp. 148-155.
- Bellingham, J. G. and Zhang, Y. (2005) Observing processes that vary in time and space with heterogeneous mobile networks; *In proceedings of the International Workshop on Underwater Robotics*, Genoa, Italy, November 2005, pp. 9-16.
- Bellingham, J. G. and Rajan, K. (2007) Robotics in remote and hostile environments; *Science*, **318**, pp. 1098-1102.
- Benesty, J. (2000) Adaptive eigenvalue decomposition algorithm for passive acoustic source localization; *Journal of the Acoustical Society of America*, **107**(1), pp. 384-391.
- Benthos (2001), *AQ-2000 Hydrophone Datasheet*,
<http://www.mksservices.co.uk/mks/files/AQ2000.pdf>

- Betke, M. and Gurvits, L. (1997) Mobile robot localization using landmarks; *IEEE Transactions on Robotics and Automation*, **13**(2), pp. 251-263.
- Bhatta, P., Fiorelli, E., Lekien, F., Leonard, N. E., Paley, D. A., Zhang, F., Bachmayer, R., Davis, R. E., Fratantoni, D. M. and Sepulchre, R. (2005) Coordination of an underwater glider fleet for adaptive ocean sampling; *In proceedings of the International workshop on Underwater Robotics*, Genoa, Italy, November 2005.
- Bingham, B. and Seering, W. (2006) Hypothesis grids: Improving long baseline navigation for autonomous underwater vehicles; *IEEE Journal of Oceanic Engineering*, **31**(1), pp. 209-218.
- Blauert, J. and Cobben, W. (1978) Some consideration of binaural cross-correlation analysis; *Acustica*, **39**, pp. 96-103.
- Bleistein, N. and Desanto, J. A. (1979) *Ocean acoustics*, Berlin, Springer Verlag.
- Bock, R. K. and Krischer, W. (1998) *The data analysis briefbook*, Sixteenth edition, Geneva, CERN, <http://physics.web.cern.ch/Physics/DataAnalysis/Briefbook/>
- Borish, J. and Angell, J. B. (1983) An efficient algorithm for measuring the impulse response using pseudo-random noise; *Journal of the Audio Engineering Society*, **31**(7), pp. 478-488.
- Borish, J. (1985a) An efficient algorithm for generating colored noise using a pseudo-random sequence; *Journal of the Audio Engineering Society*, **33**(3), pp. 141-144.
- Borish, J. (1985b) Self-contained crosscorrelation program for maximum-length sequences; *Journal of the Audio Engineering Society*, **33**(11), pp. 888-891.
- Bosworth, B. T., Bernecky, W. R., Nickila, J. D., Adal, B. and Carter, G. C. (2008) Estimating Signal-to-Noise Ratio (SNR); *IEEE Journal of Oceanic Engineering*, **33**(4), pp. 414-418.
- Bradley, J. S. (1996) Optimizing the decay range in room acoustics measurements using maximum-length sequence techniques; *Journal of the Audio Engineering Society*, **44**(4), pp. 266-273.
- Brekhovskikh, L. M. and Lysanov, I. U. P. (1982) *Fundamentals of ocean acoustics*, Berlin; New York, NY, Springer-Verlag.
- Buchner, H., Aichner, R., Stenglein, J., Teutsch, H. and Kellermann, W. (2005) Simultaneous localization of multiple sound sources using blind adaptive MIMO filtering; *In proceedings of the IEEE International Conference on Acoustics, Speech, and Signal Processing 2005 (ICASSP '05)*, Philadelphia, PA, USA, March 2005, pp. 97-100.
- Burdic, W. S. (1984) *Underwater acoustic system analysis*, Englewood Cliffs, NJ, Prentice Hall.
- Burgard, W., Moors, M., Fox, D., Simmons, R. and Thrun, S. (2000) Collaborative multi-robot exploration; *In proceedings of the IEEE International Conference on Robotics and Automation 2000 (ICRA '00)*, San Fransisco, CA, USA, April 2000, pp. 476-481.
- Caccia, M. and Veruggio, G. (1999) Acoustic motion estimation and guidance for unmanned underwater vehicles; *International Journal of Systems Science*, **30**(9), pp. 929 - 938.

- Caiti, A., Garulli, A., Livide, F. and Prattichizzo, D. (2005) Localization of autonomous underwater vehicles by floating acoustic buoys: A set-membership approach; *IEEE Journal of Oceanic Engineering*, **30**(1), pp. 140-152.
- Carter, G. C. (1981) Time delay estimation for passive sonar signal processing; *IEEE Transactions on Acoustics, Speech, and Signal Processing*, **29**(3), pp. 463-470.
- Cato, D. H. and Bell, M. J. (1992) *Ultrasonic ambient noise in Australian shallow waters at frequencies up to 200 kHz*; Technical report MRL-TR-91-23, Materials Research Labs, DSTO, Ascot Vale, VIC, Australia,
- Chan, Y. T. and Ho, K. C. (1994) A simple and efficient estimator for hyperbolic location; *IEEE Transactions on Signal Processing*, **42**(8), pp. 1905-1915.
- Chandrasekhar, V., Seah, W. K. G., Choo, Y. S. and Ee, H. V. (2006) Localization in underwater sensor networks: Survey and challenges; *In proceedings of the ACM International Workshop on Underwater Networks (WUWNet '06)*, Los Angeles, CA, USA, September 2006, pp. 33-40.
- Chen, J. C., Yao, K. and Hudson, R. E. (2003) Acoustic source localization and beamforming: Theory and practice; *EURASIP Journal on Applied Signal Processing*, **2003**(4), pp. 359-370.
- Chen, J., Huang, Y. and Benesty, J. (2005) A comparative study on time delay estimation in reverberant and noisy environments; *In proceedings of the IEEE Workshop on Applications of Signal Processing to Audio and Acoustics*, New Paltz, NY, USA, October 2005, pp. 21-24.
- Cheng, W., Teymorian, A. Y., Ma, L., Cheng, X., Lu, X. and Lu, Z. (2008) Underwater localization in sparse 3D acoustic sensor networks; *In proceedings of the IEEE Conference on Computer Communications (INFOCOM 2008)*, Phoenix, AZ, USA, pp. 236-240.
- Cheng, X., Shu, H. and Liang, Q. (2007) A range-difference based self-positioning scheme for underwater acoustic sensor networks; *In proceedings of the International Conference on Wireless Algorithms, Systems and Applications*, Chicago, IL, USA, August 2007, pp. 38-43.
- Chitre, M. A., Shahabudeen, S. and Stojanovic, M. (2008) Underwater acoustic communications and networking: Recent advances and future challenges; *Marine Technology Society Journal*, **42**(1), pp. 103-116.
- Cochard, N., Lacoume, J. L., Arzelies, P. and Gabillet, Y. (2000) Underwater acoustic noise measurement in test tanks; *IEEE Journal of Oceanic Engineering*, **25**(4), pp. 516-522.
- Cohn, M. and Lempel, A. (1977) On fast M-sequence transforms (Correspondence); *IEEE Transactions on Information Theory*, **23**(1), pp. 135-137.
- Collins, M. D. and Kuperman, W. A. (1994) Inverse problems in ocean acoustics; *Inverse Problems*, **10**, pp. 1023-1040.
- Coppens, A. B. (1981) Simple equations for the speed of sound in Neptunian waters; *Journal of the Acoustical Society of America*, **69**(3), pp. 862-863.
- Corke, P., Detweiler, C., Dunbabin, M., Hamilton, M., Rus, D. and Vasilescu, I. (2007) Experiments with underwater robot localization and tracking; *In proceedings of the IEEE International Conference on Robotics and Automation 2007 (ICRA '07)*, Roma, Italy, April 2007, pp. 4556-4561.

- Correll, N. and Martinoli, A. (2007) Modeling self-organized aggregation in a swarm of miniature robots; *In proceedings of the IEEE International Conference on Robotics and Automation 2007 (ICRA '07)*, Roma, Italy, April 2007.
- Cruz, N., Madureira, L., Matos, A. and Pereira, F. L. (2001) A versatile acoustic beacon for navigation and remote tracking of multiple underwater vehicles; *In proceedings of the MTS/IEEE Oceans 2001*, Honolulu, HI, USA, November 2001, pp. 1829-1834.
- Curcio, J. A., Leonard, J. J. and Patrikalakis, A. (2005a) SCOUT - A low cost autonomous surface platform for research in cooperative autonomy; *In proceedings of the MTS/IEEE Oceans 2005*, Washington, DC, USA, September 2005, pp. 725-729.
- Curcio, J. A., Leonard, J. J., Vaganay, J., Patrikalakis, A., Bahr, A., Battle, D., Schmidt, H. and Grund, M. (2005b) Experiments in moving baseline navigation using autonomous surface craft; *In proceedings of the MTS/IEEE Oceans 2005*, Washington, DC, USA, September 2005, pp. 730-735.
- Curtin, T. B., Bellingham, J. G., Catipovic, J. and Webb, D. (1993) Autonomous oceanographic sampling networks; *Oceanography*, 6(3), pp. 86-94.
- Curtin, T. B. and Bellingham, J. G. (2008) Progress toward autonomous ocean sampling networks; *Deep Sea Research Part II: Topical Studies in Oceanography*, 56(3-5), pp. 62-67.
- Dahl, P. D., Miller, J. H., Cato, D. H. and Andrew, R. A. (2007) Underwater ambient noise; *Acoustics Today*, 3, pp. 23-33.
- Daku, B. L. F., Salt, J. E. and McIntyre, C. M. (1992) Quality of underwater source localization in a multipath environment; *Journal of the Acoustical Society of America*, 91(2), pp. 957-964.
- Davis, R. E., Leonard, N. E. and Fratantoni, D. M. (2008) Routing strategies for underwater gliders; *Deep Sea Research Part II: Topical Studies in Oceanography*, **In Press, Corrected Proof**.
- Deffenbaugh, M., Bellingham, J. G. and Schmidt, H. (1996a) The relationship between spherical and hyperbolic positioning; *In proceedings of the MTS/IEEE Oceans 1996*, Fort Lauderdale, FL, USA, September 1996, pp. 590-595.
- Deffenbaugh, M., Schmidt, H. and Bellingham, J. G. (1996b) Acoustic positioning in a fading multipath environment; *In proceedings of the MTS/IEEE Oceans 1996*, Fort Lauderdale, FL, USA, pp. 596-600.
- Dellaert, F., Fox, D., Burgard, W. and Thrun, S. (1999a) Monte Carlo localization for mobile robots; *In proceedings of the IEEE International Conference on Robotics and Automation 1999 (ICRA '99)*, Detroit, MI, USA, May 1999, pp. 1322-1328.
- Dellaert, F., Burgard, W., Fox, D. and Thrun, S. (1999b) Using the condensation algorithm for robust, vision-based mobile robot localization; *In proceedings of the IEEE Computer Society Conference on Computer Vision and Pattern Recognition 1999*, Fort Collins, CO, USA, June 1999, pp. 588-594.
- Dellaert, F. and Stroupe, A. W. (2002) Linear 2D localization and mapping for single and multiple robot scenarios; *In proceedings of the IEEE International Conference on Robotics and Automation 2002 (ICRA '02)*, Washington, DC, USA, May 2002, pp. 688-694.

- Detweiler, C., Vasilescu, I. and Rus, D. (2007) An underwater sensor network with dual communications, sensing, and mobility; *In proceedings of the IEEE/OES Oceans 2007*, Aberdeen, Scotland, June 2007.
- Digi International (2008), *XBee™ ZNet 2.5/XBee-Pro™ ZNet 2.5 OEM RF modules product manual*, November 2008, http://ftp1.digi.com/support/documentation/90000866_C.pdf
- Dissanayake, M. W. M. G., Newman, P., Clark, S., Durrant-Whyte, H. F. and Csorba, M. A. (2001) A solution to the simultaneous localization and map building (SLAM) problem; *IEEE Transactions on Robotics and Automation*, 17(3), pp. 229-241.
- Dudek, G., Giguere, P., Prahacs, C., Saunderson, S., Sattar, J., Torres-Mendez, L.-A., Jenkin, M., German, A., Hogue, A., Ripsman, A., Zacher, J., Milios, E., Liu, H., Zhang, P., Buehler, M. and Georgiades, C. (2007) AQUA: An amphibious autonomous robot; *Computer*, 40(1), pp. 46-53.
- Dunbabin, M., Roberts, J., Usher, K. and Corke, P. (2004) A new robot for environmental monitoring on the great barrier reef; *In proceedings of the Australasian Conference on Robotics and Automation 2004 (ACRA '04)*, Canberra, ACT, Australia, December 2004.
- Dunbabin, M., Roberts, J., Usher, K., Winstanley, G. and Corke, P. (2005) A hybrid AUV design for shallow water reef navigation; *In proceedings of the IEEE International Conference on Robotics and Automation 2005 (ICRA '05)*, Barcelona, Spain, April 2005, pp. 2105-2110.
- Dunbabin, M., Usher, K. and Corke, P. (2006a) Visual motion estimation for an autonomous underwater reef monitoring robot; *Field & Service Robotics*, 25, pp. 31-42.
- Dunbabin, M., Corke, P., Vasilescu, I. and Rus, D. (2006b) Data muling over underwater wireless sensor networks using an autonomous underwater vehicle; *In proceedings of the IEEE International Conference on Robotics and Automation 2006 (ICRA '06)*, Orlando, FL, USA, May 2006, pp. 2091-2098.
- Dunn, C. and Hawksford, M. (1993) Distortion immunity of MLS-derived impulse response measurements; *Journal of the Audio Engineering Society*, 41(5), pp. 314-335.
- Eagle Tree Systems (2005), *Instruction manual for the data recorder GPS expander V3*, [http://www.eagletreesystems.com/Support/Manuals/GPS Expander Manual.pdf](http://www.eagletreesystems.com/Support/Manuals/GPS%20Expander%20Manual.pdf)
- Eagle Tree Systems (2008), *User manual for the Seagull wireless dashboard telemetry and data recorder systems*, [http://www.eagletreesystems.com/Support/Manuals/Pro, Glide, Flight and Boat Seagull and Data Recorder Instruction Manual.pdf](http://www.eagletreesystems.com/Support/Manuals/Pro,%20Glide,%20Flight%20and%20Boat%20Seagull%20and%20Data%20Recorder%20Instruction%20Manual.pdf)
- Edwards, D. B., Bean, T. A., Odell, D. L. and Anderson, M. J. (2004) A leader-follower algorithm for multiple AUV formations; *In proceedings of the IEEE/OES Autonomous Underwater Vehicles 2004*, Sebasco, ME, USA, June 2004, pp. 40-46.
- Elfes, A. (1987) Sonar-based real-world mapping and navigation; *IEEE Journal of Robotics and Automation*, 3(3), pp. 249-265.
- Erol, M., Vieira, L. F. M. and Gerla, M. (2007) Localization with dive'n'rise (DnR) beacons for underwater acoustic sensor networks; *In proceedings of the ACM International Workshop on Underwater Networks (WUWNet '07)*, Montréal, Québec, Canada, September 2007, pp. 97-100.

- Erol, M., Vieira, L. F. M., Caruso, A., Paparella, F., Gerla, M. and Oktug, S. (2008) Multi stage underwater sensor localization using mobile beacons; *In proceedings of the International Conference on Sensor Technologies and Applications 2008 (SENSORCOMM '08)*, Cap Esterel, France, August 2008, pp. 710-714.
- Etter, P. C. (2003) *Underwater acoustic modeling and simulation*, London, Spon Press.
- Eustice, R. M., Whitcomb, L. L., Singh, H. and Grund, M. (2007) Experimental results in synchronous-clock one-way-travel-time acoustic navigation for autonomous underwater vehicles; *In proceedings of the IEEE International Conference on Robotics and Automation 2007 (ICRA '07)*, Roma, Italy, April 2007, pp. 4257-4264.
- Fallon, M. and Godsill, S. (2008) Multi target acoustic source tracking with an unknown and time varying number of targets; *In proceedings of the Hands-Free Speech Communication and Microphone Arrays 2008*, Trento, Italy, May 2008, pp. 77-80.
- Farina, A. (1998) MLS impulse response measurements for underwater bottom profiling; *In proceedings of the European Conference on Underwater Acoustics 1998 (ECUA '98)*, Roma, Italy, September 1998.
- Farina, A. (1999) Target tracking with bearings-only measurements; *Signal Processing*, **78**(1), pp. 61-78.
- Farina, A., Ristic, B. and Timmoneri, L. (2002) Cramér-Rao bound for nonlinear filtering with $P_d < 1$ and its application to target tracking; *IEEE Transactions on Signal Processing*, **50**(8), pp. 1916-1924.
- Feder, H. J. S., Leonard, J. J. and Smith, C. M. (1998) Incorporating environmental measurements in navigation; *In proceedings of the Workshop on Autonomous Underwater Vehicles 1998 (AUV '98)*, Cambridge, MA, USA, pp. 115-122.
- Fenwick, J. W., Newman, P. M. and Leonard, J. J. (2002) Cooperative concurrent mapping and localization; *In proceedings of the IEEE International Conference on Robotics and Automation 2002 (ICRA '02)*, Washington, DC, USA, May 2002, pp. 1810-1817.
- Figliola, R. S. and Beasley, D. E. (2005) *Theory and design for mechanical measurements*, Fourth edition, New York, NY, John Wiley & Sons.
- Fiorelli, E., Leonard, N. E., Bhatta, P., Paley, D. A., Bachmayer, R. and Fratantoni, D. M. (2006) Multi-AUV control and adaptive sampling in Monterey bay; *IEEE Journal of Oceanic Engineering*, **31**(4), pp. 935-948.
- Fox, D., Burgard, W., Thrun, S. and Cremers, A. B. (1998) Position estimation for mobile robots in dynamic environments; *In proceedings of the conference on Artificial Intelligence/ Innovative Applications of Artificial Intelligence*, Madison, WI, USA, September 1998.
- Fox, D., Burgard, W., Dellaert, F. and Thrun, S. (1999) Monte Carlo localization: Efficient position estimation for mobile robots. *In proceedings of the 16th National Conference on Artificial Intelligence 1999 (AAAI '99)*. Orlando, FL, USA.
- Fox, D., Burgard, W., Kruppa, H. and Thrun, S. (2000) A probabilistic approach to collaborative multi-robot localization; *Autonomous Robots*, **8**(3), pp. 325-344.

- Frater, M. R., Ryan, M. J. and Dunbar, R. M. (2006) Electromagnetic communications within swarms of autonomous underwater vehicles; *In proceedings of the ACM International Workshop on Underwater Networks (WUWNet '06)*, Los Angeles, CA, USA, September 2006, pp. 64-70.
- Freitag, L., Johnson, M., Grund, M., Singh, S. and Preisig, J. (2001) Integrated acoustic communication and navigation for multiple UUVs; *In proceedings of the MTS/IEEE Oceans 2001*, Honolulu, HI, USA, November 2001, pp. 2065-2070.
- Freitag, L., Grund, M., Singh, S., Partan, J., Koski, P. and Ball, K. (2005) The WHOI micro-modem: An acoustic communications and navigation system for multiple platforms; *In proceedings of the MTS/IEEE Oceans 2005*, Washington, DC, USA, September 2005, pp. 1086-1092.
- Gay, S. L. and Benesty, J. (2000) *Acoustic signal processing for telecommunication*, Boston, MA; London, Kluwer Academic Publishers.
- Gesbert, D., Bolcskei, H., Gore, D. and Paulraj, A. (2000) MIMO wireless channels: Capacity and performance prediction; *In proceedings of the IEEE Global Telecommunications Conference 2000 (GLOBECOM '00)*, San Fransisco, CA, USA, pp. 1083-1088.
- Giraudet, P. and Glotin, H. (2006) Real-time 3D tracking of whales by echo-robust precise TDOA estimates with a widely-spaced hydrophone array; *Applied Acoustics*, **67**(11-12), pp. 1106-1117.
- Girod, L. D. (2005) *A self-calibrating system of distributed acoustic arrays*, PhD thesis, University of California Los Angeles: CA, USA.
- Girod, L. D., Martin, L., Vlad, T. and Deborah, E. (2006) The design and implementation of a self-calibrating distributed acoustic sensing platform. *ACM International Conference on Embedded Networked Sensor Systems 2006 (SenSys '06)*. Boulder, CO, USA, ACM.
- Goldsmith, A., Jafar, S. A., Jindal, N. and Vishwanath, S. (2003) Capacity limits of MIMO channels; *IEEE Journal on Selected Areas in Communications*, **21**(5), pp. 684-702.
- Golomb, S. W. (1982) *Shift register sequences*, Revised edition, Laguna Hills, CA, Aegean Park Press.
- Golomb, S. W. and Gong, G. (2004) *Signal design for good correlation: For wireless communication, cryptography, and radar*, Cambridge; New York, NY, Cambridge University Press.
- Gordon, N. J., Salmond, D. J. and Smith, A. F. M. (1993) Novel approach to non-linear/non-Gaussian Bayesian state estimation; *IEE Proceedings F Radar and Signal Processing*, **140**(2), pp. 107-113.
- Handzel, A. A. and Krishnaprasad, P. S. (2002) Biomimetic sound-source localization; *IEEE Sensors Journal*, **2**(6), pp. 607-616.
- Hernand, J.-P. and Roderick, W. I. (1993) Acoustic model-based matched filter processing for fading time-dispersive ocean channels: Theory and experiment; *IEEE Journal of Oceanic Engineering*, **18**(4), pp. 447-465.

- Hernandez, M., Ristic, B., Farina, A. and Timmoneri, L. (2004) A comparison of two Cramér-Rao bounds for nonlinear filtering with $P_d < 1$; *IEEE Transactions on Signal Processing*, **52**(9), pp. 2361-2370.
- Hoe, A. (2002) *AdaMT19937*, <http://adrianhoe.com/adrianhoe/projects/adamt19937/>
- Hofmann-Wellenhof, B., Lichtenegger, Herbert, Collins and James (2001) *Global positioning system : Theory and practice*, Wien, Springer-Verlag.
- Honary, E., McQuade, F., Ward, R., Woodrow, I., Shaw, A., Barnes, D. and Fyfe, M. (2009) Robotic experiments with cooperative aerobots and underwater swarms; *Robotica*, **27**(01), pp. 37-49.
- Howard, A., Matarić, M. J. and Sukhatme, G. S. (2002) Localization for mobile robot teams using maximum likelihood estimation; *In proceedings of the IEEE/RSJ International Conference on Intelligent Robots and Systems 2002 (IROS '02)*, Lausanne, Switzerland, October 2002, pp. 434-439.
- Howard, A., Matarić, M. J. and Sukhatme, G. S. (2003) Cooperative relative localization for mobile robot teams: An ego-centric approach; *In proceedings of the Naval Research Laboratory Workshop on Multi-Robot Systems*, Washington, DC, USA, March 2003, pp. 65-76.
- Howard, A., Parker, L. E. and Sukhatme, G. S. (2006) Experiments with a large heterogeneous mobile robot team: Exploration, mapping, deployment and detection; *International Journal of Robotics Research*, **25**(5-6), pp. 431-448.
- Huang, Y., Benesty, J. and Chen, J. (2006) Identification of acoustic MIMO systems: Challenges and opportunities; *Signal Processing*, **86**(6), pp. 1278-1295.
- Huster, A., Frew, E. W. and Rock, S. M. (2002) Relative position estimation for AUVs by fusing bearing and inertial rate sensor measurements; *In proceedings of the MTS/IEEE Oceans 2002* Biloxi, MI, USA, October 2002, pp. 1863-1870.
- Huster, A. (2003) *Relative position sensing by fusing monocular vision and inertial rate sensors*, Department of Electrical Engineering, PhD thesis, Stanford University: Palo Alto, CA, USA.
- Istepanian, R. S. H. and Stojanovic, M. (2002) *Underwater acoustic digital signal processing and communication systems*, Boston, MA, Kluwer Academic Publishers.
- Johnson-Roberson, M., Pizarro, O. and Williams, S. B. (2007) Towards three-dimensional heterogeneous imaging sensor correspondence and registration for visualization; *In proceedings of the IEEE/OES Oceans 2007*, Aberdeen, Scotland, June 2007, pp. 1-6.
- Julier, S. J. and Uhlmann, J. K. (1997) A new extension of the kalman filter to nonlinear systems; *In proceedings of the Signal Processing, Sensor Fusion, and Target Recognition VI*, Orlando, FL, USA, April 1997, pp. 182-193.
- Kalantar, S. (2006) *Field-coupled deformable formations of autonomous submersible robots*, College of Engineering and Computer Science, PhD thesis, The Australian National University: Canberra, ACT, Australia.

- Kalantar, S. and Zimmer, U. R. (2007) Motion planning for small formations of autonomous vehicles navigating on gradient fields; *In proceedings of the IEEE International Symposium on Underwater Technology 2007 (UT '07)* Tokyo, Japan, April 2007, pp. 512-519.
- Kaplan, E. D. and Hegarty, C. J. (2006) *Understanding GPS : Principles and applications*, Boston, MA; London, Artech House.
- Kasper, J. F. Jr. and Hutchinson, C. E. (1978) The OMEGA navigation system: An overview; *IEEE Communications Magazine*, 16(3), pp. 23-35.
- Kayton, M. (1988) Navigation: Ships to space; *IEEE Transactions on Aerospace and Electronic Systems*, 24(5), pp. 474-519.
- Kemppainen, A., Haverinen, J. and Röning, J. (2006) An infrared location system for relative pose estimation of robots; *In proceedings of the 16th CISM-IFTToMM Symposium of Robot Design, Dynamics and Control (ROMANSY 2006)*, Warsaw, Poland, June 2006.
- Kenn, H. and Pfeil, A. (2004) A sound source localization sensor using probabilistic occupancy grid maps; *In proceedings of the Mechatronics and Robotics 2004 (MECROB '04)*, Aachen, Germany, September 2004.
- Kilfoyle, D. B. and Baggeroer, A. B. (2000) The state of the art in underwater acoustic telemetry; *IEEE Journal of Oceanic Engineering*, 25(1), pp. 4-27.
- Kinsler, L. E. (1982) *Fundamentals of acoustics*, New York, NY, Wiley.
- Klepczynski, W. J. (1983) Modern navigation systems and their relation to time keeping; *Proceedings of the IEEE*, 71(10), pp. 1193-1198.
- Knapp, C. H. and Carter, G. C. (1976) The generalized correlation method for estimation of time delay; *IEEE Transactions on Acoustics, Speech, and Signal Processing*, 24(4), pp. 320-327.
- Konishi, M. (1993) Listening with two ears; *Scientific American*, 268(4), pp. 66-73.
- Kottege, N. and Zimmer, U. R. (2006) Acoustical localization in schools of submersibles; *In proceedings of the IEEE/OES Oceans 2006*, Singapore, May 2006.
- Kottege, N. and Zimmer, U. R. (2007) Relative localisation for AUV swarms; *In proceedings of the IEEE International Symposium on Underwater Technology 2007 (UT '07)*, Tokyo, Japan, April 2007, pp. 588-593.
- Kottege, N. and Zimmer, U. R. (2008) MLS based distributed, bearing, range and posture estimation for schools of submersibles, in Khatib, O., Kumar, V. and Rus, D. (Eds.) *Experimental robotics*. Berlin; Heidelberg, Springer, pp. 377-385.
- Kurazume, R., Nagata, S. and Hirose, S. (1994) Cooperative positioning with multiple robots; *In proceedings of the IEEE International Conference on Robotics and Automation 1994 (ICRA '94)*, San Diego, CA, USA, May 1994, pp. 1250-1257.
- Kurazume, R., Hirose, S., Nagata, S. and Sashida, N. (1996) Study on cooperative positioning system (basic principle and measurement experiment); *In proceedings of the IEEE International Conference on Robotics and Automation 1996 (ICRA '96)*, Minneapolis, MN, USA, April 1996, pp. 1421-1426.

- Kurazume, R. and Hirose, S. (1998) Study on cooperative positioning system: Optimum moving strategies for CPS-III; *In proceedings of the IEEE International Conference on Robotics and Automation 1998 (ICRA '98)*, Leuven, Belgium, May 1998, pp. 2896-2903.
- Lamport, L. (1978) Time, clocks, and the ordering of events in a distributed system; *Communications of the ACM*, 21(7), pp. 558-565.
- Larsen, M. B. (2000) Synthetic long baseline navigation of underwater vehicles; *In proceedings of the MTS/IEEE Oceans 2000*, Providence, RI, USA, September 2000, pp. 2043-2050.
- Last, J. D. (1989) Radionavigation in a time of change; *Electronics & Communication Engineering Journal*, 1(6), pp. 281-287.
- Lehmann, E. A. (2004) *Particle filtering methods for acoustic source localisation and tracking*, Department of Telecommunications Engineering, Research School of Information Sciences and Engineering, PhD thesis, The Australian National University: Canberra, ACT, Australia.
- Leonard, J. J. and Durrant-Whyte, H. F. (1991) Mobile robot localization by tracking geometric beacons; *IEEE Transaction on Robotics and Automation*, 7(3), pp. 376-382.
- Leonard, J. J., Bennett, A. A., Smith, C. M. and Feder, H. J. S. (1998) *Autonomous underwater vehicle navigation*; Technical Memorandum 98-1, Marine Robotics Laboratory, MIT, Boston, MA, USA.
- Leonard, J. J., Carpenter, R. N. and Feder, H. J. S. (2001) Stochastic mapping using forward look sonar; *Robotica*, 19(5), pp. 467-480.
- Leonard, N. E., Paley, D. A., Lekien, F., Sepulchre, R., Fratantoni, D. M. and Davis, R. E. (2007) Collective motion, sensor networks, and ocean sampling; *Proceedings of the IEEE*, 95(1), pp. 48-74.
- Li, J., Conan, J. and Pierre, S. (2006) Mobile station location estimation for MIMO communication systems; *In proceedings of the International Symposium on Wireless Communication Systems 2006*, Valencia, Spain, September 2006, pp. 561-564.
- Liang, C.-C. (1999) A study of a short-baseline acoustic positioning system for offshore vessels; *Marine Geodesy*, 22(1), pp. 19 - 30.
- Liu, H. and Milios, E. (2005) Acoustic positioning using multiple microphone arrays; *Journal of the Acoustical Society of America*, 117(5), pp. 2772-2782.
- Liu, W. (2008) *Design and modelling of adaptive foraging in swarm robotic systems*, Faculty of Environment and Technology, PhD thesis, University of the West of England: Bristol, UK.
- Locosys Technology (2006), *LS20030-3 GPS smart antenna module datasheet*, http://www.sparkfun.com/datasheets/GPS/Modules/LS20030~3_datasheet_v1.0.pdf
- Loebis, D., Sutton, R. and Chudley, J. (2002) Review of multisensor data fusion techniques and their application to autonomous underwater navigation; *Journal of Marine Engineering and Technology*, 2002(1), pp. 3-14.

- Lombard, A., Kellermann, W. and Buchner, H. (2008) A real-time demonstrator for the 2D localization of two sound sources using blind adaptive MIMO system identification; *In proceedings of the Hands-Free Speech Communication and Microphone Arrays 2008*, Trento, Italy, May 2008, pp. 41-44.
- Lucani, D. E., Médard, M. and Stojanovic, M. (2008) Underwater acoustic networks: Channel models and network coding based lower bound to transmission power for multicast; *IEEE Journal on Selected Areas in Communications*, **26**(9), pp. 1708-1719.
- Ma, N. and Goh, J. T. (2006) Ambiguity-function-based techniques to estimate DoA of broadband chirp signals; *IEEE Transactions on Signal Processing*, **54**(5), pp. 1826-1839.
- MacCurdy, E. (1948) *The notebooks of Leonardo da Vinci*, Oxford, Alden Press.
- Mackenzie, K. V. (1981) Nine-term equation for sound speed in the oceans; *Journal of the Acoustical Society of America*, **70**(3), pp. 807-812.
- Mahajan, A. and Walworth, M. (2001) 3D position sensing using the differences in the time-of-flights from a wave source to various receivers; *IEEE Transactions on Robotics and Automation*, **17**(1), pp. 91-94.
- Mahon, I., Williams, S. B., Pizarro, O. and Johnson-Roberson, M. (2008) Efficient view-based SLAM using visual loop closures; *IEEE Transactions on Robotics*, **24**(5), pp. 1002-1014.
- Majumder, S., Scheduling, S. and Durrant-Whyte, H. F. (2001) Multisensor data fusion for underwater navigation; *Robotics and Autonomous Systems*, **35**, pp. 97-108.
- Maki, T., Hashimoto, K. and Momma, H. (2005) Development of advanced secondary cable for the full ocean depth ROV Kaiko; *In proceedings of the MTS/IEEE Oceans 2005*, Washington, DC, USA, September 2005, pp. 2313-2319.
- Manley, J. E. (2007) The role of risk in AUV development and deployment; *In proceedings of the IEEE/OES Oceans 2007*, Aberdeen, Scotland, June 2007.
- Manolakis, D. E. (1996) Efficient solution and performance analysis of 3D position estimation by trilateration; *IEEE Transactions on Aerospace and Electronic Systems*, **32**(4), pp. 1239-1248.
- Mao, G., Fidan, B. and Anderson, B. D. O. (2007) Wireless sensor network localization techniques; *Computer Networks*, **51**(10), pp. 2529-2553.
- Martinelli, A., Pont, F. and Siegwart, R. (2005) Multi-robot localization using relative observations; *In proceedings of the IEEE International Conference on Robotics and Automation 2005 (ICRA '05)*, Barcelona, Spain, April 2005, pp. 2797-2802.
- Martins, A., Almeida, J. M. and Silva, E. (2003) Coordinated maneuver for gradient search using multiple AUVs; *In proceedings of the MTS/IEEE Oceans 2003*, San Diego, CA, USA, September 2003, pp. 347-352.
- Matarić, M. (1994) *Interaction and intelligent behavior*, Department of Electrical Engineering and Computer Science, PhD thesis, Massachusetts Institute of Technology: Boston, MA, USA.

- Matarić, M. J. (1997) Behavior-based control: Examples from navigation, learning, and group behavior; *Journal of Experimental and Theoretical Artificial Intelligence*, 9(2-3).
- Matos, A., Cruz, N., Martins, A. and Pereira, F. L. (1999) Development and implementation of a low-cost LBL navigation system for an AUV; *In proceedings of the MTS/IEEE Oceans 1999*, Seattle, WA, USA, September 1999, pp. 774-779.
- Matsumoto, M. (2007) *Mersenne Twister home page*,
<http://www.math.sci.hiroshima-u.ac.jp/~m-mat/MT/emt.html>
- Matsumoto, M. and Nishimura, T. (1998) Mersenne Twister: A 623-dimensionally equidistributed uniform pseudo-random number generator; *ACM Transactions on Modeling and Computer Simulation*, 8(1), pp. 3-30.
- McDowell, P., Chen, J. and Bourgeois, B. (2002) UUV teams, control from a biological perspective; *In proceedings of the MTS/IEEE Oceans 2002* Biloxi, MI, USA, October 2002, pp. 331-337.
- Milne, P. H. (1983) *Underwater acoustic positioning systems*, London, Spon Press.
- Moore, D., Leonard, J. J., Rus, D. and Teller, S. (2004) Robust distributed network localization with noisy range measurements; *In proceedings of the ACM International Conference on Embedded Networked Sensor Systems 2004 (SenSys '04)*, Baltimore, MD, USA, November 2004, pp. 50-61.
- Mourikis, A. I. and Roumeliotis, S. I. (2006) Performance analysis of multirobot cooperative localization; *IEEE Transactions on Robotics*, 22(4), pp. 666-681.
- Nebot, E. M., Durrant-Whyte, H. and Scheduling, S. (1996) Kalman filtering design techniques for aided GPS land navigation applications; *In proceedings of the First Australian Data Fusion Symposium 1996 (ADFS '96)*, Adelaide, SA, Australia, November 1996, pp. 83-88.
- Neuweiler, G. (2003) Evolutionary aspects of bat echolocation; *Journal of Comparative Physiology A: Neuroethology, Sensory, Neural, and Behavioral Physiology*, 189(4), pp. 245-256.
- Newman, P. M., Leonard, J. J., Tardós, J. D. and Neira, J. (2002) Explore and return: Experimental validation of real-time concurrent mapping and localization; *In proceedings of the IEEE International Conference on Robotics and Automation 2002 (ICRA '02)*, Washington, DC, USA, May 2002, pp. 1802-1809.
- Newman, P. M., Leonard, J. J. and Rikoski, R. J. (2003) Towards constant-time SLAM on an autonomous underwater vehicle using synthetic aperture sonar; *In proceedings of the International Symposium on Robotics Research*, Sienna, Italy, October 2003.
- Nielsen, R. O. (1991) *Sonar signal processing*, Boston, MA, Artech House.
- Odell, D. L., Hertel, K. and Nielsen, C. (2002) New acoustic systems for AUV tracking, communications, and noise measurement at NSWCCD-ARD, lake Pend Oreille, Idaho; *In proceedings of the MTS/IEEE Oceans 2002*, Biloxi, MI, USA, October 2002, pp. 266-271.
- Ögren, P., Fiorelli, E. and Leonard, N. E. (2004) Cooperative control of mobile sensor networks: Adaptive gradient climbing in a distributed environment; *IEEE Transactions on Automatic Control*, 49(8), pp. 1292-1302.

- Olson, E., Leonard, J. J. and Teller, S. (2004) Robust range-only beacon localization; *In proceedings of the IEEE/OES Autonomous Underwater Vehicles 2004*, Sebasco, ME, USA, June 2004, pp. 66-75.
- Omologo, M. and Svaizer, P. (1996) Acoustic source location in noisy and reverberant environment using csp analysis; *In proceedings of the IEEE International Conference on Acoustics, Speech, and Signal Processing 1996 (ICASSP-96)*, Atlanta, GA, USA, May 1996, pp. 921-924.
- Omologo, M. and Svaizer, P. (1997) Use of the crosspower-spectrum phase in acoustic event location; *IEEE Transactions on Speech and Audio Processing*, 5(3), pp. 288-292.
- Paley, D. A., Zhang, F. and Leonard, N. E. (2008) Cooperative control for ocean sampling: The glider coordinated control system; *IEEE Transactions on Control Systems Technology*, 16(4), pp. 735-744.
- Palmer, W. (1970) The omega navigation system as a source of frequency and time; *In proceedings of the 24th Annual Symposium on Frequency Control*, Fort Monmouth, NJ, USA, April 1970, pp. 345-360.
- Peterson, W. W. and Weldon, E. J. Jr., (1972) *Error-correcting codes*, Boston, MA, MIT Press.
- Pieng, T. S., Beng, K. T., Venugopalan, P., Chitre, M. A. and Potter, J. R. (2004) Development of a shallow water ambient noise database; *In proceedings of the IEEE International Symposium on Underwater Technology 2004 (UT '04)* Taipei, April 2004, pp. 169-173.
- Piersol, A. G. (1981) Time delay estimation using phase data; *IEEE Transactions on Acoustics, Speech, and Signal Processing*, 29(3), pp. 471-477.
- Plotnik, A. M. and Rock, S. M. (2005) Relative position sensing and automatic control for observation in the midwater by an underwater vehicle; *In proceedings of the The International Symposium on Unmanned Untethered Submersible Technology (UUST '05)*, Durham, NH, USA, August 2005.
- PNI (2004), *Application note: Multipoint calibration primer*,
[https://www.pnicorp.com/downloadResource/c40c/manuals/53/Ap+Note+Multipoint+Calibration+Primer+\(APNOTE+++1001766+++R01\).pdf](https://www.pnicorp.com/downloadResource/c40c/manuals/53/Ap+Note+Multipoint+Calibration+Primer+(APNOTE+++1001766+++R01).pdf)
- PNI (2006), *MicroMag3 Datasheet*, Revision: June 2006,
https://www.pnicorp.com/downloadResource/cMM3s/datasheets/110/MicroMag3+3-Axis+Sensor+Module_June+2006.pdf
- Pompili, D., Melodia, T. and Akyildiz, I. F. (2008) Three-dimensional and two-dimensional deployment analysis for underwater acoustic sensor networks; *Ad Hoc Networks*, 7(4), pp. 778-790.
- Postolache, O., Girão, P. and Pereira, M. (2007) Underwater acoustic source localization based on passive sonar and intelligent processing; *In proceedings of the IEEE Instrumentation and Measurement Technology Conference 2007 (IMTC 2007)*, Warsaw, Poland, May 2007.
- Priyantha, N. B., Chakraborty, A. and Balakrishnan, H. (2000) The cricket location-support system; *In proceedings of the ACM International Conference on Mobile Computing and Networking 2000 (MobiCom 2000)*, Boston, MA, USA, August 2000, pp. 32 - 43.

- Priyantha, N. B. (2005) *The cricket indoor location system*, Department of Electrical Engineering and Computer Science, PhD thesis, Massachusetts Institute of Technology: Boston, MA, USA.
- Proakis, J. G. and Manolakis, D. G. (1996) *Digital signal processing : Principles, algorithms, and applications*, Englewood Cliffs, NJ, Prentice Hall International.
- Proakis, J. G., Sozer, E. M., Rice, J. A. and Stojanovic, M. (2001) Shallow water acoustic networks; *IEEE Communications Magazine*, **39**(11), pp. 114-119.
- Proakis, J. G. and Salehi, M. (2002) *Communication systems engineering*, Upper Saddle River, NJ, Prentice Hall.
- Pugh, J. and Martinoli, A. (2006) Relative localization and communication module for small-scale multi-robot systems; *In proceedings of the IEEE International Conference on Robotics and Automation 2006 (ICRA '06)*, Orlando, FL, USA, May 2006, pp. 188-193.
- Pugh, J. and Martinoli, A. (2008) Small-scale robot formation movement using a simple on-board relative positioning system, in Khatib, O., Kumar, V. and Rus, D. (Eds.) *Experimental robotics*. Berlin; Heidelberg, Springer, pp. 297-306.
- Ramp, S. R., Davis, R. E., Leonard, N. E., Shulman, I., Chao, Y., Robinson, A. R., Marsden, J., Lermusiaux, P. F. J., Fratantoni, D. M., Paduan, J. D., Chavez, F. P., Bahr, F. L., Liang, S., Leslie, W. and Li, Z. (2008) Preparing to predict: The second Autonomous Ocean Sampling Network (AOSN-II) experiment in the Monterey bay; *Deep Sea Research Part II: Topical Studies in Oceanography*, **In Press, Corrected Proof**.
- Reeder, C. A., Odell, D. L., Okamoto, A., Anderson, M. J. and Edwards, D. B. (2004) Two-hydrophone heading and range sensor applied to formation-flying for AUVs; *In proceedings of the MTS/IEEE Oceans 2004*, Kobe, Japan, November 2004, pp. 517-523.
- Rekleitis, I. M., Dudek, G. and Milios, E. (2001) Multi-robot collaboration for robust exploration; *Annals of Mathematics and Artificial Intelligence*, **31**(1), pp. 7-40.
- Rekleitis, I. M. (2003) *Cooperative localization and multi-robot exploration*, School of Computer Science, PhD thesis, McGill University: Montréal, Québec, Canada.
- Rekleitis, I. M. (2004) *A particle filter tutorial for mobile robot localization*; Technical report TR-CIM-04-02, Centre for Intelligent Machines, McGill University, Montréal, Québec, Canada.
- Reynolds, C. W. (1987) Flocks, herds and schools: A distributed behavioral model; *Computer Graphics*, **21**(4), pp. 25-34.
- Ricker, D. W. (2003) *Echo signal processing*, Boston, MA, Kluwer Academic Publishers.
- Rife, J. and Rock, S. M. (2002) Field experiments in the control of a jellyfish tracking ROV; *In proceedings of the MTS/IEEE Oceans 2002*, Biloxi, MI, USA, October 2002, pp. 2031-2038.
- Rigby, P., Pizarro, O. and Williams, S. B. (2006) Towards geo-referenced AUV navigation through fusion of USBL and DVL measurements; *In proceedings of the MTS/IEEE Oceans 2006*, Boston, MA, USA, September 2006, pp. 1-6.

- Ristic, B., Arulampalam, M. S. and McCarthy, J. (2002) Target motion analysis using range-only measurements: Algorithms, performance and application to ISAR data; *Signal Processing*, **82**(2), pp. 273-296.
- Ristic, B. and Arulampalam, M. S. (2003) Tracking a manoeuvring target using angle-only measurements: Algorithms and performance; *Signal Processing*, **83**(6), pp. 1223-1238.
- Ristic, B. and Arulampalam, M. S. (2004) *Beyond the Kalman filter : Particle filters for tracking applications*, Boston, Artech House.
- Robotis(2007), *USB2Dynamixel users manual*,
http://www.robotis.com/data_eng/USB2Dynamixel_m.zip
- Robotis (2008), *Dynamixel RX-10 user manual*, http://www.robotis.com/zbxe/dynamixel_en
- Roland (2004), *Edirol FireWire AudioCapture FA-101 owners manual*,
http://lib.roland.co.jp/manual/en/dl_04-00303/FA-101_e4.pdf
- Roman, N. and DeLiang, W. (2003) Binaural tracking of multiple moving sources; *In proceedings of the IEEE International Conference on Acoustics, Speech, and Signal Processing 2003 (ICASSP '03)*, pp. 149-152.
- Roman, N. (2005) *Auditory-based algorithms for sound segregation in multisource and reverberant environments*, Department of Computer Science and Engineering, PhD thesis, Ohio State University: OH, USA.
- Roumeliotis, S. I. and Bekey, G. A. (2000a) Bayesian estimation and Kalman filtering: A unified framework for mobile robot localization; *In proceedings of the IEEE International Conference on Robotics and Automation 2000 (ICRA '00)*, San Fransisco, CA, USA, April 2000, pp. 2985-2992.
- Roumeliotis, S. I. and Bekey, G. A. (2000b) Collective localization: A distributed Kalman filter approach to localization of groups of mobile robots; *In proceedings of the IEEE International Conference on Robotics and Automation 2000 (ICRA '00)*, San Fransisco, CA, USA, April 2000, pp. 2958-2965.
- Roumeliotis, S. I. and Bekey, G. A. (2002) Distributed multirobot localization; *IEEE Transactions on Robotics and Automation*, **18**(5), pp. 781-795.
- Roumeliotis, S. I. and Rekleitis, I. M. (2004) Propagation of uncertainty in cooperative multi-robot localization: Analysis and experimental results; *Autonomous Robots*, **17**(1), pp. 41-54.
- Sáez, J. M., Hogue, A., Escolano, F. and Jenkin, M. (2006) Underwater 3D SLAM through entropy minimization; *In proceedings of the IEEE International Conference on Robotics and Automation 2006 (ICRA '06)*, Orlando, FL, USA, May 2006, pp. 3562-3567.
- Sarwate, D. V. and Pursley, M. B. (1980) Crosscorrelation properties of pseudo-random and related sequences; *Proceedings of the IEEE*, **68**(5), pp. 593-619.
- Schill, F. (2007) *Distributed communication in swarms of autonomous underwater vehicles*, College of Engineering and Computer Science, PhD thesis, The Australian National University: Canberra, ACT, Australia.

- Schill, F., Zimmer, U. R. and Trumpf, J. (2005) Towards optimal TDMA scheduling for robotic swarm communication; *In proceedings of the Towards Autonomous Robotic Systems (TAROS 2005)*, London, UK, September 2005.
- Schill, F. and Zimmer, U. R. (2006a) Effective communication in schools of submersibles; *In proceedings of the IEEE/OES Oceans 2006*, Singapore, May 2006.
- Schill, F. and Zimmer, U. R. (2006b) Distributed dynamical omnicast routing; *Complex Systems*, **16**(4).
- Schill, F. and Zimmer, U. R. (2007) Pruning local schedules for efficient swarm communication; *In proceedings of the IEEE International Symposium on Underwater Technology 2007 (UT '07)* Tokyo, Japan, April 2007, pp. 594-600.
- Schroeder, M. R. (1979) Integrated-impulse method measuring sound decay without using impulses; *Journal of the Acoustical Society of America*, **66**(2), pp. 497-500.
- Schulz, D., Burgard, W., Fox, D. and Cremers, A. B. (2001) Tracking multiple moving targets with a mobile robot using particle filters and statistical data association; *In proceedings of the IEEE International Conference on Robotics and Automation 2001 (ICRA '01)*, Seoul, Korea, May 2001, pp. 1665-1670.
- Singh, S., Grund, M., Bingham, B., Eustice, R., Singh, H. and Freitag, L. (2006) Underwater acoustic navigation with the WHOI micro-modem; *In proceedings of the MTS/IEEE Oceans 2006*, Boston, MA, USA, September 2006.
- Skarsoulis, E. K. and Kalogerakis, M. A. (2006) Two-hydrophone localization of a click source in the presence of refraction; *Applied Acoustics*, **67**(11-12), pp. 1202-1212.
- Serafina website, (2008), <http://serafina.anu.edu.au>
- Smith, A., Balakrishnan, H., Goraczko, M. and Priyantha, N. B. (2004) Tracking moving devices with the cricket location system; *In proceedings of the ACM International Conference on Mobile Systems, Applications and Services 2004 (MobiSys '04)*, Boston, MA, USA, June 2004, pp. 190 - 202
- Smith, S. M. and Kronen, D. (1997) Experimental results of an inexpensive short baseline acoustic positioning system for AUV navigation; *In proceedings of the MTS/IEEE Oceans 1997*, Halifax, NS, Canada, October 1997, pp. 714-720.
- Smith, S. M., Ganesan, K., An, P. E. and Dunn, S. E. (1998) Strategies for simultaneous multiple autonomous underwater vehicle operation and control; *International Journal of Systems Science*, **29**(10), pp. 1045 - 1063.
- Solberg, J. R., Lynch, K. M. and MacIver, M. A. (2008) Active electrolocation for underwater target localization; *International Journal of Robotics Research*, **27**(5), pp. 529-548.
- Somaraju, R. and Schill, F. (2007) A communication module and TDMA scheduling for a swarm of small submarines; *Turkish Journal of Electrical Engineering & Computer Sciences*, **15**(2), pp. 283-306.
- Sozer, E. M., Stojanovic, M. and Proakis, J. G. (2000) Underwater acoustic networks; *IEEE Journal of Oceanic Engineering*, **25**(1), pp. 72-83.

- Stern, R. M., Wang, D. and Brown, G. J. (2006) Binaural sound localization, in Wang, D. and Brown, G. J. (Eds.) *Computational auditory scene analysis*. Hoboken, NJ, USA, John Wiley & Sons.
- Stewart, J. L. and Westerfield, E. C. (1959) A theory of active sonar detection; *Proceedings of the IRE*, 47(5), pp. 872-881.
- Stojanovic, M. and Freitag, L. (2006) Multichannel detection for wideband underwater acoustic CDMA communications; *IEEE Journal of Oceanic Engineering*, 31(3), pp. 685-695.
- Stojanovic, M., Freitag, L., Leonard, J. J. and Newman, P. (2002) A network protocol for multiple AUV localization; *In proceedings of the MTS/IEEE Oceans 2002*, Biloxi, MI, USA, October 2002, pp. 604-611.
- Svaizer, P., Matassoni, M. and Omologo, M. (1997) Acoustic source location in a three-dimensional space using crosspower spectrum phase; *In proceedings of the IEEE International Conference on Acoustics, Speech, and Signal Processing 1997 (ICASSP-97)*, Munich, Germany, April 1997, pp. 231-234.
- Thomas, F. and Ros, L. (2005) Revisiting trilateration for robot localization; *IEEE Transactions on Robotics*, 21(1), pp. 93-101.
- Thrun, S., Fox, D., Burgard, W. and Dellaert, F. (2001) Robust Monte Carlo localization for mobile robots, *Artificial Intelligence*, 128(1-2), pp. 99-141.
- Thrun, S. (2002) Robotic mapping: A survey, in Lakemeyer, G. and Nebel, B. (Eds.) *Exploring artificial intelligence in the new millennium*. Freiburg, Morgan Kaufmann.
- Turin, G. L. (1960) An introduction to matched filters; *IRE Transactions on Information Theory*, 6(3), pp. 311-329.
- Urban, H. G. (1985) *Adaptive methods in underwater acoustics*, Boston, MA; Dordrecht, Kluwer Academic Publishers.
- Urlick, R. J. (1983) *Principles of underwater sound*, New York, NY, McGraw-Hill.
- Urlick, R. J. (1986) *Ambient noise in the sea*, Los Altos, CA, Peninsula Publishing.
- Vaganay, J., Leonard, J. J. and Bellingham, J. G. (1996) Outlier rejection for autonomous acoustic navigation; *In proceedings of the IEEE International Conference on Robotics and Automation 1996 (ICRA '96)*, Minneapolis, MN, USA, April 1996, pp. 2174-2181.
- Vaganay, J., Bellingham, J. G. and Leonard, J. J. (1999) Comparison of fix computation and filtering for autonomous acoustic navigation; *International Journal of Systems Science*, 29(10), pp. 1111-1122.
- Vaganay, J., Baccou, P. and Jouvencel, B. (2000) Homing by acoustic ranging to a single beacon; *In proceedings of the MTS/IEEE Oceans 2000*, Providence, RI, USA, pp. 1457-1462.
- Vaganay, J., Leonard, J. J., Curcio, J. A. and Willcox, J. S. (2004) Experimental validation of the moving long base-line navigation concept; *In proceedings of the IEEE/OES Autonomous Underwater Vehicles 2004*, Sebasco, ME, USA, June 2004, pp. 59-65.

- Valin, J.-M., Michaud, F., Rouat, J. and Létourneau, D. (2003) Robust sound source localization using a microphone array on a mobile robot; *In proceedings of the IEEE/RSJ International Conference on Intelligent Robots and Systems, 2003 (IROS 2003)*, Las Vegas, NV, USA, October 2003, pp. 1228-1233.
- Valin, J.-M., Michaud, F., Hadjou, B. and Rouat, J. (2004) Localization of simultaneous moving sound sources for mobile robot using a frequency-domain steered beamformer approach; *In proceedings of the IEEE International Conference on Robotics and Automation 2004 (ICRA '04)*, May 2004, pp. 1033-1038.
- Van Veen, B. D. and Buckley, K. M. (1988) Beamforming: A versatile approach to spatial filtering; *IEEE ASSP Magazine*, 5(2), pp. 4-24.
- Vanderkooy, J. (1994) Aspects of MLS measuring systems; *Journal of the Audio Engineering Society*, 42(4), pp. 219-231.
- Vasilescu, I., Kotay, K., Rus, D., Dunbabin, M. and Corke, P. (2005) Data collection, storage, and retrieval with an underwater sensor network; *In proceedings of the ACM International Conference on Embedded Networked Sensor Systems 2005 (SenSys '05)*, San Diego, CA, USA, November 2005, pp. 154-165.
- Vasilescu, I., Detweiler, C. and Rus, D. (2007) AquaNodes: An underwater sensor network; *In proceedings of the ACM International Workshop on Underwater Networks (WUWNet '07)*, Montréal, Québec, Canada, September 2007, pp. 85-88.
- Vo, B.-N., Singh, S. and Doucet, A. (2005) Sequential Monte Carlo methods for multi-target filtering with random finite sets; *IEEE Transactions on Aerospace and Electronic Systems*, 41(4), pp. 1224-1245.
- Waite, A. D. (2002) *Sonar for practising engineers*, Chichester, Wiley.
- Walker, W. G. and O'Connell, J. M. (1976) The development of LORAN-C for navigation in harbor and harbor entrance areas; *In proceedings of the MTS/IEEE Oceans 1976*, Washington, DC, USA, September 1976, pp. 123-126.
- Wallach, H. (1938) On sound localization; *Journal of the Acoustical Society of America*, 10(1), pp. 83-83.
- Wallach, H., Newman, E. B. and Rosenzweig, M. R. (1949) The precedence effect in sound localization; *The American Journal of Psychology*, 62(3), pp. 315-336.
- Ward, D. B., Lehmann, E. A. and Williamson, R. C. (2003) Particle filtering algorithms for tracking an acoustic source in a reverberant environment; *IEEE Transactions on Speech and Audio Processing*, 11(6), pp. 826-836.
- Welch, G. and Bishop, G. (1995) *An introduction to the kalman filter*; Technical report TR 95-041, Department of Computer Science, University of North Carolina, Chapel Hill, NC, USA
- Wettergreen, D., Gaskett, C. and Zelinsky, A. (1999) Autonomous guidance and control for an underwater robotic vehicle; *In proceedings of the International Conference on Field and Service Robotics (FSR '99)*, Pittsburg, PA, USA, September 1999.

- Wightman, F. L. and Kistler, D. J. (1992) The dominant role of low-frequency interaural time differences in sound localization; *Journal of the Acoustical Society of America*, **91**(3), pp. 1648-1661.
- Wijk, O. and Christensen, H. I. (2000) Triangulation-based fusion of sonar data with application in robot pose tracking; *IEEE Transactions on Robotics and Automation*, **16**(6), pp. 740-752.
- Williams, S. B., Newman, P., Dissanayake, M. W. M. G. and Durrant-Whyte, H. (2000) Autonomous underwater simultaneous localisation and map building; *In proceedings of the IEEE International Conference on Robotics and Automation 2000 (ICRA '00)*, San Francisco, CA, USA, April 2000, pp. 1793-1798.
- Williams, S. B. (2001) *Efficient solutions to autonomous mapping and navigation problems*, Department of Mechanical and Mechatronic Engineering, PhD thesis, The University of Sydney: Sydney, NSW, Australia.
- Williams, S. B., Dissanayake, M. W. M. G. and Durrant-Whyte, H. F. (2001) Towards terrain-aided navigation for underwater robotics; *Advanced Robotics*, **15**(5), pp. 533-549.
- Williams, S. B., Newman, P., Rosenblatt, J., Dissanayake, M. W. M. G. and Durrant-Whyte, H. F. (2001) Autonomous underwater navigation and control; *Robotica*, **19**(5), pp. 481-496.
- Williams, S. B., Dissanayake, M. W. M. G. and Durrant-Whyte, H. F. (2002) Towards multi-vehicle simultaneous localisation and mapping; *In proceedings of the IEEE International Conference on Robotics and Automation 2002 (ICRA '02)*, Washington, DC, USA, May 2002, pp. 2743-2748.
- Williams, S. B. and Mahon, I. (2004a) Simultaneous localisation and mapping on the great barrier reef; *In proceedings of the IEEE International Conference on Robotics and Automation 2004 (ICRA '04)* New Orleans, LA, USA, April 2004, pp. 1771-1776.
- Williams, S. B. and Mahon, I. (2004b) Design of an unmanned underwater vehicle for reef surveying; *In proceedings of the IFAC Symposium on Mechatronic Systems*, Manly, NSW, Australia, September 2004.
- Wing, M. G., Eklund, A. and Kellogg, L. D. (2005) Consumer-grade global positioning system (GPS) accuracy and reliability; *Journal of Forestry*, **103**(4), pp. 169-173.
- Zhang, F., Fratantoni, D. M., Paley, D. A., Lund, J. and Leonard, N. E. (2007) Control of coordinated patterns for ocean sampling; *International Journal of Control: Special issue on Navigation, Guidance and Control of Uninhabited Underwater Vehicles*, **80**(7), pp. 1186-1199.